Novel Metal and Silicon Oxide Engineered Substrates to Control Cell Alignment

by

Hassan Moussa

A thesis
presented to the University of Waterloo
in fulfillment of the
thesis requirement for the degree of
Doctor of Philosophy
in
Chemical Engineering

Waterloo, Ontario, Canada, 2019

Examining Committee Membership

The following served on the Examining Committee for this thesis. The decision of the Examining Committee is by majority vote.

External Examiner:	Jin Zhang Associate Professor, Western University
Supervisor:	Ting Tsui Associate Professor
Internal Member:	Yuning Li Professor
Internal Member:	Marc Aucoin Professor
Internal-external Member:	Irene A. Goldthorpe Associate Professor

AUTHOR'S DECLARATION

This thesis consists of material all of which I authored or co-authored: see Statement of Contributions included in the thesis. This is a true copy of the thesis, including any required final revisions, as accepted by my examiners.

I understand that my thesis may be made electronically available to the public.

Statement of Contribution

This thesis consists of several published manuscripts in which I, Hassan Moussa, was listed as a principal author or a contributor. Nevertheless, the list of published manuscripts could not be accomplished without collaboration within our group or externally.

Chapter 3 data is published in:

Moussa, H.I.; Logan, M.; Siow, G.C.; Phann, D.L.; Rao, Z.; Aucoin, M.G.; Tsui, T.Y., Sci. Technol. Adv. Mater. 18, 2017, 840-856

Conceptualization, Aucoin and Tsui; data curation, Moussa, Logan, Siow, Phann, and Rao; formal analysis, Aucoin and Tsui; investigation, Moussa, Logan, Siow, Phann, Rao, Aucoin, and Tsui; methodology, Moussa, Logan, Siow, Phann, Rao, Aucoin, and Tsui; resources, Tsui; supervision, Aucoin and Tsui; writing—original draft, Tsui; writing—review and editing, Aucoin, and Tsui.

Section 3.3.1.6 is a manuscript under-review, and the following is the authorship order:

H.I. Moussa, W.Y. Chan, M. Logan, M.G. Aucoin, T.Y. Tsui

Section 3.3.3 is a manuscript under-review, and the following is the authorship order:

H.I. Moussa, G. Kim, J. Tong, M. Glerum, T.Y. Tsui

Chapter 4 content is from a manuscript in a near-verbatim state which is intended for submission

Chapter 5 content is published in:

Moussa, H.I.; Logan, M.; Chan, W.; Wong, K.; Rao, Z.; Aucoin, M.G.; Tsui, T.Y., Materials 11, 2018, 1306

Conceptualization, Aucoin and Tsui; data curation, Moussa, Logan, Chan, Wong, Rao and Tsui; formal analysis, Aucoin and Tsui; investigation, Moussa, Logan, Chan, Wong, Rao, Aucoin, and Tsui; methodology, Moussa, Logan, Wong, Chan, Rao, Aucoin, and Tsui; resources, Tsui; supervision, Aucoin and Tsui; writing—original draft, Tsui; writing—review and editing, Aucoin, and Tsui.

Chapter 6 content is published in:

Moussa, H.I.; Logan, M.; Wong, K.; Rao, Z.; Aucoin, M.G.; Tsui, T.Y., Micromechanics 9, 2018, 464

Conceptualization, Aucoin, and Tsui; Data curation, Moussa, Wong, and Rao; Formal analysis, Aucoin, and Tsui; Investigation, Moussa, Logan, and Tsui; Methodology, Moussa, Logan, Aucoin, and Tsui; Supervision, Aucoin, and Tsui; Writing—Original Draft, Tsui; Writing—Review and Editing, Aucoin, and

Tsui. Tsui, T.Y.; Logan, M.; Moussa, H.; Aucoin, M.G., Materials 12, 2019, 114

Conceptualization, Tsui, and Aucoin; Data curation, Tsui; Formal analysis, Tsui; Investigation, Tsui, and Logan; Methodology, Tsui, Logan, and Moussa; Supervision, Tsui, and Aucoin; Validation, Tsui; Writing–original draft, Tsui; Writing–review and editing, Aucoin.

Abstract

Engineered biomaterials with topographical features of micron- and sub-micron-scale are designed to mimic the *in vivo* functions of extracellular matrix (ECM) to promote desirable biological changes by manipulating the behaviors of cells. We investigated three newly developed silicon oxide-based substrates, and their effect on the alignment behavior of biological cells. All substrates were fabricated using a technologically advanced integrated circuit (ICs) based technique of chemical-mechanical polishing (CMP). These substrates are not intended for biological applications.

Chapter 3 investigates the ability of a novel two-dimensional (2D) tungsten (W) and silicon oxide (SiO_2) micron and sub-micron scale patterned substrates to influence the alignment behavior of cells under different experimental conditions of (1) symmetry of the substrates comb structures, (2) cell type, (3) incubation time, and (4) serum-content in the culture media.

Results from the pattern-dependent cell behavior indicate that adherent cells on 10 μm line widths symmetric comb structures (equal W and SiO_2 parallel lines) exhibited the highest alignment performance; on which, ~54±3 % of Vero cells and ~70±4 % of prostate cancer (PC-3) cells oriented themselves within ±10° in parallel to the W lines y-axis. A time-course study to understand the pattern-dependent cell behavior indicated that after ~36 hours of incubation, cells reached a peak alignment rate of ~67±7 %. Additionally, we assessed a culture media-dependent Vero cells alignment on 10 μm line widths symmetric comb structures. Three different culture media were used, the baseline medium with fetal bovine serum (FBS), serum-free medium (SFM), and SFM supplemented with FBS. Results indicate that ~85±1 %, ~40±6 % and ~76±4 % of cells were oriented within ±10° parallel to the W lines y-axis, respectively. Results indicate that the alignment behavior of cells on symmetric comb structures is (1) W line width dependent, (2) incubation time-dependent, and (3) serum-dependent. Cells on 10 μm W lines width symmetric comb structures exhibited the highest alignment performance within ±10˚ parallel to the W lines y-axes. However, on asymmetric comb structures with unequal width of parallel W and SiO_2 lines, results indicate that the alignment of Vero cells is SiO_2 line width-dependent, rather than W line width.

A mathematical model was developed to understand and predict the geometry-dependent cell behavior on both symmetric and asymmetric comb structures. Results indicate that experimental and models are consistent.

Furthermore, we investigated the effect of antimycin A, a bacterial toxin, in the culture media on the alignment behavior of human dermal fibroblast (GM5565) cells on the same 2D W/SiO_2 substrates.

Results revealed that ~68±2 %, and ~37±5 % of GM5565 cells oriented themselves within ±20° parallel to the W lines y-axis, with and without the presence of antimycin A in the culture media, respectively. Findings demonstrate the adverse effect of antimycin A in the culture media on the alignment behavior of cells.

Chapter 4 investigates the effect of single-species protein (human and bovine serum albumin (HSA, and BSA), fibronectin (FN), vitronectin (VN), and collagen (Col-IV)), and FBS on the alignment behavior of mammalian Vero cells. Two experimental pathways were conducted, and single species proteins or FBS were used as (a) supplement for SFM, and (b) pre-adsorbed on the substrates prior to seeding the cells. Results indicate that protein as a supplement for the SFM, rather than pre-adsorbed, induced higher cell alignment.

Chapter 5 investigates the effect of a novel three-dimensional (3D) substrate of tantalum (Ta) trenches and SiO_2 (lines) fabricated to mimic the *in vivo* effect of ECM in inducing a preferential cell alignment. The results of pattern-dependent cell alignment indicate that ~91±3 % of cells on 10 μm trench's width comb structure, oriented themselves within ±10° parallel to the Ta trenches' y-axis. This was hypothesized by higher selective adhesion to Ta (trenches' sidewalls and bottom included) rather than SiO_2.

Chapter 6 investigates the effect of a novel 3D monolithic substrate of Ta lines and trenches on the alignment behavior of Vero cells as a function of topography. The substrate was developed to isolate the effect of materials (Ta) from the 3D Ta/SiO_2 substrate developed and investigated in Chapter 5. Results indicate that ~72±9 % of cells on the 10 μm trench width Ta comb structure, oriented themselves within ±10° parallel to the Ta trenches' y-axis. The decrease in cell alignment on the 3D Ta monolithic substrate in comparison to the 3D Ta/SiO_2 substrate is attributed to the Ta effect on cell alignment.

Acknowledgments

I want to express my truthful appreciation to my advisor, Dr. Ting Tsui. His knowledge, devotion, and understandings have helped me profoundly during this life-changing experience. Moreover, his continuous support, engagement, and encouragement were indispensable.

Moreover, I am grateful for the help, support, and knowledge provided by Dr. Marc Aucoin. I am also indebted to Dr. Moira Glerum for her kindness, and assistance. Additionally, I would like to express my respect for Magen Logan for her essential contribution to the success of this research.

Also, I would like to acknowledge the contribution and the hard work of all the co-operative students, especially Geoffrey C. Siow, Darron L. Phann, Zheng Rao, Kerian Sawatzky, Kingsley Wong, Wing Y. Chan, Gyeongsu Kim, Jessica Tong, and Sabin Lee. Additionally, I would like to thank the members of my committee, Dr. Yuning Li, Dr. Irene A. Goldthorpe, and Dr. Jin Zhang.

I would like to acknowledge the support of Versum Materials, LLC, especially Dr. Mark O'Neill, for providing all the chemical mechanical polished substrates used in this research.

Dedication

To my wife and kids for their true love and unconditional support;

To the memory of my beloved dad;

To my mom and my siblings; and

To all my true friends.

Table of Contents

List of Figures

List of Tables

List of Abbreviations

AFM	: Atomic force microscope
ATCC	: American type culture collection
BSA	: Bovine serum albumin
CCL-81	: Vero cell line
CMP	: Chemical-mechanical polishing
Cu-CMP	: Copper chemical-mechanical polishing
DAPI	: 4′,6-diamidino-2-phenylindole
DMEM	: Dulbecco's Modified Eagle Media
D-PBS	: Dulbecco's phosphate-buffered saline
DEV	: Deep ultraviolet light source
ECACC	: European Collection of Cell Cultures
ECM	: Extracellular matrix
EUV	: Extreme ultraviolet light source
FBS	: Fetal bovine serum
NEAA	: Non-essential amino acid
PECVD	: Plasma-Enhanced Chemical Vapour Deposition
PVD	: Physical Vapour Deposition
SEM	: Scanning electron microscope
W-CMP	: Tungsten chemical-mechanical polishing

Chapter 1
Introduction

1.1 Thesis Background

Researchers design engineered biomaterials with the objective of creating extracellular matrix (ECM) like micron and sub-micron scale structures that can mimic the impact of extracellular matrix on prompting desirable biological changes (Biggs et al., 2007; Anselme and Bigerelle, 2005; Cukierman, Pankov, and Yamada, 2002; Cousins et al.; 2004; Dalby et al.; 2002). These changes may include, but are not limited to, change in the morphology of cells, cytoskeletal organization, adhesion, migration, proliferation, and differentiation (Ning et al., 2016; Kim et al., 2006; Hasirci and Kenar, 2006). Many researchers agree that the biological functions of cells are topographical features and are size-dependent; thus, a slight change in the size of the topographical features could lead to unexpected changes in the results (Gong et al., 2015; Biggs et al., 2007; Cousins et al.; 2004; Dalby et al.; 2002). Many studies argue that this is a simplistic approach to a much-complicated problem (Khalili and Ahmad, 2015; Gong et al., 2015; Ryoo et al., 2010). This debate is extensively addressed in the literature (Khalili and Ahmad, 2015; Martino et al., 2012; Rabe, Verdes, and Seeger, 2011), where researchers indicate that growing healthy biological cells *in vitro* conditions is a complex process that involves highly controlled environment and parameters, which are (1) physical (biomaterials or substrates), (2) chemical (biomolecules or culture media), and (3) source or cells. Enhancing *in vitro* behaviors of cells requires a deep understanding of the individual effect of each of the previously-mentioned environments, and the potential interactions among the three of them on inducing the desirable change in the behavior of cells (Huang, Antensteiner, Liu, Lind, and Vogler, 2016; Lv et al., 2015; Khalili and Ahmad, 2015; Martino et al., 2012; Rabe et al., 2011; Hakkinen, Harunaga, Doyle, and Yamada, 2011).

The thesis is written based on data from four published manuscripts (Moussa et al., 2017; Moussa et al., 2018a; Moussa et al., 2018b; Tsui, Logan, Moussa, and Aucoin, 2019), and supplemented with supportive data from manuscripts under review and unpublish data.

1.2 Thesis Motivation

The ability to manipulate biological behaviors of cells on engineered biomaterials and the associated benefits are undisputable (Sung, Yang, Yeh, and Cheng, 2016; Qi, et al., 2013; Yim et al., 2010; Anselme et al., 2010; Yang, et al., 2009), and it is extensively assessed and studied in literature (Ning et al., 2016; Gong et al., 2015; Kolind et al., 2010). Nevertheless, the mechanisms at which these changes happen are

complex, and often reliant on a broad variety of factors such as surface roughness (Carré and Lacarrière, 2010; Qu et al., 2007; Oshida and Lim, 2001), surface contact angle (Huang, et al., 2012; Kao, et al., 2010; Valamehr et al., 2008), geometrical features (Lv et al., 2015b; Anselme et al., 2010; Stevenson and Donald, 2009), and protein type (Rapuano and MacDonalda, 2011; Wilson, Clegg, Leavesley, and Pearcy, 2005; Vaidya and Ofoli, 2005). The above-reviewed literature reported engineered substrates fabricated using materials, such as silicon (Seo et al., 2017; Choi, Alford, and Honsberg, 2015; Mann et al., 2012), silicon oxide (Delivopoulos et al., 2015; Hashimoto and Imazato, 2015; Teixeira, McKie, Foley, Bertics, and Nealey, 2006), polymers such as polystyrene (Biazar, Heidari, Asefnezhad, and Montazeri, 2011; Hu et al., 2014), polyvinyl alcohol (Nakamoto, Wang, Kawazoe, and Chen, 2014), polydimethylsiloxane – PDMS (Cheng, LeDuc, and Lin, 2011), hydrogel (Aubin et al., 2010), polycarbonates (Fujita, Ohshima, and Iwata, 2009), and protein patterns (Joo et al., 2016; Poudel, Lee, Tan, and Lim, 2013), with the exception of few scholars who discussed substrates fabricated using metals and metal oxides such as aluminium oxide (Hashimoto and Imazato, 2015), nickel and palladium (Jahed et al., 2014), and titanium (Anselme and Bigerelle, 2005; Huang et al., 2004). Nevertheless, no literature addressed neither two-dimensional (2D) nor three-dimensional (3D) (metal and SiO_2)_substrates. The studies mentioned above focus on inducing the desirable change in the behavior of cells as a result of external mechanical stimuli, mainly surface roughness. Rupp et al. (2018), Lin et al. (2014), Shibata and Tanimoto (2015), Rosales-Leal et al. (2010), and Huang et al. (2004) reported a minimum surface roughness of 0.05 μm required to stimulate the initial cell-substrate interaction *in vitro* (e.g., on surgical implants) and thus, all subsequent cellular functions. An exception is one research group that successfully fabricated silicon and nano-porous silicon one-dimensional substrate with an average roughness of 0.2 and 1.1 nm, respectively (Muñoz-Noval et al., 2012; Torres-Costa et al., 2012). Nevertheless, the substrates were fabricated using techniques that is not scalable, and may not be suitable for all materials. Moreover, the range of line widths studied in the previously mentioned studies was often restricted to within two orders of magnitude and to topographies at a micron scale. The previously evaluated literature assessed the behaviors of cells that adhered to uniform substrates (either with or without topographical features), but never concurrently, and on the same surface with varied topographical features, specially textured and un-textured (flat) surfaces, or lines/groves vs. flat surfaces (Lamers et al., 2010; Yang et al., 2009; Fujita et al., 2009; Loesberg et al., 2007). Furthermore, substrates with micro and nano topographies undergo interactions between and among them. To name few; Van der Waals (Rance, Marsh, Bourne, Reade, and Khlobystov, 2010), photo-induced magnetic forces (Guclu, Tamma, Wickramasinghe, and Capolino, 2015) and self-organization forces (Pohl et al., 1999). These forces may influence nanostructures (e.g., nanowires) to the

cluster, especially if the spacing is insignificant. These factors, in addition to others, may restrict the fabrication of nanoscale structures with high precision and small spacing. Additionally, the delicate nature of the reviewed substrates in terms of mechanical dependability and sensitivity make them hard to be reworked, reused, and cleaned without altering the topographical geometries and hindering their effectiveness (Jahed et al., 2014).

Thus, the motivation of this thesis is to address the limitations identified in the above-reviewed literature, using three newly developed silicon-based substrates that were fabricated using an advanced fabrication technique of chemical-mechanical polishing (CMP). These substrates were developed initially to be used as integrated circuits and not intended to be used for biological applications. The three substrates are (i) two-dimensional (2D) tungsten (W) and silicon oxide (SiO_2) substrate of micron and sub-micron scale tungsten lines inlaid in silicon oxide film; (ii) three-dimensional (3D) tantalum (Ta) and silicon oxide (SiO_2) micron and sub-micron scale of parallel SiO_2 lines and Ta trenches (sidewalls and flat bottoms) comb structures; and (iii) three-dimensional (3D) silicon oxide (SiO_2) comb structures with parallel lines and trenches coated with a thin layer of tantalum (Ta). The comb structures have parallel lines and trenches with equal width, fabricated with high precision in terms of dimensions and surface roughness. The width of the parallel lines and lines/trenches in each comb structure is equal and varies in the range of 0.18 to 100 μm. Thus, this thesis covers more than three orders of magnitude of comb structures and lines / trenches with widths from nano- to micro- scale and is believed to be the broadest range assessed by one research. The surface roughness of silicon oxide, tungsten and tantalum were measured to be ~0.01 nm, ~0.44 nm, and ~0.5 nm, respectively. In comparison to substrates with conventional topographical features, the two-dimensional (2D) W/SiO_2 micron and sub-micron scale patterned substrates can be easily cleaned and reworked by simple means, as this thesis will discuss and illustrate in Chapter 3. Furthermore, the three-dimensional tantalum-based monolithic substrates provide the opportunity to observe and characterize the behavior of cells when adherent simultaneously on two substrates with different topographies, mainly flat and comb structures.

1.3 Hypotheses

Hypothesis I: if biological cells are deposited and incubated on the newly developed 2D W/SiO_2 substrates, the micron and sub-micron scale patterned structures will cause a preferential cell adhesion by attracting the adherent cells to targeted locations of W lines, and the unique designs of the symmetric and asymmetric comb structures would induce the desired change in the alignment of cells. The latter is hypothesized by a pattern-dependent, time-dependent, and serum-dependent cell behavior. The

preferential cellular behavior of adherent cells on tungsten lines could be driven by higher surface energy and roughness of tungsten in comparison to silicon oxide lines. A mathematical model is developed to understand and predict the observed cell geometry-dependent behavior.

Hypothesis II: if biological cells are deposited and incubated on the newly developed 3D Ta/SiO_2 substrates, a preferential change in the behavior adherent cells will be observed driven a higher selective adhesion to tantalum rather than silicon oxide.

1.4 Thesis Objectives

This thesis aims to explore the potential applications of newly developed 2D and 3D substrates in manipulating behaviors of biological cells. These novel substrates are fabricated using chemical-mechanical polishing (CMP), a technologically advanced industrial fabrication technique mainly used to produce integrated circuits for the semiconductor industry. The objectives of this thesis are:

1. Developing and investigating the effect of a novel 2D tungsten and silicon oxide micron and sub-micron scale patterned substrate on the behavior of cells in the absence of external mechanical stimuli. Herein, the focus is on the effect of the material composition of the substrate (W vs. SiO_2) on the behavior of cells.
2. Developing and investigating the impact of a new 3D tantalum and silicon oxide micron and sub-micron scale patterned substrate on the behavior of cells as a function of surface topographical features (lines vs. ditches), and the materials composition of the substrate (Ta vs. SiO_2).
3. Isolating the material effect - addressed in objective 2- from the 3D Ta/SiO_2 micron and sub-micron patterned scale substrate by developing a novel monolithic 3D substrate of thin-film tantalum-coated silicon oxide lines and trenches to investigate the potential to manipulate the behavior of cells. This objective considers the effect of surface topographies only, in comparison to the effect of materials and topography in objective 2.

The comprehension and outcomes attained from this work will be useful for the discovery of (i) a new generation of highly durable, reusable, and active synthetic (SiO_2 and metal) substrates that can mimic the functions of extracellular matrix *in vitro*, and (ii) promising applications of thin film tantalum coatings for the improvement of the biocompatibility and bioactivity performances of surgical implants.

1.5 Thesis Structure

This thesis comprises of seven chapters, and four appendixes organized as follows:

Chapter 1 is intended to provide an introduction to this thesis and includes background, motivation, objectives, and thesis structures and chapters. Chapter 2 introduces the necessary literature review that is critical to understanding the experimental results presented in the subsequent chapters of this thesis. Chapter 3 presents a novel two-dimensional tungsten and silicon oxide micron and sub-micron scale patterned substrate. The 2D micron and sub-micron scale substrate is used to manipulate the alignment behaviors of the adherent (mammalian Vero, human prostate cancer, and human fibroblast) cells under different experimental conditions. Chapter 4 investigates the manipulation of cellular behaviors on the same 2D micron and sub-micron scale patterned (W and SiO_2) substrate discussed in Chapter 3 as a function of single-species serum proteins and fetal bovine serum (FBS) when (i) added individually as a supplement to the serum-free medium, and (ii) pre-adsorbed on the 2D substrates prior to seeding the cells. Chapter 5 investigates the effect of an original 3D micron and sub-micron scale patterned substrate of silicon oxide lines, and tantalum trenches on manipulating the behavior of mammalian (Vero) cells. The intended outcome is to understand the impacts of materials and topography on the behavior of cells. Chapter 6 presents a novel monolithic 3D tantalum thin-film coated on silicon oxide structures of lines and trenches to study the cell-substrate interactions as a function of the substrate topographies only. The monolithic 3D substrate is developed to isolate the effect of materials from the 3D micron and sub-micron scale patterned substrate addressed in Chapter 5 on manipulating the behavior of cells. Finally, Chapter 7, will conclude and present an outlook for future works.

Chapter 2
Literature Review

2.1 Fabrication of Chemical-Mechanical Polishing Integrated Circuits

2.1.1 Nanotechnologies and Nanomaterials

The Royal Society and The Royal Academy of Engineering (2004) defines nanotechnologies as "the design, characterization, production, and application of structures, devices and systems by controlling shape and size at nanometer scale." (p. vii). Materials with crystallites or grains in size range of 1-100 nm are called nanomaterials (Koch, 2009; Suryanarayana and Koch, 2000). However, there is no consensus among researchers on the definition of nanomaterials. For example, some definitions take into account the percentage of atoms to the total number of atoms in a grain boundary (Pakiela, Lewandowska, and Kurzydlowski, 2011). Others take into account the improvement of properties due to the refinement of structure (Baker, 2001). Industries and governmental agencies widely recognize the potential benefits of nanotechnologies, which may include drug delivery, healthcare and biotechnology (Nikalje, 2015; Filipponi and Sutherland, 2013); energy harvesting, and environment (Filipponi and Sutherland, 2013; Walther and Ahn, 2011; Vullers et al., 2009); electronics and Microsystems (Schwierz, 2010; Anker et al., 2008); optics and photonics (Rycenga et al., 2011; Uppuluri et al., 2010). Thus, the contribution of nanotechnologies to the benefit of humankind is indubitable (Pimpin and Srituravanich, 2012). However, despite the anticipated benefits, different stakeholder groups and the public have pointed to many challenges and concerns, such as the potential health, safety and environmental adverse impacts and the social, ethical and regulatory issues (Filipponi and Sutherland, 2013; Yao, 2007; Tomellini et al., 2006; The Royal Society, 2004).

Literature indicates that the number of research groups and industries involved in nano-related research and development are increasing exponentially worldwide; especially in the fields of drug delivery, nanomedicine, enhanced imaging, and biotechnology (Nikalje, 2015; Singhana et al., 2014; Filipponi and Sutherland, 2013; Boisseau and Loubaton, 2011; Ludwig et al., 2011; Lymberis, 2010; Tsytsikova, 2009; Tomellini et al., 2006; Cheung and Renaud, 2006; Li et al., 2006; Robert and Freitas Jr., 2005; Pimpin and Srituravanich, 2012; Nikalje, 2015). It is essential to highlight that nanomaterials used for medical applications must fulfill two vital requirements, (1) biocompatibility and, (2) flexibility of materials (Filipponi and Sutherland, 2013; Tomellini et al., 2006). Taking into consideration that the

physical, mechanical and toxic characteristics (e.g., energy and electrical conductivity, color, strength, and weight) of nanomaterials are different from those at the bulk scale, thus, nanomaterials are unique.

2.1.2 Classification of Nanomaterials

Gleiter (1995) categorized nanomaterials according to composition, morphology and nanocrystalline distribution. Nanomaterials are metals, ceramics, polymers and composite materials that contain grains made of nanocrystalline (e.g., tungsten), amorphous (e.g., silicon oxide) or quasicrystalline (e.g., si-ZnMgHo) phases (Gleiter, 1995). The classification by Gleiter (1995) was considered incomplete by many scholars since the dimensionality of nanostructures (0D, 1D, 2D, and 3D) was not taken into account (Tiwari et al., 2012; Hussainova, 2010; Koch, 2009; Pokropivny and Skorokhod, 2007; Suryanarayana and Koch, 2000).

The classification of nanomaterials based on their dimensionality may not be the best way to categorize them, but, it is the most common one. Kim (2013), Tiwari et al. (2012), Dong et al. (2011), Jin et al. (2010) and Suryanarayana and Koch (2000) indicate that literature deals extensively with 3D nanostructures, followed by 1D- and 2D-nanostructures. The main focus of this study will be on both 2D (Chapter 3 and Chapter 4) and 3D (Chapter 5 and Chapter 6) structures.

Nanomaterials are fabricated using two main approaches, the top-down (lithography), and the bottom-up (chemical vapor deposition). In the top-down approach, micron and sub-micron sized materials are fabricated from bulk materials (Acikgoz et al., 2011; Cheung et al., 2006), whereas the bottom-up approach refers to a chemical process in which individual atoms are stacked to form molecules. These molecules self-assemble to form the required nanostructures (Khanna, 2016; Silva, 2006). According to Khanna (2016), the mechanisms that drive the molecular self-assembly are the physical and chemical forces at a nanoscale. In these methods, the control over fabrication and eco-system conditions is critical to the quality of the fabricated nanomaterials (Filipponi and Sutherland, 2013). Chuvilin (2015) and Banhegyi (2015), indicate that the uniformity, consistency, scalability, and cost of materials fabricated using the top-down approach are better in comparison to the bottom-up approach.

In this thesis, the chemical-mechanical polishing (CMP) method will be discussed in detail since it is relevant to this work.

2.1.3 Chemical-Mechanical Polishing Nanofabrication

The chemical-mechanical polishing (CMP) technology is an ultra-precision process for the fabrication of inlaid micron and sub-micron structures. This technique has become increasingly predominant over the last three decades as the semiconductors industry continues to produce integrated circuits (ICs) with

smaller dimensions, higher density, and higher performance (Coutinho, Mudhivarthi, Kumar, and Gupta, 2008; Banerjee and Rhoades, 2008; Coutinho and Gupta, 2011). These integrated circuits consist of multiple inlaid metallization layers that are extremely flat and smooth (Banerjee and Rhoades, 2008; Rhoades, 2008). A demonstration of the chip characterization, especially roughness, will be discussed in details in Chapter 3, Section 3.2.2. CMP has become a mainstream process in the semiconductor industry at and below the 0.35μm technology node (Zhao and Lu, 2013; Lee, Lee, Choi, and Park, 2009; Banerjee and Rhoades, 2008). The technology was initially developed and patented by the *International Business Machines* Corporation (IBM) laboratories in the 1980s for the fabrication of ICs (Li, 2007; Brusic et al., 2003).

As the name indicates, the CMP process involves a combination of chemical and mechanical forces in order to generate substrates with extremely smooth inlaid surfaces. A rotating wafer is pressed facing down against a rotating polishing pad, and an aqueous suspension of abrasive (slurry) is pressed against the wafer's face by the pad, resulting in both mechanical and chemical effects (Beaudoin, Boning, and Raghavan, 1999). A specific balance of the two processes is required. However, if the polishing part is too mechanical, it can lead to surface scratches, and if it is too chemical, it can lead to a lack of planarity (Steigerwald et at., 1995). The CMP process involves the use of mechanical energy to remove groups or uneven particles from the surface in order to achieve a flat surface (Steigerwald et al., 1995). The chemical component is a material-dependent slurry of chemicals, which have two main functions; (1) removing the particles from the surface by dissolving them, and (2) preventing the dissolution of materials that are not in contact with the soft polymer polishing pad (Lee, Lee, and Jeong, 2016), from the low areas on the wafer surface ensuring local planarity (Steigerwald et al., 1995). The slurry must dissolve the particles because otherwise, the particles can redeposit as metal or metal oxide, which will inhibit the mechanical abrasion (Steigerwald et al., 1995). Typical CMP slurry comprises of abrasive spherical particles, mainly silicon oxide (SiO_2) or aluminum oxide (Al_2O_3) with a diameter in the range of 0.1–2.0 μm. These particles are suspended in an aqueous oxidizing solution (Siddiqui and Frederick, 2005). Particles with a diameter higher than 2.0 μm will cause a higher metal removal rate, and particles smaller than 0.1 μm will increase the removal rate of silicon oxide (Siddiqui and Frederick, 2005). It is essential to indicate that the composition of the slurry plays an essential role in increasing surface uniformity leading to surfaces free from defects (Lee et al., 2016; McConnell, and Hurst, 2014a; McConnell, and Hurst, 2014b). The slurry can prevent the continuous passivation of the desired material by reacting with the metal to produce a film such as metal oxide which will protect the surface from further reaction. The chemical reaction which happens on the metal surface is explained by Lee et al.

(2016) in three general steps involving the metal (M), oxidizer (Ox), stabilizing (chelating) agent (C), pH adjustor (A), and corrosion inhibitor (I) as listed in Equations 2.1, 2.2, and 2.3, respectively (Lee et al., 2016):

$$\text{Metal [M]} + \text{Oxidizer [Ox]} \rightarrow \text{Metal oxide [M} - \text{Ox]} \quad 2.1$$

$$\text{M} - \text{Ox} + \text{Stablizer [C]} + \text{pH adjustor [A]} \rightarrow \text{Metal complex} \quad 2.2$$

$$\text{M} + \text{Corrosion inhibitor [I]} \rightarrow \text{Metal} - \text{inhibitor [M} - \text{I]} \text{ complex} \quad 2.3$$

In Equation 2.1, the oxidizer yields a metal oxide that is partially soluble, which is a favorable state. A soluble metal oxide leads to removal rate without topographical selectivity, and an insoluble layer will prevent further oxidation. In the presence of the pH adjustor, the stabilizer helps to form a metal complex from the metal oxide, as indicated in Equation 2.2. This step is essential to compensate for the insufficient metal oxide layer. Adding corrosion inhibitors to the process (Equation 2.3), protects the polished surfaces from being affected by the chemicals, thus preventing surface defects such as dishing and scratching (Lee et al., 2016). Any layers with higher undesirable thickness will be removed mechanically, allowing the metal layer to react again chemically. As a result, only the high areas on the surface are removed until the entire area is one smooth surface.

The CMP process has significant advantages over other techniques such as the elimination of step-coverage concerns and improvement of lithographic resolution by minimizing the depth of field variations (Zantye, Kumar, and Sikder, 2004). Currently, CMP is the only available, reliable solution to achieve such kind of faultless surfaces (Coutinho and Gupta, 2011; Steigerwald et al., 1995) with high material removal rates (MRRs) (Zhang, Liu, Song, and Hu, 2010) and competitive cost. These are the primary reasons for choosing CMP as the main method for producing ICs, instead of many other planarization techniques, such as Spin Etch Planarization and doped glass reflow (Atiquzzaman, 2012). CMP is a complex process due to a large number of process parameters, inputs, outputs, and random variables that are hard to optimize (Lai, 2001). These variables are what influence, to a great extent, the scope and performance of the CMP process.

Originally, aluminum was widely used as an “interconnecting material” (Gupta, 1979) for “metallization” (Banerjee and Rhoades, 2008), but, due to its higher interconnect resistance, and lower electro-migration (Banerjee and Rhoades, 2008; Lai, 2001; Singer, 1998; Steigerwald et al., 1995), the semiconductor industry turned to copper (Cu) as a replacement. The use of copper has grown exponentially over time, to include other materials, such as tungsten (Banerjee and Rhoades, 2008; Feeney, 2010). This study uses IC chips manufactured using tungsten CMP (W-CMP), and copper CMP (Cu-CMP), which both will be discussed in later chapters.

The integrated circuits (ICs) fabrication process (Damascene integration) starts with the deposition of a silicon oxide layer (~500-700 nm thick) on a 200mm silicon substrate (wafer). The ~300 nm deep inlaid structures in the SiO_2 layer are fabricated using patterning and etching processes to prepare the surface for the deposition of the metal layer (W or Cu). Prior to the metal physical deposition process, a thin barrier layer of Ti/TiN or Ta/TaN is deposited into the silicon oxide layer to prevent possible metal diffusion and to improve the adhesion between tungsten and silicon oxide in case of Ti/TiN. The barrier layer is less than 20 nm thick. The metal deposition process is carried out using physical vapor deposition techniques, leading to a surface with the uneven and rough finish of stacked layers of metal deposition. This process is followed by the chemical-mechanical polishing (CMP) stage, which is used as an "enabling technology" to generate an exceptionally smooth and flat surface. A simplified CMP process schematic based on Murarka, Verner, and Gutmann (2000) is shown in Figure 2-1.

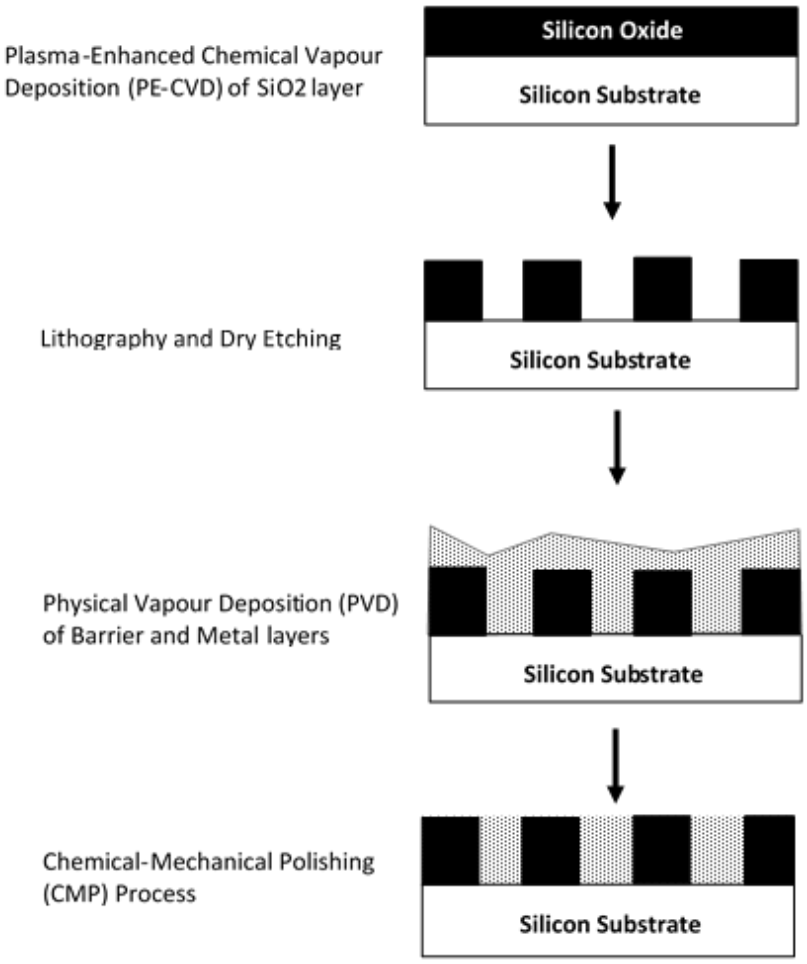

Figure 2-1 Simplified illustration of the damascene integration process (based on Murarka et al., 2000).

2.2 Manipulating the Morphology of Biological Cells on Nanostructures

This section provides a review on the *in vitro* interactions between biological cells and nano-biomaterials. The objective is to understand how these interactions are addressed in academic literature, taking into consideration the different experimental conditions.

2.2.1 Background

When a biological cell comes in contact with a biomaterial, it naturally reacts with its surface creating a surface-bound layer. The performance and cellular functions of this layer were found to be dependent on the topographical, physical, and chemical properties of the biomaterial. These cellular functions include proliferation, change in morphology, the organization of the cytoskeleton, and focal adhesion (Kolind et al., 2010; Dalby et al., 2004a; Kasemo, 2002). Lord et al. (2010) indicate that even though the cellular functions are influenced to a great extent by the "speciation, conformation and orientation of the surface-bound proteins" (p. 68), nevertheless, a large body of literature focuses on assessing the impact of biomaterial topography instead.

In this work, the focus will be on fibroblast cells (GM5565) and epithelial (Vero and PC-3) cells, which are selected based on their common characteristics (e.g., source, species, and growth model), and their uncommon characteristics (e.g., tissue of origin, and cell type/morphology). These characteristics will be discussed in more details in section 3.2.3, and Table 3-3.

2.2.2 Manipulating the Behaviour of Biological Cells in Literature

Researchers design micron and sub-micron structures with the aim of replicating the structures of the extracellular matrix (ECM), in order to study the impact of these mimicked ECM on the changes in the biological functions of cells, such as change in morphology, cytoskeletal organization, adhesion, motility, proliferation, differentiation, etc. (Ning, et al., 2016; Kim et al., 2006; Hasirci and Kenar, 2006). There is a consensus among nanobiologists that the biological functions of cells depend on the size of the nanostructure size. A slight change in the size of a nanostructure could lead to unexpected changes in results (Gong et al., 2015). Many studies argue that this notion is only half the story (Ryoo et al., 2010; Gong et al., 2015). This study discusses the effect of different materials used in the fabrication of nanostructures, topography, and dimensions (e.g., spacing) individually or combined on inducing a preferential change in the biological functions of cells.

Kolind et al. (2010) studied the impact of topographical features (1D, 2D or 3D), dimensions (e.g. rectangle size and inter-rectangles gap size), projected pillar area (a/A), which represents the ratio of top

cross-sectional pillar area to the total pillar area, distribution of microstructures and culture duration on the proliferation and morphology, and organization of cytoskeleton and focal adhesion (FAs) contacts of human fibroblast cells. Results show that cell proliferation and morphology, cytoskeleton, and FAs are insignificantly dependent on pillars shape and distribution, but highly dependent on gap and pillar size. For example, a wider gap size will allow a higher diffusion of the cytoskeleton and fewer FAs points; thus, a higher proliferation rate. This is explained by the lower stress imposed on the actin cytoskeleton, which allows higher free intercellular pathways that are responsible for cell proliferation and development (Ning et al., 2016; Kolind et al., 2010). Kolind et al. (2010) observe that the effect of both gap and pillar size becomes more distinct with the progression of culture time. With time, FAs tend to shift from the cell boundary toward the center. Results underlined the correlation between the a/A ratio and cell proliferation rate. The study shows no correlation during the early culture time; however, with time, there is an increase in the proliferation rate with the increase of a/A up to a maximum value of 30 % at seven-day of culture duration. Beyond that point of time and ratio, the study finds the insignificant influence of a/A on the proliferation rate. The observations by Kolind et al. (2012) were similar to the findings of Lord et al. (2010) and Chen et al. (2004). Researchers continue to investigate the ability to influence and alter the biological functions of cells using well-designed nanostructures.

Biggs et al. (2007), Cousins et al. (2004), and Dalby et al. (2002) examined the impacts of surface roughness on manipulating the adhesion, spreading, and proliferation abilities of fibroblast cells. Results indicated that nanoparticles reduced cells' ability to adhere, spread, and proliferate. Nanoclusters (10–13 nm), on the contrary, improved the adhesion, spreading, and proliferation of the cells under study. Nevertheless, Dalby et al. (2002) indicate that increasing the size of nanoclusters beyond a critical size (to 50 nm and 95 nm) will have an inverse impact on the assessed properties, similar to the effect of the surface with nano-particles. Observations show that cells on nanocolumns have a more elongated morphology, settling and adapting with the profile of the surface projection. Choi et al. (2009) studied the impacts of 3D nanostructures with different dimensions (low, medium and high) and shapes (posts and grates) on the spreading and elongation rates of fibroblast cells. Results indicated that cells spread and flattened in a similar way on flat surfaces and low aspect ratio structures. However, elongation observed to happen in cells that are located on surfaces with low aspect ratios. With the increase of structures height, cells spreading rate becomes insignificant, while cells exhibited a rounded morphology. With time (from three-to-seven days), Choi et al. (2009) observed substantial growth in cells sizes, population, and spreading rates. The growth happened on all the four surfaces but decreased

with height increase. Additionally, results indicate that cells tend to elongate in a preferred direction, along with the nanopattern.

A review paper by Martínez et al. (2009) assessed the impacts of different micro- and nanostructures and materials on the orientation, adhesion, cell morphology, proliferation and differentiation of a wide range of cells (fibroblasts, stems, nerve wires, and osteoblasts), indicated that all the cells under the study have a preferred elongation and alignment direction, which correlates with the findings of Thakar et al. (2003) and Dalby et al. (2003). Findings indicate that cell orientation and structure depth are positively correlated, whereas structures' width and cell orientation are inversely correlated. Nevertheless, the adhesion process was found to be cell-type dependent. The proliferation of cells and gene expression were found to be cell and structure dependent. Teixeira et al. (2006) observed that epithelial cells changed their alignment from parallel to perpendicular and their focal adhesion distribution with the reduction in the size of the structures from 4 μm to 0.4 μm. Martínez et al. (2009) indicated that "cell membrane conforms to the large grooves but tend to bridge the narrowest and deepest groove" (p. 130). This observation was found to be cell-type independent. Furthermore, it confirmed the adverse impact of topographical features on the morphology of cells, and cytoskeletal development. This behavior is influenced to a great extent by the mechanical forces (tensile and relaxation) that cells experience when they are in contact with these structures (Wood, 1988; Meyle et al., 1995; Baac et al., 2004; Teixeira et al., 2006; Charest et al., 2004).

Pennisi et al. (2009) investigated the interaction between cells (fibroblast and glial) and surface nano-topography; in particular, cell proliferation, cytoskeletal organization, and cell morphology. Results indicate that cells growth and spread rates increase with decreased surface roughness. However, results also indicate that surface topography has a minimum impact on glial cells proliferation in comparison with fibroblast cells. The latter is explained by the higher standard rate of proliferation of fibroblast cells compared to glial cells (central nervous system).

Hu et al. (2010) examined the impact of structures topography and aspect ratios on some of the surface properties of nanostructures (e.g., energy and wettability) and the interaction with fibroblast cells (e.g., spreading). Results indicate that the spreading of cells is inversely proportional to the topographical features of the surface, and the pillars' aspect ratio. Cells on nanopillars tend to aggregate and spread poorly (40-50 % less) in comparison with their behavior on a flat surface. This is attributed to the influence of surface topography, not surface wettability (hydrophobicity/hydrophilicity) properties. Cells tend "to form effective adhesion complexes ... at the tops of the pillars." (Hu et al., 2010, p. 6). These findings are similar to those of Park et al. (2007) and Sniadecki et al. (2006).

Ryoo et al. (2010) studied the impact of different nanotube materials on the proliferation, focal adhesion, spreading, and gene transfection of fibroblast (NIH-3T3) cells. The study shows that different nanomaterials can alter cell morphology, viability, and proliferation. Similar to Ponsonnet et al. (2003), Ryoo et al. (2010) observed that the behavior of cells was dependent on the physicochemical properties (e.g., wettability and roughness) of nanostructures.

In their work, Chung, Li and Wang (2013), argue that the biological functions of cells, such as adhesion, proliferation, migration, and differentiation, can be altered using nanostructures with different mechanical, chemical, physical, and topographical characteristics. These findings are similar to findings by Kolind et al. (2010), Hu et al. (2010), Ryoo et al. (2010), Choi et al. (2009), and Biggs et al. (2007).

Jahed et al. (2014) studied the effect of complexity, aspect ratio, spacing, and surface interfacial strength of different metallic nanopillars on the interaction, adhesion, and spreading mechanisms of fibroblast cells. Jahed et al. (2014) indicated that the adhesion and spreading of cells are linked to "filopodia" (arm-like cytoplasmic extensions). Filopodia are significantly involved in sensing the substrate nanotopographies upon the initial contact between the cells and the substrate. These findings are similar to findings by Albuschies and Vogel (2013), Dalby et al. (2004b) and Bornschlögl et al. (2013). Albuschies and Vogel (2013) reported that filopodia tend to spread toward nanostructures rather than the flat substrate. According to Jahed et al. (2014), cells tend to stop spreading during the proliferation process before continuing to spread again. Also, cells show the tendency to connect and form filopodia-like connections in high-density areas, even after they have retracted and disconnected (Jahed et al., 2014; Hoelzle and Svitkina, 2012). Similar to Beningo et al. (2001), Tan et al. (2003) and Albuschies and Vogel (2013), Jahed et al. (2014) observed that for high aspect ratio (elastic) nanopillars, the filopodia traction force pulls these pillars in the direction of the cell; causing the pillars to completely detach from the substrate if the interfacial strength between the flat substrate and the nanopillar is weaker than the filopodia traction force (Jahed et al., 2014).

Wang et al. (2014) and Wang et al. (2011) studied the impact of nanopillar diameter and spacing on cell capture yield. These two factors play a key role in the behavior of cells and capture yield. Results indicate that cell capture yield, the ideal diameter of the nanopillar and spacing among them are inversely interrelated. Such behavior was attributed to the contact area for interaction between cells and nanopillars. Similarly to Jahed et al. (2014) observed the formation of cells filopodia and pseudopodia, which are "a form of the actin machinery that is essential to understanding a cell's functional interactions." (Mejillano et al., 2011, Abstract). These two formations are highly reliant on cell-substrate adhesion, in addition to elution strength and shear direction.

Gong et al. (2015) studied the effect of size, shape, and surface properties of gold nanostructures on cellular uptake in terms of internalization (intake of proteins), penetration, and distribution. Identifying the optimal size that achieves the highest cellular intake continues to divide and confuse many researchers. Chithrani et al. (2006), Trono et al. (2011), and Albanese and Chan (2011) represent a classic case of uncertainty identifying the ideal size of a gold nanoparticle required to provide the maximum intake by a cell. Three studies provide three different answers. Gong et al. (2015), Wang et al. (2013), and Chithrani et al. (2006) show that cellular uptake is not only size dependent but also shape dependent. They used a wide range of nanostructures (spherical, rods, cages, and hexapods). Results indicate that branched nano-structures (spherical) have a higher uptake by cells in comparison with rod and cube nanostructures. Spherical nanostructures tend to have a smaller contact surface with receptors of cell membrane than nanorods and nanocages. Thus, a higher number of free binding sites is available. Salatin et al. (2015) and Alkilany and Murphy (2010) agree with the general notion of shape-dependent cellular uptake, but the results were different.

Rasmussen et al. (2016) and McNamara et al. (2010) addressed the effect of surface stiffness, and topography, respectively, on the differentiation of human stem cells. They emphasized that manipulating the features of nanostructures is a durable approach to influencing cell differentiation rather than trying to impose changes on the cell surface chemistry. These mechanical properties are controlled using geometrically designed nanopillars with a high aspect ratio. Similarly to Fu et al. (2010), Rasmussen et al. (2016) indicate that nanopillars with high aspect ratios are often softer than the ones with low aspect ratios. Rasmussen et al. (2016) also indicate that the efficiency of cells induction (signaling events) on nanopillars is higher than that on a flat surface. This finding confirms a general consensus among researchers on the more significant influence of textured/structured surfaces on the behaviour of cells in comparison with that of flat surfaces (Ning et al., 2016; Kolind et al., 2010; Choi et al., 2009; Darling et al., 2007; Thakar et al., 2003). Notably, results by Rasmussen et al. (2016) and McNamara et al. (2010) confirm the notion that stem cells differentiation can be influenced by the use of nanostructures as external factors (Smith et al., 2009; Nur-E-Kamal et al., 2006; Levenberg et al., 2003). Results indicate that nanostructures may provide the potential for sustaining the abilities of biological cells to self-renewal and proliferation. Findings by Rasmussen et al. (2016) indicate that soft (high aspect ratio) pillars do not support the proliferation of cells; instead, they support the migration of cells. Gadegaard (2016) explained the findings of Rasmussen et al. (2016) by weak cell adherence (Gadegaard, personal communication, April 29, 2016). McNamara et al. (2010) identified some of the factors (e.g., cell adhesion) that may contribute to the differentiation of cells due to interaction with the substrate.

Ning et al. (2016), Thakar et al. (2003), and Darling et al. (2007) observed the role of cell type, and surface topography on the proliferation, growth, spreading, elongation (relates to organization, stiffness, and contractility of cytoskeleton), orientation rates and stiffness (due to actin fibers) of cells. Results indicate that fibroblast cells tend, initially, to proliferate at a higher rate on a flat surface than on a surface with nanostructures. However, with time, the opposite happens. This was explained by the ability of nanostructures to maintain the viability and growth rate of cells, contrary to flat surfaces. Furthermore, Ning et al. (2016) and Thakar et al. (2003) indicate that the growth and spread rates and stiffness of fibroblast cells were found to be dependent on the shape (channels vs. pillars vs. flat surface) and dimensions (micro vs. nano). The growth of fibroblast cells growth and spread rates are higher on channels than on pillars and flat surfaces and higher on micro- than on nanostructures. This is explained by the ability of fibroblast cells "to create more traction force and focal adhesion sites." (Ning et al., 2016, p. 2721). Observations by Ning et al. (2016), Thakar et al. (2003) and Dalby et al. (2003) indicate that cells have a preferred growth and elongation direction, which is mainly the direction of the long axis and direction of channels. This was due to cells contact guidance. Results illustrate that the change in the biological functions of the cells is cell- and structure-dependent.

2.2.3 Summary

The impact of the micron and sub-micron topographical features on the behavior of biological cells has been the subject of many scholarly studies. Results indicate that the *in vitro* behavior of cells can be considerably altered using highly controlled physical and chemical complex environments and variables. This has been made possible due to the advancements in fabrication and monitoring technologies. However, there seems to be a consensus among scholars in regards to the complexity of mimicking *in vivo* environments. Thus, researchers indicate that some of the findings and observations can be generalized, but the majority cannot. This can be justified by the limited data available on the different and multiple variables, which may have an influence individually and collectively on the assessment processes and its results. Section 2.3 briefly discusses these complex physical and chemical environments and variables.

2.3 Factors that Influence Cell-Substrate Interactions

2.3.1 Background

Growing healthy biological cells *in vitro* conditions is a complex process. The process involves highly controlled physical (biomaterial or substrate) and chemical (biomolecule or culture media) environments and variables to be met. Optimizing the *in vitro* behavior (e.g., adhesion, alignment, migration, spreading, proliferation, and differentiation) of cells, requires an in-depth understanding of the interactions between these environments and conditions (Huang et al., 2016; Khalili and Ahmad; 2015; Martino et al., 2012; Rabe et al., 2011; Anselme et al., 2010; Ochsner et al., 2007; Michaelis et al., 2011; Hong et al., 2006; Anselme et al., 2000; Michaelis, Robelek , and Weg, 2011; Poncbe et al., 2010; Sagvolden, et al., 1999, Norde, 2003 as cited by Baujard-Lamotte et al., 2008). Table 2-1 lists some of these factors that may influence the *in vitro* behavior of cells.

Table 2-1 The main parameters that may affect the in-vitro behavior of biological cells

<table>
<tr><th colspan="2">Substrate Properties</th><th colspan="2">Cells</th><th colspan="2">Culture Medium</th></tr>
<tr><td>Wettability (contact angle)</td><td rowspan="3">Huang et al. (2016)
Khalili and Ahmad (2015)
Martino et al. (2012)
Rabe et al. (2011)
Anselme et al. (2010)
Ochsner, et al. (2007)
Michaelis et al. (2011)</td><td rowspan="3">Cell line and source</td><td rowspan="10">Huang et al. (2016)
Lv et al. (2015)
Martino et al. (2012)
Carré and Lacarrière (2010)
Anselme et al. (2010)</td><td>Type (serum-free vs. serum-containing)</td><td>Huang et al. (2016)
Carré and Lacarrière (2010)</td></tr>
<tr><td>Topographies distribution (e.g., random vs. ordered)</td><td>Protein type (serum vs. single-species)</td><td rowspan="8">Rabe et al. (2011)
Hakkinen et al. (2011)
Schmidt et al. (2009)</td></tr>
<tr><td>Scale of topographies (e.g., micron vs. sub-micron)</td><td rowspan="2">pH
Proteins are positively charged at pH<7, and negatively charged at pH>7</td></tr>
<tr><td>Type of topographies (e.g., lines vs. trenches)</td><td rowspan="2">Martino et al. (2012)
Hakkinen et al. (2011)</td><td rowspan="3">Seeding density</td></tr>
<tr><td>Fabrication Process</td><td>Ions content (Mg^{+2} and Ca^{+2})</td></tr>
<tr><td>Chemical composition (e.g., metal vs. oxide, or organic vs. inorganic)</td><td>Huang et al. (2016)
Lv et al. (2015)</td><td rowspan="2">Protein concentration</td></tr>
<tr><td>Surface homogeneity (monolithic vs. composite)</td><td rowspan="3">Martino et al. (2012)
Carré and Lacarrière (2010)</td><td rowspan="3">Incubation time</td></tr>
<tr><td>Surface functionalization</td><td rowspan="2">Protein size</td></tr>
<tr><td>Electrical properties (e.g., adding conductive particles to polymers)</td></tr>
</table>

Researchers agree on the complexity of the *in vitro* cells' adhesion process (Huang et al., 2016; Khalili and Ahmad; 2015; Martino et al., 2012; Rabe et al., 2011; Anselme et al., 2010; Ochsner et al., 2007), however, there is no consensus in literature when addressing the major stages for the attachment and adhesion of cells. These stages start after the initial contact between biomaterial (substrate) and biomolecules (medium) as listed in Table 2-2 and discussed in scholarly works. Literature listed in Table 2-2 discusses in detail the different phases involved in the interactions between biological cells and a substrate, namely, the adsorption of protein(s) from a bulk solution (e.g., culture media) onto the substrate, which happens rapidly (Vogler, 2012; Barnthip, Noh, Leibner, and Vogler, 2008), followed by the adhesion of the biological cells.

Table 2-2 Different stages of biological cell-substrate interaction as described in the literature

Number of Stages	Events	Literature
2	Short-term (< 24 hrs.): Includes adhesion and spreading of cells	Anselme and Bigerelle (2006), Anselme and Bigerelle (2005) Bigerelle et al. (2002), and Anselme et al. (2000)
	Long-term (24 hrs. – 21 days): Includes proliferation and differentiation of cells	
2	Stick phase: Initial adhesion stage involves "integrin-ligand" binding (Van der Waals and Ionic forces)	Garcia and Gallant (2003)
	Grip phase: Spreading of cells and the formation of focal adhesion (increase the area of contact)	
3	Stage I: Initial attachment	Khalili and Ahmad (2015) Helenius et al. (2008)
	Stage II: Flattening	
	Stage III: Fully spreading and Structural Organization	
3	Stage I: Sedimentation	Hong et al. (2006)
	Stage II: Initial attachment and spreading	
	Stage III: Stable adhesion	
3	Stage I: Flattening considers the initial cell-surface interaction	Pierres, Benoliel, and Bongrand (2002)
	Stage II: Alignment increases the cell membrane-surface interaction	
	Stage III: Spreading involves increasing the membrane fitting on the surface	
3	Stage I: Attachment (~9 min to 1 ½ hrs)	Vogler and Bussian (1987) as cited in Parhi, Golas, and Vogler (2010)
	Stage II: Adhesion and spreading (~ 1 ½ hrs till 3hrs)	

Number of Stages	Events	Literature
	Stage III: Proliferation (~3 till 30 hrs)	
3	Stage I: Attachment	Murphy-Ullrich (2001)
	Stage II: Spreading	
	Stage III: Focal adhesion and the formation of stress fiber	
4	Stage I: Typical spherical-shaped cells with sensing Filopodia (10 min)	Chierico, Joseph, Lewis, and Battaglia (2014)
	Stage II: Cells undergo attachment to the substrate (30 min)	
	Stage III: Spreading of cells and the growth of focal points (1 hr.)	
	Stage IV: Full spreading of cells (16 hrs.)	
4	Stage I: Attachment of cells to the substrate (during the 1st hour)	Huang et al. (2003) LeBaron and Athanasiou (2000)
	Stage II: Cell flattening and spreading	
	Stage III: Organization of actin skeleton	
	Stage IV: Focal adhesion formation	
4	Stage I: Protein adsorption (seconds)	Carré and Lacarrière (2010) Jager et al. (2007)
	Stage II: Cellular attachment (minutes)	
	Stage III: Cellular adhesion (hours)	
	Stage IV: Migration, proliferation, and differentiation (days-weeks).	
4	Stage I: Proteins from the bulk solution (culture media) are adsorbed on the substrate (seconds)	Anselme et al. (2000)
	Stage II: Cells are attached and spread on the substrate (minutes)	
	Stage III: Reorganization of the cytoskeleton and active spreading on the substrate (hours)	
	Stage IV: Synthesizing of ECM proteins by cells (days)	
4	Stage I: Protein adsorption	Barngrover (1986) Vogler (1988) (as cited in Parhi, Golas, and Vogler, 2010)
	Stage II: Cell-substrate contact	
	Stage III: Cell-substrate attachment	
	Stage IV: Cell adhesion and spreading	

2.3.2 In Vitro Adsorption of Proteins

This section will focus on the effect of protein adsorption onto a substrate on the adhesion of cells, and their subsequent functions while discussing the mechanisms involved in this critical step (Chierico et al., 2014; Anselme et al., 2010; Carré and Lacarrière, 2010; Ponche et al., 2010; Baujard-Lamotte et al., 2008; Jager et al., 2007; Wilson et al., 2005). Vogler (2012), Michaelis et al. (2011), Williams (2008), Wilson et al. (2005), and Krishnan et al. (2004) indicate that the rapid adsorption of protein from a bulk phase onto a substrate is the initial biological response when immersed in a culture medium. It is widely accepted among scholars that as a result of strong protein and surface interactions, the adsorbed protein(s) plays an essential role in controlling the biocompatibility of the substrate for cell adhesion (Chierico et al., 2014; Vogler, 2012; Carré and Lacarrière, 2010; Williams, 2008; Krishnan et al., 2004; Jager et al., 2007). This is important to regulate the biological functions of adherent cells, such as migration, mitosis, and differentiation (Michaelis et al., 2011; Hong et al., 2006; Burridge and Wennerberg, 2004; Geiger et al., 2001). However, if the number and types of the adsorbed proteins onto a substrate is unknown, defining the adsorption mechanisms will be difficult to comprehend (Vogler, 2011; Barnthip et al., 2009; Zhuo, Siedlecki, and Vogler, 2006). A review paper by Vogler (2012) suggests a strategy that may help to understand the "protein-adsorption problem" based on addressing three main issues.

I. How can the relationship between the different properties of a substrate influence the proteins' adsorption mechanism? What general rules can be used to design a substrate for a specific application?

II. How can protein(s) from a complex biological environment (i.e., culture medium) selectively adsorbed (in single or multiple layers) onto a substrate predict the composition of these layers?

III. How does the adsorption of protein(s) on a substrate help in guiding the subsequent interactions between the substrate and biological cells?

The lack of consensus among researchers is typical when discussing the mechanisms by which proteins adsorbed on to a substrate; thus, seeing broad consistency is widely accepted in the "protein-adsorption literature" (Vogler, 2012; Hakkinen et al., 2011; Parhi, Golas, and Vogler, 2010; Carré and Lacarrière, 2010; Oshida and Lim, 2001). This is mainly explained by the complex factors that influence the process of protein adsorption as listed in Table 2-3 (based on Vogler, 2012).

It is essential to consider all the possible types of physical-chemical complex interactions between the different components of the system to understand the protein-surface adsorption mechanism. Such may include protein-protein, protein-surface, protein-water, and water-surface. This study focuses on protein-surface interactions.

Table 2-3 Summation of variables and factors that influence the process of protein adsorption

Variable	Factor	Comment	Literature
Protein	The molecular weight (MW) and the size of protein - the impact of a protein diffusion rate	Proteins with higher MW are adsorbed on a substrate more than lower MW proteins. Proteins with higher MW can form multiple layers when adsorbed on a substrate. Lower MW proteins diffuse faster than higher MW proteins but form a smaller number of contact points in comparison with higher MW. The diffusion-constant ratio for two proteins with a spherical-like shape (Barnthip et al., 2009). $(\frac{\mathrm{Di}}{\mathrm{Dj}}) = \left(\frac{\mathrm{MWj}}{\mathrm{MWi}}\right)^{\frac{1}{3}}$	Noh et al. (2008) Noh and Vogler (2007) Noh et al. (2006) Parhi et al. (2009) Schmidt et al. (2009) Dee et al. (2002) Rabe et al. (2011) Sun et al. (2003) as cited in Schmidt et al. (2009) Barnthip et al. (2009)
	Concentration	Solutions with a higher concentration of protein cause faster adsorption than diluted ones.	Seigel et al. (1997) as cited in Vogler (2012) Schmidt et al. (2009)
	Source	Proteins from different sources (animal vs. human) tend to be adsorbed in a similar but not identical way. The source of protein affects the way they shape on a surface (elliptical, rod and heart like and Y-shaped).	Krishnan et al. (2006) Lu, Su, and Penfold (1999) Rabe et al. (2011) Wilson et al. (2005) Hakkinen et al. (2011)
	Competitive adsorption among proteins (based on the number of proteins in the solution)	Adsorption from single-protein solution is different from adsorption from multiple-proteins solution. Diffusion of proteins is size and MW dependent.	Vogler (2012) Barnthip et al. (2009) Barnthip et al. (2008) Noh et al. (2007) Vaidya and Ofoli (2005) Schmidt et al. (2009)
	The affinity of proteins to the substrate surface	Partially affected by the size of the protein. Proteins with higher molecular weight have a higher number of binding sites in comparison to smaller proteins. Unlike symmetric rigid particles, proteins behave differently in terms of adsorption and desorption when approaching a substrate from a bulk solution.	Schmidt et al. (2009) Dee et al. (2002) Horbett (2004) Rabe et al. (2011) Dee et al. (2002) Sun et al. (2003) as cited in Schmidt et al. (2009)
	structural stability and rigidity	Once in contact with a substrate, proteins with higher structural stability tend to unfold at a lower rate than unstable proteins, and thus, they form fewer contact points and bonds. On neutral charge substrates, proteins have a higher adsorption rate.	Schmidt et al. (2009) Dee et al. (2002) Horbett (2004) Wilson et al. (2005)

Variable	Factor	Comment	Literature
Substrate	Surface hydrophilicity and hydrophobicity and surface features	There is no general agreement in the literature on a standard definition or measures. However, the most agreed upon definition in the context of cell adhesion and protein adsorption literature is the one by Vogler (2001) Hydrophobic surface: $\theta > 65^{o}$ Hydrophilic surface: $\theta < 65^{o}$ ($\pm 15^{o}$ range)	Gao and McCarthy (2009) Vogler (2001) Anselme (2000) as cited in Parhi et al. (2010) Vogler (2012) Vogler (2011) Schmidt et al. (2009) Dee et al. (2002) Rabe et al. (2011) Wilson et al. (2005) Ruggeri and Jackson (2013) Tighe and Mann (2011) Zhang and Webster (2013) Michaelis et al. (2011) Valamehr et al. (2008) Huang et al. (2016)
	Protein adsorption vs. absorption	The two, unlike phenomena, are very hard to distinguish. In principle, protein should be adsorbed faster to none water-wetted surface in comparison to a wetted one due to the low energy required to replace surface-bound water	Schmidt et al. (2009) Rabe et al. (2011) Aveyard and Haydon (1973) as cited in Vogler (2012)

2.3.2.1 Protein Adsorption: Kinetics

Upon adding a single, binary, or multi-component protein solution onto a substrate, a diffusion followed by mass adsorption of protein molecules is induced closer toward the solution-substrate interphase (Vogler, 2012). Herein, the concentration of the adsorbed protein(s) is greater on a substrate than in a bulk solution. Thus, it is useful to remember that proteins from different sources show relatively similar adsorption mechanisms (Krishnan et al., 2006; Cha et al., 2008; Noh and Vogler, 2007; Ariola, Krishnan, and Vogler, 2006).

It is essential to indicate that the adsorption of proteins will not cause the depletion of the bulk solution unless the substrate area to the solution volume is very high (Vogler, 2012). It was observed that the protein adsorption (rate-of-mass) from a single protein solution is more significant than adsorption from a binary or multi-proteins solution (Barnthip et al., 2008; Barnthip et al., 2009). The adsorption kinetics to a hydrophobic substrate from a single-protein solution (I) and a binary-proteins (competitive adsorption) solution (II) is documented in Figure 2-2, which is adapted from Vogler (2012) under license.

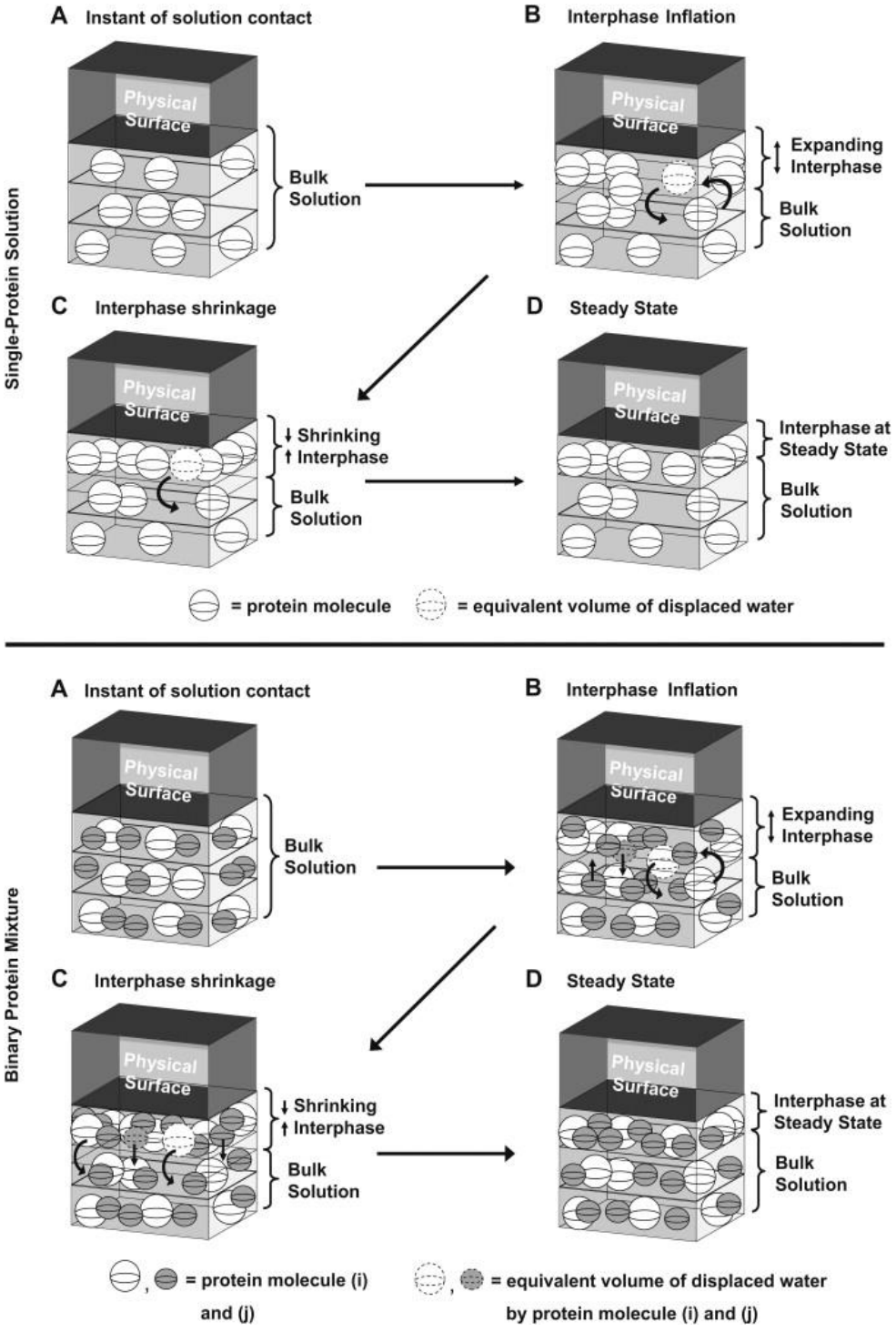

Figure 2-2 Adsorption kinetics of (I) single-protein solution and (II) binary-protein solution (competitive adsorption) on to a hydrophobic substrate (Vogler, 2012). Reused under Elsevier license number 4532750215581)

The detailed description of a single-protein and binary-protein adsorption as illustrated in Figure 2-2 is explained in Table 2-4 based on Rabe et al. (2011), Michaelis et al. (2011), Kao et al. (2010), Barnthip et al. (2009), Schmidt et al. (2009), Barnthip et al. (2008), Baujard-Lamotte et al. (2008), Noh et al. (2007), Wilson et al. (2005), Krishnan et al. (2004), Sun et al. (2003) (as cited in Schmidt et al., 2009), and. Dee et al. (2002).

Table 2-4 Single- and binary-protein adsorption mechanism on a substrate (based on literature in the paragraph above)

Stage	Single-protein Solution	Binary-Protein Solution (competitive adsorption)
(A) Surface immersion and protein diffusion	Spontaneous hydration of the surface followed by fast diffusion of a single protein from the bulk phase to form a 3D interphase separating the substrate from the liquid	Natural hydration of the surface, followed by diffusion of the binary proteins, where the lower molecular weight protein diffuses faster from the bulk phase to form a 3D interphase. Their size and molecular weight directly influence the competitive diffusion and adhesion of proteins.
(B) The dehydration of the interphase	The diffused single-protein replaces the water molecules from the interphase, causing surface dehydration. The interphase area expands. In interphase, the single protein is less organized and concentrated. Stage (B) controls the maximum capacity of the adsorbed protein, which is related to the surface contact angle.	The diffused protein with the lower molecular weight replaces the water molecules from the interphase cause surface dehydration. The interface area expands. Proteins in the interphase layer(s) are less organized and less concentrated. Stage (B) controls the max capacity of adsorbed protein(s), which is related to the surface contact angle.
(C) Interphase layer volume shrinkage	The volume of the interphase layer is becoming thinner as a result of more organized and concentrated protein layer(s)	
(D) Interphase at a steady-state	Interphase thickness shrinks to reach the thinnest possible thickness (volume). The adsorbed protein concentration becomes higher as a result of full surface/interphase dehydration.	Interphase thickness becomes very thin. The concentration of adsorbed proteins in the interphase increases. This happens due to total expulsion and replacement of water molecule (dehydration), and initially adsorbed low molecular weight protein

Rabe et al. (2011) indicate that proteins roam freely in a bulk solution, while on a substrate, proteins adapt particular shape (elliptical, rod-like, heart-like, and Y-shaped) and orientation that controls "which part of the protein interacts with the substrate and which part is exposed to the bulk solution." (p. 90). On a substrate, an elliptical-shaped protein indicates a structurally stable protein, which is

parallelly oriented along the long axis of the substrate (side-on) or perpendicularly attached along the substrate short axis (end-on).

2.3.3 In Vitro Cell Adhesion

This section addresses the impacts of hydrophilicity/hydrophobicity of a substrate on the cell-substrate interaction. The process of cell adhesion, which happens *in vitro* in a static culture medium is described by Khalili and Ahmed (2015) as a "passive adhesion" process, and according to Huang et al. (2016), and Michaelis et al. (2011), it is a complex process, and to a large extent remains ambiguous. The protein adhesion may involve multiple forces such as, gravitational (Bizzarri, Monici, and van Loon, 2015; Wagner et al., 2008), thermal (Matsuzaka et al., 2013; Rico et al., 2010), and surface (interfacial) forces (Huang, et al., 2012). These forces move cells from the bulk medium to proximity (short-distance) from the medium-surface interface. On Glass, this distance was found to be approximately 10 nm, as stated by Curtis (1964) and cited in Carré and Lacarrière (2010). The forces also include interactions between cell receptors (integrins) and surface adsorbed ligands (Bacakova et al., 2011; Wolfenson et al., 2013). It is vital to indicate that the initial cell-protein interaction happens through transmembrane receptors (integrins), which induce the cell-ECM adhesion (Grzesik, 1997; Grzesik and Robey, 1994).

2.3.3.1 Impact of Surface Hydrophilicity and Hydrophobicity

Table 2-1, Section 2.3.1 lists the main parameters that may influence the *in vitro* interaction mechanisms between a living cell and a substrate. Nevertheless, the hydrophilicity and hydrophobicity of the surface are among the most important factors (Zhang and Webster, 2013; Ruggeri and Jackson, 2013; Vogler, 2012; Rabe et al., 2011; Tighe and Mann, 2011; Michaelis et al., 2011; Carré and Lacarrière, 2010; Jager et al., 2007; Zhao et al., 2005; Redey et al., 2000).

Vogler (1998) quantitatively defines the terms "hydrophobicity" and "hydrophilicity" as a function of the water contact angle (θ). In a biology context, a hydrophobic surface is a surface with a contact angle $\theta > 65°$, while a surface is considered hydrophilic if the surface exhibits a contact angle $\theta < 65°$. In a subsequent paper, Vogler (2001) (as cited in Vogler, 2012) indicates that bio-adhesion excels in the range of $\pm 15^{o}$ around water contact angle $\theta = 65°$. Findings by Valamehr et al. (2008) point in the same direction as Vogler (2001) and indicate that increasing the contact angle (surface hydrophilicity) from 45° and decreasing the contact angle (surface hydrophobicity) from 105° will lead to an increase in the cellular interaction with the surface. Vogler (2001) differentiates between two types of substrates and their biological response; (1) cell promoting (active /hydrophilic), and (2) cell demoting (inactive /

hydrophobic). The definitions of hydrophilicity and hydrophobicity of a surface as defined by Vogler (1998) are widely used in literature (Wilson, 2005; Parhi et al., 2010; Lim et al., 2004; Liu et al., 2007), and thus, they will be used as a reference in this work as well.

However, the impact of a surface's hydrophilicity and hydrophobicity on the adhesion of cells is a debatable issue. Zhao et al. (2005) and Redey et al. (2000) discuss how a surface with higher hydrophilicity improves the adhesion of cells and the synthesis of ECM. Whereas, Qu et al. (2007) contradict these findings and indicate that surfaces with lower wettability (hydrophobic surfaces) are better for protein adhesion and cell attachment. Michaelis et al. (2011) agree with Zhao et al. (2005) and Redey et al. (2000) and indicate that the only consensus in this debate is the fact that proteins and cells react and bind differently on surfaces with different hydrophilic and hydrophobic properties. Figure 2-3 adapted from Michaelis et al. (2011) indicates the different interactions between protein/cell and a substrate. Highly hydrophilic surfaces tend to dissociate water molecules to form a hydroxylated surface.

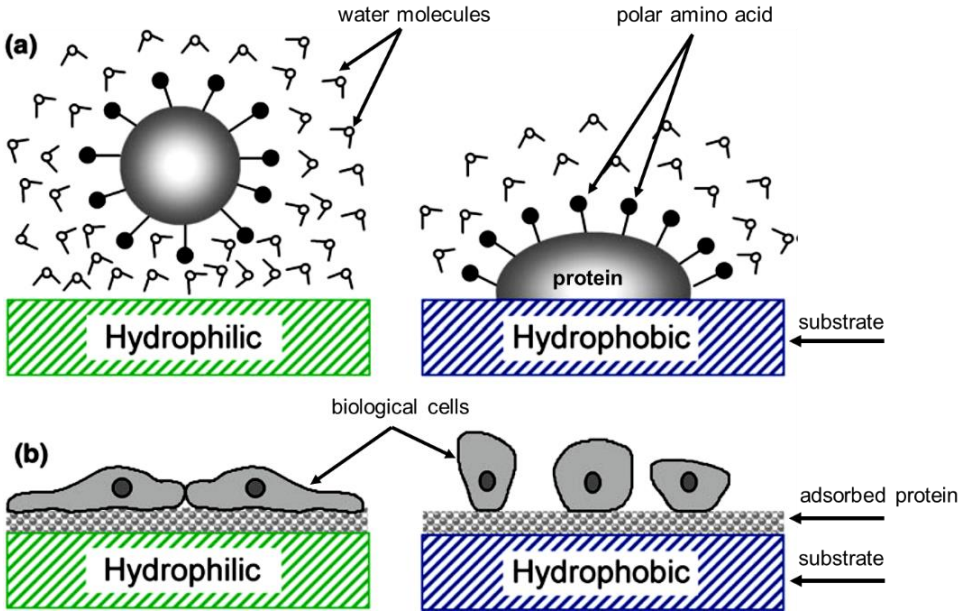

Figure 2-3 In vitro biological substances-substrate interaction on hydrophilic and hydrophobic surfaces. (a) Protein adsorption, and (b) Cell adhesion (modified - Michaelis et al., 2011). Reused under Springer Nature permission license number 4543101232576.

Thus, no protein structural rearrangements will happen, leading to insufficient and regularly revocable adsorption (Vogler, 1998). However, on less hydrophilic substrates, the interaction with water molecules will happen due to hydrogen bonding, leaving the water molecules undissociated. Proteins on hydrophobic surfaces with weak tendency to bind with H_2O, can easily dehydrate the substrate, creating

entropic forces that induce irreversible adsorption of proteins on a hydrophobic substrate and leading to significant conformational changes in the protein molecule structures with partial or total unfolding (Michaelis et al., 2011; Norde and Haynes, 1995).

Likewise, Sagvolden et al. (1999) discussed how cells tend to attach to a hydrophobic surface initially; however, with time, cells become spherical and detach from the surface. Thus hydrophobic surfaces are generally referred to and used in literature as non-adhesive surfaces (Orner et al., 2004). This behavior is observed between fibronectin and other glycoproteins on the one hand, and high concentration of albumin in a serum-containing culture medium on the other hand (Anselme et al., 2010; Lewandowska et al., 1992, as cited in Kyriakides, 2015; Sagvolden et al., 1999; Baujard-Lamotte et al., 2008; Scotchford et al., 2002; Roach et al., 2005). This is explained by albumin's higher affinity for hydrophobic surfaces in comparison to glycoproteins (Scotchford et al., 2002; Dee et al., 2002; Sun, Yue, Huang, and Meng, 2003; Schmidt et al., 2009), leading to a weak mammalian cells adhesion onto a hydrophobic substrate. Parhi et al. (2010) explain the weak adhesion of mammalian cells from a serum-containing medium with a high concentration of albumin to a hydrophobic substrate, as a result of the higher adsorption of in comparison to glycoproteins. Literature refers to such competitive adsorption behavior of proteins as the "Vroman effect" (Parhi et al., 2010; Noh and Vogler, 2007; Krishnan, 2004 as cited in Parhi et al., 2010; Brash, 1988; Horbett, 1982). The notion in regards to albumin is consistent with the findings by Kyriakides (2015), Michaelis et al. (2011), Carré and Lacarrière (2010), Wilson et al. (2005), Sousa et al. (2005) (as cited in Zhang and Webster, 2013), and Yang, Cavin, and Ong (2003), in which they referred to albumin as a cell-adhesion inhibiting protein and to fibronectin and other glycoproteins as adhesion-promoting proteins. Similarly to the scholars mentioned above, Orner et al. (2004) and Yang et al. (2003) emphasize on a number of factors that have an impact on the *in vitro* adhesion of cells on a substrate; (a) the concentration (density) of the adsorbed protein; (b) the type of the adsorbed protein (related to the hydrophobicity and hydrophilicity of the surface); and (c) time-course as explained by Rapuano and MacDonald (2011), and Meyer et al. (1988) and cited by Michaelis et al., (2011). Parhi et al. (2010), and Anselme et al. (2010) agree on the notion of surface hydrophobicity and indicate that attachment, adhesion, and proliferation of mammalian cells are more efficient on hydrophilic surfaces than on hydrophobic ones. Such dependency is considered a general phenomenon (Parhi et al., 2010; Lim, Liu, Vogler, and Donahue, 2004; Liu et al.; 2007; Fan et al. 2000). Anselme et al. (2010), Wilson et al. (2005), Schoen and Mitchell (2004) (as cited in Parhi et al., 2010), Dee et al. (2002), and Horbett (1982) discuss how cells do not respond or sense a bare substrate, instead they sense a surface covered with a layer of protein adsorbed from a culture media (Parhi et al., 2010). However, Berne et al. (2015), Orgovan

et al. (2014), Renner and Weibel (2011), Parhi et al. (2010), and MacDonald et al. (2004) challenge the notion described by Anselme et al. (2010) and Wilson et al. (2005), and suggest that the initial interaction and attachment of cells on a substrate is mainly due to physiochemical interactions rather than biological ones.

2.3.4 Summary

The factors that may impact the protein-substrate adsorption behaviors, and subsequently cells-substrate adhesion via cells-protein interactions, have been briefly reviewed. This section discussed how proteins adsorption on hydrophilic substrates is lower than on hydrophobic ones. This was found to be mainly due to the nature of water-substrate interactions and the ability of a higher affinity protein to replace the adherent water molecules. On the contrary, proteins were found to adhere the best on hydrophilic substrates rather than hydrophobic ones. Additionally, this chapter highlighted that the interaction between a biological matter and a substrate excels in the range of $\pm 15^{o}$ around water contact angle θ=65°.

Chapter 3
Manipulating Cell Behaviour on a Novel 2D Tungsten/Silicon Oxide Patterned Substrate

This chapter is based on the following publication:
Moussa, H.I.; Logan, M.; Siow, G.C.; Phann, D.L.; Rao, Z.; Aucoin, M.G.; Tsui, T.Y., Sci. Technol. Adv. Mater. 18, 2017, 840-856.

The goal of this chapter is to develop a new 2D tungsten, and silicon oxide micron and sub-micron scale patterned substrate fabricated using an advanced industrial key enabling technology of tungsten chemical-mechanical polishing (W-CMP) to manipulate and alter the behavior of mammalian cells (Section 3.3). This is the first time in literature that such substrates are used in nanobiotechnology related-context, that is, for non-intended applications that are related to the semiconductors industry. Section 3.3.1 investigates the *in vitro* use of the newly developed 2D W/SiO_2 micron and sub-micron scale patterned substrates to manipulate the behavior of Vero cells to control their alignment in a preferential orientation (in Sub-section 3.3.1.1) Sub-section 3.3.1.2, presents a mathematical model to describe the Vero cells dynamics and behavior on the 2D W/SiO_2 micron and sub-micron scale patterned substrate. Additionally, sub-section 3.3.1.3, studies the alignment behaviors of Vero cells as a function of incubation time. The effect of serum concentration in the culture media (serum-containing and serum-free media), on the alignment behavior of Vero cells is demonstrated in sub-section 3.3.1.4. The novel substrates used in Chapter 3 for manipulating the morphology of cells are distinguished from other substrates in their ability to remove the surface contaminations (biological and dust) using a simple mechanical rework process that is chemical-free, without affecting their functionality, as will be demonstrated in sub-section 3.3.1.5. All the above-mentioned experiments were done on symmetrical comb structures with equal width of tungsten and silicon oxide lines. Thus, it is essential to assess, the effect of silicon oxide width (spacing) on the alignment behaviors of cells using multiple asymmetrical comb structures as demonstrated in sub-section 3.3.1.6. Sub-section 3.3.2 will demonstrate the ability of the 2D micron and sub-micron scale patterned substrate under-study to induce a similar behavior for different types of cells, in particular, prostate cancer (PC-3) cells. This is essential since related-literature indicates that cell-substrate interactions are cell-type dependent. Sub-section 3.3.3 studies the effect of a bacterial toxin (antimycin A) in the culture media on the ability of human dermal fibroblast (GM5565) cells to interact with the 2D micron and sub-micron scale patterned substrate, and thus, on manipulating the alignment behaviors of GM5565 cells.

3.1 Background

To properly maintain the functionality of organs in humans and animals, cells need to organize and reposition themselves in specific patterns with their extracellular matrix (ECM) and elongate in the direction of a common axis (Bourget, Guillemette, Veres, Auger, and Germain, 2013). Such behavior was observed by Koubassova and Tsaturyan (2011) while studying the change in the collective alignment behavior of smooth and skeletal muscles in order to effectively generate the proper mechanical forces (contraction and relaxation) required for the movement of the human body. It is essential to emphasis on the role of ECM (*in vivo*) and ECM-like biomaterials (*in vitro*) in controlling the behaviour and fate of biological cells (Ning, et al., 2016; Kim et al., 2006; Hasirci and Kenar, 2006), which was discussed earlier in Section 2.2.2.

In the last decade, a considerable body of literature was accumulated and published with interest in tissue engineering (Michaelis et al., 2011; Ponche, Bigerelle, and Anselme, 2010; Hasirci and Kenar, 2006), cell interaction with implanted medical devices (Nikalje, 2015; Cheung and Renaud, 2006), and differentiation of cells (Rasmussen et al, 2016; McNamara et al, 2010) using engineered biomaterial (scaffolds) fabricated to mimic the functions of ECMs. These engineered biomaterials are either self-assembled monolayers and structures (Arima and Iwata, 2015; Hudalla and Murphy, 2011) or patterned structures on silicon or polymer-based substrates. They include, nanopillars (Rasmussen et al., 2016; Wang, Wan, and Liu, 2014), nanoscale pits (Biggs et al., 2007; Dalby et al., 2004b), grooves (Martínez et al., 2009; Yang, et al., 2009), and nanotubes (Ryoo et al., 2010; Park et al., 2007), to name few. Micropatterned proteins such as laminin (Joo et al., 2015), and collagen (Poudel et al., 2013) are also used to alter the behavior of cells. However, in spite of the rapid growth in the fabrication and the use of these nano biomaterials for research purposes, their commercial applications are still facing health, safety, and regulatory issues and concerns (Filipponi and Sutherland, 2013; Yao, 2007; Tomellini et al., 2006; The Royal Society, 2004). This is partly due to the limited mechanical durability and reliability of these structures that may result in irreversible damage when biological cells or bacterial cells are seeded on top. Damages refer to mechanical deformation, detachment from the substrate (Jahed et al., 2014) and bending (Kuo, Chueh, and Chen, 2014). Furthermore, substrates with micron and sub-micron topographical features undergo interactions between and among them. This may include, but are not limited to, Van der Waals (Rance, Marsh, Bourne, Reade, and Khlobystov, 2010), photo-induced magnetic forces (Guclu, Tamma, Wickramasinghe, and Capolino, 2015), and self-organization forces (Pohl et al., 1999). These forces could influence nanostructures (e.g., nanowires) to the cluster, especially if the spacing between them is small. Thereby, they will lose their effectiveness in manipulating cells. Thus, the design and

fabrication of nanostructures with very high precision and small spanning using the conventional nanofabrication techniques will be problematic. Jahed et al. (2014) demonstrated that bacteria (e.g., S. aureus) are attracted to metallic nanostructures rather than flat substrates, and their adhesion, survival and colonization rates are dependent on the dimensions and shapes of these nanostructures. This could increase the potential for surface contamination. This notion was confirmed by Mortimer, Burke, and Wright (2016), Szunerits, Barras, Khanal, Pagneux, and Boukherroub (2015), Krotz (2014), Armentano et al. (2014), and Puckett, Taylor, Raimondo, and Webster (2010). However, others may disagree (Wu, Zuber, Brugger, Maniura-Weberc, and Ren, 2016). In addition to a higher potential of bacterial contamination, foreign particles (e.g., dust) or adherent biological cells could settle in between the small structures, with a slim chance of removing them without causing permanent damage to the existing topographies, leading to an ineffective substrate. Thus, the rework-ability and reusability of similar topographical substrates are almost impossible without a high price tag. Additionally, protein-based printed devices are chemically fragile, and protein molecules will readily decompose with time, and thus, they cannot be cleaned.

The 2D W/SiO_2 substrates are silicon-based substrates fabricated using an ultra-precision and an advanced tungsten chemical-mechanical polishing technology of integrated circuit (IC) (Coutinho and Gupta, 2011; Banerjee and Rhoades, 2008). The technique is referred to in this work as W-CMP. The specimens consist of highly dense micron and sub-micron scale W metal lines inlaid in SiO_2 blanket (Rhoades, 2008; Coutinho et al., 2008). The surface of the specimen is exceptionally continuous, flat, and smooth with an average root-mean-square (RMS) roughness of less than 10 nm (Jing et al., 2013; South Bay Technology, 2017; Seo and Lee, 2007; Seo and Lee, 2005; van Kranenburg et al, 1997; Thomas et al., 1996; Abe et al., 1992). In comparison to molybdenum (in the same group in the periodic table), tungsten is superior in terms of physical, chemical, and mechanical properties. To list few, surface energy (Tran et al., 2016), hardness (Saha and Nix, 2002), modulus elasticity, melting point, density (among the heaviest metals), electrical conductivity, and heat capacity (Plansee, 2016; Royal Society of Chemistry (RSC), 2019; Haynes et al., 2015; Coursey et al., 2015; International Tungsten Industry Association (ITIA), 2011; Emsley, 2011). These and other physical, chemical, and mechanical properties of tungsten are listed in Table 3-1. Silicon oxide has a hardness of 8.3 GPa (Liu, Lin, and Zhang, 2008), modulus of elasticity of 69.3 GPa (Oliver and Pharr, 1992), and the surface energy of chemical-mechanical polished W of 0.0296 J/m^2 (Thomas, Kaufman, Kirleis, and Beisky, 1996) as listed in Appendix A, Table S1. Thus, both silicon oxide and tungsten provide cost-effective, stable, reliable, mechanically durable, and reusable structural backbone of the substrates understudy, as this chapter will demonstrate.

Table 3-1 The physical, chemical and mechanical properties of tungsten

Property	Value/Description	Literature
Physical State at 20 °C and Appearance	A solid, shiny, silver-white metal	Haynes et al. (2015) ITIA (2011) Emsley (2011) Kim, Jang, and Greer (2010) Liu et al. (2008) Saha and Nix (2002) Lassner and Schubert (1999) Oliver and Pharr (1992)
Group of Metals	Refractory Metal	
Hardness at 20 °C	14-15 GPa	
Modulus of Elasticity at 20 °C	390-410 GPa	
Surface Energy	~3.3 J/m^2	Tran et al. (2016) Thomas et al. (1996) Lassner and Schubert (1999)
Density at 20 °C	19.3 g/cm^{-3}	Haynes et al. (2015) RSC (2019)
Thermal Conductivity at 20 °C	1.75 W/cm. K	Emsley (2011) ITIA (2011)
Electrical Resistivity at 20 °C	5.28 μΩ.cm	Haynes et al. (2015) ITIA (2011)
Electrical Conductivity	$18x10^6$ 1/Ω.m	
Melting Point	4322-3414 °C	Haynes et al. (2015) ITIA (2011) RSC (2019)
Boiling Point	5500-5900 °C	
Vapour Pressure at 2000 °C	$8.15x10^{-8}$ Pa	Emsley (2011) ITIA (2011)
Crystal structure	Body-centred Cubic (BCC)	
Lattice Constant	0.3165 nm	Coursey et al., 2015 Emsley (2011)
Specific Heat Capacity at 20 °C	132-135 J/kg. K	Haynes et al. (2015) RSC (2019)
Enthalpy of Fusion	46 kJ/mol^{-1}	Coursey et al., 2015 Emsley (2011)
The coefficient of Linear Thermal Expansion at 20 °C	$4.20\text{-}4.68x10^{-6}$ K^{-1}	Haynes et al. (2015) ITIA (2011) Emsley (2011)
Application	Used as an alloy with other metals (improves melting points) arc welding electrodes (high temp applications), and in cutting and drilling tools. Scanning probe for SEM and AFM	Kim, Jang, and Greer (2010) Lassner and Schubert (1999)

This chapter will demonstrate the ability of the newly developed 2D W/SiO_2 micron and sub-micron scale patterned substrate to manipulate the behavior of mammalian (Vero) cells by attracting cells to targeted locations, in particular, tungsten parallel lines without the presence of external mechanical stimuli.

3.2 Materials and Methods

3.2.1 2-Dimensional Tungsten and Silicon Oxide Patterned Substrates

Versum Materials, LLC (Tempe, AZ, USA) provided the 2D W/SiO_2 substrates used in this study. As discussed in Section 2.1.3, the substrates were fabricated on 200 mm silicon wafers using a cutting-edge ICs industrial technique (Cogez et al., 2011; Li, 2007; Doering and Nishi, 2007; Chen, 2007; Baravelli, 2005). Figure 3-1 presents a simplified illustration of the fabrication of W-CMP substrates. Inlaid patterns were transferred to the silicon oxide thin layer that was coated on the top of the silicon wafer using photolithography and plasma etching techniques, as shown in Figure 3-1(a) and (b). The etched patterns were filled with a thin barrier layer of titanium (less than 20 nm) and tungsten, as shown consecutively in Figure 3-1(c). The excess tungsten, titanium, and silicon oxide were removed using the W-CMP techniques. The polishing step consists of two significant components, both happening simultaneously, as discussed in Section 2.1.3. The chemical component includes the use of a slurry of oxidizers such as hydrogen peroxide (H_2O_2) and ferrite nitrate ($Fe(NO_3)_3$) for the oxidation of the metal and the mechanical removal of the oxidized by-product of the surface. According to Lim, Lee, Son, Lee, and Kim (2006), the concentration of both oxidizers (H_2O_2 and, $Fe(NO_3)_3$) to be 5 wt. % of the slurry. However, Lee et al. (2016) reported that the preferred concentration of H_2O_2 in the slurry was in the range of 0.5-5 %. Lim, Park, and Park (2013) suggested that the concentration of ferric nitrate in the slurry was in the range between 0.1-1.0 wt. %. The slurry also contains abrasive materials such as silicon oxide and aluminum oxide. These particles have a diameter in the range of 0.1 to 2.0 μm (Siddiqui et al., 2005). The final surface is smooth, flat, continuous, and defect-free, as in Figure 3-1(d) (Banerjee and Rhoades, 2008; Rhoades, 2008; Beaudoin, Boning, and Raghavan, 1999; Steigerwald et at., 1995). The reactions between the substrate and the slurry components are discussed in Section 2.1.3.

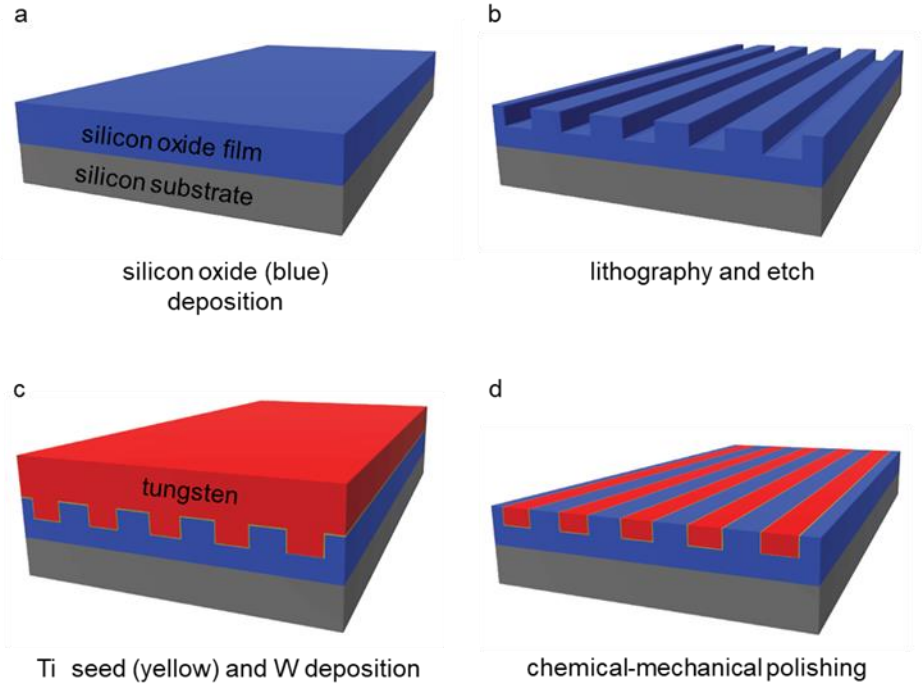

Figure 3-1 A demonstrative sketch of the 2D W/SiO_2 substrate specimen fabrication process. Silicon substrate in grey, silicon oxide in blue, thin titanium (Ti) seed layer in yellow, and the tungsten layer in red (Moussa et al., 2017).

3.2.2 Structure Characterizations

The substrates topographical features and roughness are characterized in this work using a Scanning Electron Microscope (SEM) and Atomic Force Microscope (AFM) for measuring the roughness of the surface. SEM instrument brand was Zeiss LEO-1550 (Carl Zeiss AG, Oberkochen, Germany) and it operated with 3-7 kV electron high tension (EHT) using a secondary electron detector (SE2). Samples required no gold sputtering unless otherwise stated. AFM instrument brand was Dimension 3100 Scanning Probe Microscope (Veeco, New York, USA).

3.2.2.1 Scanning Electron Microscope (SEM)

Figure 3-2 illustrates typical top-down SEM micrographs with low and high magnification isolated lines, and parallel tungsten line comb structures. Figure 3-2(a) shows a low magnification 0.25 µm parallel tungsten comb structures with alternating equal widths of W (light gray) and SiO_2 (dark gray) lines in addition to isolated W lines that are 0.25 µm wide. Figure 3-2(b) shows a high magnification image of W isolated lines inlaid in a SiO_2 continuous phase referred to in this work as "Field Oxide." The two isolated lines are ~1.5 mm long and 50µm apart. Figure 3-2(c)-(f) shows some of the other inlaid tungsten comb

structures. Adding to the structures presented in Figure 3-1, structures with line widths of 0.18, 0.25, 0.5, 1, 2, 5, 10, 50, and 100 μm were also assessed in this work.

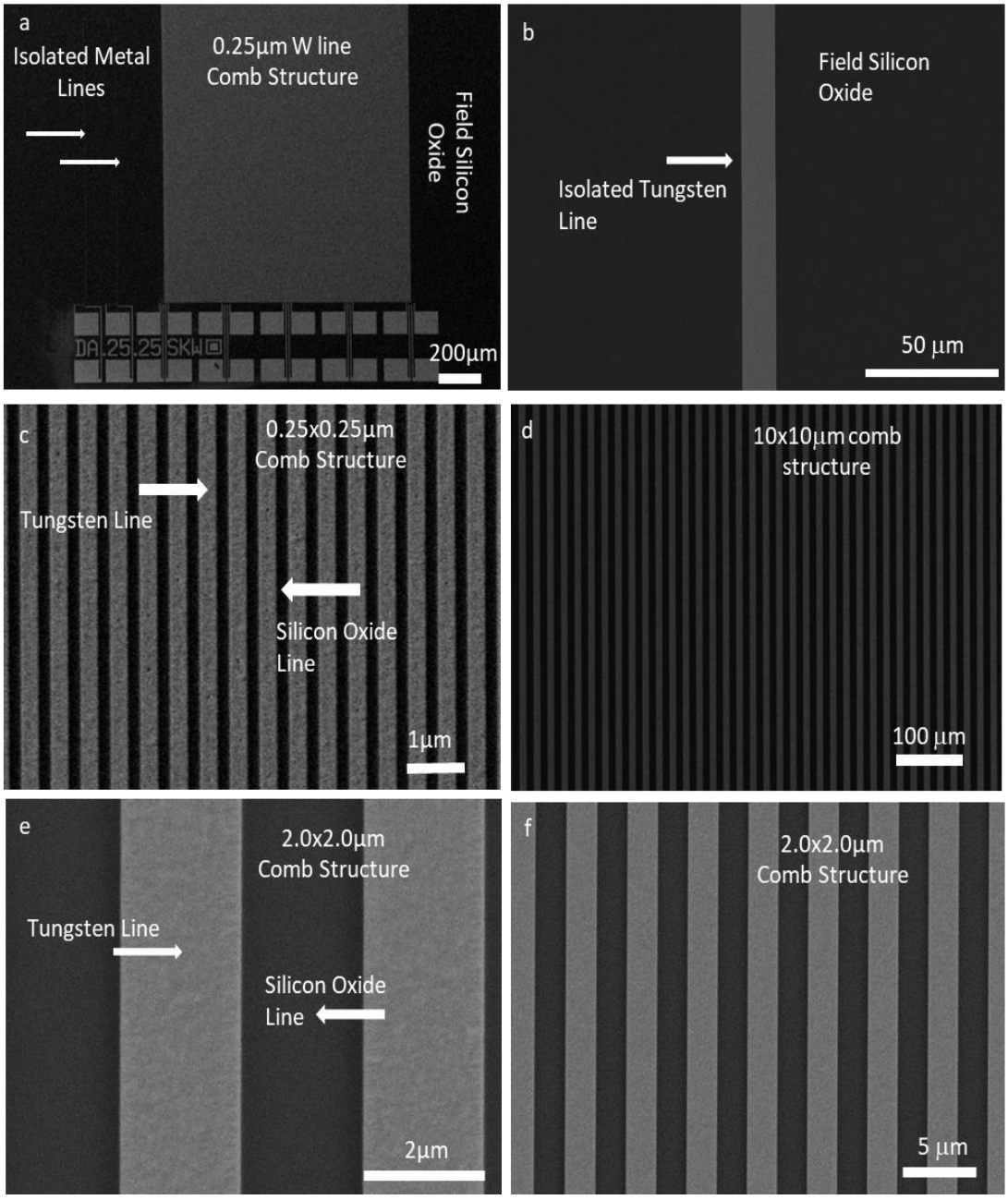

Figure 3-2 Top-down SEM micrographs show the different widths of inlaid tungsten lines (dispersed) in the silicon oxide continuous phase. (a) Tungsten/silicon oxide structure where lines are invisible due to magnification, (b) 0.25x0.25 μm tungsten/silicon oxide (equal width line and spacing) parallel lines (comb structure), and (c) 2.0x2.0 μm tungsten/silicon oxide (equal width line and spacing) parallel lines (comb structure).

Typical SEM images from Figure 3-2 indicate that the surface of the substrates is free from defects, scratches, and residues, and the W line sidewalls appear to be smooth and continuous. Table 3-2 provides a summary of the actual dimensions of the inspected parallel lines comb structures.

Table 3-2 Summary of the actual dimensions of the inspected parallel lines comb structures

Structure Type	Line Width		Comb Structure		Total Area	Measured Area*
	Tungsten	SiO_2	Width	Height		
	(μm)	(μm)	(μm)	(μm)	(μm^2)	(μm^2)
Comb Structures With Parallel Silicon Oxide and Tungsten Lines	0.18	0.18	1,258	1,606	2.02×10^6	1.73×10^6
	0.25	0.25	1,258	1,606	2.02×10^6	1.73×10^6
	0.5	0.5	1,258	1,606	2.02×10^6	1.73×10^6
	1	1	1,258	1,606	2.02×10^6	1.73×10^6
	2	2	1,258	1,606	2.02×10^6	1.73×10^6
	5	5	2,193	1,603	3.52×10^6	3.14×10^6
	10	10	1,258	1,606	2.02×10^6	1.73×10^6
	50	50	2,984	2,984	8.90×10^6	8.31×10^6
	100	100	2,984	2,984	8.90×10^6	8.31×10^6
Field Tungsten (Solid)	no parallel lines, just an area of tungsten		1,258	1,606	2.02×10^6	1.73×10^6

* All grids were measured without an edge area of 50x50 μm on all sides to avoid the edge effect impact on the cell alignment

Typical low- and high-magnification SEM micrographs of 70° tilted and 90° (cross-sectional) samples were essential for characterizing and demonstrating the topographical features of the W-CMP surfaces understudy. These included the roughness, flatness, and uniformity of the SiO_2, and W surfaces and lines. The desired micrographs were achieved, and the tungsten and silicon oxide lines and fields appeared clear after the substrate had been cleaved perpendicular to the metal lines. The cross-sectional samples were inspected and imaged after gold sputtering was completed. Typical images with low and high magnification were done, and the results are demonstrated in Figure 3-3 for 70° tilted samples, and in Figure 3-4 for 90° tilted samples. Figure 3-3(a)-(b) shows ~0.5 μm wide tungsten lines separated by ~0.5 μm of silicon oxide. Figure 3-3(c)-(d) presents field tungsten and field oxide side by side. Likewise, the 90° cross-sectional micrographs from Figure 3-3(a)-(b) and (c)-(d) show W/SiO_2 parallel lines comb structure with metal lines 0.5 μm, and 3.0 μm and oxide spacing 1.5 μm and 1.0 μm wide. As anticipated, the polished surfaces were continuous and flat. The silicon oxide film had a uniform thickness of ~0.5 μm, and the tungsten lines were inlaid to a depth of ~0.3 μm in the oxide film.

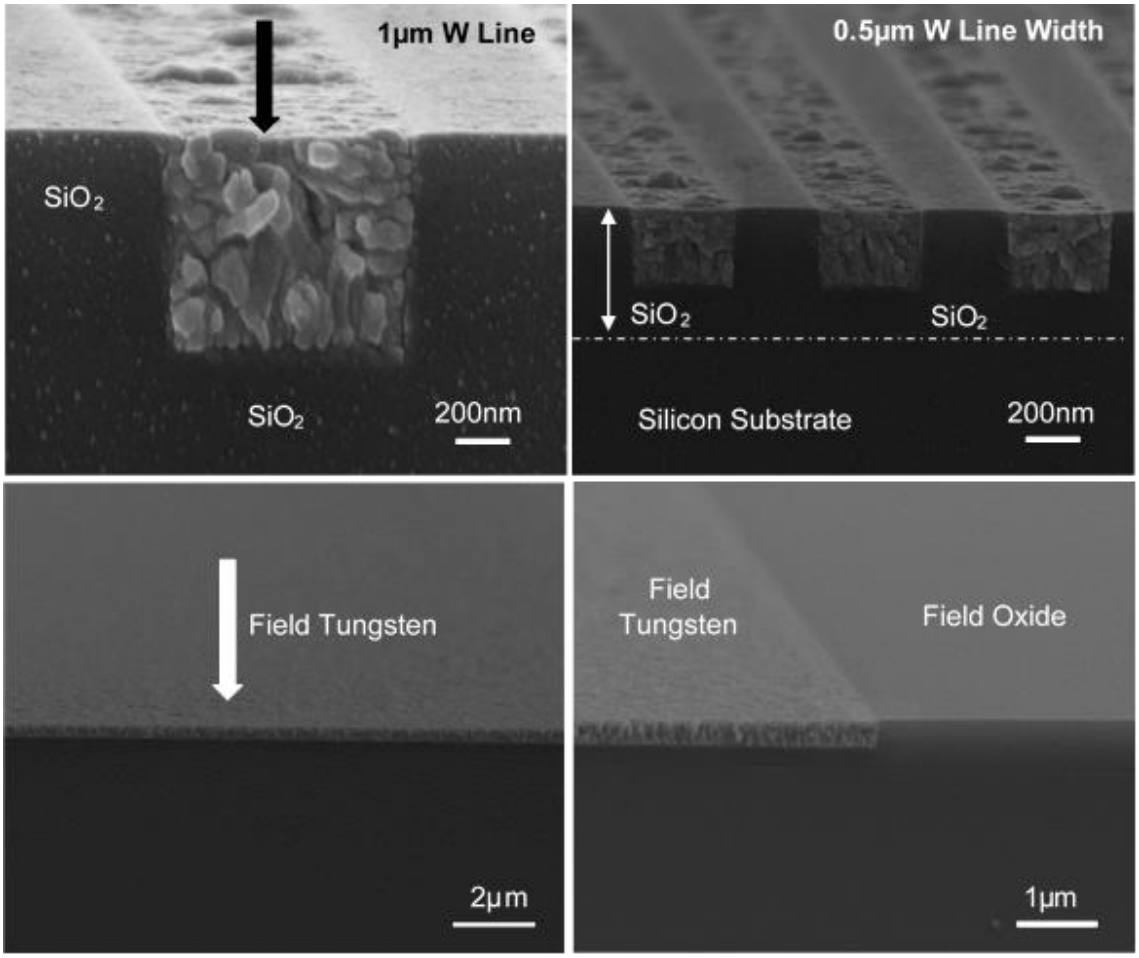

Figure 3-3 Typical 70° tilted SEM micrographs with substrates (a) 1µm wide tungsten line inlaid in silicon oxide continuous phase, (b) 0.5x0.5 µm tungsten and silicon oxide parallel lines, (c) field tungsten (solid), and (d) field tungsten and field silicon oxide side by side. The dotted line separates the silicon oxide area from the silicon substrate.

3.2.2.2 Atomic Force Microscope (AFM)

In addition to the micrographs generated from SEM, AFM was used to generate micrographs (as shown in Figure 3-5), and the root-mean-square (RMS) roughness of the 2D W/SiO_2 substrates was measured using Gwyddion (version 2.5.2), an open-source data visualizing and analysis software for scanning probe microscopy (SPM). Results indicate that the average RMS roughness of W and SiO_2 (fields and comb structures) was analyzed to be in the scale of ~0.44 ± 0.14 nm, and ~0.26 ± 0.06 nm, respectively. Data spreads represent one standard deviation. AFM scanning areas were 5µm x 5µm for field SiO_2, and 50x50 µm for W/SiO_2 comb structure. These analyzed roughnesses are consistent with or better than values reported in the literature for CMP surfaces (Jing et al., 2013, Zantye, Kumar, and Sikder, 2004; van Kranenburg et al., 1997; Thomas et al., 1996).

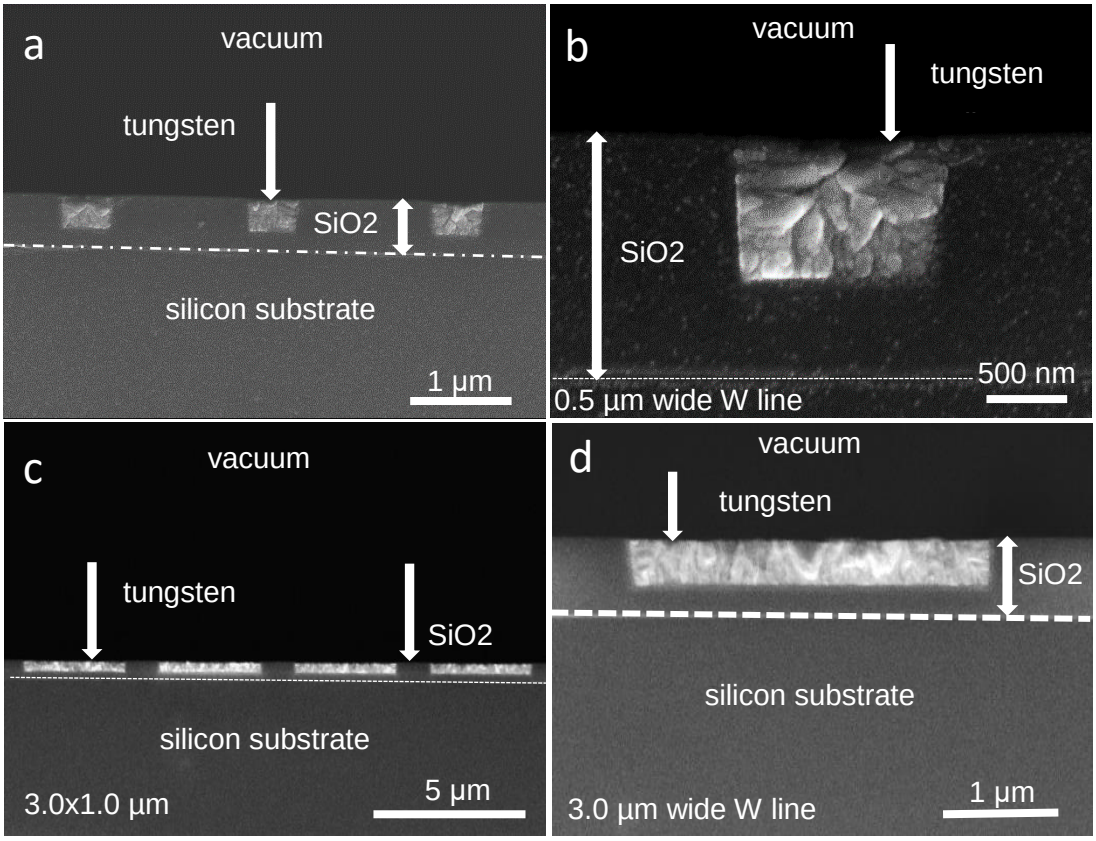

Figure 3-4 SEM micrographs with 90° tilted (cross-sectional) high and low magnification, (a)-(b) low and high magnification of a comb structure with 0.5 µm wide tungsten lines and 1.5 µm silicon oxide spacing, (c)-(d) low and high magnification of a comb structure with 3.0x1.0 µm tungsten and silicon oxide parallel lines. The dotted lines separate the silicon oxide from the silicon substrate.

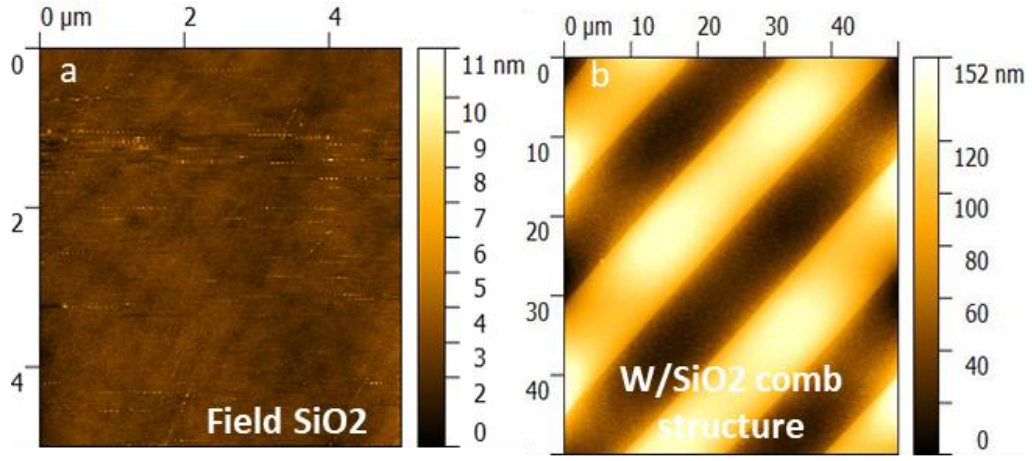

Figure 3-5 AFM micrographs of (a) field silicon oxide with a scanned area of 5x5 µm and (b) W parallel lines comb structures with a scanned area is 50x50 µm.

3.2.3 Cell Culture, Fixation, Ethanol-Dried and Staining Protocols

This section discusses in detail the different cell lines used in the experimental work as well, their incubation procedures, fixation, and staining protocols. This includes Vero cells (CCL-81), human prostate cancer cells (PC-3), and human dermal (skin) fibroblast cells (GM5565). Vero and prostate cancer cells are epithelial cells, while GM5565 and QT are fibroblasts. Table 3-3 provides a detailed description of these cell lines.

Table 3-3 Description of the cell lines understudy

Description	Vero Cells	Prostate Cancer	Dermal Fibroblast	Quail Tail
Cell Line Name	CCL-81™	PC-3	GM5565	QT-35 ™
Supplier	ATCC™	ATCC™	ATCC™	ECACC™
Source	Normal Adult Male	Adenocarcinoma Male Adult	Normal Adult Male	Fibrosarcoma
Species	African Monkey (mammalian)	Human (mammalian)	Human (mammalian)	Quail (bird)
Tissue of Origin	Kidney	Prostate; derived from Bone	Skin	Muscle
Growth Model	Adherent	Adherent	Adherent	Adherent
Morphology / Cell Type	Epithelial	Epithelial	Fibroblast	Fibroblast
Literature	Sigma-Aldrich (2016a) Adams et al. (2015)	Cunningham and You (2015) Russell and Kingsley (2003)	Bauer et al. (1993)	Sigma-Aldrich (2016a)

3.2.3.1 Vero Cells (CCL-81)

Vero cells (CCL-81) obtained from the American Type Culture Collection (ATCC, USA) were cultured in a 1:1 mix of Dulbecco's Modified Eagle Medium (DMEM) and Ham's F12 (Corning Cellgro, USA) nutrient mixture. The DMEM/F12 medium was supplemented with 4 mM L-glutamine (Sigma-Aldrich, USA) and 10 % fetal bovine serum (FBS) (Gibco, USA). Cells were incubated in 5 % CO_2 at 37 $^{\circ}$C. The average diameter of a Vero cell is 14.65 μm, as measured during the experiment using Countess II FL Automated cell counter.

The ATCC via their distributor CedarLane Labs (Burlington, ON) indicated that the average diameter of Vero cells falls between 12.39–16.64 μm, with an average of 14.52 μm, and the majority of cells' diameter at 14.75 μm (Achankunju, personal communication, October 15, 2016). The polished specimens

were sterilized in 2 mL of 70 % ethanol for 30 seconds before cell depositions. Specimens were air-dried, then rinsed with 2 mL Dulbecco's phosphate-buffered saline (D-PBS) to remove residual contaminants. Sterilized specimens were inoculated with a specific confluence and incubated for a specified period. The confluence of cells and incubation periods varied depending on the specific experiment parameters. The incubation process was conducted in 6-well plates (Nunc, Thermo Scientific, Denmark). After the incubation period, the spent media was removed and rinsed with 2 mL of Dulbecco's Phosphate-Buffered Saline (D-PBS) solution. The adherent cells on specimen surfaces were fixed using 2 % methanol-free formaldehyde (Sigma-Aldrich, USA) for one hour at room temperature, and then dehydrated by submerging them sequentially in 50 %, 75 %, and 95 % ethanol solutions for ~ 10 minutes, followed by a 15-minute soak using 100 % ethanol. Specimens were dried gently with high purity nitrogen after the final ethanol soak (Moussa et al., 2017).

Staining was done according to the following protocol. The adherent cells were fixed, as previously mentioned, using 2 mL of 2 % methanol-free paraformaldehyde (Sigma-Aldrich). The permeabilization process of the cell membrane was done using 2 mL of 0.1% Triton-X100 (Sigma-Aldrich) for five minutes. Two milliliters of 1 % (w/w) bovine serum albumin (BSA) (Sigma-Aldrich) were used to block the cells before adding the deep red CytoPainter F-Actin stain (ab112127 Abcam, Cambridge, MA, USA). The F-Actin stain was diluted by a factor of 1,000 in 1 % BSA. This step happens in the dark, at room temperature for an hour. The cells were then exposed for 5 minutes to 2 ml of 4’ ,6-diamidino-2-phenylindole (DAPI) (Life Technologies™, Carlsbad, CA, US), and then washed twice using 2 mL of D-PBS. The staining process ends, when four drops of the anti-fade agent are added before specimens are stored in the dark at 4 °C prior to imaging (Moussa et al., 2017).

3.2.3.2 Prostate Cancer Cells (PC-3)

The American Type Culture Collection (ATCC, Manassas, VA) was the source of the human prostate cancer cells (PC-3) used in this experiment. Ham’s F-12K (Kaighn’s) a modified version of Ham’s F-12 culture medium was used for cell incubation. Since the F-12K culture medium is protein-free, the medium was supplemented with 10 % FBS (Thermo Fischer, Whitby, ON), and 1 % of penicillin-streptomycin. Cells were incubated in 5 % CO_2 at 37 $^{\circ}$C. The polished specimens were sterilized in 2 mL of 70 % ethanol for 30 seconds prior to cell depositions. Specimens were air-dried, then rinsed with 2 mL Dulbecco’s phosphate-buffered saline (D-PBS) to remove residual contaminants. Sterilized specimens were seeded with cells with a confluence of $1.5x10^5$ cells/ mL and incubated for 48 hours. After the end of the incubation period, the wasted medium was removed, the incubated cells were fixed at room

temperatures using a process that is widely used in literature (Seo et al., 2017; Li et al., 2014; Pan et al., 2012).

3.2.3.3 Human Dermal Fibroblast Cells (GM5565)

Human dermal fibroblast (GM5565) cells from ATCC (Manassas, VA) were seeded on 2D W/SiO_2 micron, and sub-micron scale patterned substrates and cultured for 72 hours in an incubator at 37 °C with 5 % of CO_2 Corning, NY) in two different culture media A, and B. Both are serum containing media of Dulbecco's Modified Eagle Medium (DMEM) supplemented with 10 % (v/v) Gibco™ FBS (Thermo Fischer, Whitby, ON), but medium B was supplemented with 5 μM antimycin A (Sigma-Aldrich, St. Louis, Missouri) at a concentration that is sufficient to induce a change in the function of the mitochondria, but not to result in immediate failure (Stefano, Samuel, and Kream, 2017; Kalghatgi et al., 2013). The 2D micron and sub-micron scale patterned substrates were rinsed and dried with ethanol prior to seeding the GM5565 cells with an initial concentration of $1x10^5$ cells/mL in 35 mm plates (Falcon, Thermo Fischer, Whitby, ON).

3.2.3.4 Quail Tail Cells (QT-35)

Quail tail cells (QT-35) were obtained from the European Collection of Authenticated Cell Cultures (ECACC). The cells were cultured in a Modified Eagle Medium (MEM) with 1 % of Non-Essential Amino Acid (NEAA) solution (Corning Cellgro, USA) supplemented with 4 mM L-Glutamine (Sigma-Aldrich, USA) and supplemented with 10 % (v/v) Gibco™ FBS (Thermo Fischer, Whitby, ON, Canada). The cells containing solutions were kept in a 5 % carbon dioxide environment at 37 °C prior to cell deposition. Sterilized specimens were submerged in the culture medium for 48 hours at 37 °C. The incubation of cells was conducted in Nunc Delta Surface 6 well plates made by Thermo Scientific (Denmark) at an initial concentration of cells was $5.0x10^4$ cell/mL for 24 hours. The spent media was removed and rinsed with 2 mL of D-PBS solution. The adherent cells on the specimen surfaces were fixed by submerging them in 4 % methanol-free formaldehyde (Sigma-Aldrich, USA) for 1 hour at room temperature, and then dehydrated using ethanol. The substrates were dried gently with high purity nitrogen after the final ethanol soak.

3.2.4 Quantifying the Dimensions and Orientation of Cells Nuclei

This section is intended to demonstrate the quantification method of cell-substrate interaction in terms of the orientation and alignment of nuclei for the different cells (Vero, PC-3, and GM5565) under study. Orientation is represented by the angle ϕ that exists between the major axis of the elliptically-shaped

nuclei and the metal line axis (y-axis). A schematic drawing illustrating the angle ϕ between these axes is shown in Figure 3-6. The angle ϕ is equal to 0° when the nucleus' major axis is perfectly aligned in parallel to the metal line axis (y-axis). The angle ϕ is equal to 90° when the nucleus' major axis is perpendicularly oriented to the metal line axis (x-axis). The elongation ratio of cells is calculated as a ratio between cell's major (L) and minor (S) axes (L/S), as illustrated in Figure 3-6, and the L/S ratio is always bigger than 1. The center of the cell nucleus (C) is identified by the point at which the short and long axes intercept. These measurements were conducted manually as lines of best fit, based on a visual estimate of the nucleus boundaries by using the Image Processing and Analysis in Java (ImageJ) software (National Institute of Mental Health, Bethesda, Maryland, USA) built-in application tools. Cells situated within the 50 μm region from the boundary of the comb structures were excluded in order to avoid possible edge influences.

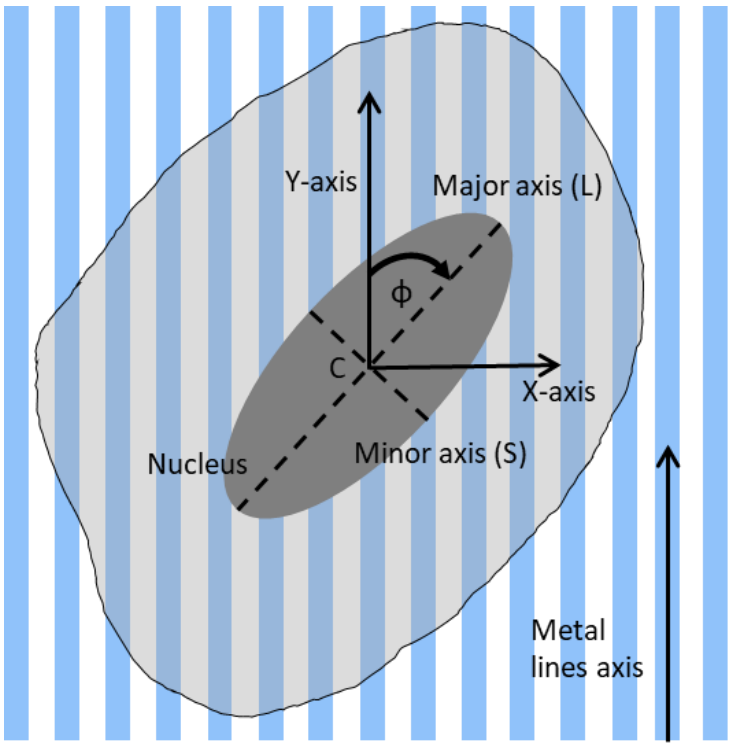

Figure 3-6 Representative sketch of a cell on a tungsten and silicon oxide comb structure showing the nucleus deviation angle ϕ from the tungsten lines y-axis, and the long (L), and short (S) axes of the cell. "C" is the point at which the two axes connect, and form a right angle (Moussa et al., 2017).

3.3 Results and Discussion

This section discusses the potential changes in the behavior of cells adherent on a newly developed 2D W/SiO_2 micron and sub-micron scale patterned substrate as a result of different experimental parameters.

This includes different cell lines, culture media, the protein concentration in the culture media, the effect of silicon oxide lines widths (spacing), and the effect of the bacterial toxin on the behaviors of cells, GM5565 in particular.

The conducted experiments and their results that are listed and discussed in this section are intended to prove that the 2D W/SiO_2 substrates can be used to induce a preferential change in the alignment and orientation behaviors of adherent cells. This was demonstrated to be possible in the absence of any external mechanical stimuli that are responsible for the biological and biochemical responses of cells as a result of cell-substrate interaction.

This section is divided into three main sub-sections based on the type of assessed cells.

3.3.1 Vero Cells (CCL-81)

3.3.1.1 Patterns-dependent Cell Alignment

This experiment was conducted to demonstrate the ability of the 2D W/SiO_2 substrates to alter the geometry, orientation, and alignment behaviors of Vero cells on both un-patterned surfaces (e.g., field oxide, field tungsten, and bare silicon) and patterned surfaces (comb structures). For this experiment, Vero cells were incubated on two 2D W/SiO_2 substrates for 24 hours at a similar initial concentration of $2x10^5$ cells per mL. After the end of the incubation period, one chip was prepared, and cells were fixed and dried as discussed in Section 3.2.3.1 to be later imaged using SEM. SEM micrographs were obtained using EHT between 3-7 kV and SE2 electron detector (Section 3.2.2). The second chip was fixed and stained ready, to obtain high-resolution images using a confocal fluorescence microscope (Leica Microsystems, GmbH, Germany). The Leica TCS SP5 used to obtain fluorescence images was done at the University of Guelph (Canada) and equipped to obtain signals from five different wavelengths at the same time. Blue DAPI and red CytoPainter F-Actin fluorescence stains were inspected with wavelengths in the ranges of 436–482 nm, and 650–700 nm, respectively. Similarly to the structures (with no cells on) imaged by SEM and published in Figure 3-2, images of Vero cells adherent on different surfaces and W parallel lines comb structures with different line widths, are shown in Figure 3-7.

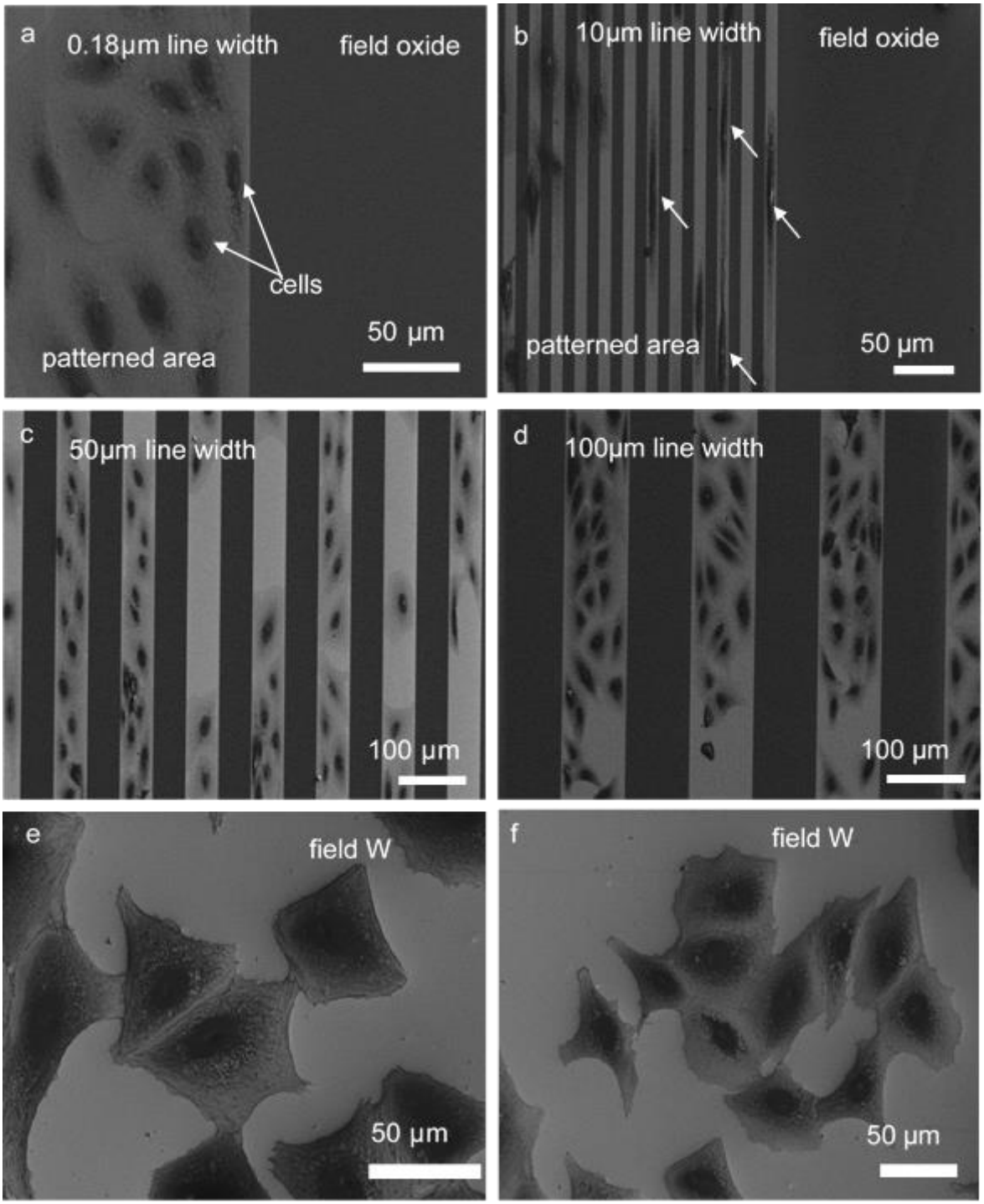

Figure 3-7 SEM images capture the change in the cell adhesion patterns on different structures with different tungsten line widths: (a) 0.18 μm (lines are unnoticeable due to magnification), (b) 10 μm, (c) 50 μm, (d) 100 μm, (e)-(f) filed tungsten (0 μm). SEM micrographs indicate symmetrical widths of tungsten lines and silicon oxide spacing in the comb structure

The dimensions of the imaged and inspected comb structures and field tungsten are listed Table 3-2. Since the width of W and SiO_2 comb structures alternating lines were identical, it is reasonable to assume that W and SiO2 lines covered almost half of the inspected areas, except for field metal and field oxide. As Figure 3-7 indicates, Vero cells on 0.18 μm (a), 50 μm (c), and 100 μm (d) wide W lines comb structures and field tungsten (e-f) show that they were randomly distributed with no orientation preference or preferential geometrical shape. The majority of cells inspected on 50 μm (c), and 100 μm (d) wide W lines comb structures remained entirely within the tungsten lines (light grey) with no contact on SiO_2 lines (dark grey). However, on a 10 μm wide W lines comb structure (b), cells behaved in a more organized manner, by aligning themselves in parallel to the W lines. To further confirm the observations obtained from the SEM micrographs in Figure 3-7, it was essential to obtain high-resolution micrographs using a confocal fluorescence microscope. The fluorescence micrographs will help to understand the alignment behavior of cell nuclei stained and labeled in blue, and actin microfilaments stained with red.

The staining protocol of Vero cells is described in Section 3.2.3.1. Additionally, the fluorescence confocal micrographs will be used for the mathematical modeling intended to describe the alignment behaviors of the adherent cells and compare them with the experimental data from Section 3.3.1.1.

Qualitatively, the confocal fluorescence images on isolated tungsten lines and W/SiO_2 dense parallel lines comb structures Figure 3-8 confirm that the cell-substrate interactions, observed previously in Figure 3-7, happened without the presence of external mechanical forces or stimuli, but they were only driven by preferred cell-tungsten lines interactions as a result of the tungsten high surface energy (Table 3-1). Figure 3-8(a) shows that on a bare silicon substrate (black-background), there was no preferred alignment behavior (nuclei stained in blue and actin microfilaments stained in red). However, cells show a change in the alignment behavior when adhered to isolated W lines, regardless of the width of the isolated W line (0.18, 2.0, and 10 μm). Isolated lines refer to W lines (~1.5 mm long) inlaid in field oxide; those are 50 μm apart (as discussed in Section 3.2.2.1). Figure 3-8 (b, c, d, and e) illustrates that cells on these isolated W lines tend to elongate into a long thin strand. It was observed that the largest width of the cell was near the nucleus, which in turn was deformed into a diamond-like shape. Vero cells underwent severe stress on 0.18 μm isolated lines micrograph (b) in order to stretch and fit along the W isolated lines. However, despite the stress and change in shape, the majority of the cells remained broader than the 0.18 μm W lines. This is understandable since the average diameter of Vero cells is 14.75 μm (Section 3.2.3.1). This preferential adhesion behavior is driven and influenced by the width of tungsten lines even though the width of the isolated W line is ~1.1% of the average diameter of the cell. These observations show a limitation of the nucleus ability to deform as a result of the mechanical forces

transmitted between the extracellular matrix (in this case the substrate) and the cytoskeleton (F-actin filaments). The deformation magnitude is cell-type dependent. Fibroblast and endothelial cells deform less than epithelial cells because of the higher stiffness of nucleus (Wang et al., 2018; Haase et al., 2016; Belaadi, Aureille, and Guilluy, 2016; Lammerding, 2011).

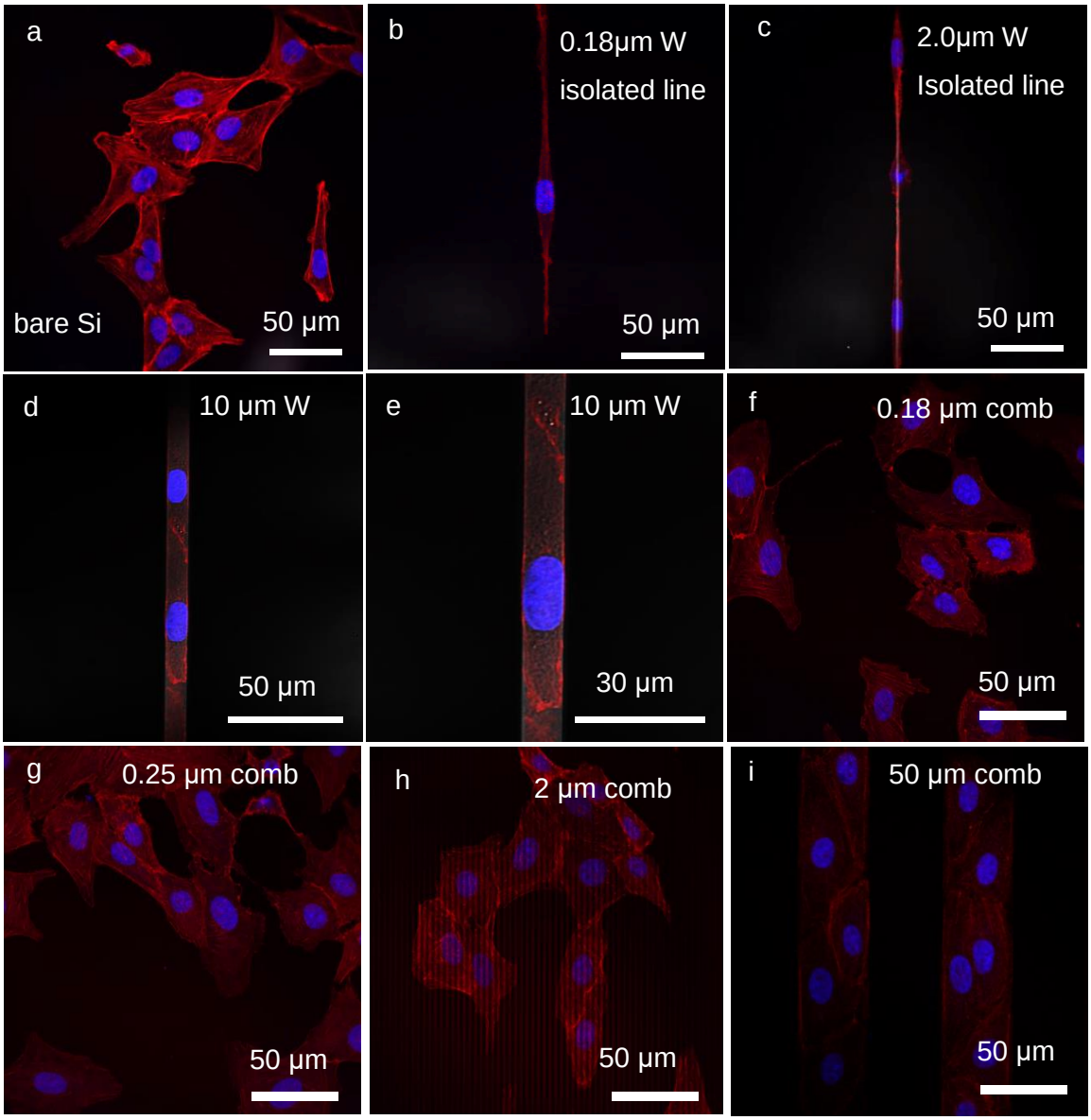

Figure 3-8 (a) Fluorescent confocal image of Vero cells on the bare silicon substrate. (b), (c), (d), and (e) Images of adherent cells on 0.18 µm, 2.0 µm, and 10 µm (high and low magnification) wide isolated tungsten lines, respectively. (f), (g), (h), and (i) Micrographs of adherent cells on 0.18 µm, 0.25 µm, 2.0 µm, and 50 µm comb structures, respectively. Cell nuclei are stained in blue using DAPI, and F-actin microfilaments are stained in red using fluorescent phalloidin conjugate. All cells were incubated for 48 hours (Moussa et al., 2017).

The notion of cell-W lines interaction is also observed on 2.0 μm isolated tungsten lines (c) and 10 μm (d)-(e) isolated W lines. Contrarily to the attachment behavior of Vero cells on 0.18 μm and 2.0 μm isolated W lines, cells fit entirely on 10 μm isolated W lines with less deformation on the shape and dimensions of the nucleus. Figure 3-8 (b)-(c) reveals that the nuclei of the non-dividing elongated cells on isolated 0.18 μm and 2.0 μm isolated tungsten lines were similar. This suggests a limited deformation ability determined by the maximum amount of force generated by the F-actin filaments and the compliance of the cell nuclei (Moussa et al., 2017).

Figure 3-8 (j)-(k) shows a Vero cell likely in anaphase, going through mitosis while severely elongated on 0.18 μm isolated tungsten line. Figure 3-8(k) reveals two identical groups of condensed chromosomes that are aligned away from the tungsten line y-axis (Moussa et al., 2017), and it further demonstrates the formation of two developed nuclei in not fully-separated cells. This image indicates that the severe elongation of the adherent cell did not prevent it from dividing. Similarly to Figure 3-8 (j)-(k), Figure 3-8 (l)-(m) shows another dividing cell (in the dotted white box) on 2.0 μm isolated tungsten line, but at a different stage of mitosis, probably in metaphase.

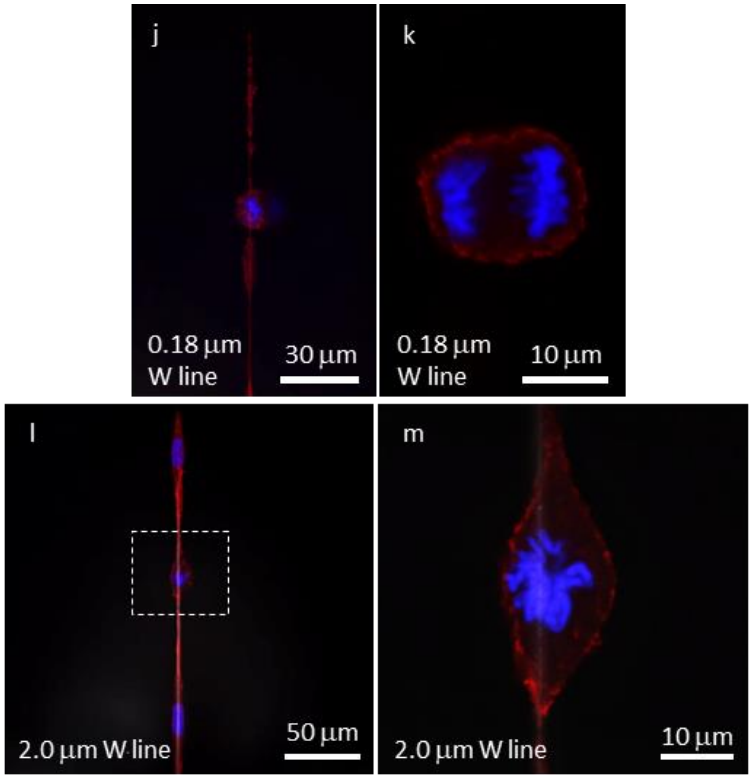

Figure 3-8 (j)-(k) Low and high magnification images of a dividing cell on 0.18 μm isolated tungsten line. (l)-(m) Low and high magnification images of a dividing cell on 2.0 μm isolated tungsten line.

The orientation and alignment behavior of Vero cells were characterized using the method described in Section 3.2.4. The angle ϕ exists between the major axis of the elliptically-shaped nuclei and the metal line axis (y-axis), as demonstrated in Figure 3-6. This angle was measured for cells adherent on the assessed structures. A total of 5,804 cells were assessed and measured on comb structures with different W/SiO_2 line widths, bare silicon, field tungsten, and field oxide areas. Results from Figure 3-9(a)-(b) confirm the visual observations and show a broad distribution of alignment behavior of cells. Quantitatively, only 13.6 % of cells on bare silicon, 11.4 % of adherent cells on field tungsten (solid), 4.8 % of cells on field silicon, and 16 % of cells adherent on 0.18μm comb structure align in the range of ±10° in parallel to W lines; thus, adherent cells on these assessed areas and structures show no preferred alignment.

Data indicate that with the increase in the width of tungsten line from 0.25 μm to 10 μm, adherent cells show an increase in the percentage of aligned cells the range of ±10° from 22 % to 56 %, respectively. The tendency of cells to preferably align at a peak on 10μm W line comb structure will decline (misaligned) at W line widths larger than 10μm, for example, 50μm and 100μm. This is further demonstrated in Figure 3-9(b), in which the percentage of cell alignment within ±10° and ±20° of the tungsten lines y-axes was illustrated as a function of the line widths of the comb structures. These findings agree with results from Joo et al. (2015), Nakamoto et al. (2014), Poudel et al. (2013), and Aubin et al. (2010). These publications indicate that cells showed a preferred alignment behavior along the line axes at a specific line width (vary depending on the cell type); however, on larger or smaller line width, cells tend to misalign. The number of Vero cells assessed on each area and comb structure is labeled on each chart as n.

Additionally, the deformation in the nuclei shape (described in the L/S ratio, cell nuclei long axis to short axis) on bare silicon, field tungsten, and field oxide was found to be in the same range of 1.4±0.2, 1.5±0.3, and 1.7±0.4, respectively.

Furthermore, results indicate that the average L/S ratio of adherent cells increases with the increase of W line width to peak at 10 μm with 169 % higher than average L/S ratio for adherent cells on field tungsten. Thus, the above-given results demonstrate that the alignment of adherent Vero cells is a pattern-dependent behavior. The summary of data from Section 3.3.1.1 is briefed and listed in Table 3-4.

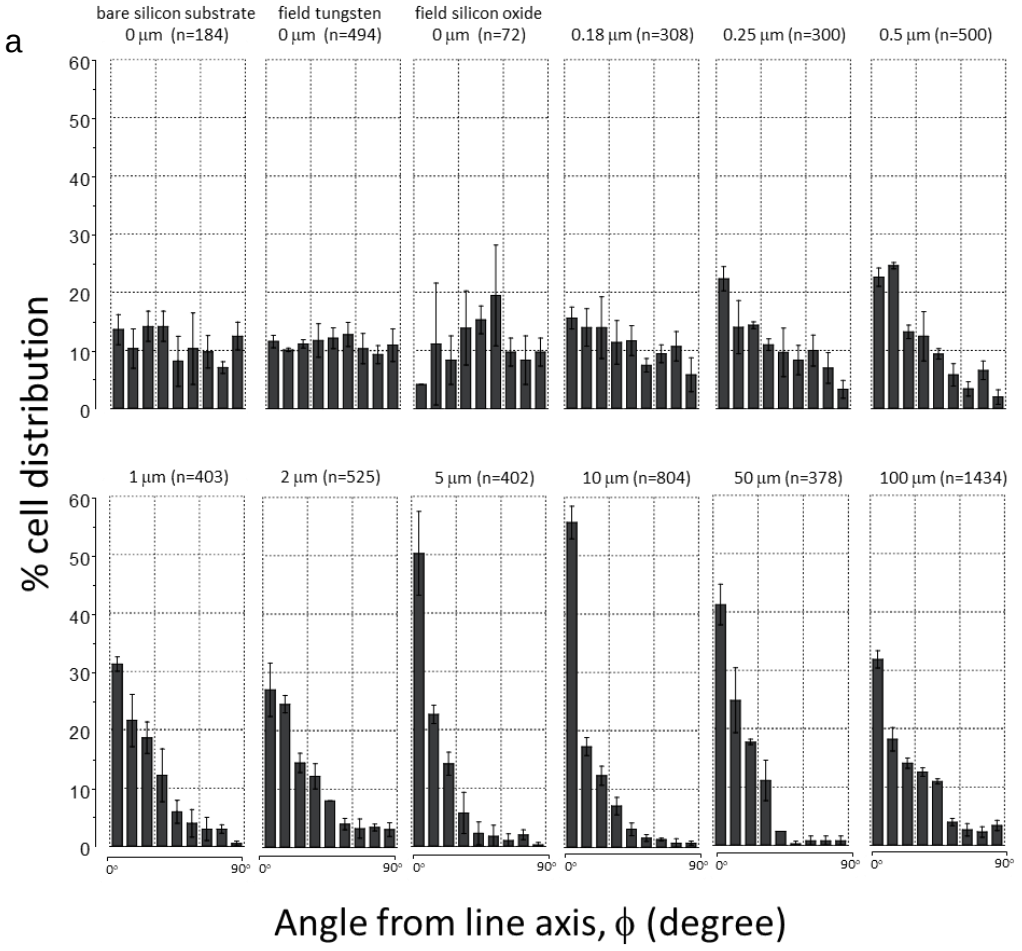

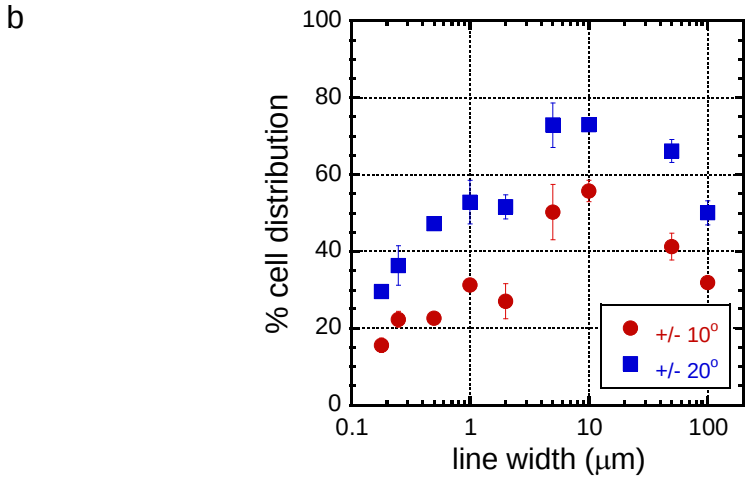

Figure 3-9 (a) The alignment of Vero cells characterized as the angle ϕ from W lines y-axis and the width of W line, from 0 μm (field oxide, field W, and bare silicon) to 100 μm. Value "n" is the number of cells inspected on each structure. Each bar represents the percentage of cells in a ±10° bin of deviations from the line axis. (b) Distribution of cell alignment as a function of line width for ±10° and ±20°. Error bars correspond to one standard deviation (Moussa et al. 2017).

Table 3-4 Data summary for the alignment of Vero cells as a function of W and SiO_2 lines width dimensions, comb structure area, number of assessed cells, and percentage of cell aligned within ±10° and ±20° of the W lines y-axis.

Structure	Comb Structure Lines Width	Measured Comb Structure Area	Cell Number in Structure	Cell Density	Cell Distribution Aligned ± 10° from W Lines	% Cell Distribution Aligned ± 20 ° from W Lines
		(mm^2)	(n)	($cells/mm^2$)	(%)	(%)
1	Bare silicon	-	184	-	14 ± 3	24 ± 2
2	Field tungsten	1.73	494	286	12 ± 2	22 ± 1
3	Field oxide	-	75	-	4 ± 0	15 ± 8
4	0.18x0.18	1.73	308	178	16 ± 2	30 ± 2
5	0.25x0.25	1.73	300	173	22 ± 2	36 ± 5
6	0.5x0.5	1.73	500	289	23 ± 2	47 ± 1
7	1.0x1.0	1.73	403	233	31 ± 1	53 ± 6
8	2.0x2.0	1.73	525	303	27 ± 5	52 ± 5
9	5.0x5.0	3.14	402	128	50 ± 7	73 ± 6
10	10x10	1.73	804	466	56 ± 3	73 ± 1
11	50x50	8.31	378	45	41 ± 3	66 ± 3
12	100x100	8.31	1,434	173	32 ± 1	50 ± 3

Note: Initial cell confluence was 2×10^5 cells/ml. Data spread corresponds to one standard deviation.

To summarize this section, Vero cells showed the tendency to preferentially adhere to isolated tungsten lines and tungsten parallel lines comb structures, rather than field oxide or silicon oxide parallel lines. The adherent Vero cells elongated and aligned themselves in the direction of the W lines y-axes to maximize their contact with these lines. The maximum cell alignment was observed and quantified on comb structure with tungsten lines 10 μm wide. This happened without the presence of external mechanical forces or stimuli, but was only driven by preferential cell-tungsten lines interactions.

3.3.1.2 Mathematical Model for Line Width-Dependent Cell Behavior

This section is intended to demonstrate the ability of a newly developed mathematical model to predict the alignment behaviors and dynamics of the adherent cells. The developed model was based on experimental data from Section 3.3.1.1, which shows a strong correlation between the widths of symmetric tungsten and silicon oxide lines in the comb structure and the elongation and alignment behaviors (deformation characteristics) of cells. Observations based on Figure 3-7, Figure 3-8, and

experimental data from Figure 3-9 and Table 3-4 demonstrate that adherent cells on 10x10 μm lines widths comb structure showed the highest elongation and alignment behaviors in comparison with other comb structures. This shows a tungsten linewidth dependent behavior, driven by the tendency of cells to maximize their contact area with tungsten line. A mathematical model was developed to predict the geometry-dependent cell behavior by calculating the percent of tungsten area coverage of an adherent cell, A(W), as a function of comb structure tungsten line widths (Equation 3.1). A visual demonstration is provided in Figure 3-10. Two cell geometries were modeled based on monolithic un-patterned surfaces (field tungsten, and bare silicon) based on actual adherent cells and two isolated tungsten line widths of 0.18 and 2.0 μm as illustrated in Figure 3-10 (a) and Figure S1 (Appendix B). The geometries signify the shape of cells observed in these different areas and isolated tungsten lines. On monolithic un-patterned surfaces, cells are randomly oriented with irregular geometries with dimensions of ~97 μm long and ~107 μm wide. On polished oxide, cells showed similar randomness and irregularity with ~56 μm long and ~58 μm wide dimensions. The elongated cell on 2.0 μm wide isolated tungsten line was measured to be ~ 179 μm long and ~ 11 μm wide, whereas cell on 0.18 μm wide line was ~ 228 μm long and ~ 9 μm wide. To determine the correlation between the width of metal lines and the portion of the cell that was in contact with the tungsten lines, symmetrically parallel lines were overlaid on these cell geometries as demonstrated in Figure 3-10(a)-(b). The yellow diamond shapes symbolize the potential cell morphology that can be observed. The data generated from the simulation represent the cell alignment comparative to the width of the tungsten line on the comb structure. Results were presented in Figure 3-10(c). It was assumed that the center of the modeled cell was always positioned on a tungsten line; thus, a modeled cell would be either in full contact with one metal line (100 % coverage), or 50 % of the cell area was in contact with the simulated tungsten lines, in which cell-tungsten coverage is considered to be 50 %.

The portion of the cell area on (in contact with) tungsten lines ΣA_i, represented in Figure 3-10(b) in blue was calculated using Equation 3.1, as a percentage of total cell area on both tungsten lines (in blue) and silicon oxide lines (in yellow). i = 5 for circle shaped (pink) cell, and i = 3 for diamond shaped (yellow) cell, in Figure 3-10(b). Equation 3.1 displays cell's geometry-dependent behavior

$$A(W) = \frac{\sum A_i}{\text{total cell area}} \text{ x } 100 \qquad 3.1$$

The "i" index represents the number of the tungsten lines that the adherent cell was in contact with. Value i = 1 is for a cell that was fully adherent on a metal line, and the coverage is considered to be 100 %. i = n, which depends on the total number of tungsten lines in contact with a cell.

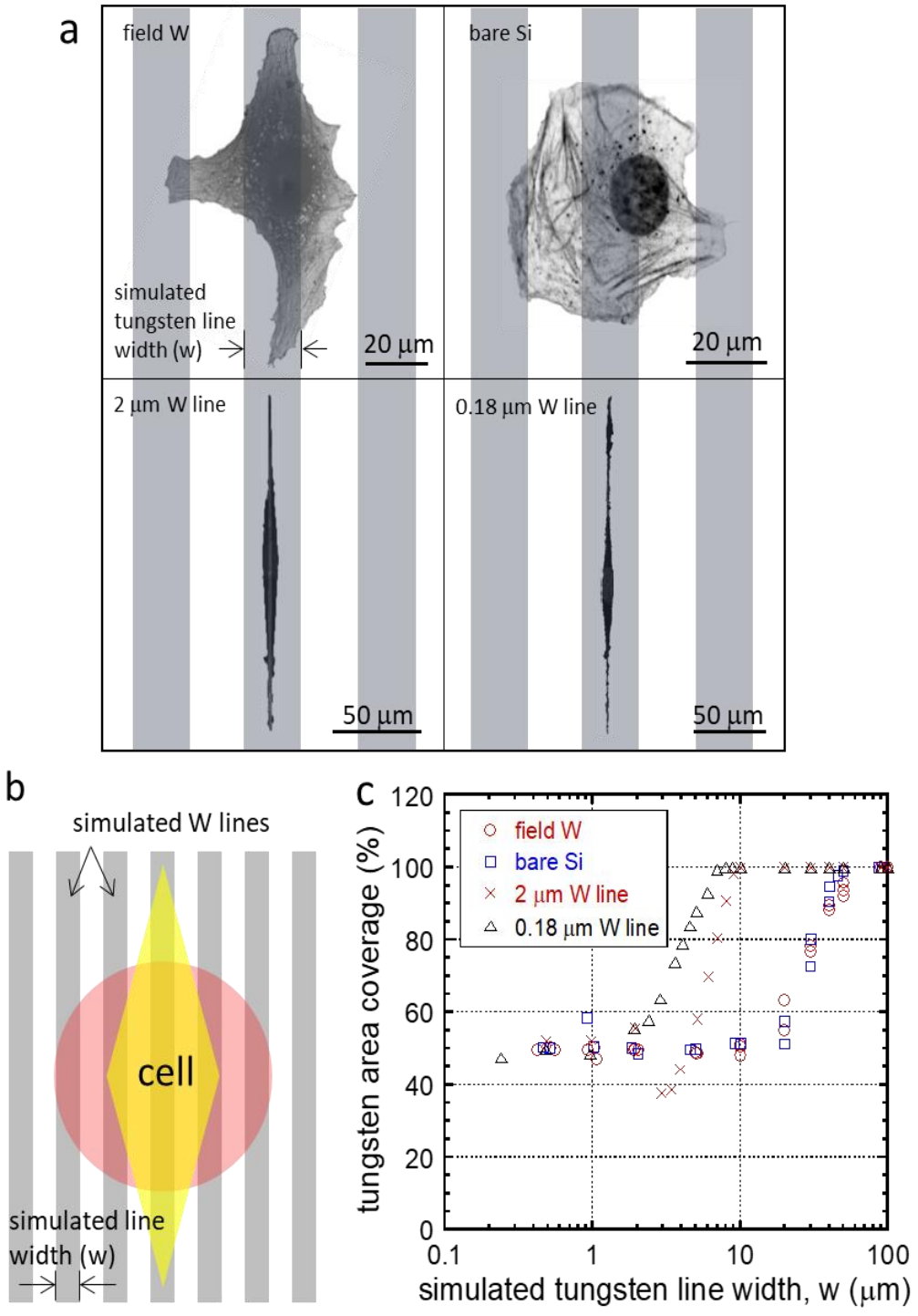

Figure 3-10 (a) Cells with different morphologies on field W, bare Si, 2.0 µm, and 0.18 µm wide isolated tungsten lines overlaid on simulated W (gray) and SiO_2 (white) lines. (b) A representative diagram of the orientation of cells compared to the simulated W and SiO_2. (c) The tungsten coverage area on a cell plotted as a function of simulated tungsten line widths (w) (Moussa et al., 2017).

Figure 3-10(c) shows that for the randomly-shaped cells such as the ones observed on field tungsten and bare silicon (Figure 3-10(a)), the cell covered ~50 % of the tungsten lines when placed on the simulated tungsten lines with widths smaller than 10 μm. The cell-tungsten coverage was observed to increase with the increase in the width of the tungsten lines wider than 20 μm. Cells were found to be in full contact with tungsten lines 100 μm wide, at which point the entire cell was in contact with tungsten. On isolated tungsten lines, the elongated-shaped cells showed ~50 % coverage when simulated metal lines were smaller than 2 μm wide. This value is similar to that observed on randomly oriented cells, but with tungsten lines thinner than 10 μm. This finding indicates that cells will not benefit from deforming their geometries to elongate and fully fit within these tungsten lines to increase the cell-tungsten contact area. However, on lines with widths of ~6-10 μm, the elongated cells showed an increase in the cell-tungsten area to about 70 %. This coverage percentage is considerably higher than that of the irregular shaped cells. Therefore, on tungsten lines ~2 and 10 μm wide, cells will substantially benefit from deforming their geometries to align along the tungsten lines, as illustrated in Figure 3-10(c). However, for tungsten lines larger than 10 μm, cells will tend to be in full contact with metal lines.

This finding is consistent with the experimental data, which indicates that cells on field tungsten and field oxide are randomly oriented with irregular geometries; however, on comb structures of 0.18 μm tungsten lines width and beyond, cells show the tendency to align in the direction parallel to the metal lines y-axes, where alignment rate peaks at ~10 μm lines width comb structures. Beyond this critical line width, cells tend to orient themselves randomly.

3.3.1.3 Time-Dependent Cell Alignment

Figure 3-8 provides a snapshot of the preferential adhesion and alignment behavior of Vero cells on the 2D W/SiO_2 substrate after 24 hours of incubation time. The change in the behavior of the adherent cells over the time course of the experiment is still ambiguous. The literature discussed in Table 2-2, Section 2.3.1, provides overall information on the different phases involved in the interaction between biological cells from a bulk phase (cells in the culture medium) and the substrate, but not the change in the behavior of cells in detail. Thus, to understand these changes, this section will assess the attachment and alignment behavior of Vero cells on 10x10μm W/SiO_2 comb structure (Figure 3-2(d)) throughout the time course of 49.25 hours, the total incubation period of the experiment. Each of these 10x10μm comb structures occupies an area of ~ 1.8mm^2. The experiment was performed using Vero cells incubated with an initial concentration of ~0.5×10^5 cells/mL on ten 2D W/SiO_2 substrates; each incubated for one of the following times: 0.5, 1.25, 2.25, 4.3, 6, 8.25, 12.2, 26, 36.2, and 49.25 hours. In total, 2,702 cells were

manually measured using the characterization method described in Figure 3-6, Section 3.2.4. The 70^{o} tilted SEM micrographs of the adherent cells after each of the incubation periods are revealed in Figure 3-11 (Moussa et al., 2017). Images show a step-by-step change in the morphology and alignment of the adherent cells over the time course of the study, from initial seeding until the end of the incubation period. After the initial seeding of cells and for a period of ~0.5 hours, the adherent cells maintained a dense spherical shape with small cytoplasmic extensions projected out onto the surface. These observations are consistent with findings by Chierico et al. (2014), Khalili and Ahmad (2015), and Grolas and Vogler (2010). After one hour of incubation, cells tended to spread over the W (light grey) and SiO_2 (dark grey) parallel lines without a preferential direction, covering individually in some cases up to three or more metal lines. SEM images show cytoplasmic projections preferentially extended on the W lines rather than on SiO_2. Such behavior became dominant with time. After eight hours, cells showed a tendency to retract perpendicularly toward the W and SiO_2 line axes. However, the cytoplasmic projections were observed to extend further along the tungsten lines.

This tendency continued to be in effect after 26 hours of incubation, while a significant portion of the adherent cells came in contact with one or two tungsten lines. Between 36 hours of incubation time and the end of the experiment at 49.25 hours, cells were found to be elongated and aligned in the direction of the W metal lines and in full contact with them in a preferential adhesion behavior. Additional 70° tilted SEM images further describe the change in the morphology and alignment behavior of Vero cells on 10x10 μm comb structures as a function of time from 0.5 hours (incubation time) to 49.25 hours (end of incubation period) similar to Figure 3-11 is demonstrated in Appendix B, Figure S2.

Observations from Figure 3-11 were quantitatively assessed, and the percentage of cells aligned parallel in to the W lines y-axes on 10x10μm comb structures as a function of time was plotted as illustrated in Figure 3-12. In total, 2,702 adherent Vero cells were characterized. Results show an increase in the alignment of cells between 0.5 and 2:25 hours, followed by a decrease between 4.30 and 12.2 hours, and then an increase, where cells' alignment rate peaks at 36.2 hours of incubation time, followed by a drop in the alignment rate at the end of the experiment at 49.25 hours.

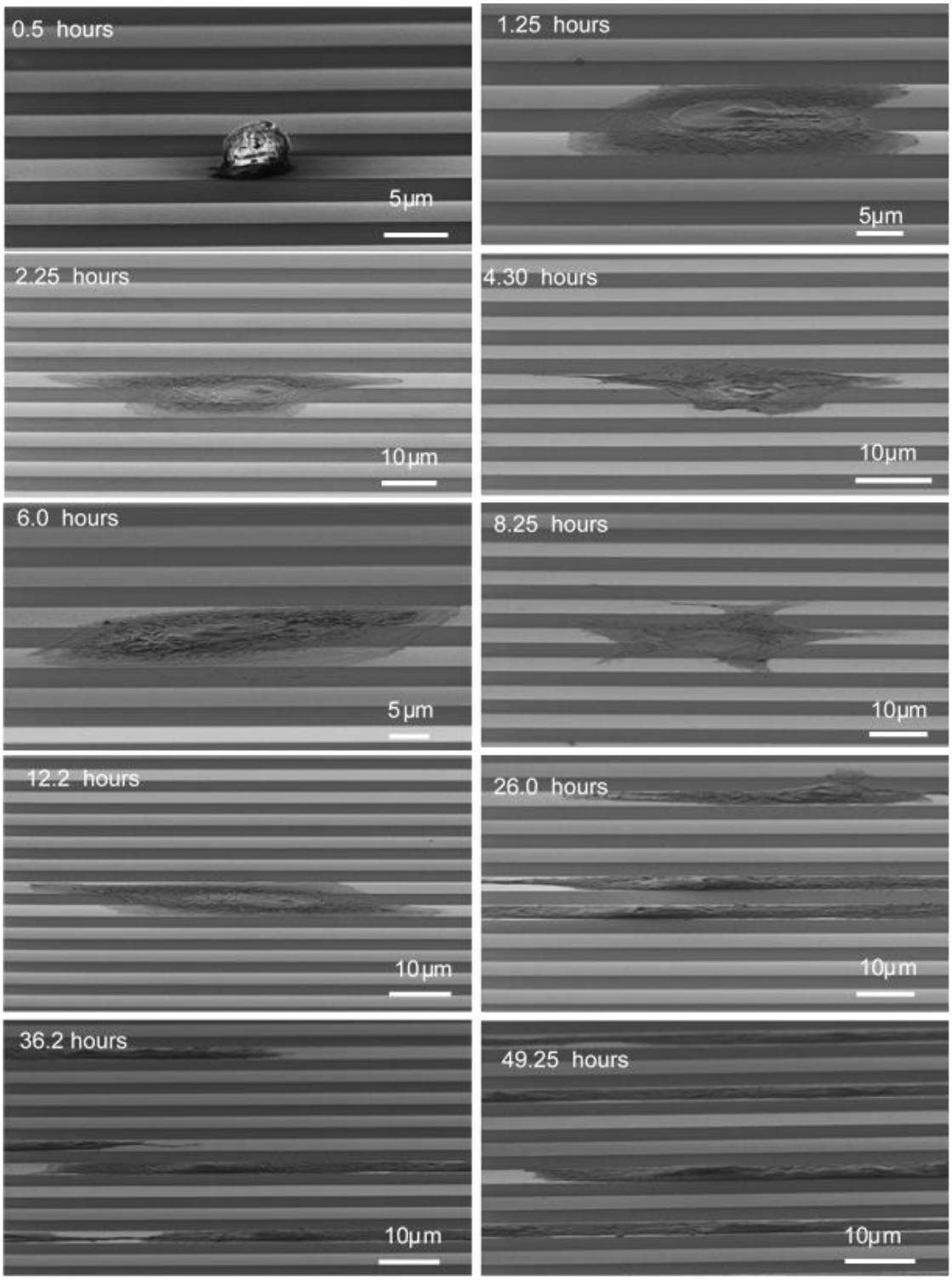

Figure 3-11 SEM 70^{o} tilted micrographs of Vero cells at different incubation periods on 10x10 µm comb structures. The time of 0.5 hours is the initial seeding time and 49.25 hours represent the end of the incubation time.

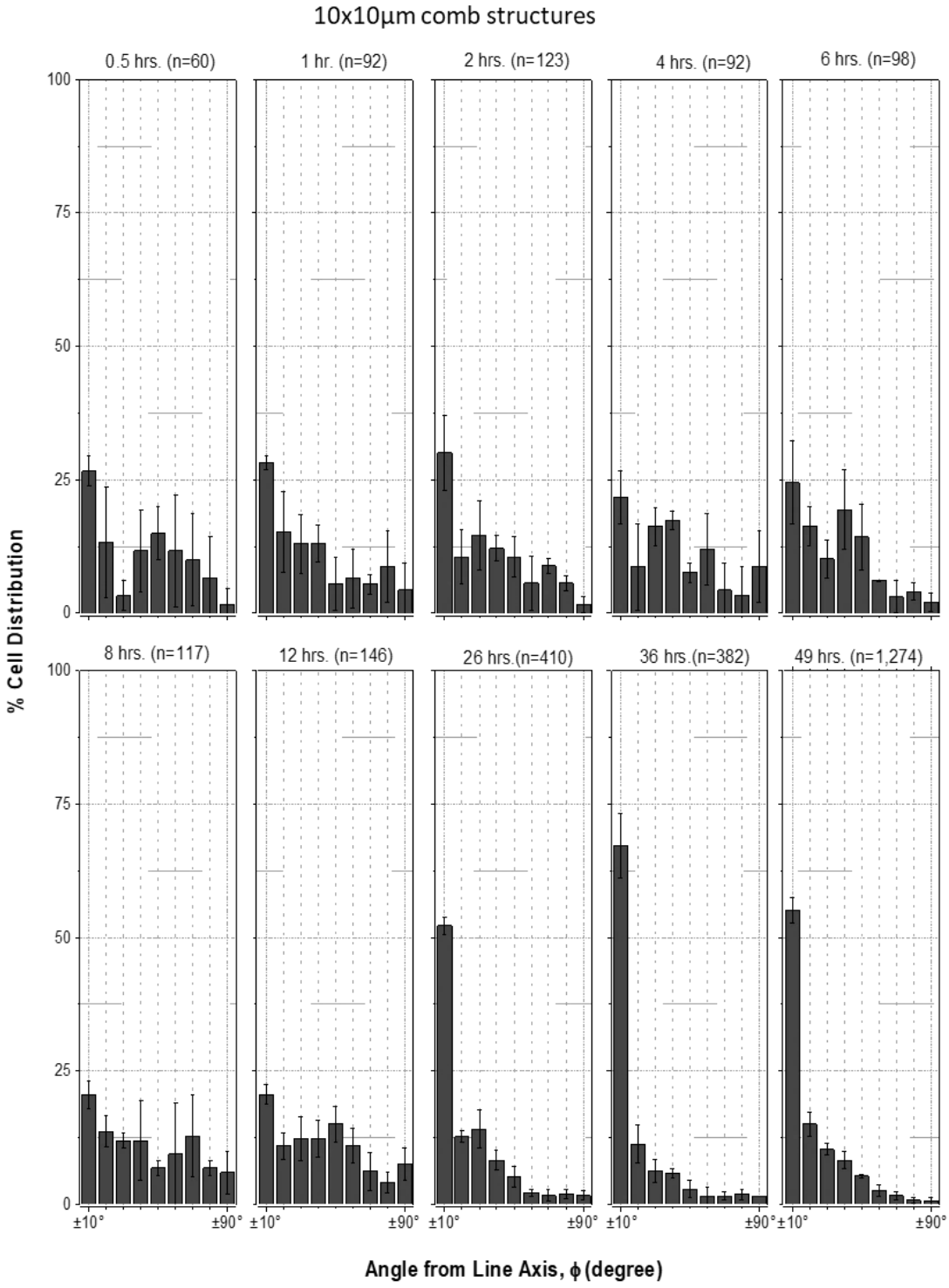

Figure 3-12 Percentage of cells aligned parallel to the W lines on 10x10 µm comb structure as a function of incubation time. The time of 0.5 hours represents the initial seeding time, and 49.25 hours is the end of the incubation period. The number of inspected cells is n. Error bars correspond to one standard deviation.

The quantitative data from the time-dependent cell adhesion experiment (Figure 3-13) show an increase in the number of cells on the 10x10 µm comb structures (concentration of cells measured in cell/mm^2) as a function of time as in Figure 3-13. As indicated before, the area of a 10x10 µm comb structure is ~1.8 mm^2. As predicted data from Figure 3-13 confirm the visual observations (qualitatively) of the proliferation behavior of the adherent cells throughout the time-course of this experiment. Data in Figure 3-13 were best fitted by an exponential function with a pre-exponential factor, exponent coefficient, and coefficient of determination (R^2) of 37.71 cells/mm^2, 0.0537, and 0.9445, respectively.

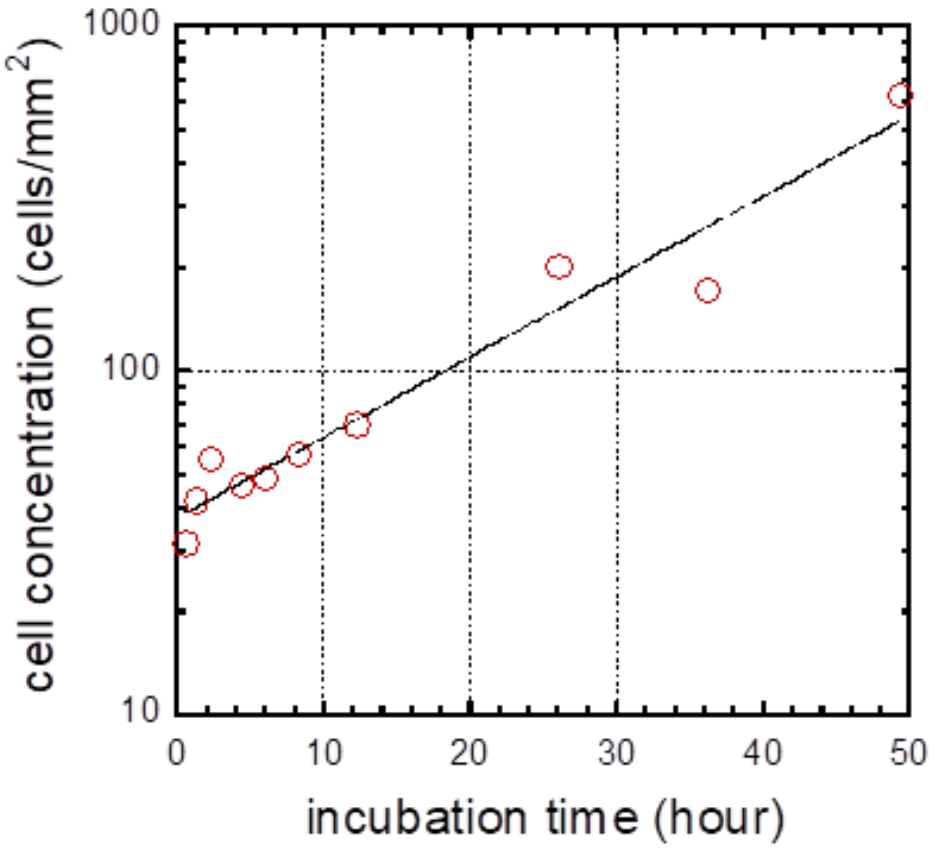

Figure 3-13 The concentration of adherent Vero cells as a function of time on a 10x10 µm comb structure

Additionally, the location of the adherent Vero cells centers (c) as characterized in Figure 3-6 is plotted in Figure 3-14, which shows that more than half of cell nuclei population was located on the tungsten lines at all incubation time. For example, after half an hour of incubation, ~70 % of nuclei adhered to tungsten lines, while the rest to the silicon oxide. This suggested that the preferential adhesion of cells onto tungsten begins shortly after seeding of cells and continues throughout the experiment.

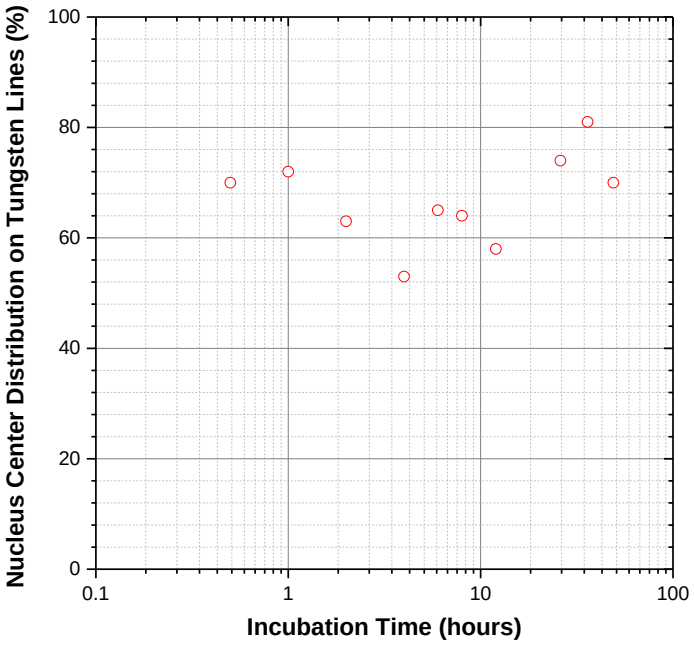

Figure 3-14 Plot of the location of adherent cell nuclei centers on the 10x10 µm W comb structure as a function of incubation time. The location of the center determines whether the cell on metal or oxide line, even if the cell nucleus is spread on multiple W and oxide lines.

3.3.1.4 Culture Media-Dependent Cell Alignment

Section 3.3.1.3 demonstrated that incubation time is one of the significant parameters that can induce a preferential cell-tungsten lines attachment behavior mainly on 10x10µm tungsten comb structures. As listed in Table 2-1, there are some driving forces that may individually or collectively play an important role in altering the cell-substrate attachment behavior in general and cell-tungsten in particular. This section will focus on the effect of different culture media and the concentration of protein within them, on promoting a preferential cell-tungsten adhesion behavior. The adhesion of protein molecules plays a critical role in enhancing the cell-substrate interaction behavior (Teixeira et al., 2003). However, the surface energy, surface roughness, and the ability of the surface to adsorb proteins play an essential role in the overall cell-substrate interaction (Rabe et al., 2011; Schmidt et al., 2009; Hobertt, 2004). Researches by Parhi et al. (2009), Baszkin and Lyman (2004), and Hallab et al. (2001) highlighted that in general substrates with higher surface energy promote higher cell-substrate interaction. Thus, it is important to remind the reader about essential facts concerning the surface properties of chemical-mechanical polished tungsten surfaces. Tran et al. (2016) indicate that W has a surface energy of ~3.3 J/m^2, one of the highest surface energies among metals. This value is more than 100 times greater than the surface energy of virgin (0.0272 J/m^2) and chemical-mechanical polished silicon oxide (0.0296 J/m^2) as

reported by Thomas et al. (1996). As a result, one can claim that this is one of the reasons for the preferential adhesion behavior of cells on tungsten CMP structures. Also, the surface roughness of the chemical-mechanical polished W surfaces in comparison to SiO_2 surfaces is probably another factor in the preferential adhesion behavior of cells on the substrates understudy. The results of the surface characterization using AFM, which are discussed in 3.2.2.2, indicate that the tungsten CMP surfaces have an average root-mean-square (RMS) roughness of ~0.44 nm that is ~ 1.7 times higher than average roughness of the chemical-mechanical polished SiO_2 surfaces (~0.26 nm) on the same substrates. Khan, Auner, and Newaz, (2005) studied the ideal roughness of silicon oxide substrate for the adhesion of neural cells in particular. Findings indicate that the surface roughness (R_a) must fall in between 20 and 100 nm. Considering the different type of cells used in the current study (Vero cells), this is the factor that needs to be taken into account, especially the polished SiO_2 used falls out of the range indicated in Khan et al. (2005). The effect of roughness on the adhesion of protein claim came in agreement with the findings of other scholars (Khalili and Ahmad, 2015; Biazar et al., 2011; Khan et al., 2005; Ponsonnet et al., 2003; Hallab et al., 2001; Anselme et al., 2000; Martin et al., 1995), even though, the reported materials (platinum, tantalum, and titanium) were not the same. The surface energy and the average roughness of a substrate affect the hydrophobic and hydrophilic nature of the surface, which eventually influence to a great extent the interaction between cells and a substrate as discussed in Sectio 2.4.1 based on literature by Zhang and Webster (2013), Ruggeri and Jackson (2013), Vogler (2012), Rabe et al. (2011), Tighe and Mann (2011), and Michaelis et al. (2011). The contact angles of a DMEM/F12 and 10 % FBS culture media droplet were measured on a bare silicon substrate (with a native thin layer of SiO_2 at the surface) and W/SiO_2 patterned surfaces to be ~50.0° and ~29.7°, respectively. A close-up photograph of a droplet from the culture media on both substrates was taken using a high-resolution camera. A horizontal line was drawn along the surface, and the contact angle Θ was measured using the tangent-method, as the angle between the droplet outline and the horizontal surface line (Extrand, 2016).

We studied and assessed the direct impact of culture media on manipulating the adhesion and alignment behavior of Vero cells on the 2D W/SiO_2 substrates. Vero cells with an initial concentration of ~0.5×10^5 cells/ml were incubated, fixed, and dried using the detailed procedures described in Section 3.2.3.1. The incubation of cells was done for 48 hours in three different culture media. These media differ in the content of serum content. The three media are: (1) 10 % FBS (serum) containing media referred to as "baseline;" (2) ultra-low protein Gibco® OptiPRO™, a serum-free cell culture medium (SFM); and (3) OptiPRO™ with 10 % FBS. FBS contains ~38 mg/mL of proteins and other

active ingredients, such as albumin, creatinine, gamma globulin, glucose, lactate dehydrogenase, and glutamic products. OptiPRO™, the ultra-low protein medium, contains ~7.5 µg/mL of proteins.

The orientation of the adherent cells on 10 µm comb structures, from the three media, were quantified based on the characterization method discussed in Section 3.2.4, and graphed as illustrated in Figure 3-15, excluding data from cells located within the 50 µm region from the inward boundaries of the comb structures in order to eliminate the edge effects on the alignment of cells. Each of the bars represented the fraction of adherent cells (as a percentage of the total number on the cells assessed on the 10 µm comb structure) aligned in an angular interval in the range of ±10° from line axis of the nucleus. If a cell aligned with an angle ϕ of ±11°, would be automatically added to the second group of bins, which consisted of a population of aligned cells with an angular interval of $\pm 10° < \phi \leq \pm 20°$. Error bars indicate one standard deviation from three groups of measurements.

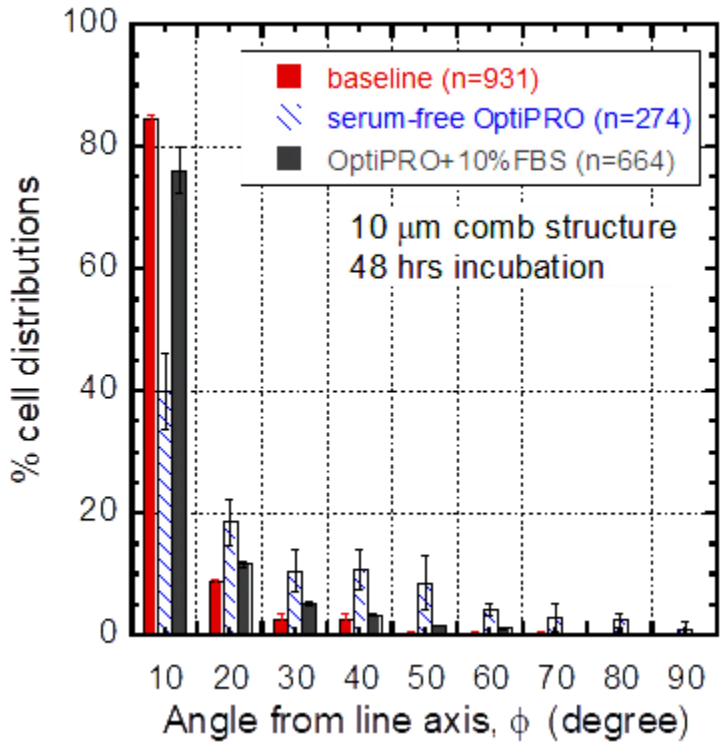

Figure 3-15 Distribution of adherent Vero cells orientated on 10 µm wide W lines comb structure cultured in the baseline, OptiPRO™, and OptiPRO™ + 10 % FBS culture media. (n) Denotes the number of the cells measured, excluding those around the edge and situated inward within the 50 µm region from the boundary of the comb structures to avoid the edge effect. Error bars indicate one standard deviation from three groups of measurements (Moussa et al., 2017)

Alignment data from cells incubated in 10 % FBS culture medium (the baseline) indicates that ~85±1% of adherent cells fall in the range of ±10°, and this percentage falls by ~50 % to become ~40±6 % for

cells incubated in OptiPro™. The drop in the percentage of cells aligned in the range of ±10° is accompanied by a critical drop in the number of assessed cells from 931 cells to 274 cells, respectively. Remarkably, the alignment rate of the incubated cells in the range of ±10° tends to grow drastically to ~76 ± 4 %, while the number of assessed cells increases to 664 cells when incubated in OptiPRO + 10 % FBS culture media. These numbers demonstrate the essential role of fetal bovine serum (FBS) as a source of protein in the culture medium proves its ability to induce a preferential cell alignment behavior on the assessed 2D W/SiO2 patterned substrates. Thus, it is acceptable to say that the cellular preferential alignment on the W/SiO_2 micron and sub-micron patterned scale substrate is not only dependent on tungsten line widths, as demonstrated in Figure 3-9, but also on serum. This means that cells can recognize a surface by sensing the protein(s) adsorbed on it as indicated by Wilson, Clegg, Leavesley, and Pearcy (2005). The enhancement in the rate of alignment and number of adherent cells in the baseline (1) and 10 % FBS containing OptiPRO (3) culture media is regarded to the existence proteins and growth factors on the tungsten lines prior to cell adhesion on the same substrates. Results come in agreement with findings by Fang, Wu, Fang, Chen, and Chen (2017); Petiot et al. (2010); de Oliveira Souza, da Silva Freire, and Castilho (2005); Teixeira et al. (2003); Matsushita, Kawakubo, Sawano, and Funatsu (2000); and Miyamoto, Izumi, Ishizaka, and Hayashi (1989) in which a change in the behaviour of incubated cells in terms of growth patterns and alignment when using serum-free media or FBS alternative media, respectively.

It is a common practice in literature to supplement cell culture media with bovine serum (FBS), serum albumin (human or bovine), and ECM proteins (e.g., fibronectin, collagen, and laminin) to experimentally induce specific biological changes such as proliferation, and differentiation (Poudel et al., 2015; Felgueiras , Evans , and Migonney, 2015; Nakamoto et al., 2014; Xu and Mosher, 2011; Aubin et al., 2010; Fujita et al., 2009; Vaidya a and Ofoli, 2005; LeBaron and Athanasiou, 2000; Steele, Johnson, and Underwood, 1992; Underwood and Bennett, 1989). Thus, Chapter 4 will study and evaluate in detail the role of individual protein components of fetal bovine serum (FBS) on the alignment behavior of cells.

3.3.1.5 Mechanically Reworked Dependent Cell Adhesion

The W-CMP specimens used in this work were fabricated using a chemically and mechanically robust fabrication technique. As demonstrated in Section 3.2.1 and Section 3.2.2, the surfaces of the 2D W/SiO2 substrates are smooth and defect-free. Hence, it is possible to remove fall-on particles, residues, or other contaminants using mechanical rubbing without compromising the integrity and effectiveness of the surface. This post-CMP cleaning procedure is a common practice in the semiconductor industry, which is

widely used to improve the production yield and the quality of the final surfaces (Keswani and Han, 2015). This post-CMP cleaning technique provided this work with a unique advantage of substrate workability and reusability. The mechanical workability of the 2D W/SiO_2 substrate was tested using, quail fibrosarcoma cells (QT-35) obtained from the European Collection of Authenticated Cell Cultures (ECACC). These cells served as controlled adherent cell contaminants and were deposited on virgin W-CMP comb structures. QT-35 cells were incubated for 24 hours using the incubation, fixation, and dehydration protocols described in Section 3.2.3.4. The initial concentration of QT-35 cells used in this experiment was ~ $0.5x10^5$ cells/mL. The dehydrated specimens were stored in a high purity nitrogen environment for four days. This was done to simulate typical cell alignment experiments and SEM specimen storage conditions.

Quail tail cells were removed from the substrate by manual scrubbing using regular size cotton balls (Equate Brand from Walmart, Canada) and wetted with deionized water. The manual rubbing process was conducted under ambient conditions in a wet lab (no cleanroom environment). The substrates were then rinsed by ethanol and dried using high purity nitrogen. The process will supposedly be able to remove all the adherent cells. The effectiveness of the mechanical rubbing process in removing the adherent QT cells was confirmed by examining the cleaned substrate using an optical microscope. Figure 3-16(a)-(b) compares the results of the contaminated specimens before (left column) and after (right column) the cleaning process of three comb structures with W and SiO_2 parallel line widths of 10x10 µm, and 0.18x0.18 µm. It is evident that all adherent cells were removed by the simple cleaning process used, with no visible damage, patterns distortion, scratches, and residues. This demonstrated the mechanical workability and reusability of the tested substrates.

However, to prove that the cleaning process did not affect the properties of the cleaned substrates, Vero cells were deposited on these cleaned surfaces with an initial concentration of ~$0.5x10^5$ cell/mL and incubated for 48 hours on these cleaned substrates using the same protocol discussed in Section 3.2.3.1. The orientation and alignment behaviors of the adherent Vero cells were characterized using the standard method described in Section 3.2.4 and used throughout this work. Results were compared with data from the baseline sample characterized in Figure 3-15, Section 3.3.1.1, and illustrated in Figure 3-17.

Figure 3-17 illustrates the alignment results of both, the baseline and reworked substrates. The total number of cells assessed in this experiment was slightly over 9,000 cells. Results from the comparison outcomes indicate that adherent cells on all assessed structures showed a similar orientation and alignment behaviors before (control sample) and after (reworked sample) cleaning. Cells adherent on to field tungsten and 0.18x0.18 µm comb structures exhibited no preferential orientation or alignment

behavior, as was expected. In contrast, cells on the 10x10 µm comb structures tend to align in parallel to the tungsten lines y-axes preferentially. The accumulative percentage of cells aligned within ±20° (this include cells aligned in both ±10° and ±20°) on both of the samples, control, and reworked samples were measured to be ~93 ± 1 % and ~97% ± 1 %, respectively.

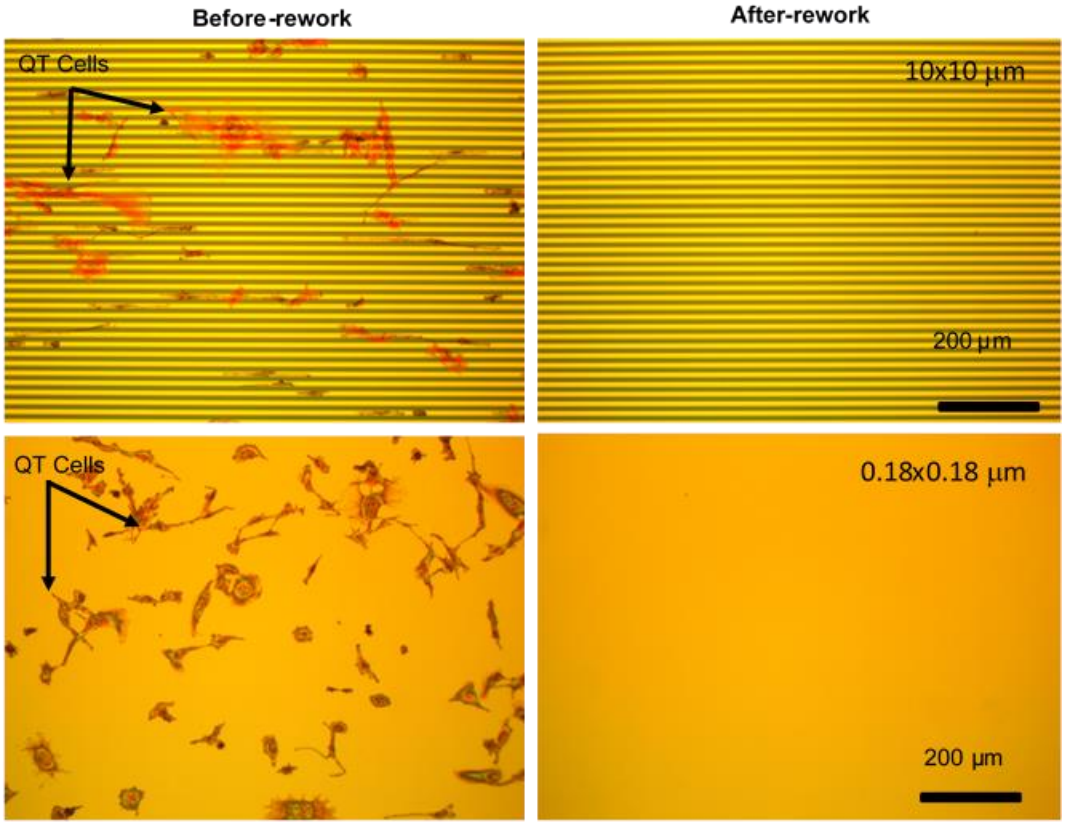

Figure 3-16 Comparison between comb structures prior and after the rework and cleaning process performed on tungsten and SiO_2 parallel lines comb structures with (a) 10x10 µm, and (b) 0.18x0.18 µm.

This indicates that the cleaning technique proposed and executed had no negative impact on the mechanical and physiological performance of the substrates understudy. Cleaned substrates demonstrated their ability to induce a preferential cell-substrate interaction, especially on 10x10 µm comb structures in a trend similar to their ability before cleaning. In spite of the different intended applications, it was proven that maintaining the performance of the 2D W/SiO_2 substrates used in this study is possible without the need for the technologically advanced and highly expensive processes that are often used in large-scale manufacturing to clean substrates and increase the production yield as demonstrated in the two patents by Inbe (2004) and Shih and Tuw (2000). To our best knowledge, this is the first time in literature in which a

patterned substrate that is pre-used for manipulating the behavior of cells regained its functionality and workability after a mechanical cleaning process that is simple and chemical-free (besides ethanol).

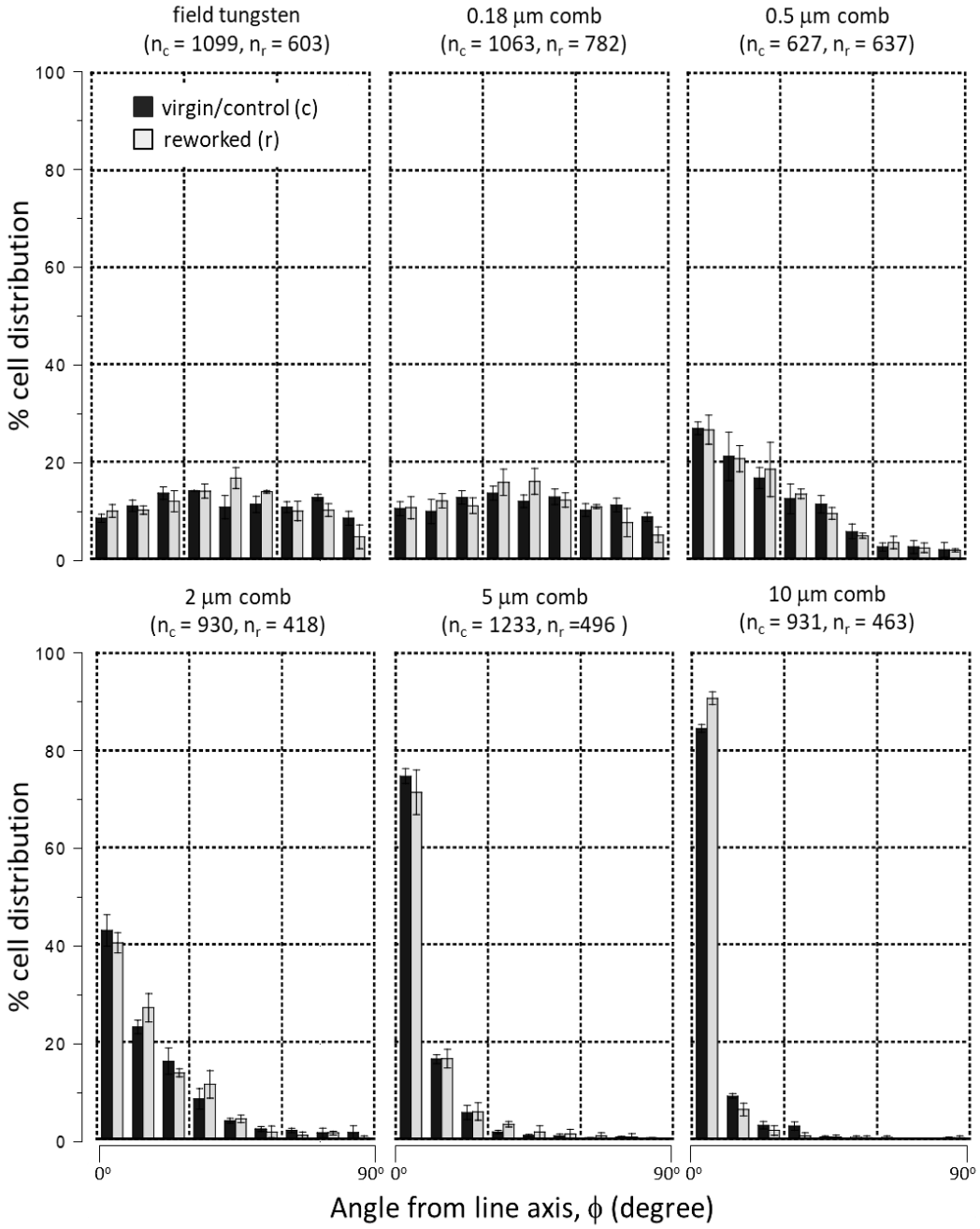

Figure 3-17 Orientation of adherent Vero cells on control (c) and reworked (r) substrates. The values n_c and n_r refer to the numbers of cells assessed on the different comb structure on both clean and reworked samples. Error bars correspond to one standard deviation. The initial concentration of cells is 5×10^4 cells/mL (Moussa et al., 2017).

3.3.1.6 Asymmetrical Line Widths Dependent Cell Alignment

This section looks at the effect of asymmetric tungsten and silicon oxide line widths in the comb structures on the alignment behavior of Vero cells.

In the previous sections, the focus was on assessing the change in cellular behavior of Vero cells adherent to 2D W/SiO_2 micron and sub-micron scale patterned substrates with symmetrical parallel line comb structures. Similar substrates with equal parallel line width geometries are often reported in the literature to induce a preferential cellular behavior (Moussa et al., 2017; Ning et al., 2016; Teixeira et al., 2006). Nevertheless, the characterization of cell behavior on symmetrical geometries failed to prove whether the tungsten or silicon oxide lines were responsible for driving the preferential behavior of cells. This is critical to design and develop active substrates that can yield the highest preferential alignment rate among the population of adherent cells under study.

The 2D W/SiO_2 substrate used in this section was prepared identically to the substrates prepared and characterized, as discussed in Sections 3.2.1 and 3.2.2. However, unlike the symmetrical comb structures, the 2D W/SiO_2 substrate used in this section consists of asymmetrical alternating W, and SiO_2 lines range from 1 to 100 µm. Figure 3-18 reveals the typical top-down scanning electron images of some asymmetric grids.

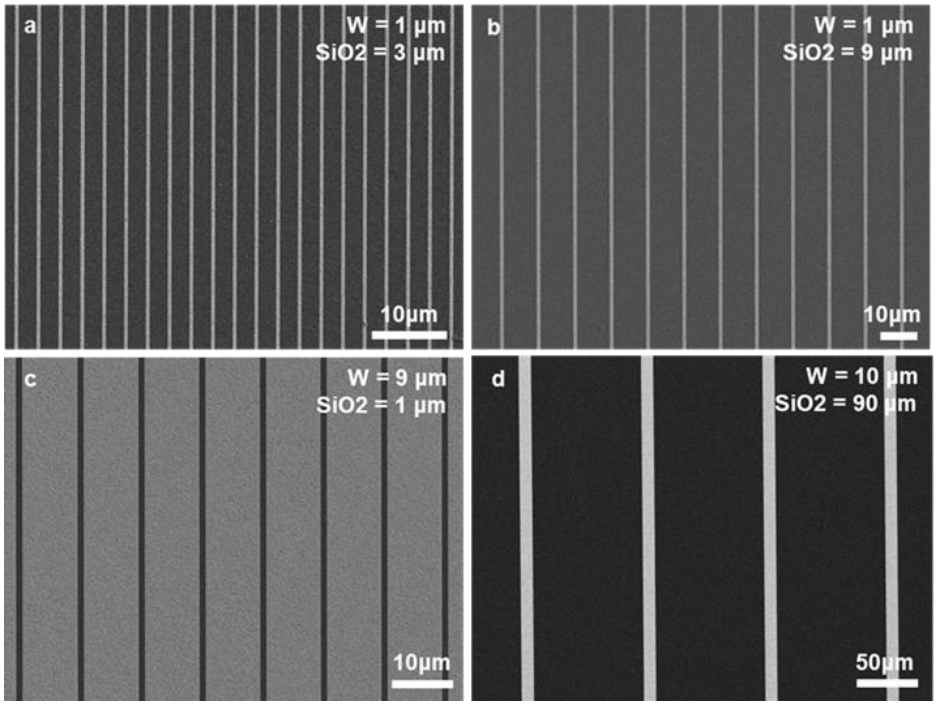

Figure 3-18 Typical scanning electron micrographs of alternating tungsten (light gray) and silicon oxide (dark grey lines with widths of (a) 1x3 µm, (b) 1x9 µm, (c) 9x1 µm, and (d) 10x90 µm.

The mammalian Vero cells used in this section were cultured, fixed, and dehydrated using the protocols discussed in Section 3.2.3.1.

Scanning electron images show the morphology of adherent cells on asymmetric (complex) line patterns as published in Figure 3-19. The SEM micrographs on the left from (a) to (e) show comb structures containing tungsten lines with fixed widths of 1 μm with alternating silicon oxide lines with increasing widths of (a) 3 μm, (b) 5 μm, (c) 9 μm, (d) 50 μm, and (e) 100 μm. These micrographs demonstrate a trend of increasingly aligned cells in the direction of the tungsten lines y-axes as the width of the silicon oxide line increases. In contrast, cells on structures with the same line geometrical patterns, but with inverted material widths, show a weak orientation preference, as demonstrated in Figure 3-19(f) – (j). These structures hold a 1.0 μm wide silicon oxide line and various tungsten line widths of (f) 3 μm, (g) 5 μm, (h) 9 μm, (i) 50 μm, and (j) 100 μm. Observations denote the importance of the alternating tungsten and silicon oxide width on manipulating the morphology of cells.

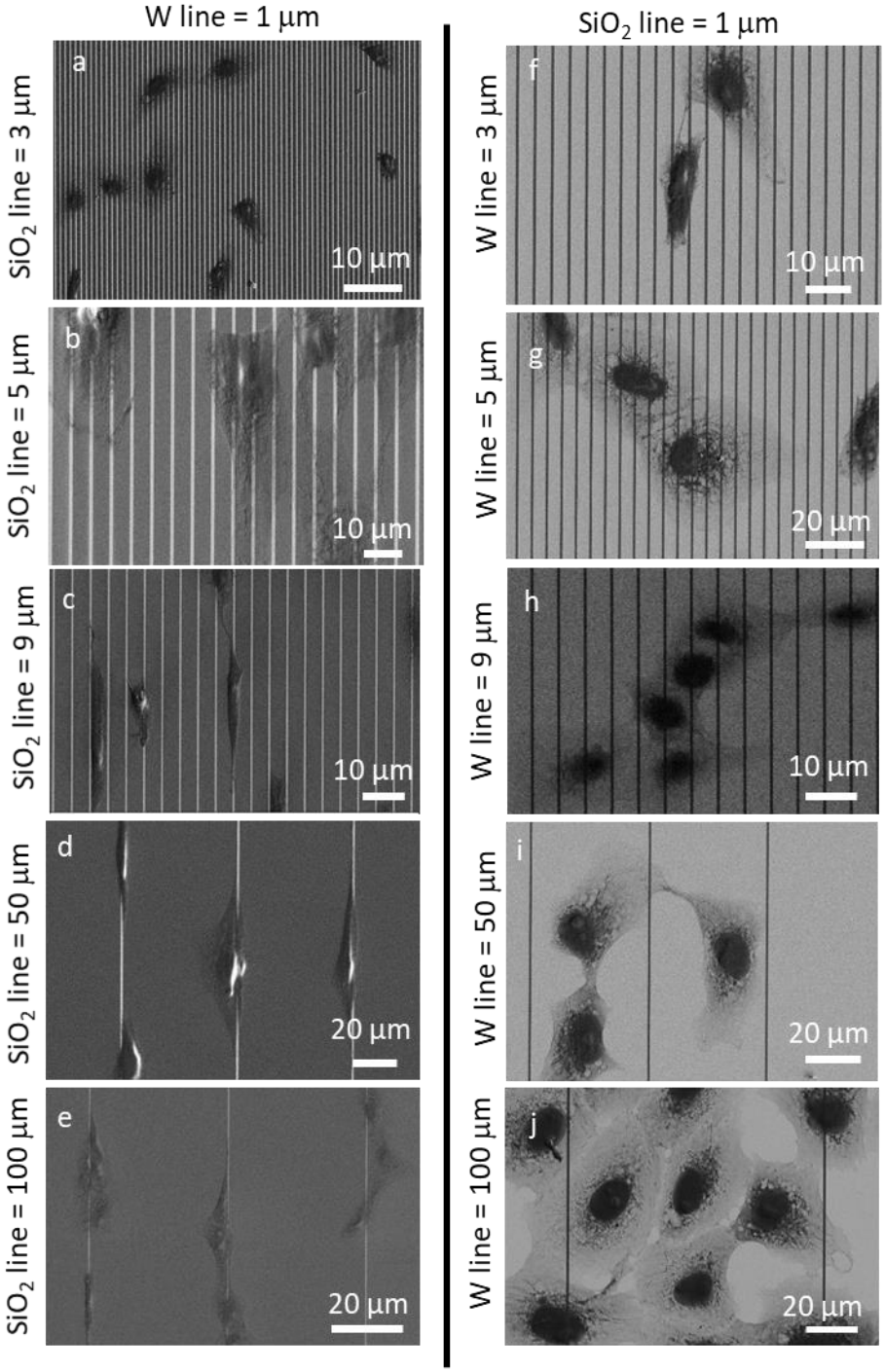

Figure 3-19 SEM micrograph of adherent cells on comb structures with different combinations of tungsten and silicon oxide line widths. (a-e) Substrates with a fixed tungsten line width of 1 µm and silicon oxide line widths of (a) 3 µm, (b) 5 µm, (c) 9 µm, (d) 50 µm, and (e) 100 µm. Additional substrates consist of fixed 1.0 µm silicon oxide lines and tungsten lines with widths of (f) 3 µm, (g) 5 µm, (h) 9 µm, (i) 50 µm, and (j) 100 µm.

To quantify the observations from Figure 3-19, the percent of cell population was oriented within ±20˚ of W line axes as a function of SiO_2 line widths, and the percent of cell population was oriented within ±20˚ of SiO_2 line axes as a function of W line widths, are presented in Figure 3-20 (a) and (b), respectively. The total number of cells (n) measured in (a) and (b) is included in the corresponding plot.

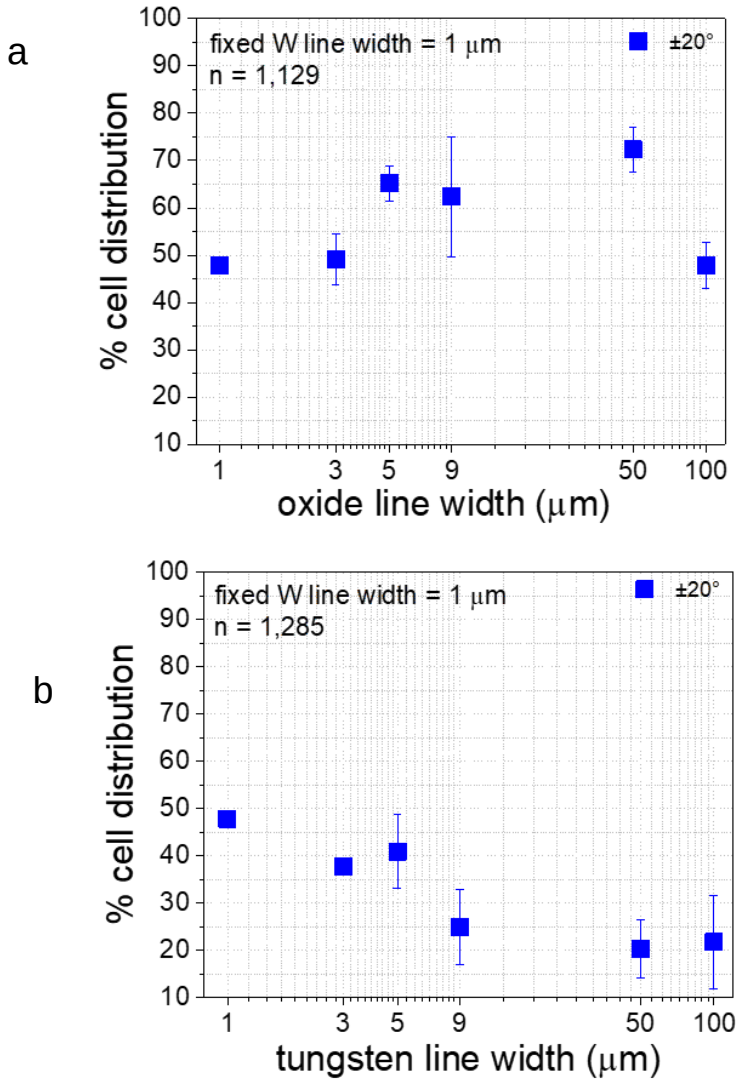

Figure 3-20 (a) Percent of cell population oriented within ±20° of the tungsten line y-axes as a function of silicon oxide line widths. (b) Percent of cell population oriented within ±20° of the silicon oxide line y-axes as a function of tungsten line widths. Error bars correspond to one standard deviation from three independent data groups.

Figure 3-20 shows the results of the orientation of adherent Vero cells on 2D W/SiO_2 substrates with asymmetric comb structures with (a) 1 μm fixed W lines and varying SiO_2 line widths (1-100 μm), and (b) 1 μm fixed SiO_2 lines and varying W line widths (1-100 μm). As a point of reference, the results from

the 1x1 μm (symmetric) comb structure are also included in both figures (a) and (b). Results from Figure 3-20(a) show that 72.3±4.8 % of cells aligned within ±20˚ of the tungsten line y-axes for SiO_2 spacing of 50 μm, and fixed-width tungsten lines of 1 μm.

On the contrary, the alignment performance of adherent Vero cells on asymmetric comb structures with a fixed silicon oxide lines of 1 μm, and varying W line widths were lower in magnitude at 40.9±7.8 % of cells aligned within ±20˚ of the SiO_2 line y-axes for W spacing of 5 μm, as shown in Figure 3-20(b).

Results from Figure 3-20 (a)-(b) indicate that the alignment and change in the morphology of adherent cells are more sensitive to silicon oxide line widths rather than tungsten lines. This further demonstrates the role of material placed in a defined surface pattern in the alignment behavior of adherent cells. A significant difference in cellular behavior is observed when material placement is inverted. Table 3-5 summarizes the results of Section 3.3.1.6.

Table 3-5 Adherent cells alignment behaviors on asymmetric patterned comb structures.

Line Width (μm)		Cell Counted (n)	% Cell Alignment within the range of Φ = ±20°
Tungsten	Silicon Oxide		
1	1	299	47.8 ± 1.6
1	3	171	49.1 ± 5.3
1	5	164	65.2 ± 3.7
1	9	205	62.4 ± 12.7
1	50	155	72.3 ± 4.8
1	100	135	47.8 ± 4.8
3	1	201	37.8 ± 1.7
5	1	193	40.9 ± 7.8
9	1	169	24.9 ± 7.9
50	1	187	20.3 ± 6.2
100	1	236	21.7 ± 9.9

Note: Tungsten and silicon oxide line widths varied independently in the range of 1 and 100 μm. Alignment angle ϕ = ±20˚

The mathematical model developed and presented in Section 3.3.1.2 was tested on adherent Vero cells on symmetrical comb structures (with equal line widths of W and SiO_2). The model was useful in predicting the minimum width of tungsten lines on symmetric comb structures required to induce the preferential cellular alignment behavior. However, the model was never tested to predict the alignment behaviors of adherent cells on asymmetrical structures, with unequal line widths of W and SiO_2. Results from

Figure 3-20 and Table 3-5 indicate that the alignment behavior of the adherent Vero cells was found to be dependent on silicon oxide linewidth for asymmetric comb structures with fixed W lines and variable SiO_2 line widths. Nevertheless, the minimum width of SiO_2 lines at which the preferential alignment behavior could be induced is still unknown. Thus, the mathematical model developed and used in Section 3.3.1.2 was used to calculate the percentage of a cell area that is in contact with simulated tungsten lines on various patterns. Illustrations of the two potential cell geometries used in this section are presented in Figure 3-21. Two potential cell geometries were considered and modeled: (1) irregular cell geometry as illustrated in Figure 3-21 (a)-(b) and (2) elongated cell geometry as demonstrated in Figure 3-21(c)-(d).

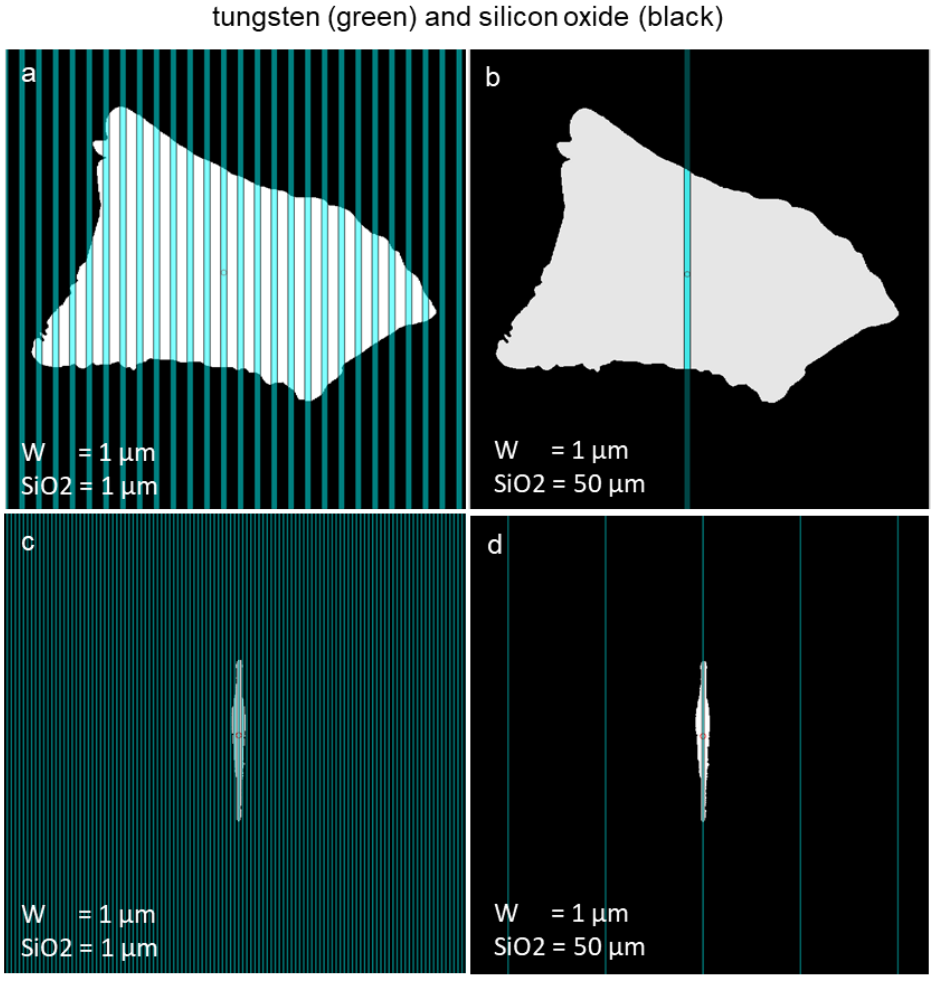

Figure 3-21 Representative images of cell figures on simulated asymmetric W/SiO_2 lines generated from the mathematical model used to calculate the portion of cell area on W lines (green) and SiO_2 lines (black). Irregular-shaped and elongated cell models are displayed in (a-b) and (c-d), respectively. (a, c) Modeled symmetric 1x1 µm comb structures of equal W and SiO_2 lines. (b, d) Asymmetric comb structures with 1x50 µm W and SiO_2.

3.3.2 Human Prostate Cancer (PC-3) Cells

PC-3 cells are stage IV, adenocarcinoma cells that originate in the prostate epithelial tissue (primary site) of a 65 years old Caucasian adult male and spread beyond the prostate to other parts of the body, particularly bones, where they are collected (metastatic site) (ATCC, 2016; Seim et al., 2017; Dolfi et al., 2013; Picollet-D'hahan et al., 2013). PC-3 cells present the aggressive type of prostate cancer cells both *in vitro* and *in vivo* conditions, which are commonly used in literature (Seo et al., 2017; Tai et al., 2011; Dolfi et al., 2013; Surdo and Bauer, 2012; Gaupel et al., 2013). An average size of PC-3 cells was found to be 18.08±2.69 μm as indicated by Nexcelom Bioscience (2013), Surdo and Bauer (2012), and Dolfi et al. (2013). Park et al. (2014) and Lighart et al. (2013) reported a slightly different average size of ~15.21±2.62 μm. The PC-3 cells were chosen for their similarity to Vero cells in terms of cell type/morphology since both are epithelial. Cells were incubated at an initial confluence of $1.5x10^5$ cells/mL using the protocol described in Section 3.2.3.2. The alignment behaviors of PC-3 cells were characterized and conducted in a similar way to the method used for Vero cells and described in Section 3.3.1.1. This experiment was done to understand whether the novel 2D W/SiO_2 micron and sub-micron scale patterned substrate understudy will have the same effect on other epithelial cells.

The alignment behavior of adherent PC-3 cells on the 2D W/SiO_2 substrate was quantified using the same method used for Vero cells and described in 3.2.4. The angle ϕ that exists between the major axis of the elliptically shaped nuclei and the tungsten lines y-axis, as demonstrated in Figure 3-6, was measured for cells adherent on the assessed structures. A total of 2,921 cells were assessed and measured on comb structures with different W/SiO_2 line widths, field tungsten, and field oxide areas. The number of PC-3 cells assessed on each area and comb structure is labeled on each chart as (n). The number of PC-3 adherent cells is ~50 % lower than the number of the Vero cells assessed (n = 5,804) in Section 3.3.1.1. This is consistent with Kwon et al. (2007) and Palmer et al. (2008), who indicated that cancer cells have a lower adhesion in comparison to healthy cells regardless of the substrate topographical features and incubation time.

Results from Figure 3-22 indicate a broad distribution of PC-3 cell alignment behaviors. Only 13.8 % of adherent cells on field oxide and 11.8 % on field tungsten (solid) align in the range of ±10° in parallel to W lines y-axes, indicating that cells have no preferred alignment on these substrates. However, cells showed an increase in the alignment rates from 13.8 % to 70.4 % (peak value) when the width of W lines increased from 0.18 μm to 10 μm, respectively forming an elliptical-shaped cell. A similar observation was reported by Koch et al. (2012), indicating that PC-3 were elongated with spindle-like morphology. However, cells on tungsten lines wider than 10 μm showed a tendency to misalign on 50 μm and 100 μm

W line widths from 26.9 % to 22.3 %, respectively. This was additionally demonstrated in Figure 3-23, in which the cell alignment angle ϕ within ±10° and ±20° of the tungsten lines y-axes were graphed as a function of the tungsten line widths on each assessed comb structure. Such line width-dependence alignment behavior was observed by Joo et al. (2015), Nakamoto et al. (2014), Poudel et al. (2013), and Aubin et al. (2010), in which they reported a peak in the alignment rates of adherent cells when deposited on specific line widths, but these alignment rates showed misalignment on wider or thinner lines. Additionally, the elongation (deformation) in the nuclei shape (described in the L/S ratio, cell nuclei long axis to short axis) was observed to increase until a peak average value for cells adherent on W line with of 10 μm.

The cancerous and non-cancerous cells are different in their cellular behaviors and activities, which may include, but are not limited to, migration potential, cell viability, repair mechanisms, cell-cell communication, and other cellular activities (Ai et al., 2017; Rao et al., 2014; Shaw et al. 2014; Tai et al., 2011; Rao et al., 2010). However, the assessed PC-3 cells showed similar alignment behaviors to the ones observed for Vero cells on the same substrates.

The summary of data from Figure 3-22 and Figure 3-23 is listed in Table 3-6 and includes; tungsten and silicon oxide line widths, cell count on each area and comb structure, cell density, and cells alignment rates within ±10° and ±20° from the lines y-axes.

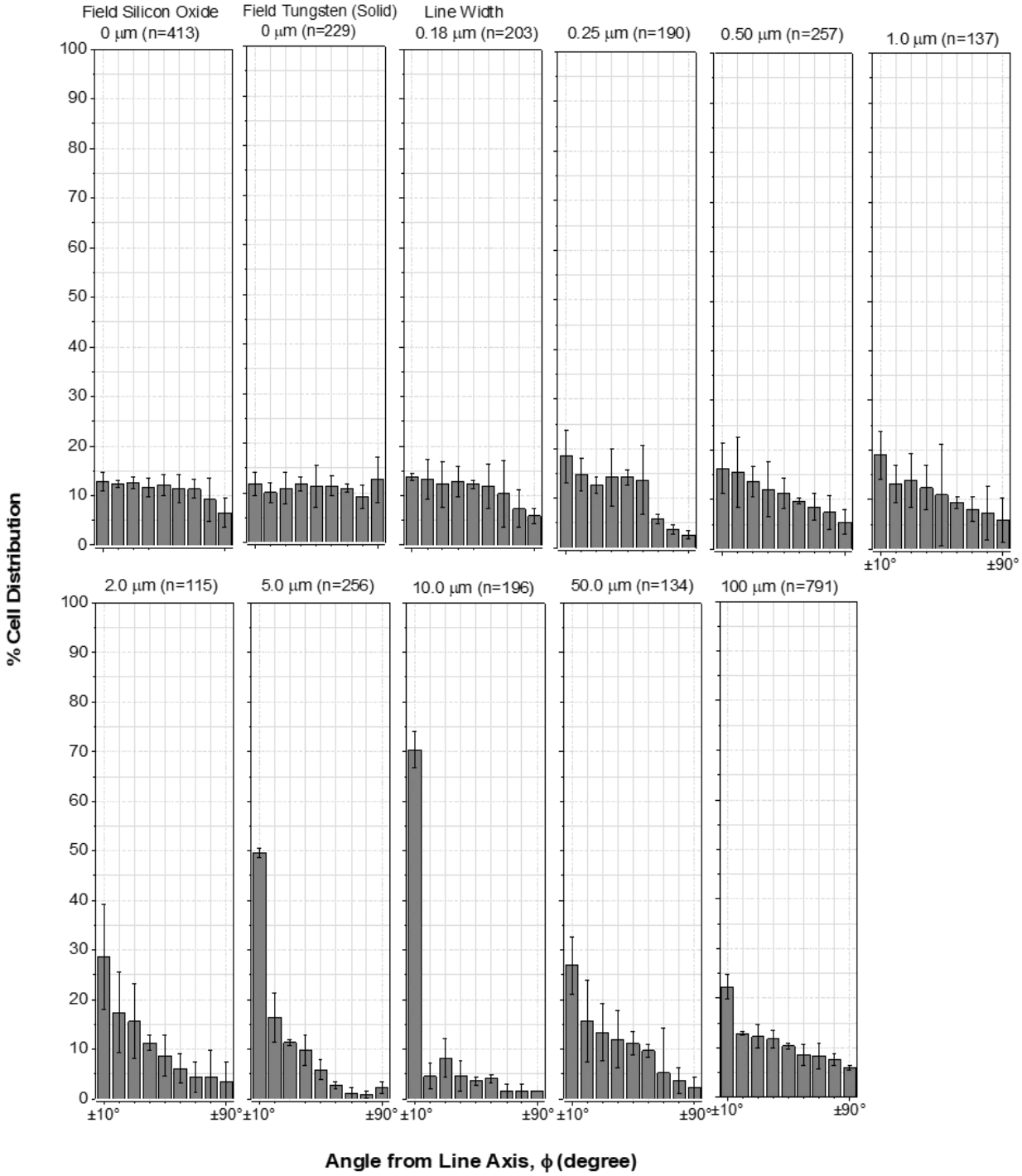

Figure 3-22 Percentage of cells aligned as a function of angle ϕ from line axis and W line width, from 0 μm (field oxide, field W, and bare silicon) to 100 μm. The number of cells inspected in each structure (n). Each bar represents the percentage of cells in a ±10° bin of deviations from the line axis. i.e., a cell with ϕ is +9° would be counted in the first bar from the right in each plot. Error bars correspond to one standard deviation.

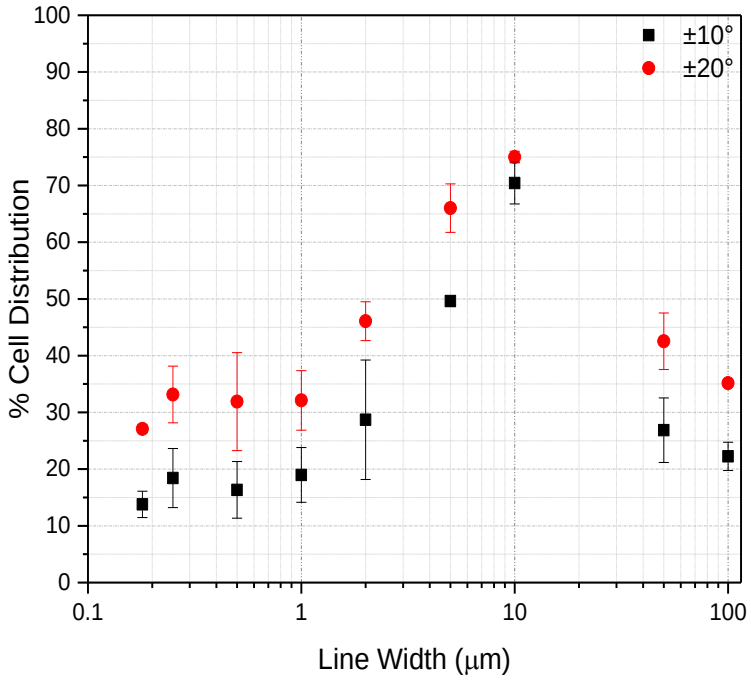

Figure 3-23 Distribution of cell alignment as a function of line width for ±10° and ±20°. Error bars correspond to one standard deviation

Table 3-6 Adherent PC-3 cells alignment behaviors on symmetric patterned comb structures

Line Width (μm)		cell counted (n)	Pattern area (mm^2)	Density ($cells/mm^2$)	% cell distribution ±10°	% cell distribution ±20°
Tungsten	Silicon Oxide					
Field Silicon Oxide (0 μm)		413	-	-	12.8 ± 1.9	25.2 ± 1.6
Field Tungsten (0 μm)		229	1.73	132	11.8 ± 2.3	21.8 ± 0.7
0.18	0.18	203	1.73	117	13.8 ± 0.8	27.1 ± 4.5
0.25	0.25	190	1.73	110	18.4 ± 5.2	33.2 ± 5.0
0.5	0.5	257	1.73	149	16.3 ± 5.0	31.9 ± 8.6
1.0	1.0	137	1.73	79	19.0 ± 4.8	32.1 ± 5.3
2.0	2.0	115	1.73	66	28.7 ± 10.5	46.1 ± 3.4
5.0	5.0	256	3.14	148	49.6 ± 0.9	66.0 ± 4.3
10	10	196	1.73	113	70.4 ± 3.7	75.0 ± 1.0
50	50	134	8.31	16	26.9 ± 5.7	42.5 ± 5.0
100	100	791	8.31	95	22.3 ± 2.5	34.6± 2.6

Note: Tungsten and silicon oxide line widths varied in the range of 0 (filed oxide and tungsten) and 100 μm. Alignment angle ϕ in the range of ±10° and ±20° from the lines y-axes

3.3.3 Human Dermal Fibroblast (GM5565) Cells - The Effect of a Bacterial Toxin on the Alignment of Cells

This section is intended to characterize the adhesion and alignment behaviors of human dermal fibroblast (GM5565) cells on the newly developed 2D W/SiO_2 micron, and sub-micron scale patterned substrates as a function of tungsten and silicon oxide line widths when exposed to a bacterial toxin such as antimycin A.

3.3.2.1 Background

While a substantial body of literature accumulated focusing on understanding the cell-substrate interactions (Khalili and Ahmad, 2015, Anselme et al., 2010; Huang et al., 2003; Sagvolden et al., 1999), there is insignificant number of published papers discussing the effect of antimycin A in the culture media on the alignment behavior of cells. Antimycin A is an antibiotic material produced by Streptomyces species that hinders the mitochondrial respiration and may reduce the level of adenosine triphosphate (ATP) in the cell (Chen, Ma, Han, Chen, and Zhu, 2017; Zhu et al., 2014). In the presence of antimycin A, the production of "reactive oxygen species" ROS increases causing cellular damage (Sabharwal and Schumacker, 2014), and negatively affect the physiological functions of cells (Sena and Chandel, 2012; Lisdero et al., 2004). Mitochondria are essential organelles present in all mammalian cells, and they perform various functions (Shadel and Horvath, 2015). This complex organelle inhabits a considerable part of the cytoplasm volume of an animal cell (Alberts et al., 2002).

Despite its toxicity, antimycin A is used as a pesticide "management tool" by fish farmers (Finlayson et al., 2011), and it has also been used as a fungicide, insecticide, and miticide (Greene and Pohanish, 2005). Shadel and Horvath (2015), and King and Radicchi-Mastroianni (2002) reported that a high concentration of Antimycin would cause cell apoptosis; nevertheless, using antimycin A in lower dosages will not cause cells to die, but will have a depleting effect on the production of ATP (Shadel and Horvath, 2015) (Nir and Nieva, 2003). Additionally, Du et al. (2010), Sáenz-Morales et al. (2006), Raman and Atkinson (1999), and Nir and Nieva (2003) highlighted the fact that a brief exposure to antimycin A was proven to prevent the polymerization of the actin, thus leading to deprived cell adhesion. A similar adverse effect was observed to be caused by cyanide, another toxin that changes the membrane potential of the the mitochondria (Prahalad et al., 2004; Kroshian, Sheridan, and Lieberthal, 1994), signifying that a reduction in the ATP demand and the activity of the mitochondria will negatively affect the growth and the morphology of cells (You and Park, 2010). Nevertheless, the effect of antimycin A on the behavior

and morphology of cells adherent on engineered micron and sub-micron scale patterned substrates remains unidentified.

The GM5565 cells were cultured for 72 hours, at an initial cell confluence of 1 x 10^5 cells/mL, then fixed and dehydrated using the protocols discussed in Section 3.2.3.3. In brief, cells were cultured on multiple substrates using two culture media. Medium A contained a modified medium supplemented with serum, and the serum-containing medium B was supplemented with 5 μM of antimycin A, a bacterial toxin. This concentration was sufficient to cause mitochondrial dysfunction, but not enough to cause vital damage (Kalghatgi et al., 2013). No antibiotics (penicillin and streptomycin) were added to the culture media due to the adverse impact on mitochondrial function and growth of cells (Llobet, Montoya, López-Gallardo, and Ruiz-Pesini, 2015; Kalghatgi et al., 2013).

3.3.2.2 Bacterial Toxin Effect on Manipulating the Behavior of Cells

Fibroblast cells were seeded on 2D W/SiO_2 micron, and sub-micron scale patterned substrates fabricated using the technology described in Section 3.2 and incubated in two different culture media: media (I) containing only the components described in Section 3.2.3.3 and media (II) supplemented with 5 μM antimycin A. To obtain SEM micrographs, fibroblast cells were deposited on eight different comb structures with line widths of 0.18 μm, 0.25 μm, 0.5 μm, 1 μm, 2 μm, 5 μm, 10 μm, and 50 μm. Qualitative observations from Figure 3-24 demonstrate that cells on 0.18 μm dense comb structures are randomly oriented, with or without the presence of antimycin A. However, in both media (I, and II), cells show the tendency to increase its alignment rates with the increase in the tungsten lines width approaching the 10μm wide metal lines. Moreover, cells adherent on tungsten lines wider than 10 μm shows higher misalignment. It is important to underline that the alignment magnitude for fibroblast cells in the presence of antimycin A was observed to be much lower than in the absence of antimycin A.

The alignment behaviors of adherent GM5565 fibroblast cells, as observed in Figure 3-24 were quantified by measuring the displacement angle ϕ as described in Section 3.2.4. The alignment behaviors of adherent fibroblast cells as a function of the tungsten line width was measured and plotted in Figure 3-25. Error bars correspond to one standard deviation from three independent groups of data. The total number of adherent cells (incubated without antimycin A) was assessed to be 6,892 toxin-free, while in the presence of antimycin A, the number of inspected and characterized cells was 4,696. Results indicate that as the line width increases, the percentage of cells, which tends to aligned within $\pm 20^o$ in parallel to the tungsten lines, y-axes remains almost constant, as demonstrated in Figure 3-25. This is

observed to be true regardless of the media composition, in which ~ 41 % of nuclei on the 2 μm comb structures oriented within ±20^{o} of the line axes.

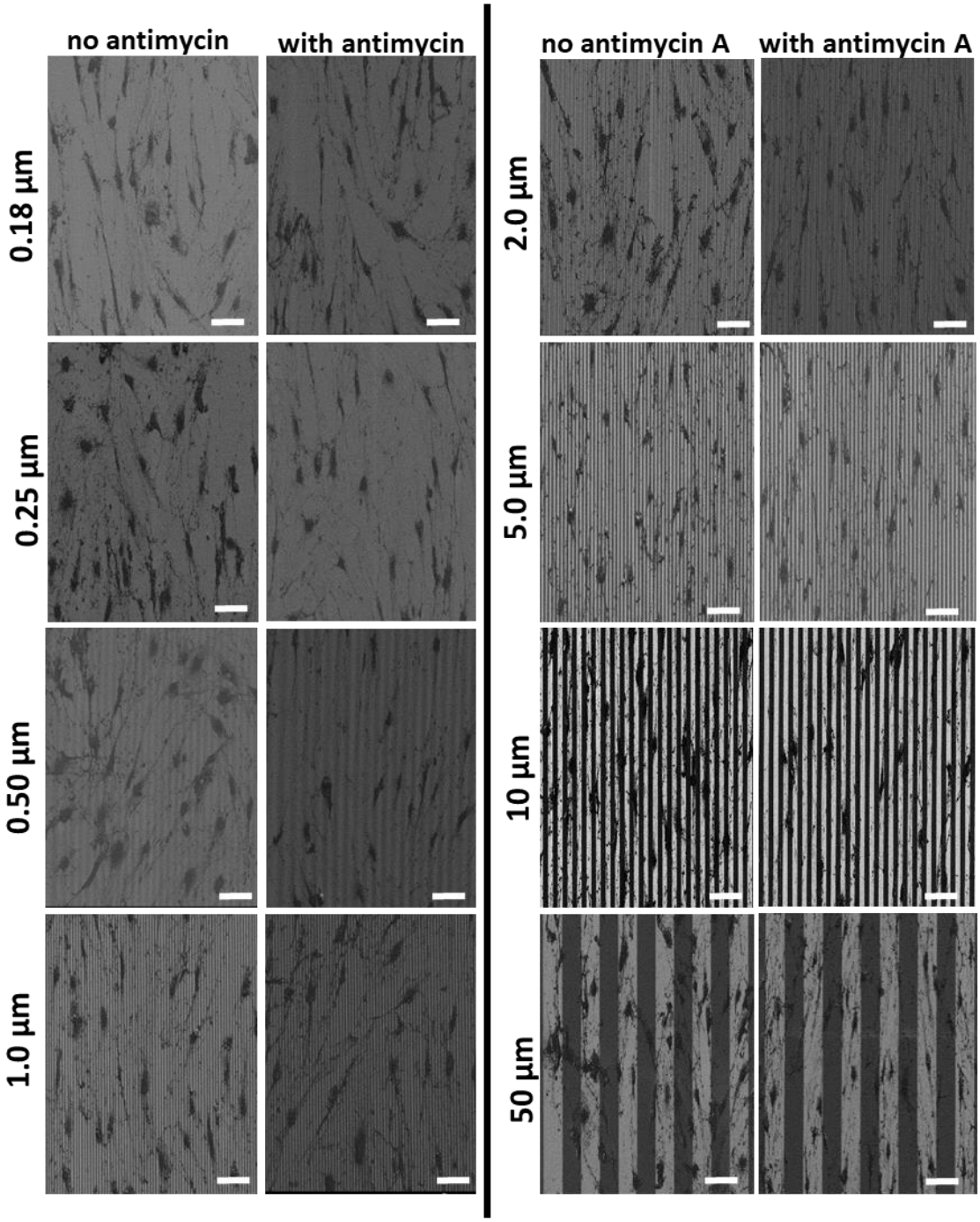

Figure 3-24 Top-down SEM micrographs of cells incubated on comb structures in media with or without antimycin A. Eight comb structures with line widths of 0.18, 0.25, 0.5, 1, 2, 5, 10, and 50 μm were tested. Initial cell concentrations were maintained at 1 x 10^5 cells/mL. All cells were incubated on the engineered surfaces for 72 hours. Scale bars correspond to 50 μm

The alignment of the adherent cells on tungsten lines (incubated in the absence of antimycin A) increases and reaches a peak value of 67.5±1.6 % on comb structures with line widths of 10 μm, while the alignment rate of cells incubated in the presence of antimycin A remains constant. As previously observed in Figure 3-24, cells adherent to comb structures with 50 μm line widths display an alignment rate smaller than 10 μm. However, the alignment rate of cells without antimycin on 50 μm line widths continues to surpass the alignment rate of those cells with antimycin.

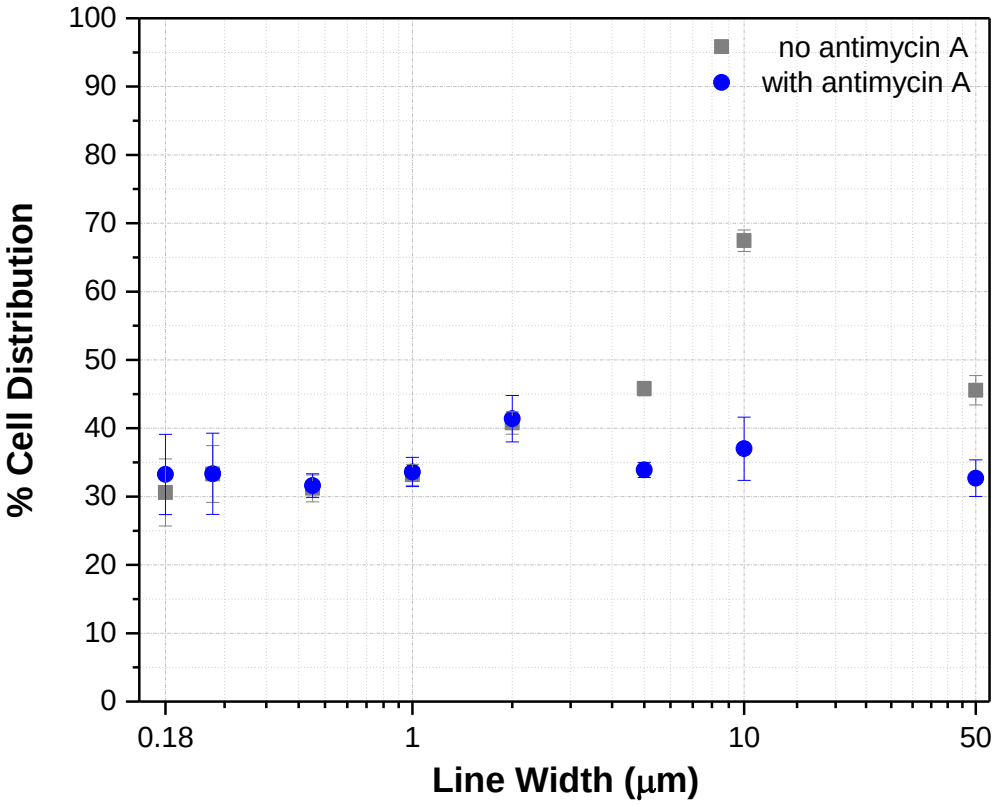

Figure 3-25 The percentage of cells that are aligned within ± 20° of the tungsten line y-axes of various line widths. Cells adhered to the 10 μm wide lines have the tightest alignment performance. Incubation time is 72 hours.

The outcomes of Figure 3-25 indicate that 10 μm tungsten lines continue to induce the strongest alignment behavior for GM5565 cells incubated in the absence on antimycin A, but not for the ones incubated with antimycin A. Results demonstrate the negative impact of antimycin A on the alignment behavior of the adherent GM5565 cells.

3.3.2.3 Summary

The results of this section demonstrate the adverse effect of antimycin A on the alignment behavior of human dermal fibroblast (GM5565). Results prove that cells incubated in the absence of antimycin A showed a preferential alignment on tungsten lines compared to silicon oxide lines. Cell adherent on comb structure with 10 μm tungsten line widths demonstrated the maximum alignment rate in comparison with other comb structures. This is similar to the preferential behavior observed for mammalian Vero cells, and the human prostate cancer cells. However, in the presence of antimycin A, it was observed that the total number of adherent cells and the percentage of cells aligned within ±20° of the tungsten lines y-axis were significantly lower.

Chapter 4
Single-Species Protein-Dependent Cell Alignment

In this section, the effect of the single-species protein component of fetal bovine serum (FBS) on the adhesion and alignment behaviors of mammalian (Vero) cells were studied and assessed. These single species are; human and bovine serum albumin (Alb), fibronectin (FN), vitronectin (VN), and collagen (Col). Two sets of experiments were conducted as part of this chapter. (a) the effect of single species protein as a supplement to serum-free medium, and (b) the effect of single protein pre-adsorption, on the adhesion and alignment behaviors of cells.

4.1 Background

The adsorption of protein(s) onto a substrate is a natural event and is considered the initial step in many biological phenomena (Rabe et al., 2011; Hakkinen et al., 2011; Wilson et al., 2005; Horbett and Schway, 1988). Proteins, in general, were found to stimulate different cellular morphological responses by binding to protein-specific receptors causing cytoskeletal components to rearrange differently (Mahesparan et al., 1997). However, specific proteins are required by cells for anchorage-dependent adhesion and interaction with the extracellular matrix, which is vital for the following biological functions (Wilson et al., 2005). Surfaces with strong hydrophilic characteristics promote stronger cell adhesion and ECM synthesis (Zhao et al., 2005; Redey et al., 2000). Nevertheless, others may disagree, stating that surfaces with high hydrophilic properties have a minimum impact on the adsorption of proteins such as fibronectin and albumin (Kern, Yang, Glover, and Ong, 2005). These proteins vary in terms of size and weight. Thus their adsorption on a substrate will be affected by the topographical features of the substrate (Zinger et al., 2004).

The molecular weights, sources, and functions of each protein component used in this experiment are listed in Table 4-1, based on - but not in any particular order - Zhang and Webster (2013), Plantman, 2013; Ruggeri and Jackson (2013), Tighe and Mann (2011), Michaelis et al. (2011), Anselme et al. (2010), Kao et al. (2010), Parhi et al. (2010), Golas, and Vogler, 2010)Stevenson and Donald (2009), Barnthip, Parhi, Golasb, and Vogler (2009), Zhu, Robey, and Boskey (2008), Barnthip, Noh, Leibner, and Vogler (2008), Anselme and Bigerelle (2006), LeBaron and Athanasiou (2000), Sagvolden et al. (1999), Lu, Su, and Penfold (1999), Groth and Altankov (1996), Casaroli Marano and Vilaro (1994), Lutanie, et al. (1992), Hayman , Pierschbacher , Suzuki, and Ruoslahti (1985), and Silver and Birk (1984).

Table 4-1 Molecular weight of the different protein components in FBS serum-containing medium

Description	Source	Molecular Weight	Function	Literature
Albumin Human / Bovine	Produced by the liver, with high levels in plasma	HAS ~66 kDa BSA ~69 kDa	Helps to promote the stability of culture media. Reduces the cell membrane damage due to destructive oxidation	Tanaka (2013) Shen et al. (2012) Francis (2010) Ellmerer et al. (2000)
Vitronectin (VN)	Plasma protein secreted by the liver	65-75 kDa	Forms focal adhesion points and promote adhesion, migration, and change in morphology	Su and Riesbeck, 2018 Kyriakides, 2015 Tighe and Mann, 2011 Zhu et al., 2008
Collagen and isoforms	ECM glycoprotein assembles the basal lamina	~280-289 kDa	Minimal effect on cell differentiation, change in morphology	Xiao et al. (2016) Byron et al. (2013) Prewitz et al. (2013) Coelho et al. (2011)
Fibronectin (FN)	ECM glycoprotein	~430-460 kDa	Cell adhesion, morphology changes, migration, the organization of the cytoskeleton, the formation of focal adhesion and cell differentiation	Kyriakides (2015) Anselme et al. (2010) Wilson et al. (2005) Sagvolden et al. (1999)

4.1.1 Bovine and Human Serum Albumin Effect on Cell Behavior

Albumins are secreted by the liver and account for ~50-60 % of plasma proteins (Tanaka, 2013; Francis, 2010; Jefferson and Shankland, 2008; Ellmerer et al., 2000). In addition to their role in enhancing the interaction between cells and biomaterials (tissues or engineered substrates), albumin functions as an anti-oxidant, and provide temporary storage of amino acids, while binding and transporting ligands, hormones, and metal ions (Shen, Ly , and Hoang, 2012; Francis, 2010; Ellmerer et al., 2000). Edwars et al. (1987) identified serum to act as a "spreading factor." For the growth of cells. Albumins are frequently used in research and industry as a supplement for culture media due to their biological neutrality.

Additionally, supplementing a culture medium with albumins will help improve its stability (Sigma-Aldrich, 2017; Francis, 2010). Albumin plays the role of a free radical sink and decreases the potential destructive oxidation of the cell membranes (Sitterley, Karmiol, Manaster, and Ryn, 2008). Albumin may also play a role of adhesion inhibitor of human T cells (a subtype of white blood cell) as highlighted by Kim et al. (2006). Generally speaking, the adsorption of albumin on a substrate is reversible for short adsorption periods. However, over longer adsorption times, the adsorption becomes less reversible as indicated by Vaidya and Ofoli (2005). Albumin excels in supporting the adhesion of cells on hydrophilic substrates (Kyriakides, 2015; Wertz and Santor, 2001), and this is due to the fact that the ultimate albumin coverage on hydrophilic surfaces was found to be higher than on hydrophobic surfaces.

4.1.2 Vitronectin Effect on Cell Behavior

Vitronectin (VN) is an abundant plasma glycoprotein that is predominantly produced by the liver and found in nearly all mammalian tissues (Su and Riesbeck, 2018; Ruggeri and Jackson, 2013). VN is found side by side with fibrillar collagen, even though VN is found in basement membranes (Zhu et al., 2008). The adsorption of VN on engineered biomaterials is influenced to a great extent by the hydrophobic nature of the biomaterial and the content of calcium and magnesium ions in the culture media (Kyriakides, 2015; Tighe and Mann, 2011; Matsushita et al. 2000). This is caused by the ability of vitronectin to enhance the organization of the cell adhesion integrin subunits (Matsushita et al. 2000). Thus, it is expected that vitronectin will not support the adhesion and alignment of cells on the 2D W/SiO2 structures since the comb structures are hydrophilic, and also because OptiPRO^{TM} is low in calcium content. Miyamoto et al. (1989), and Hayman et al. (1985) indicate that vitronectin alone is the active component in bovine serum that influences the cell spreading behavior. Although vitronectin is the main adhesive protein in FBS (Hayman, Pierschbacher, Suzuki, and Ruoslahti, 1985), when used alone in the culture media, VN loses its ability to support any type of cell-spreading behaviour, leading to the assumption that other species of protein, which exist alongside the vitronectin in the FBS, are what activate the vitronectin-dependent cell behavior (Miyamoto et al., 1989; Yatohgo, Izumi, Kashiwagi, and Hayashi, 1988). It is worth saying that vitronectin exists at a much higher concentration than fibronectin in FBS the serum-containing medium (Hayman et al., 1985).

4.1.3 Collagen Effect on Cell Behavior

Collagen (Col) is a structural glycoprotein protein and a predominant component of ECM. It is highly available in animals and can accumulate growth factors (Byron, Humphries, and Humphries, 2013; Gonzalez-Perez, Udina, and Navarro, 2013). This less soluble ECM protein accounts for one-third of the total proteins in the human body (Coelho, Gonzalez-Garcia, Salmeron-Sanchez, and Altankov, 2011; Shoulders and Raines, 2009). The behavior of collagen in the interfaces between the substrate and the bulk liquid phase is limited (Coelho et al., 2011). Nevertheless, collagen is known to adhere to hydrophilic surfaces. The ability of collagen to induce a substantial proliferation and differentiation of cells as a single species protein is insignificant, according to Philp et al. (2005). In comparison to fibronectin, collagen was observed to produce an inferior ECM (Prewitz et al., 2013; Xio et al., 2016), but performed better than vitronectin (Plantman, 2013). It is essential to note that collagen is dependent on the polymerization of fibronectin to be included in the ECM structure (Byron, Humphries, and Humphries, 2013; Kinsey et al. 2008; Sottile and Hocking 2002).

4.1.4 Fibronectin Effect on Cell Behavior

Fibronectin is a high molecular weight glycoprotein that is found as part of the ECM in an insoluble form, while, in serum and blood plasma is found in a soluble form. Similar to vitronectin, fibronectin involves in the cell adhesion process, but not involved in the initial cell-substrate interaction as indicated by Wilson et al. (2005), and Vaidya and Ofoli (2005), mobility and differentiation of cells. Fibronectin is capable of forming a fiber-like matrix to induce the adhesion and mobility of cells (Xio et al., 2016). The adsorption of fibronectin - in general – as a function of time is irreversible as observed by Vaidya and Ofoli (2005). Fibronectin is widely observed in literature to enhance a higher integrin-induced adhesion of cells on both hydrophobic (Kyriakides, 2015; Stevenson and Donald, 2009; Baujard-Lamotte, Noinville, Goubard, Marque, and Pauthe, 2008) and hydrophilic (Parhi et al., 2010; Anselme et al., 2010; Wilson et al., 2005; Sagvolden et al., 1999) substrates. However, on hydrophilic surfaces, higher adsorption of fibronectin was observed, while upholding its functionality leading to an increase in cell-surface interaction. The opposite happened when fibronectin was adsorbed on hydrophobic surfaces (Wilson et a., 2005). A study by Kim et al. (2006) indicates that a serum-free medium (e.g., OptiPRO^{TM}) supplemented with fibronectin alone - in the absence of other glycoproteins or serum - will be able to induce and support the adhesion and spreading of cells in the absence of other glycoproteins or serum (Miyamoto, 1989). Additionally, it was experimentally demonstrated by Yatohgo et al. (1988) that fibronectin supports a more extensive expansion of the peripheral cytoplasm in comparison with vitronectin.

4.2 Materials and Methods

4.2.1 2D Tungsten and Silicon Oxide PatternedSubstrates

The substrates used in this chapter were identical to the ones used in Chapter 3, and their fabrication process was discussed in details in Section 3.2.1 and demonstrated in Figure 3-1. In brief, silicon oxide-based micron and sub-micron scale patterned substrates were fabricated using very-large-scale-integration (VSLI) process, which is an advanced technology that is widely used in the semiconductor industries. The substrates consist of dense comb structures of tungsten equal widths parallel lines inlaid in thin film SiO_2 blanket. The final surfaces are smooth, flat, continuous, and defects free.

4.2.2 Vero Cells Culture, and Fixation Protocols

Vero cells obtained from the American Type Culture Collection (ATCC, Manassas, Virginia, USA), and were incubated for 48 hours on the 2D substrates according to the protocol discussed in Section 3.2.3.1,

with a twist to fit the context of the two experiments done herein. All Vero cells were incubated at an initial concentration of $0.5x10^5$ cell/mL. Gibco® ultra-low protein OptiPRO™ cell culture medium was used instead of 1:1 DMEM/F12 culture medium used in Section 3.2.3.1. Prior to cell deposition, the 2D W/SiO_2 substrates were all decontaminated for 30 seconds using 2 mL of 70 % ethanol and were air-dried, then rinsed with 2 mL of Dulbecco's phosphate-buffered saline (D-PBS) to remove residual contaminants. The incubation was done in 6-well tissue culture plates (Nunc, Thermo Scientific, Roskilde, Denmark). OptiPRO™ was used to eliminate the potential conflict or competitive adhesion between the proteins contained in the media, and those are used to supplement the medium or pre-adsorbed on the substrates. The single proteins used in the experiment are in a purified form (purity >95 %). Although these proteins are structurally distinct, have different surface charge and zeta potentials, but they show similar solubility in water, functions and cell recognition sequence (Lin et al., 2014; Aumailley, 2013; Sitterley et al., 2008).

Figure 4-1 represents the proposed protein experiment pathways; the individual serum proteins or FBS used to supplement the SFM (OptiPRO), and the individual serum proteins or FBS pre-adsorbed onto the substrate prior to seeding the cells. A detailed description of all the protein-dependent experiments, including the type of proteins, pre-adsorption period, initial cell confluence, and cell incubation period is listed in Table 4-2.

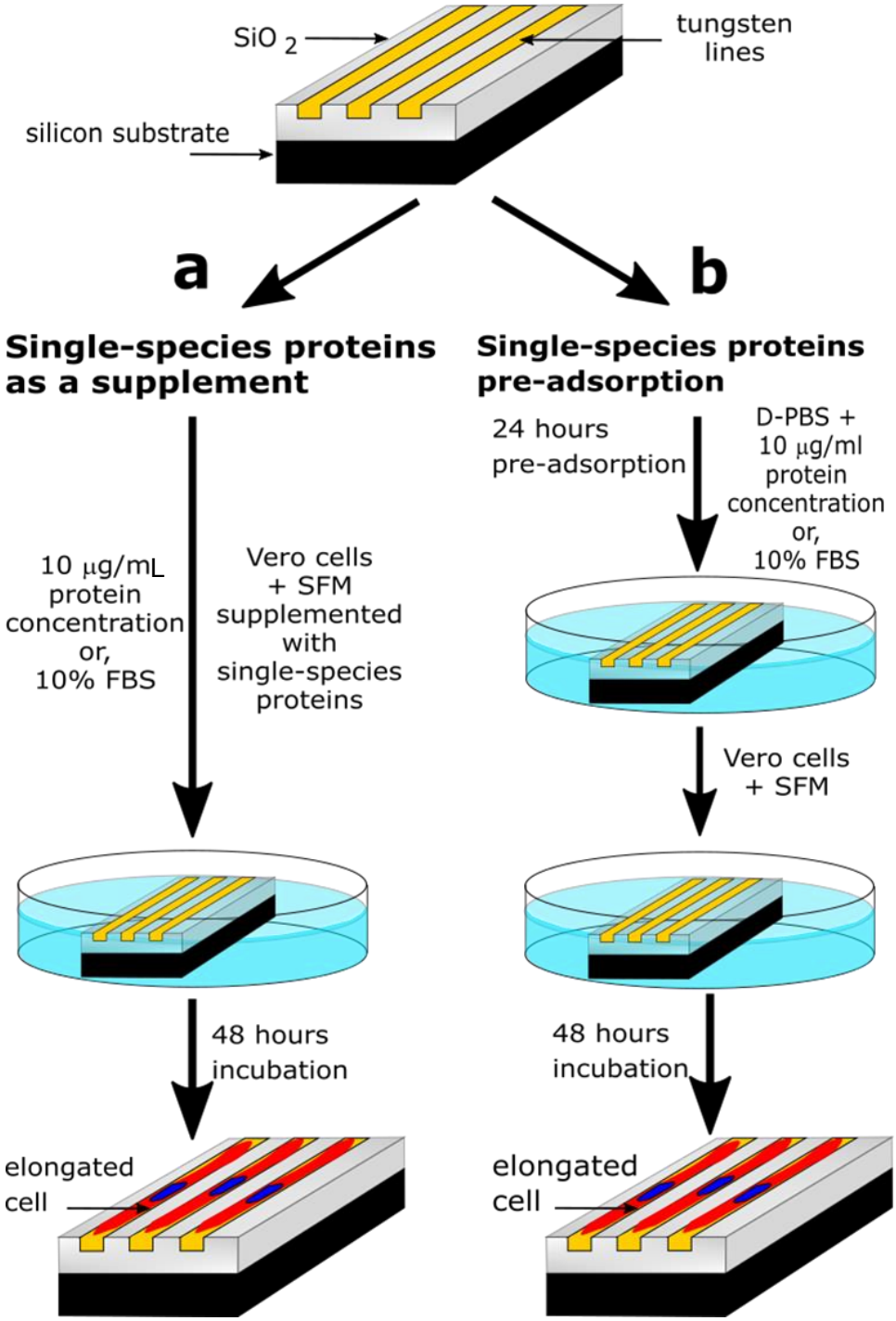

Figure 4-1 Proposed protein experiment pathways. (a) individual serum proteins or FBS used to supplement the SFM (OptiPRO). (b) Single-species serum proteins or FBS pre-adsorbed onto the substrate before seeding the cells. Single-species proteins used at a concentration of 10 μg/mL. Proteins pre-adsorption was done for 24 hours, and cells were incubated for 48 hours. All single proteins and FBS were diluted with D-PBS for the pre-adsorption experiments. All spent D-PBS was removed before cell seeding.

Table 4-2 List of all protein-dependent experiments, and their parameters; including the concentration of proteins, pre-adsorption periods, cells initial concentration, incubation period, post-incubation treatments, experimental objectives, and characterization method.

Sample Number	Figure Number	Cell Confluence (Cell/mL)	Protein Pre-absorption	Protein Concentration	Protein Incubation (hrs.)	PBS Rinse	Culture Medium	Vero Incubation (hrs.)
OptiPRO - Control Sample								
1	4-3	5.00E+04	N/A	N/A	N/A	No	OptiPRO	48
4.2.3.1 SFM Supplemented with Single Protein-Dependent Cell Alignment								
2	4-4	5.00E+04	N/A	10 µg/mL	N/A	No	OptiPRO + HSA	48
3	4-5	5.00E+04	N/A	10 µg/mL	N/A	No	OptiPRO + BSA	48
4	4-6	5.00E+04	N/A	10 % (v/v)	N/A	No	OptiPRO + FBS	48
5	4-7	5.00E+04	N/A	10 µg/mL	N/A	No	OptiPRO + VN	48
6	4-8	5.00E+04	N/A	10 µg/mL	N/A	No	OptiPRO + Col	48
7	4-9	5.00E+04	N/A	10 µg/mL	N/A	No	OptiPRO + FN	48
4.2.3.2 Single Protein Pre-adsorption Dependent Alignment								
8	4-11	5.00E+04	Fibronectin	10 µg/mL	24	No	OptiPRO	48
9	4-12	5.00E+04	Collagen	10 µg/mL	24	No	OptiPRO	48
10	4-13	5.00E+04	FBS	10 % (v/v)	24	Yes, prior to cell seeding	OptiPRO	48
11	4-14	5.00E+04	FBS	10 % (v/v)	24	No	OptiPRO	48
12	4-15	5.00E+04	Vitronectin	10 µg/mL	24	No	OptiPRO	48

All cells from the protein-dependent experiments were fixed, and ethanol dried before characterization step using scanning electron microscope (SEM)

4.2.2.1 Single protein as a Supplement for Culture Media Experiment

Vero cells were cultured for 48 hours in Gibco® ultra-low protein OptiPRO™ cell culture media, supplemented with 10 μg/mL of one of fetal bovine serum essential proteins (Sigma-Aldrich, Oakville, Canada). These proteins are (1) bovine serum albumin (BSA), (2) human serum albumin (HSA), (3) fibronectin, (4) vitronectin, and (5) collagen. Two additional samples were prepared for comparison (i) only using OptiPRO™ as a culture medium, and (ii) OptiPRO™ supplemented with 10 % FBS. The two samples were prepared according to the protocols discussed in Section 3.3.1.4.

4.2.2.2 Single protein Pre-adsorption Experiment

The 2D W/SiO_2 substrates were sterilized using 2 mL 70 % ethanol and rinse with 2 mL D-PBS (Ca^{2+} and Mg^{2+} free). Prior to cells incubation, substrates were immersed in solutions of 10 μg/mL single species proteins diluted in sterile D-PBS for 24hrs in a fridge at 4 °C. The extra D-PBS was removed, and cells were cultured on the substrates with the pre-adsorbed single proteins on them, in Gibco® ultra-low protein OptiPRO™ culture media for 48 hours. Cells were fixed and dehydrated. It is essential to mention that two additional samples were prepared, in which the substrates were pre-incubated for 24 hours prior to cell deposition, in a D-PBS solution containing 10 % FBS. However, after removing the spent D-PBS, and before seeding the cells, one of the samples was rinsed two times with D-PBS, while the other was not. Then, cells were cultured in Gibco® ultra-low protein OptiPRO™ culture media for 48 hours.

4.2.3 Results and Discussion

The orientation and alignment behaviors of the adherent Vero cells from both experiments (with and without pre-adsorbed single proteins) were quantitatively assessed, and the deviation angle ϕ between the nuclei long axis and the metal lines y-axes were measured as discussed in Section 3.2.4. All experiments were conducted simultaneously and under the same conditions, using the same type of cells, with the same passaging number. OptiPRO™ is a culture medium that has an ultra-low content of serum and calcium cations in comparison to FBS (Elhofy, 2014; Arora, 2013). Figure 4-1 represents the different experimental pathways used in the proteins experiment.

4.2.3.1 Proteins as a Supplement Dependent Cell Alignment

The alignment and orientation behaviors of Vero cells incubated in seven different culture media (as previously discussed in Section 4.2.2.1) were qualitatively characterized and quantitatively quantified. The visual observations of the preferential cellular alignment behaviors on comb structures 10 μm parallel tungsten lines are demonstrated in Figure 4-2. Qualitatively, incubated cells show three main alignment

behaviors in response to the culture medium they are incubated in. Figure 4-2. (a, d, and g) represents Vero cells incubated in culture media contains OptiPRO as a control sample, OptiPRO supplemented with 10 % (v/v) FBS, and OptiPRO supplemented with 10 μg/mL fibronectin, respectively show that cells (pointed to in red arrows) in these three-culture media tend to align, but do not elongate much. Moreover, Figure 4-2. (b, c) represents cells incubated in culture media contains OptiPRO supplemented with bovine serum albumin (BSA), and OptiPRO supplemented with human serum albumin (HAS), correspondingly, demonstrates that the majority of cells preferentially align and elongated parallel to the metal lines y-axes. However, images from Figure 4-2. (e, and f) which represents cells incubated in OptiPRO supplemented with vitronectin and OptiPRO supplemented with collagen, respectively, indicate that the majority of the observed cells lose their alignment and elongation performances. Additional SEM images illustrating the alignment behaviors of cells incubated in different culture media are available in Appendix C.

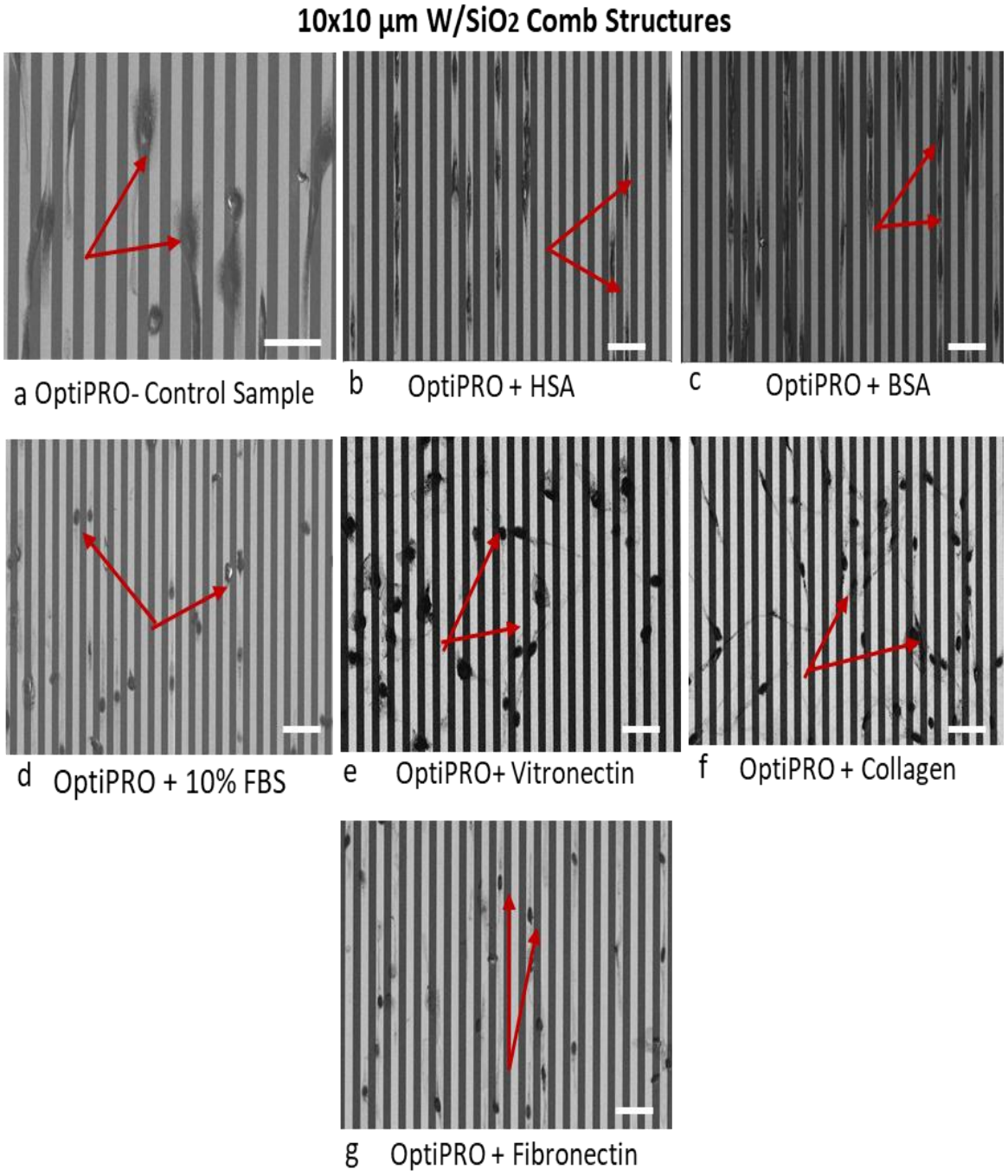

Figure 4-2 Typical top-down SEM images of Vero cells in OptiPRO™ supplemented with single-species serum proteins or FBS. Images reveal changes in the alignment and elongation behaviors of cells in response to the type of protein used to supplement OptiPRO™, the serum-free medium. (d, and g) cells are aligned but not elongated. (b, c) Cells are aligned, and elongated, and (a, e, and f) cells are neither elongated nor aligned. Cells pointed at in red arrows confirm the observations. Each scale bar corresponds to 50 µm. W lines in light gray, and SiO_2 lines in dark gray.

To quantitatively confirm our visual observations a total of 27,910 cells were measured and assessed. Results indicate that in comparison with the alignment performances of cells incubated in ultra-low protein Gibco® OptiPRO™ (Figure 4-3), which was found to be 38.1±1.1, cells incubated in the OptiPRO™ supplemented with 10 µg/mL of HAS (Figure 4-4), BSA (Figure 4-5), and in 10 % FBS (Figure 4-6) have the highest percentage of cells aligned at ±10° from the W lines y-axes with 96.0±1.0 %, 95.3±0.7 %, and 61.6±2.7 %, respectively. However, when comparing it with data from OptiPRO™ supplemented with 10 µg/mL of one of the single-species serum proteins, such as vitronectin (Figure 4-7), collagen (Figure 4-8), or fibronectin (Figure 4-9), results indicate that only OptiPRO™ containing fibronectin was able to induce some preferential alignment at a rate of 45.7±4.0. Nonetheless, the impacts the other single-species proteins like vitronectin, and collagen were found to be minimal, and alignment rates were measured to be 24.9±3.3, and 29.9±1.7, respectively. (n) is the number of the assessed cells on each structure in every culture medium. It was observed that the total number of cells assessed in HSA (n = 2,409), and BSA (n = 3,726) were lower than those assessed from OptiPRO™ (n = 3,100) and 10 % FBS (n = 5,446). This is reasonable since FBS contains higher concentrations of hormones and growth factors in comparison to OptiPRO™, and albumin (Elhofy, 2014; Arora, 2013; Brunner et al., 2010). The different quantified adsorption behaviors are consistent with the literature (Krishnan, Cha, Liu, Allara, and Vogler, 2006; Lu et al., 1999). Consistent with the visual observations in regards to the elongation behaviors of the adherent cells as attained from Figure 4-2, the characterization of cell elongation or deformation behaviors were measured and calculated as a ratio between the nucleus long and short axial (L/S). Results indicate that cells incubated in HAS, and BSA had the highest elongation with L/S average values of 2.53±0.58, and 2.34±0.50. This comes in agreement with the data on the alignment of Vero cells in the presence of BSA and HAS in comparison with the other proteins. As expected, the elongation of adherent cells in the presence of fibronectin or FBS as a supplement for OptiPRO, the SFM, was found to be smaller in comparison with BSA and HAS. Fibronectin and FBS induced a deformation (elongation) in the shape of the nuclei of the adherent cells with axial ratios of 1.64±0.37, and 1.78±0.39, respectively. Moreover, the lowest cell elongation axial ratio was induced by culture media supplemented with VN, and Col. The positive correlation observed between the tendency of cells to align parallel to the metal lines y-axes, and cell elongation to maximize their contact with metal lines comes in consensus with the findings from Chapter 3, Section 3.3.1.1; and confirmed by the mathematical model developed and presented in Section 3.3.1.2.

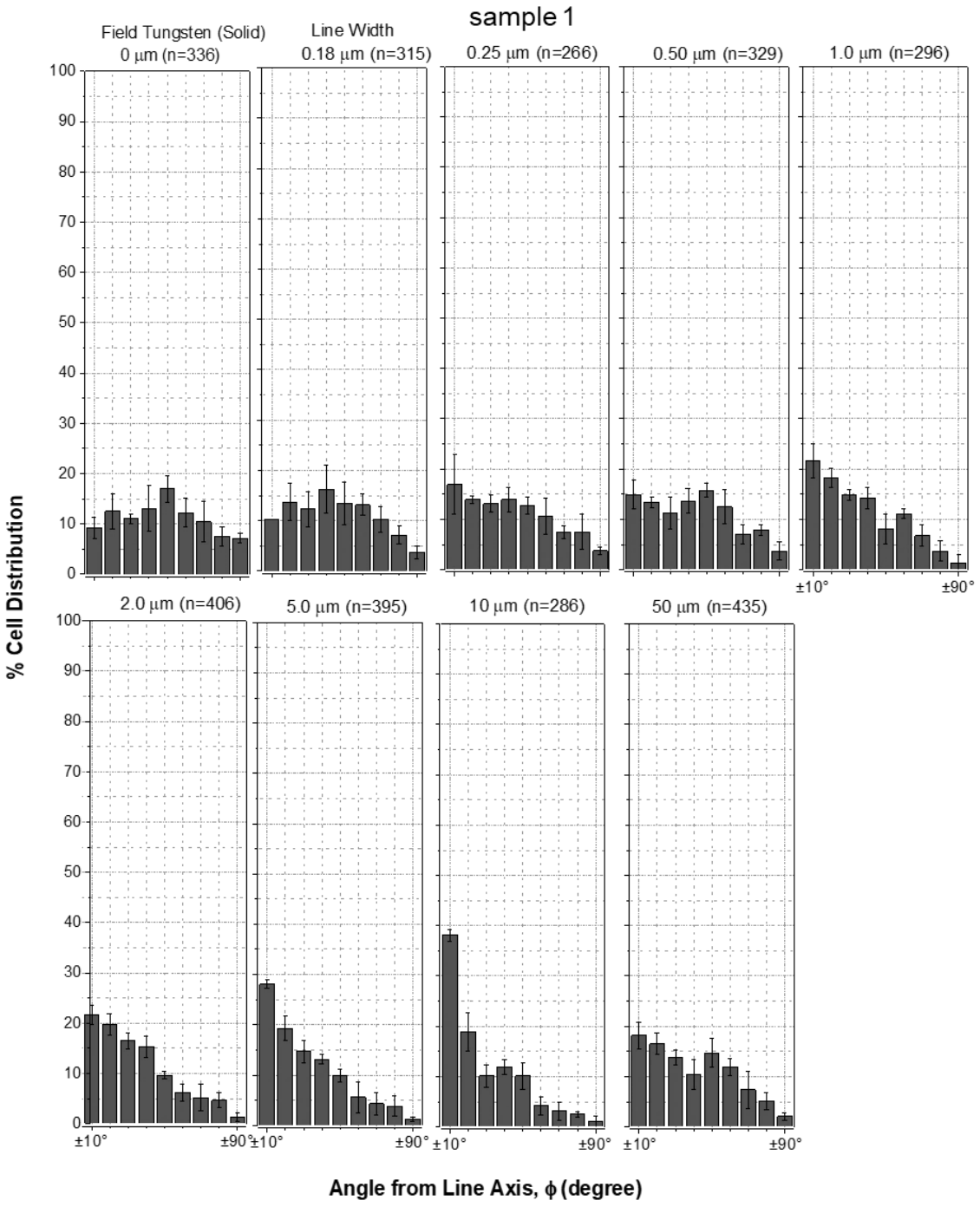

Figure 4-3 Percentage of Vero cells (incubated in OptiPRO™ culture medium) aligned parallel to the metal line as a function of W line width. From 0 μm (field oxide and field tungsten) to 50 μm. "n" is the number of cells inspected on each structure. Each bar represents the percentage of cells in a ±10° bin of deviations from the line axis. i.e., a cell with ϕ is +9° would be counted in the first bar from the right in each plot. Error bars correspond to one standard deviation

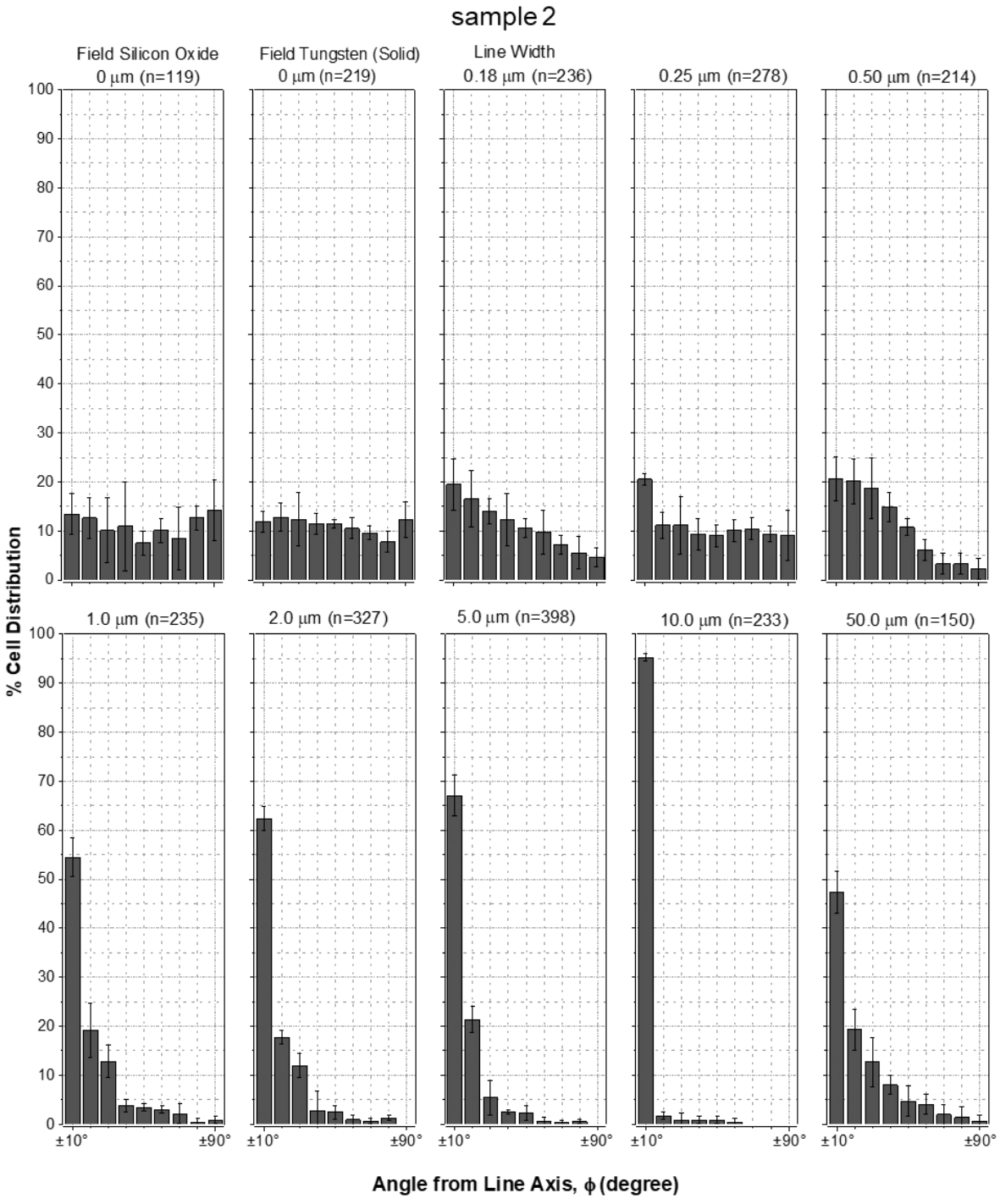

Figure 4-4 Percentage of Vero cells (incubated in OptiPRO™ and human serum albumin (10 μg/mL) culture media) aligned parallel to the metal line as a function of W line width. From 0 μm (field oxide and field tungsten) to 50 μm. "n" is the number of cells inspected on each structure. Each bar represents the percentage of cells in a ±10° bin of deviations from the line axis. i.e., a cell with ϕ is +9° would be counted in the first bar from the right in each plot. Error bars correspond to one standard deviation.

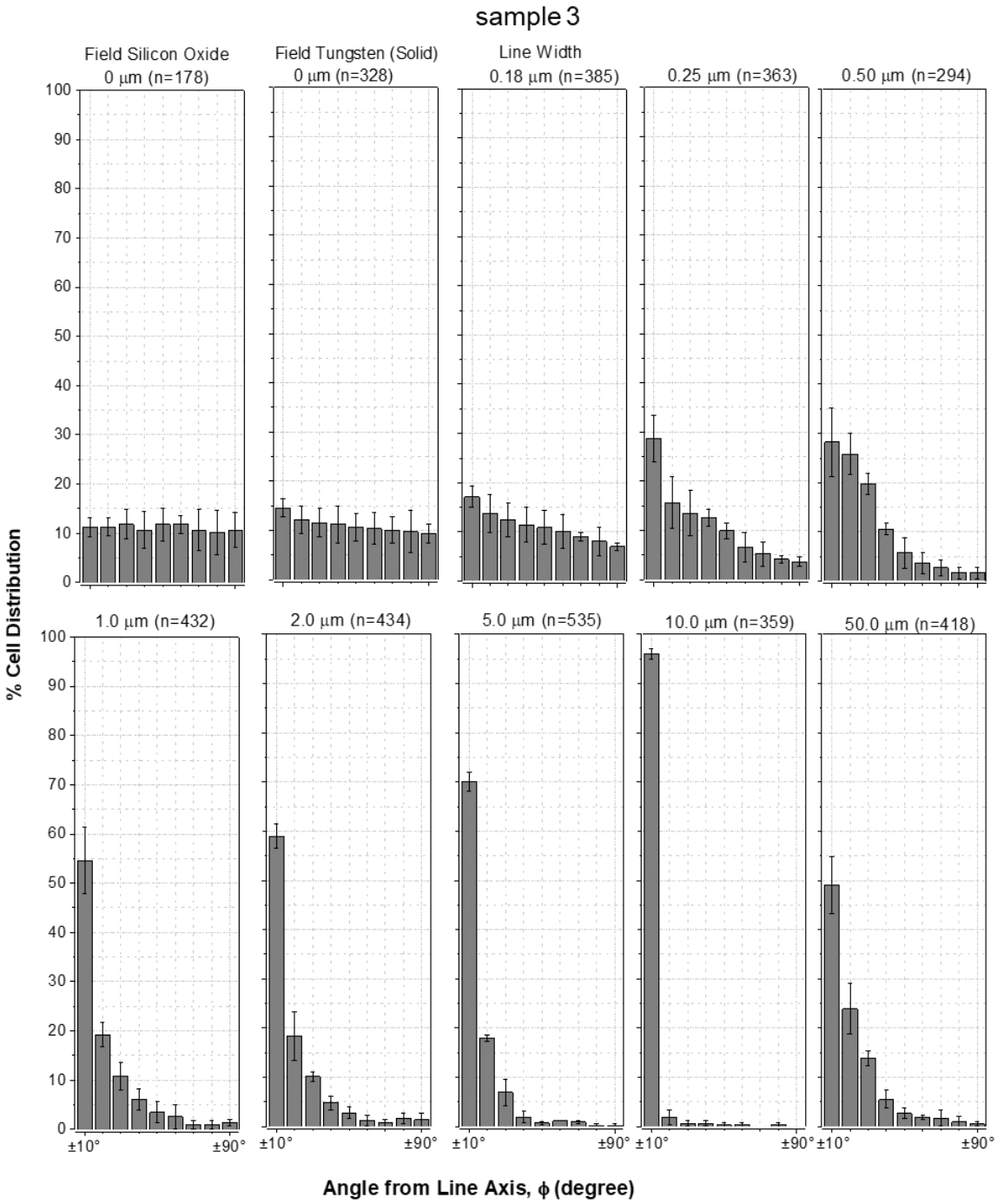

Figure 4-5 Percentage of Vero cells (incubated in OptiPRO™ and bovine serum albumin (10 μg/mL) culture media) aligned parallel to the metal line as a function of W line width. From 0 μm (field oxide and field tungsten) to 50 μm. "n" is the number of cells inspected on each structure. Each bar represents the percentage of cells in a ±10° bin of deviations from the line axis. i.e., a cell with ϕ is +9° would be counted in the first bar from the right in each plot. Error bars correspond to one standard deviation

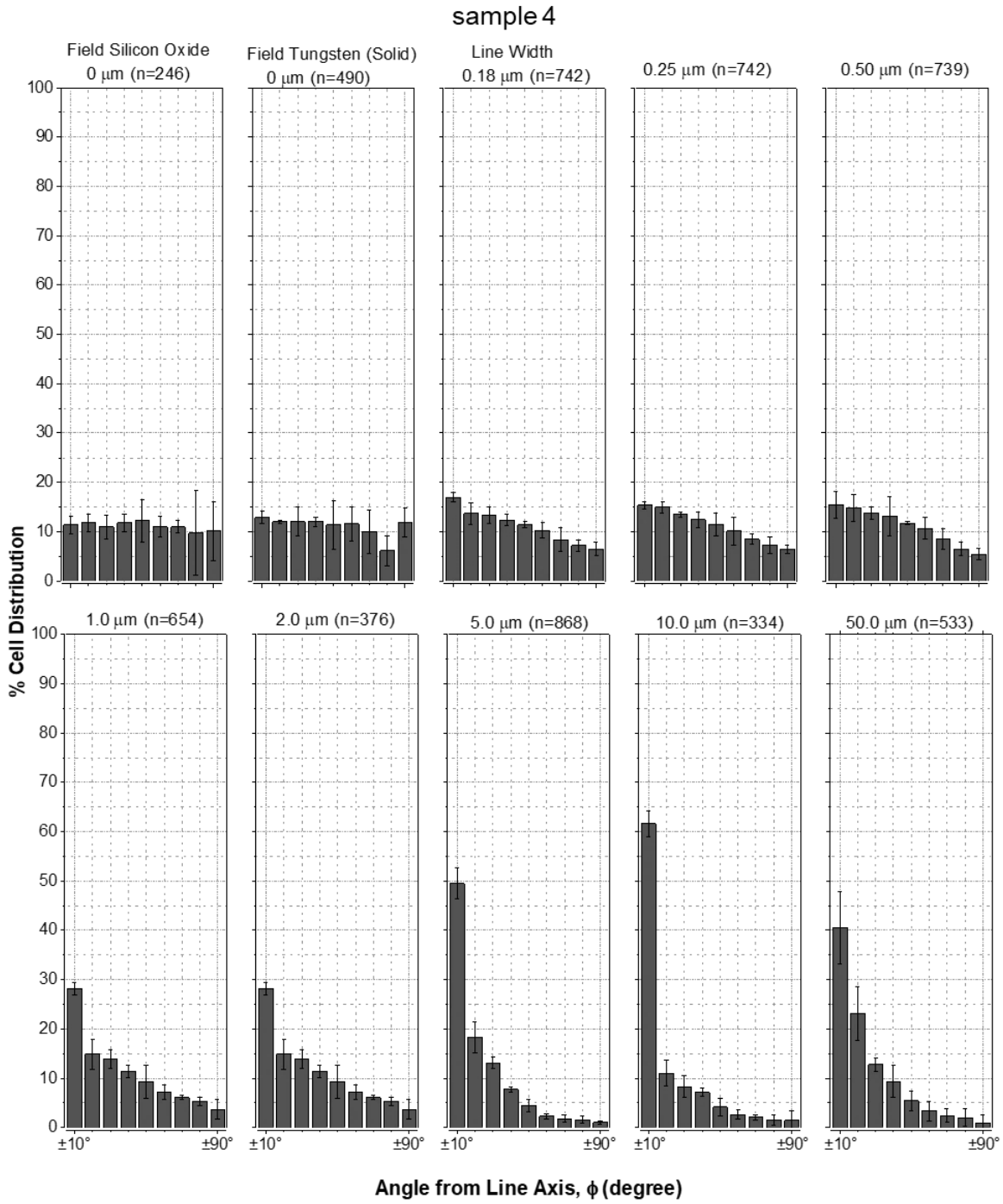

Figure 4-6 Percentage of Vero cells (incubated in OptiPRO^{TM} and 10 % FBS) aligned parallel to the metal line as a function of W line width. From 0 μm (field oxide and field tungsten) to 50 μm. "n" is the number of cells inspected on each structure. Each bar represents the percentage of cells in a ±10° bin of deviations from the line axis. i.e., a cell with ϕ is +9° would be counted in the first bar from the right in each plot. Error bars correspond to one standard deviation.

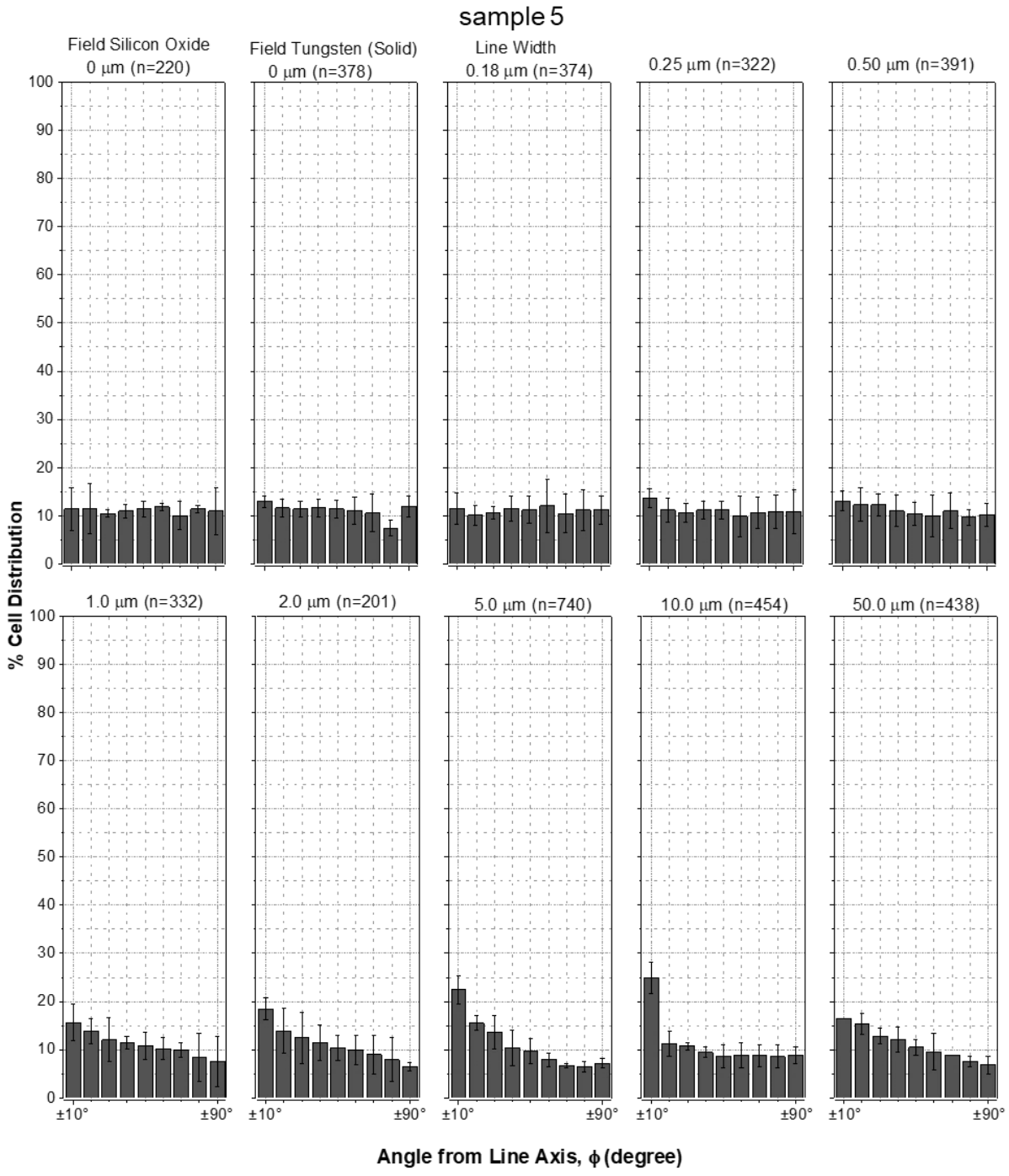

Figure 4-7 Percentage of Vero cells (incubated in OptiPRO™ culture medium and 10 µg/mL vitronectin as a supplement) aligned parallel to the metal line as a function of W line width. From 0 µm (field oxide and field tungsten) to 50 µm. "n" is the number of cells inspected on each structure. Each bar represents the percentage of cells in a ±10° bin of deviations from the line axis. i.e., a cell with ϕ is +9° would be counted in the first bar from the right in each plot. Error bars correspond to one standard deviation.

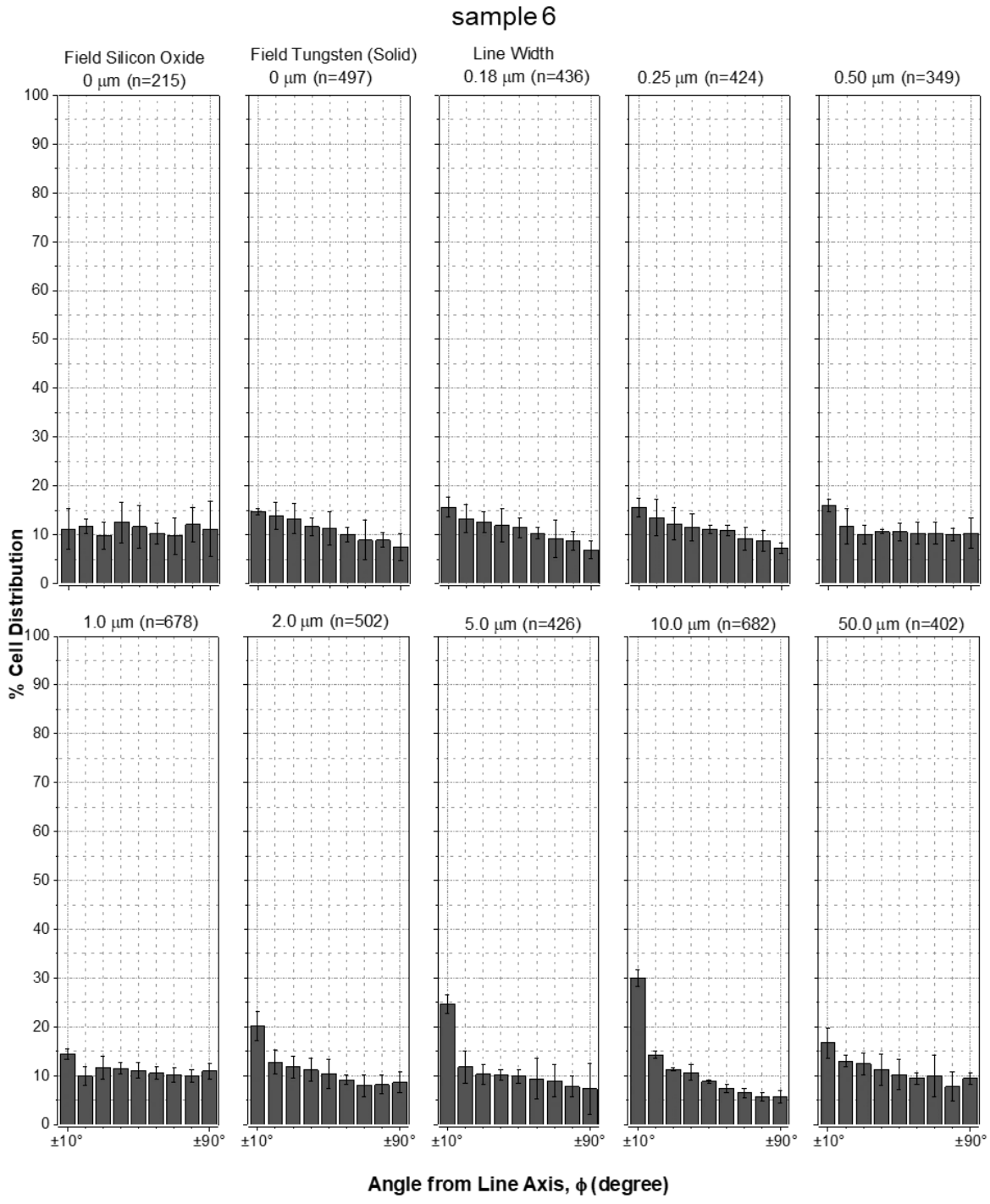

Figure 4-8 Percentage of Vero cells (incubated in OptiPRO™ culture media, and 10 µg/mL collagen as a supplement) aligned parallel to the metal line as a function of W line width. From 0 µm (field oxide and field tungsten) to 50 µm. "n" is the number of cells inspected on each structure. Each bar represents the percentage of cells in a ±10° bin of deviations from the line axis. i.e., a cell with ϕ is +9° would be counted in the first bar from the right in each plot. Error bars correspond to one standard deviation.

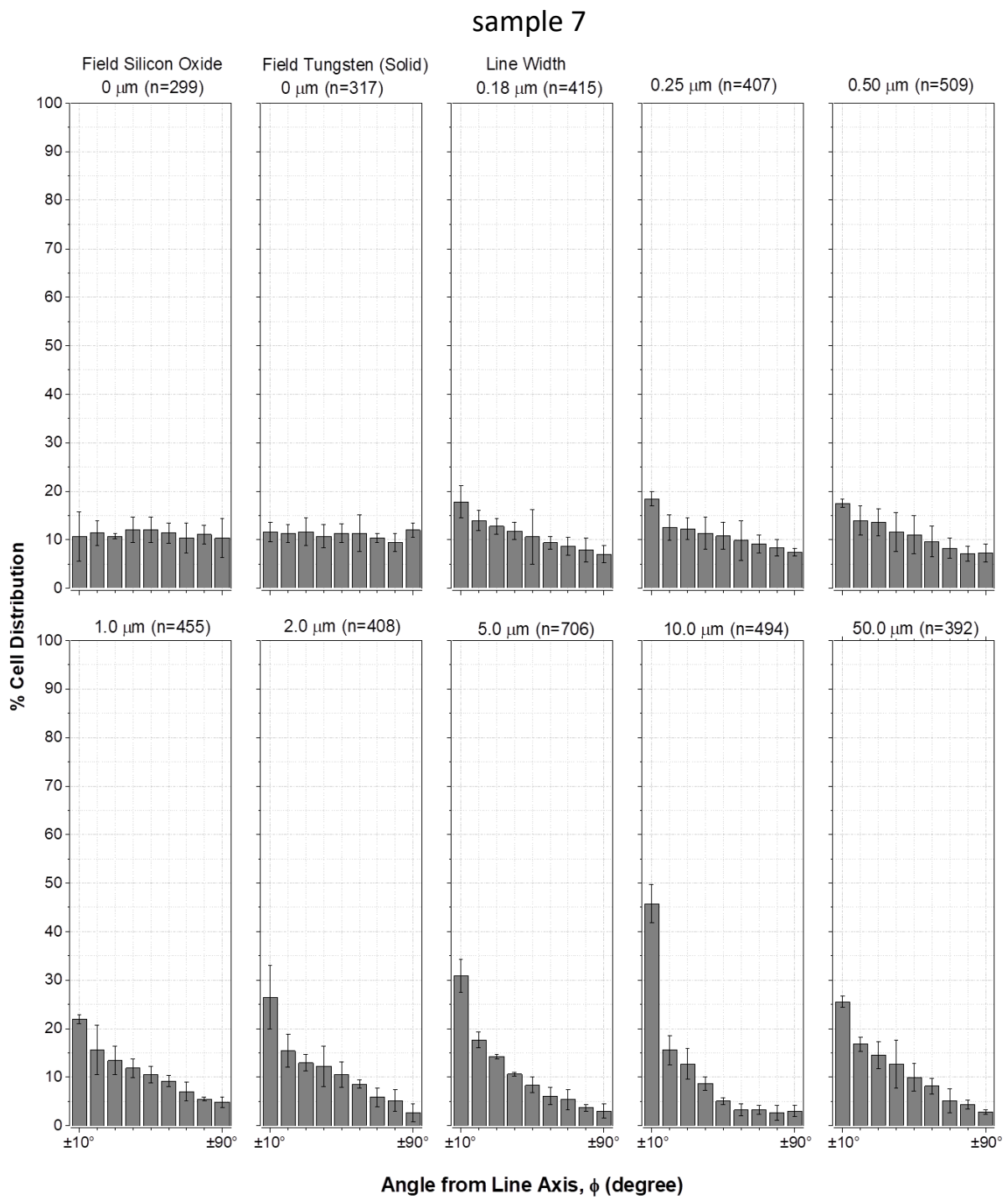

Figure 4-9 Percentage of Vero cells (incubated in OptiPRO™ serum-free medium, and 10 μg/mL fibronectin as a supplement) aligned parallel to the metal line as a function of W line width. From 0 μm (field oxide and field tungsten) to 50 μm. "n" is the number of cells inspected on each structure. Each bar represents the percentage of cells in a ±10° bin of deviations from the line axis. i.e., a cell with ϕ is +9° would be counted in the first bar from the right in each plot. Error bars correspond to one standard deviation.

The summary of cell alignment data (ϕ in the range of $\pm 10°$) on 10x10 µm W and SiO_2 parallel lines comb structure presented in Table 4-3. The 10x10 µm tungsten and silicon oxide parallel lines comb structure was proven to be the pattern with the most potential to induce the highest preferential cell-substrate interaction.

Table 4-3 Summary of cell alignment distribution data incubated in different culture media on 10x10µm comb structures with an area of ~2.7 mm^2: number of measured cells, cell density, % population of cells and standard deviation (SD) with angle ϕ at ± 10° and ± 20° of the metal line axes, and L/S. Initial cell concentration 5×10^4 cells/mL. SD represents one standard deviation from three independent groups of samples.

Sample Number	Matching Figures	Medium	Protein Concentration	Total Cell Count	Density (cell/mm^2) 10x10µm grid	% cell distribution	
						±10°	±20°
1	4-3	OptiPRO™	N/A	3,100	172	38.1±1.1	57.0±2.7
2	4-4	OptiPRO™ + HAS as a supplement	10 µg/mL	2,409	86	95.3±0.7	97.0±0.7
3	4-5	OptiPRO™ + BSA as a supplement	10 µg/mL	3,726	132	96.0±1.0	97.9±1.4
4	4-6	OptiPRO™ + FBS as a supplement	10 % FBS (v/v)	5.446	123	61.6±2.7	72.6±1.4
5	4-7	OptiPRO™ + VN as a supplement	10 µg/mL	3,850	167	24.9±3.3	36.1±3.4
6	4-8	OptiPRO™ + Collagen as a supplement	10 µg/mL	4,977	251	29.9±1.7	44.2±1.6
7	4-9	OptiPRO™ + FN as a supplement	10 µg/mL	4,402	182	45.7±4.0	61.3±1.0

The above-given results demonstrate that even under the most favorable experimental conditions, there is no culture medium (among the ones assessed in this section) that can achieve - at the same time – the highest alignment rate and support the highest cell growth. Thus, the choice of the culture medium is an outcome-dependent process. Otherwise, the best choice is a medium that can achieve the best of the intended outcomes. However, understanding why, is a complex process, which is to a great extent remains ambiguous (Huang et al., 2016; Khalili and Ahmad, 2015; Michaelis et al., 2011). The process – as discussed before - involves many interrelated parameters and conditions as listed in Table 2-1, and discussed in Section 2.3.1 (Wolfenson et al., 2013; Vogler, 2012; Michaelis et al., 2011; Bacakova et al., 2011; Vogler; 2011; Barnthip et al., 2009; Williams, 2008; Zhuo, Siedlecki, and Vogler, 2006; Krishnan

et al., 2004). Herewith, the discussion is based on the proven hypothesis (as demonstrated in Section 3.3.1) that the preferential alignment behaviors of cells are the direct consequence of protein content in the culture medium, thus on the substrate (protein-dependent). This could be further explained by (1) protein-substrate adsorption rate (Sitterley et al., 2008), (2) the concentration of Ca^{+} ions the culture medium (Sitterley et al., 2008; Norde and Lyklea, 1990; Edwards, Robson, and Campbell, 1987).

Though, FBS, albumins, and glycoproteins are frequently used to induce a preferential cell-substrate spreading and adhesion (Xu and Mosher, 2011; Shinji et al., 2011; Nelea and Kaartinen, 2010; Sitterley, 2008; Underwood and Bennett, 1989), yet their purity and concentration(s) in the culture medium what play an important role in the their adhesion, and subsequently the cell attachment patterns (Baszkin and Lyman, 2004).

Vero cells like all mammalian cells are anchorage-dependent cells (Merten, 2015; Parhi et al., 2010; Ammerman et al., 2008), which means that their survival depends on a cell-substrate interaction. It was found that such cells are adherent on hydrophilic surfaces rather than hydrophobic ones (Parhi et al., 2010). Thus, differentiating between hydrophobic substrates that induce good protein adsorption, and hydrophilic substrates that support good cell growth is essential for understanding the cell-protein-substrate interactions, indicating that all the proteins assessed in this experiment do not adsorb well on hydrophilic surfaces, similar to 2D W/SiO_2 substrates understudy. Water, not the adsorbed protein(s) was found to play the ultimate role in controlling the initial cell adhesion *in vitro*, indicating that the adhesion of cells from a bulk protein-containing medium is mediated by biological recognition involving surface-adsorbed ligands for cell receptors (Martini, Bonechi, Foletti, and Rossi, 2013; Huggins, Marsh, and Payne, 2011; Parhi et al., 2010). Proteins interaction with hydrophobic and hydrophilic surfaces are well documented in the literature, indicating that these interactions are protein-dependent. For example, the adsorption of FN on a hydrophobic substrate (hydroxyapatite - calcium phosphate) is higher than albumin (Alb), indicating that the Albumin adlayer is smaller in mass and lower in density (Tagaya, Ikoma, Hanagata, Yoshioka, and Tanaka, 2011). A similar observation was found, but the adhesion was assessed on a glass (hydrophilic) substrate (Kim et al., 2006). This was explained by the FN higher molecular weight (~7 times higher) than Albumin. Nevertheless, this contradicts with our experimental data, which indicate that on 10x10 μm comb structures, FN had a lower alignment rate of 45.7±4.0 % in comparison to HSA and BSA, with 95.3±0.7 % and 96.0±1.0 %, respectively. A different result was observed by Polyudova, Eroshenko, and Korobov (2017) indicating that bovine serum albumin (BSA) supported higher adhesion of bacteria cells (we acknowledge cellular behavior of bacteria and mammalian cells are different). However, FN demonstrated the ability to induce a better adhesion behavior (n = 4,402 cells)

than HSA (n = 3,726 cells), and BSA (n = 2,409). This comes in agreement with Garcia et al. (1998) as cited by Felgueiras et al. (2015) indicating that the effect of BSA on the attachment of cells in the absence of FN or VN is insignificant. The other single species proteins (e.g., collagen, and VN) showed similar performance in comparison to FN. The results by Felgueiras et al. (2015) and Kim et al. (2006) indicate better performance of FN over serum, VN, and collagen. Seiffert and Smith (1997) indicate that VN induced adhesion is a dose-dependent process. Lacouture, Schaffer, and Klickstein (2009) observed that under strain, the single-species protein might behave differently in a protein density-dependant behavior. At a low density of 1,000 molecules per μm^2, collagen supported higher cell adhesion than both fibronectin and vitronectin, in contrast, VN performed better than collagen and FN for high protein density ($\geq$ 2,500 molecules per μm^2). This indicates that cell-protein-substrate interaction mechanisms are hard to predict, taking into consideration the different conditions of each experiment. The number of moles of a single protein adsorbed on the substrate varied by nearly 10-fold when equivalent concentrations (e.g., 10 μg/mL in our experiment) are compared and used. At similar protein concentrations, higher molecular weight proteins (e.g., FN, and Col) will have fewer molecules (molecules per cell) in the solution in comparison to smaller ones, such as albumin and vitronectin (Parhi et al., 2009; Lacouture et al., 2009; Hajj, et al., 2007). Cooke et al. (2008) indicate that collagen-IV pre-coated on a glass surface (highly hydrophilic), but not if added as a supplement to the culture medium, will support higher cell growth in comparison to fibronectin. This contradicts with the findings of our experiment, which indicate (as listed in Table 4-3) the ability of collagen to support higher cell growth (n = 4,977 cells) in comparison to fibronectin (n = 4,402 cells). This happened on the 2D W/SiO_2 micron, and sub-micron scale patterned substrate even though collagen does not adhere well on hydrophilic surfaces, thus cannot form complex crosslinked polymeric networks (Coelho et al., 2011). However, when studying the adhesion behavior of cells on a different substrate, such as polystyrene (tissue culture flasks) using single ECM proteins or serum as a supplement for the serum-free medium results were different. Mahesparan et al. (1997) indicate that at the same concentration (μg/mL) of a single protein, fibronectin supported the adhesion of a higher number of human glioma (A-172 MG) cell line, in comparison to collagen. This behavior was found to be similar for all assessed cells (Mahesparan et al., 1997). Notably, collagen IV effect on the adhesion of cells was comparable to the uncoated substrate. Single species proteins stimulate the same cell differently, suggesting that ECM protein-specific interaction and binding can stimulate different cytoskeletal components within the cell (Mahesparan et al., 1997). Individual ECM proteins such as collagen IV, was reported to not able to induce cell migration, indicative to the fact that cells may not have a functional receptor that could interact with that specific

protein (Berens, Rief, Loo, and Giese, 1994; Giese, Rief, Loo, and Berens, 1994). It was noted by Mahesparan et al. (1997) that the stimulatory effect of fibronectin on the mobility of cells is independent of the protein synthesized by the cell, and given the fact that many cells are capable of self-producing fibronectin, this may increasingly replicate a more familiar environment (Wilson et al., 2005). Nevertheless, the existence of a single ECM protein in the culture medium is not enough to stimulate a peak change in the adhesion and alignment behavior of cells because it requires the involvement of all ECM protein, which each one of them is capable of stimulating different cellular function (Yang et al., 2017; Xio et al., 2016). This, in addition to other reasons, could explain why fibronectin, and not the other ECM proteins, was capable of stimulating a higher preferential cellular alignment behavior. However, the comparison between fibronectin and albumin indicates that albumin stimulated a much higher alignment rate than fibronectin. This can be explained and justified by the fact that albumin is adsorbed more on hydrophilic surfaces (Scotchford et al., 2002) and faster (Roach et al., 2005) than FN. Additionally, albumin remains active (folded) and experiences less denatured changes in comparison to FN on hydrophilic substrates (Kyriakides, 2015; Baujard-Lamotte et al., 2008)., which in addition to the fact that hydrophilic surfaces, in general, attract less amount of proteins explain the lower cell population on albumin (Baujard-Lamotte et al., 2008).

The protein-substrate (Patrauchan, Sarkisova, and Sauer, 2005), cell-protein (Tharmalingam et al., 2011), and cell-cell (Ko, Arora, Bhide, Chen, and McCulloch, 2001; Takeichi and Osada, 1972) adhesions are mediated by the calcium content in the culture medium (Cao, Chen, and Schreyer, 2012; Gigout et al., 2005; Ko et al., 2001; Norde and Lyklea, 1990). This happens via the *calcium-sensing receptor* (CaSR); a protein receptor that is involved in regulating the mobility of cells, and becomes activated by a specified concentration of extracellular divalent cations such as calcium and magnesium (Tharmalingam et al., 2011). Beckman Institute (2011), Sitterley (2008), Arora et al. (2001), Edwards et al. (1987) indicated that the adhesion and spreading of cells on to a substrate covered with FBS and BSA is mainly attributed to the calcium concentration in the range of 10^{-4}- 10^{-2} mole/liter in the culture medium. In a low-calcium at below 10^{-6} mole/mL environment, the adhesion and spreading behaviors of cells decline substantially. This decrease can be reversed by increasing the concentration of fibronectin in the serum. However, despite the fact that vitronectin and collagen are both glycoproteins like fibronectin, but the use of a purified vitronectin or collagen instead of the serum or as a single supplement for serum-free medium will not enhance the spreading of cells, unless supplemented with calcium (Ca^{+2}) concentration in the range of 10^{-4} -10^{-3} mole/liter (Gigout et al., 2005; Edwards et al., 1987). Comparing the cell adhesion performance of fibronectin and calf serum pre-coated on a glass substrate (as a function

of time) in the absence of divalent cations mainly calcium and magnesium, indicate that fibronectin highly inductive, while serum performance is comparable to the uncoated surface (Edwards et al., 1987). Calcium cations were found to mediate the assembly of polymeric collagen networks (Yurchenco and Cheng, 1993). Similar to fibronectin, albumin was found to induce the migration of neutrophils disregards to the concentration of calcium cations in the medium (Marks, Hendey, and Maxfield, 1991).

In general, the adhesion of proteins happens the best on hydrophobic substrates (mainly polymeric materials are studies), while hydrophilic surfaces (mainly glass is used in literature) can stimulate a preferential cell adhesion. The findings of this section to a great extent come in alignment with literature in regards to the ability of single-species proteins as a supplement for serum-free media to support the adhesion and alignment of cells, while taking into consideration the protein type and concentration, surface characterization, and calcium content in the culture medium. Bovine serum albumin and human serum albumin were proven to have the utmost ability to induce a preferential cell alignment behavior on the 2D W/SiO_2 substrates. Furthermore, based on literature and as predicted, in comparison with other ECM proteins, fibronectin was proven to be superior in stimulating a preferential adhesion and alignment behaviors. Thus, albumin and fibronectin as part of the FBS, are the main driving elements for preferential cell-substrate behavior.

These observed behaviors can be hypothesized by; (1) tungsten has the highest surface energy among metals at ~3.3 J/m^2 (Tran et al., 2016). A higher surface energy substrate promotes higher cell-surface interaction, as earlier discussed in Section 3.3.1.4, that (Parhi et al., 2009; Baszkin and Lyman, 2004; Hallab et al. 2001), in spite of the disagreement in regards to the magnitude of involvement of the surface energy and adsorbed protein on the adhesion of cells and the potential change in their behavior (Parhi, Golas, and Vogler, 2010). (2) The wetting angle of W/SiO_2 comb structures was measured to be ~29.7° -, this indicates that the comb structures are hydrophilic. Vogler (2001) as cited by Vogler (2012), indicates that bio-adhesion excels in the range of $\pm 15^{o}$ around water contact angle θ=65°. The findings by Valamehr et al. (2008) point in the same direction in regards to the ideal contact angle for cell adhesion.

4.2.3.2 Protein Pre-adsorption Dependent Alignment

In this section, the intention is to test whether the pre-adsorption of single-species protein on bio-mimicked engineered substrates, would improve the alignment behaviors of adherent cells. Results from this section will be compared with results from Section 4.2.3.1, in which the same single proteins were added as supplements to the serum-free medium. However, the question remains, whether the change in the behaviors of cells – in this particular case - is a protein-specific phenomenon. Furthermore, whether

pre-adsorption of a protein and supplementing an SFM with the same protein will have an equal impact on the behavior of the same cells.

The effect of the pre-adsorption of individual proteins onto engineered scaffolds or biomaterials on steering the adhesion of cells is widely addressed in biology-related literature (Lv, Huang , Mercadé-Prieto, Wu, and Chen, 2015; Nune and Misra, 2014; Hook, 2014; Cho and Chae, 2009; Eskin et al., 2004; Yang, Cavin, and Ong, 2003; Ying, Jin, and Tao, 2001; Tamada and Ikada, 1993; Silver, Lin , and Cooper, 1993; Fabrizius-Homan, Cooper, and Mosher, 1992). Balcells and Edelman (2002) demonstrated the role of pre-adsorption of specific proteins on increasing the mobility of cells in comparison to supplementing the culture medium with these specific proteins. Lv et al. (2015), discussed the positive effect of protein pre-adsorption on reducing the fouling under pasteurization conditions. Tamada and Ikada (1993) studied the effect of protein pre-adsorption on the changes in the contact angle of a substrate, indicating that the contact angle of polyethylene (PE) pre-coated with either collagen or fibronectin, decreased by ~77 % from 96±4° to 43±3°, causing an improvement in the substrate hydrophilicity. Lv et al. (2015) reported a similar effect, but on stainless steel, instead of polyethylene, in which the contact angle of the substrate decreased from 72±2° to 32±1°.

These observations were consistent with Nune and Misra (2014), reporting substantial changes on the *in vitro* cellular activities as a function of pre-adsorption of proteins. Silver et al. (1993) reported an increase in the thrombogenic activities on substrates pre-coated with a single protein. These responses were found to be protein type-dependent. For example, fibronectin increased the potential of formation clots, while albumin caused the opposite. Yang et al. (2003) observed that the adhesion of cells and the pre-absorbed amount of protein are directly proportional. Such correlation was found to be protein-type dependent, as reported by Silver et al. (1993). On titanium substrates, FN was found to be adsorbed at a significantly higher concentration in comparison to albumin (Yang et al., 2003). While Balcells and Edelman (2002) reported a similar conclusion on tissue culture polystyrene (TCPS) when comparing FN with other single proteins, Eskin et al. (2004) observed the effect of the pre-adsorption of single protein onto a substrate, on the subsequent adhesion of cells, indicating a protein-dependent effect, similar to that discussed above. The pre-adsorption of FN would cause an increase in the number of adherent cells and spreading behaviors in comparison to albumin. It was demonstrated that the pre-adsorption of FN would increase the spreading of cells by ~100 % if FN concentration increased in the pre-adsorption solution from 0.03 to 3 μg/mL. This was observed on tissue culture polystyrene (Eskin et al., 2004).

A study by Webb, Hlady, and Tresco (1998) demonstrated that a highly hydrophilic substrate (contact angle of ~7.3°, at pH 7.5), pre-coated with bovine serum albumin (BSA), induced higher adhesion,

spreading, and cytoskeletal deformation (no specifics were given on the type of deformation). However, on a substrate with a higher contact angle of ~59.7°, the adverse effect was observed. Nevertheless, when the same substrates were pre-coated with collagen IV, and FN, rather than albumin, the adverse effect was observed, in which higher cell density was obtained on a hydrophilic substrate with ~59.7° contact angle, in comparison to a substrate with ~7.3° contact angle. It is worthy of indicating that the density of adherent cells on substrates pre-adsorbed FN was highly dependent on the substrate contact angle. A higher number of cells were found adherent on substrates with a contact angle of ~59.7°, rather than on substrates with ~7.3°.

Moreover, the number of adherent cells on substrates with pre-adsorbed FN was much higher than on substrates pre-coated with collagen (Webb et al., 1998). Vitronectin behaved in the same way as collagen in terms of adsorption and adhesion of cells (Fabrizius-Homan and Cooper, 1991). Tamada and Ikada (1993) proved that the pre-absorption of FN on a substrate with a contact angle of ~70° enhanced the adhesion of cells. However, results show a noticeable difference in cell adhesion when comparing substrates with and without protein pre-adsorption. Substrates with pre-adsorbed FN induced higher substrate-cell affinity. It was noted that pre-coated FN provides the substrate with ligands for the cell membrane receptors.

Additionally, Lin et al. (2014a) assessed the adsorption of ECM proteins on gold substrates with zeta potentials in the range between +6.8 mV to -187 mV. One of the substrates had a zeta potential of ~79 mV, which is similar to the zeta potential of the 2D W/SiO_2 substrate under study (~80 mV). The adsorption density of collagen is better than FN at such substrate (Lin et al., 2014a). Similarly, Chang et al. (2016), Chang et al. (2014), and Wu, Wang, Chen, and Wang (3013), demonstrated that substrates with surfaces with a zeta potential of ~79 mV would induce higher cell adhesion and proliferation. Altankov et al. (2003) indicated that higher zeta potential substrates improves the adhesion and spreading behavior of fibroblast cells. This was later confirmed by Chang et al. (2016) and Chang et al. (2014), using epithelial cells. It was observed that the increase in the surface potential, will cause an increase in the number of adherent cells, as well as, a change in the morphology of cells, from bi-polar (elongated) shape, to flat, denoting a higher cell-substrate adhesion (Chang et al., 2014). This is, to some extent, similar to findings by Zhang et al. (2008). The above could be explained by the fact that some cells are more sensitive to the change in the surface chemistry, in particular, surface potential than other cells (Chang et al., 2014). Furthermore, the change in the morphology of adherent cells is an indication of the physiological condition of cells after adhesion (Costa, Hucker, and Yin, 2002).

This section examined the adhesion and alignment behaviors of Vero cells incubated on 2D W/SiO_2 substrates. Each substrate was incubated for 24 hours in a D-PBS solution containing 10 μg/mL of a single ECM protein such as FN, VN, and Col, or containing 10 % FBS, prior to the incubation of cells. In the case of the pre-adsorption with FBS experiments, and prior to seeding of Vero cells, the substrates were either rinsed (a couple of time) with a buffer-saline solution or was not rinsed. This was done to understand the effect of rinsing FBS prior to seeding cells on their alignment and adhesion behaviors. In total, six different substrates were used. The outcomes of this experiment were compared with results from Figure 4-33, and Figure 4-4, which denote alignment and adhesion data of Vero cells cultured in (1) OptiPRO™ as a culture medium, and (2) OptiPRO™ supplemented with 10 % FBS, respectively.

The visual observations of the preferential cellular alignment behaviors on comb structures with 10 μm wide tungsten lines are demonstrated in Figure 4-10. Qualitatively, cells adherent on protein pre-incubated substrates demonstrates two main alignment behaviors. Substrates pre-adsorbed with FN and FBS, half of the adherent cells show preferential alignment behavior, as demonstrated in Figure 4-10(b, e). However, the majority of cells adherent on substrates with pre-adsorbed collagen, FBS (rinsed prior to cell seeding), and VN show the tendency to misalign parallel to the W lines y-axes as observed from Figure 4-10(c, d, and f). Nevertheless, cells adherent on all pre-adsorbed proteins displays a similar tendency not to elongate, independent of their alignment behavior. Supplementary SEM micrographs describing the behavior of cells on substrates with pre-adsorbed proteins are available in Appendix C.

A total of 19,898 cells were assessed and characterized to quantify the observations obtained from the SEM micrographs Figure 4-10. "n" is the number of assessed cells from each sample. Results from Figure 4-6 and Figure 4-14 demonstrate that the number of adherent cells is independent of whether the FBS is pre-adsorbed on the substrate (n=5,446) or used as a supplement to the culture medium (n=5,495). This is logical due to the unique composition of FBS.

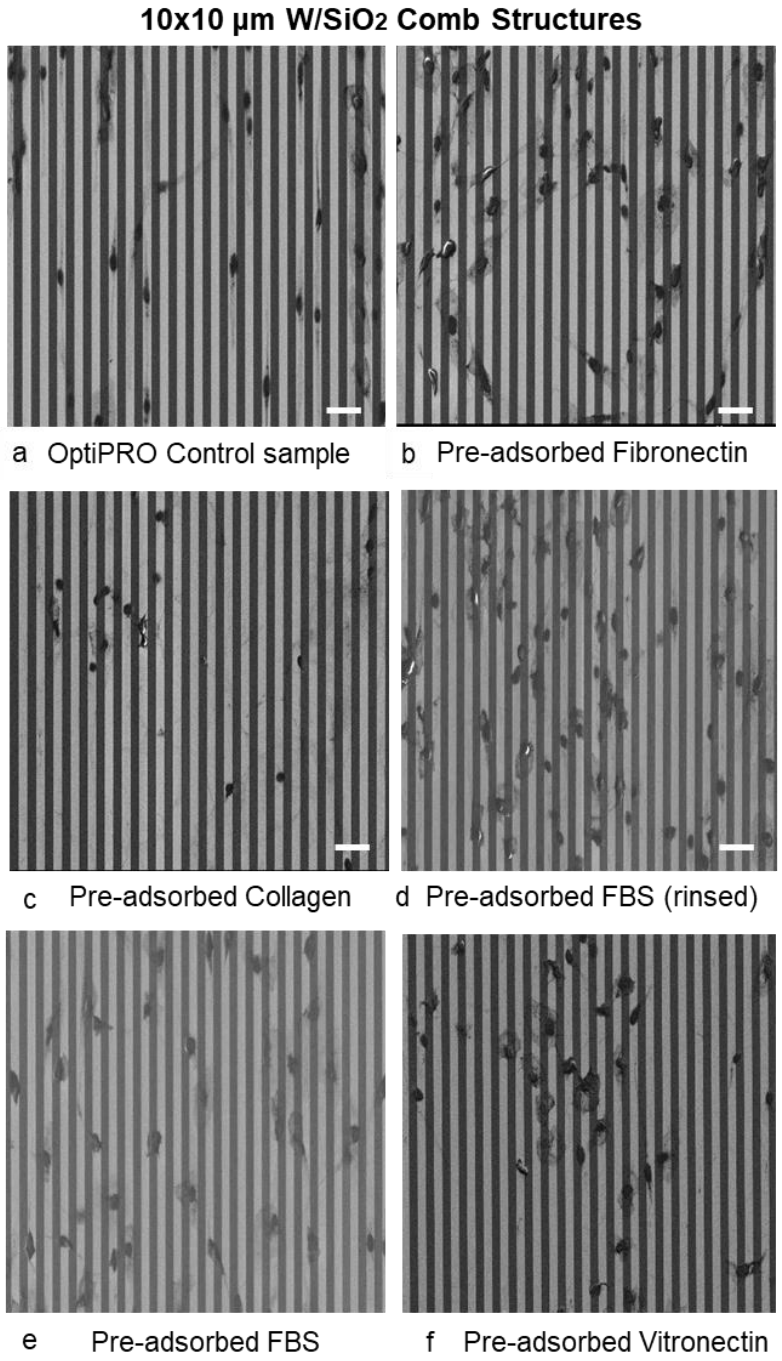

Figure 4-10 Typical top-down SEM images of Vero cells incubated in the OptiPRO™ culture media on a 2D substrate pre-adsorbed with different single-species serum proteins or FBS. The alignment and elongation behaviors of cells are dependent on the type of pre-adsorbed protein on the 2D substrates prior to seeding the cells (a) cells in OptiPRO™ used as a reference for comparison, (b, and e) Less of half of cells adherent on FN and FBS are aligned, and (c, d, and f) the majority of cells on pre-adsorbed Col, rinsed FBS, and VN are randomly oriented. Scale bars correspond to 50 µm.

However, when the pre-adsorbed FBS was rinsed using D-PBS, the number of adherent cells after seeding dropped by almost 11.8 % (n=4,855) as shown in Figure 4-13. This could be explained by the gradual desorption of the pre-adsorbed FBS from the substrate. The effect of FBS on the adhesion of cells as reported previously comes in agreement with findings by Wangen et al. (2018), Ye et al. (2017), and Tamada and Ikada (1985) when tested using albumins instead of FBS. The comparison between albumins and FBS could be justified (since albumin is the major component of FBS) in regards to adsorption and desorption of FBS. In comparison with pre-adsorbed FBS, fibronectin supported the adhesion of a lower number of cells (n=3,746) as illustrated in Figure 4-11, results came in consensus with findings by Wilson et al. (2005), and Yang et al. (2003). Webb et al. (1998) reported that the adhesion of NIH 3T3 fibroblast cells on a glass substrate is considerably higher when pre-coated with FN in comparison to collagen. This is similar to the results presented in this section and demonstrated for FN (n=3,746) as in Figure 4-12 in comparison to collagen (n=2,266) as confirmed in Figure 4-12. Pre-adsorbed VN induced the adhesion of a slightly fewer (-5.8 %) number of cells (n=3,536) in comparison to FN (n=3,746), as illustrated in Figure 4-15, and Figure 4-11, respectively. In comparison to other individual serum proteins, and as expected, substrates with pre-adsorbed FBS supported the highest number of adherent cells (Hook, 2014; Tamada and Ikada, 1992), followed by FN, VN, and Collagen.

In regards to the alignment behavior of cells as a function of the pre-adsorbed single proteins or FBS, results indicate that substrates pre-incubated with FBS (without rinsing) or fibronectin induced the highest alignment rates of 41.4±8.3 % (Figure 4-15), and 41.4±1.5 % (Figure 4-12), respectively. Moreover, rinsing the pre-adsorbed FBS with D-PBS negatively affected the ability of FBS to support cell alignment (33.0±2.2 %) as demonstrated in Figure 4-14. Expectedly, vitronectin and collagen-induced the lowest cell alignment with 21.7±1.4 % as in Figure 4-16, and 27.0±3.2 % as in Figure 4-13, respectively. For single species proteins, this can be explained by the effect of molecular weight and, the orientation of proteins on the substrate as discussed by Tamada and Ikada (1985). It is essential to take into account the adverse effect of pre-adsorbed single proteins on the adhesion and alignment of cells. Research by Hughes, Pena, Clark, and Dourmashkin (1979) reported that a substrate with a pre-adsorbed single protein becomes natural-like surface as to change the behavior of cells.

Hughes (1979) discussed how pre-adsorbed proteins provide the substrate with ligands for the cell membrane integrins. Additionally, Chelli et al. (2014) reported the positive impact of pre-adsorbed albumin on the alignment of human astrocytoma cells by creating cell-adhesive regions (like the tungsten lines) side by side with cell repulsive regions (like silicon oxide lines). Cai et al. (2009) and Blau et al. (2001) reported that the adhesion-promoting properties of a single protein are substrate-dependent.

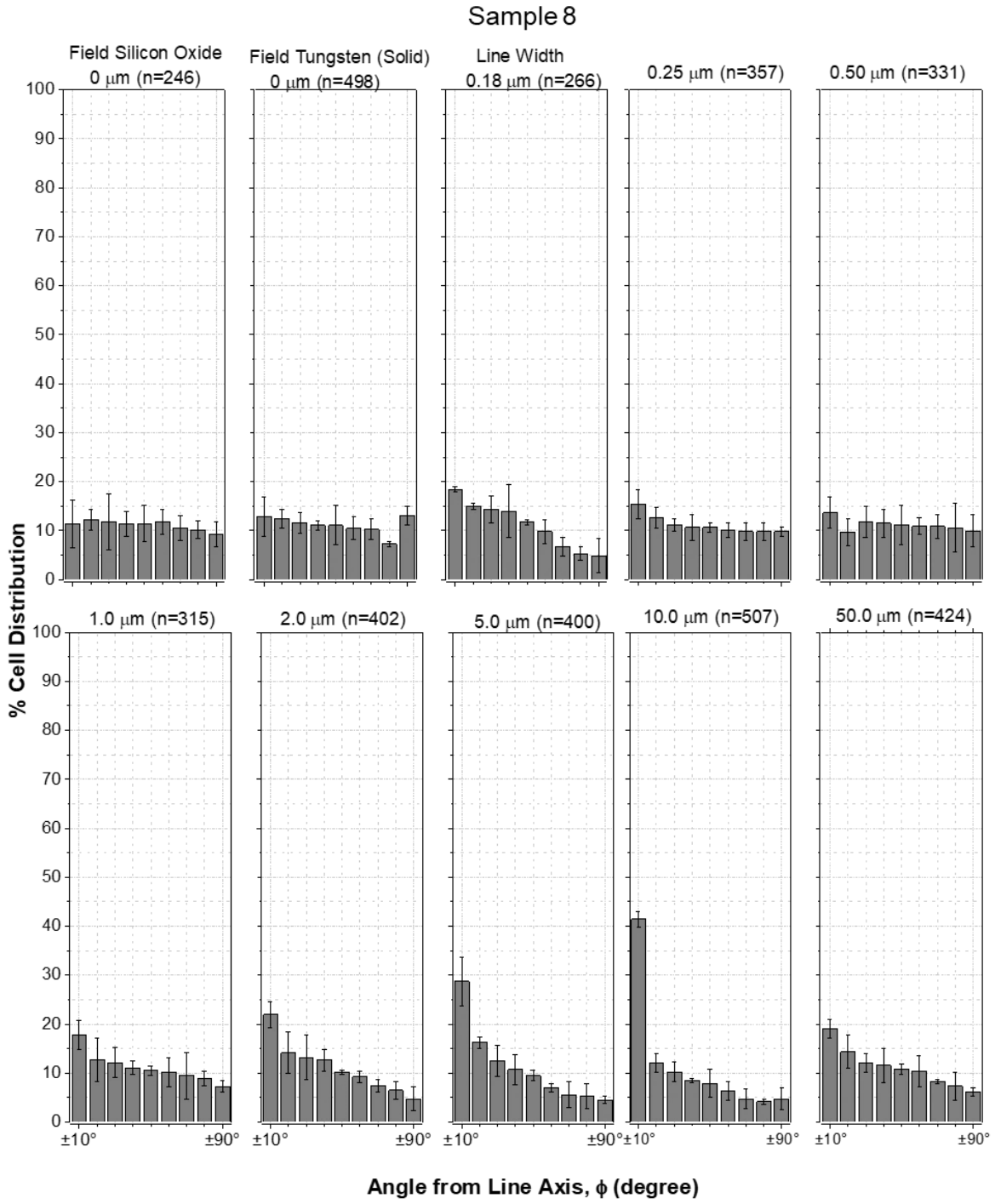

Figure 4-11 Alignment of Vero cells (incubated on pre-adsorbed fibronectin) as a function of metal lines width. From 0 μm (field oxide and field tungsten) to 50 μm. "n" is the number of cells inspected on each structure. Each bar represents the percentage of cells in a ±10° bin of deviations from the line axis. i.e., a cell with ϕ is -11° would be counted in the second bar from the right in each plot. Error bars correspond to one standard deviation from three different bins.

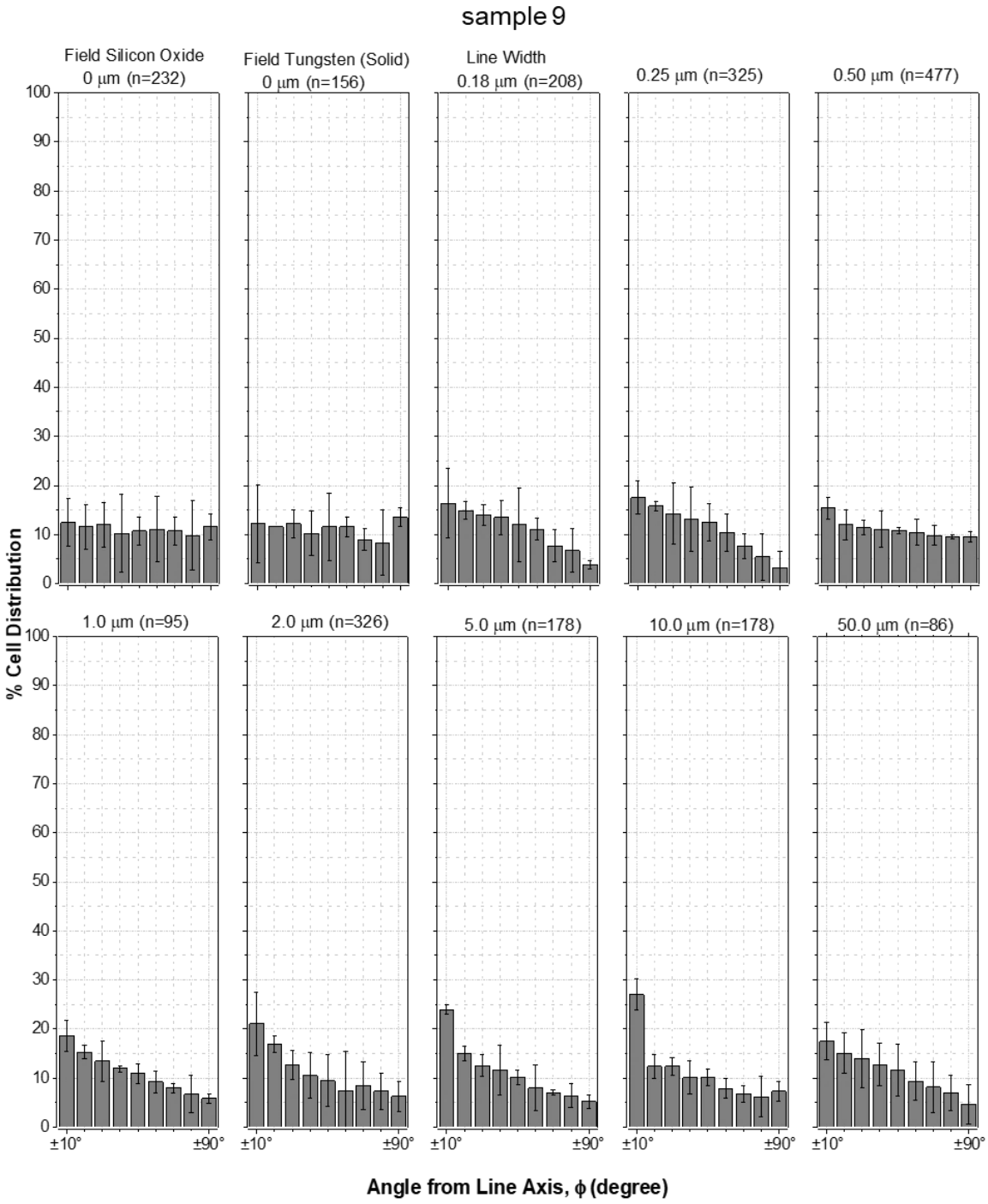

Figure 4-12 Percentage of cells alignment rates (incubated on pre-adsorbed collagen) as a function of metal lines width. From 0 μm (field oxide and field tungsten) to 50 μm. "n" is the number of cells inspected on each structure. Each bar represents the percentage of cells in a ±10° bin of deviations from the line axis. i.e., a cell with ϕ is -11° would be counted in the second bar from the right in each plot. Error bars correspond to one standard deviation from three different bins.

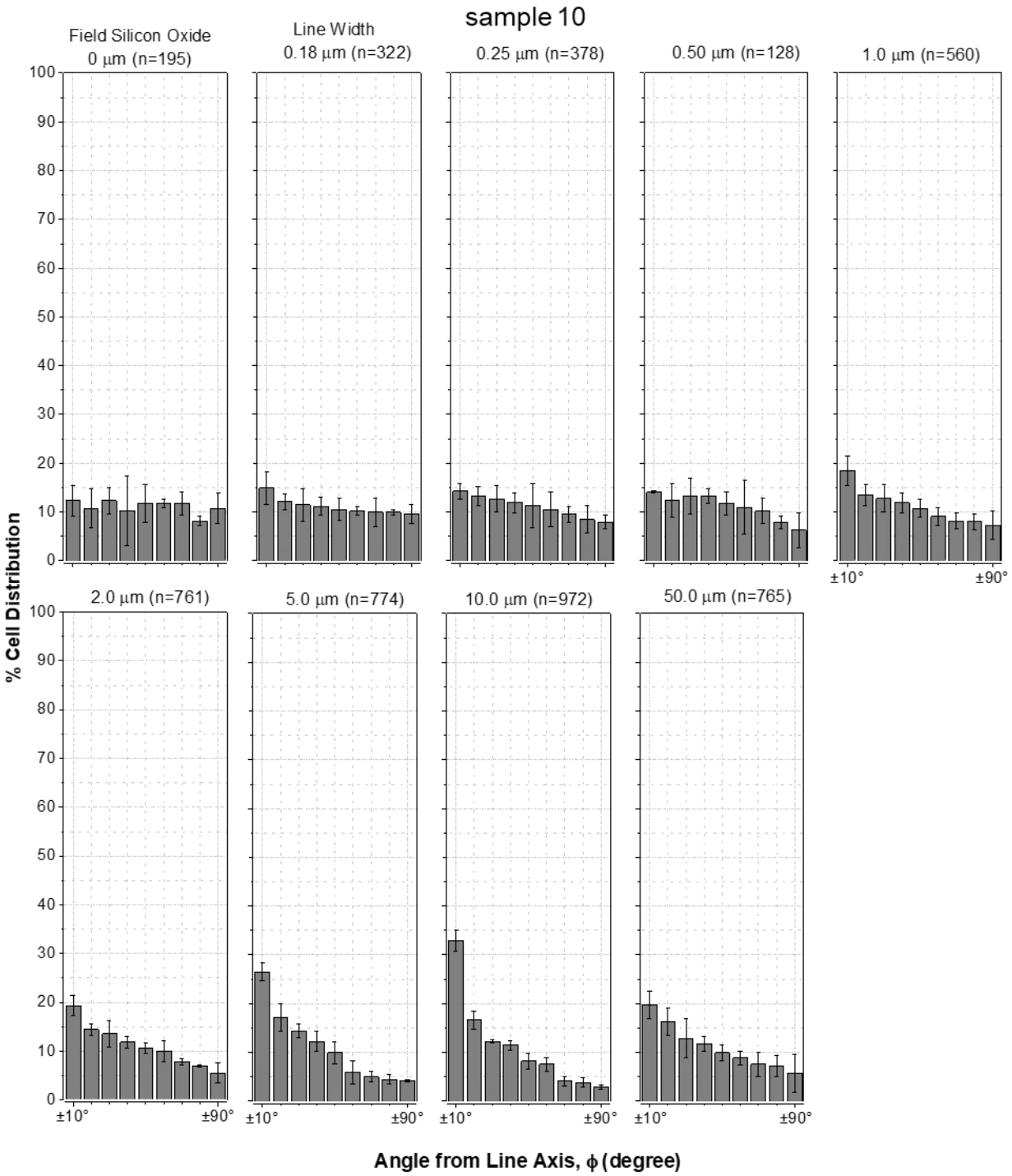

Figure 4-13 Alignment of Vero cells (incubated on pre-adsorbed 10 % FBS, rinsed using D-PBS prior to cell seeding) as a function of metal lines width. From 0 μm (field oxide and field tungsten) to 50 μm. "n" is the number of cells inspected on each structure. Each bar represents the percentage of cells in a ±10° bin of deviations from the line axis. i.e., a cell with ϕ is -11° would be counted in the second bar from the right in each plot. Error bars correspond to one standard deviation from three different bins.

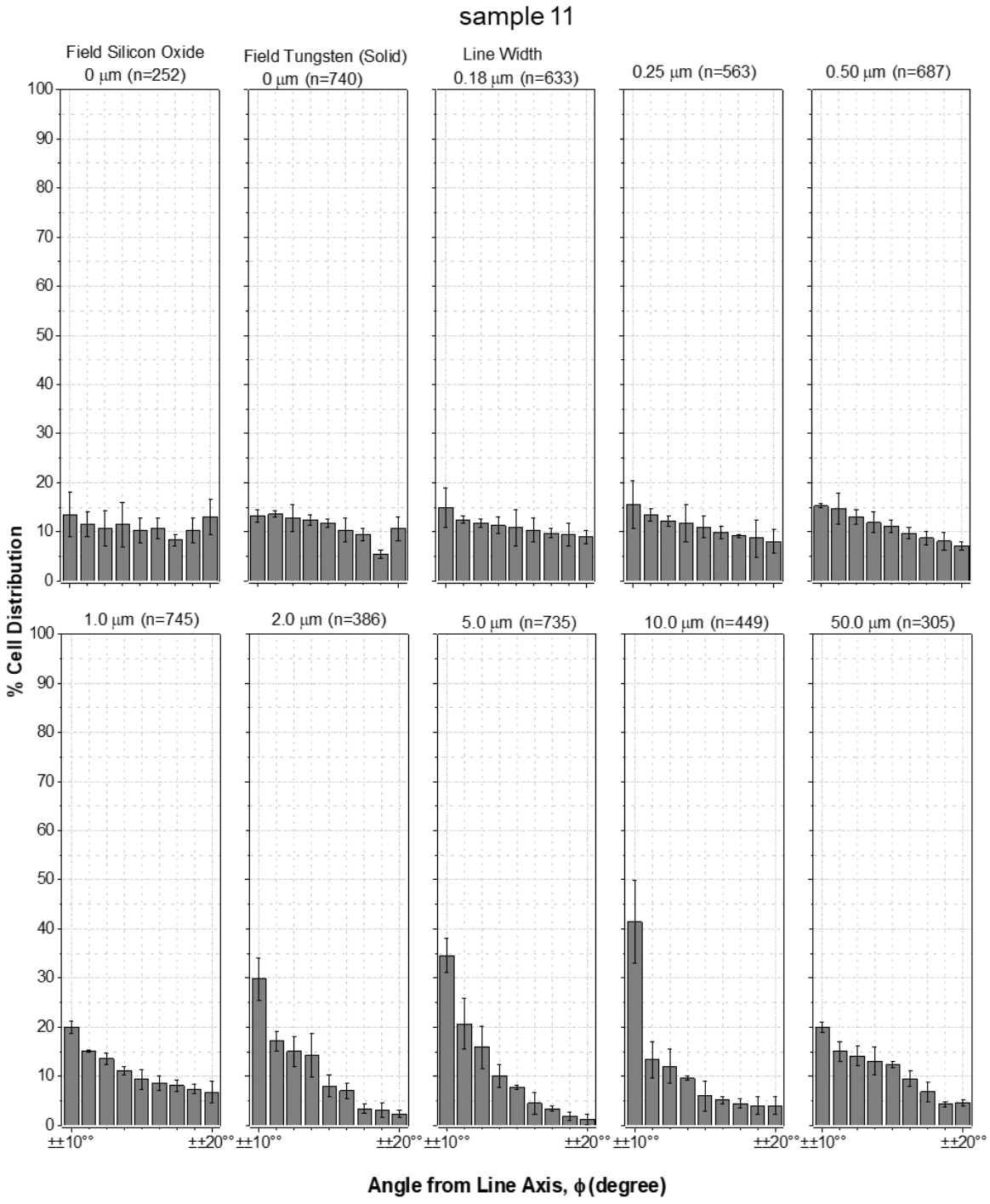

Figure 4-14 Alignment of Vero cells (incubated on pre-adsorbed 10 % FBS) as a function of metal lines width. From 0 μm (field oxide and field tungsten) to 50 μm. "n" is the number of cells inspected on each structure. Each bar represents the percentage of cells in a ±10° bin of deviations from the line axis. i.e., a cell with ϕ is -11° would be counted in the second bar from the right in each plot. Error bars correspond to one standard deviation from three different bins.

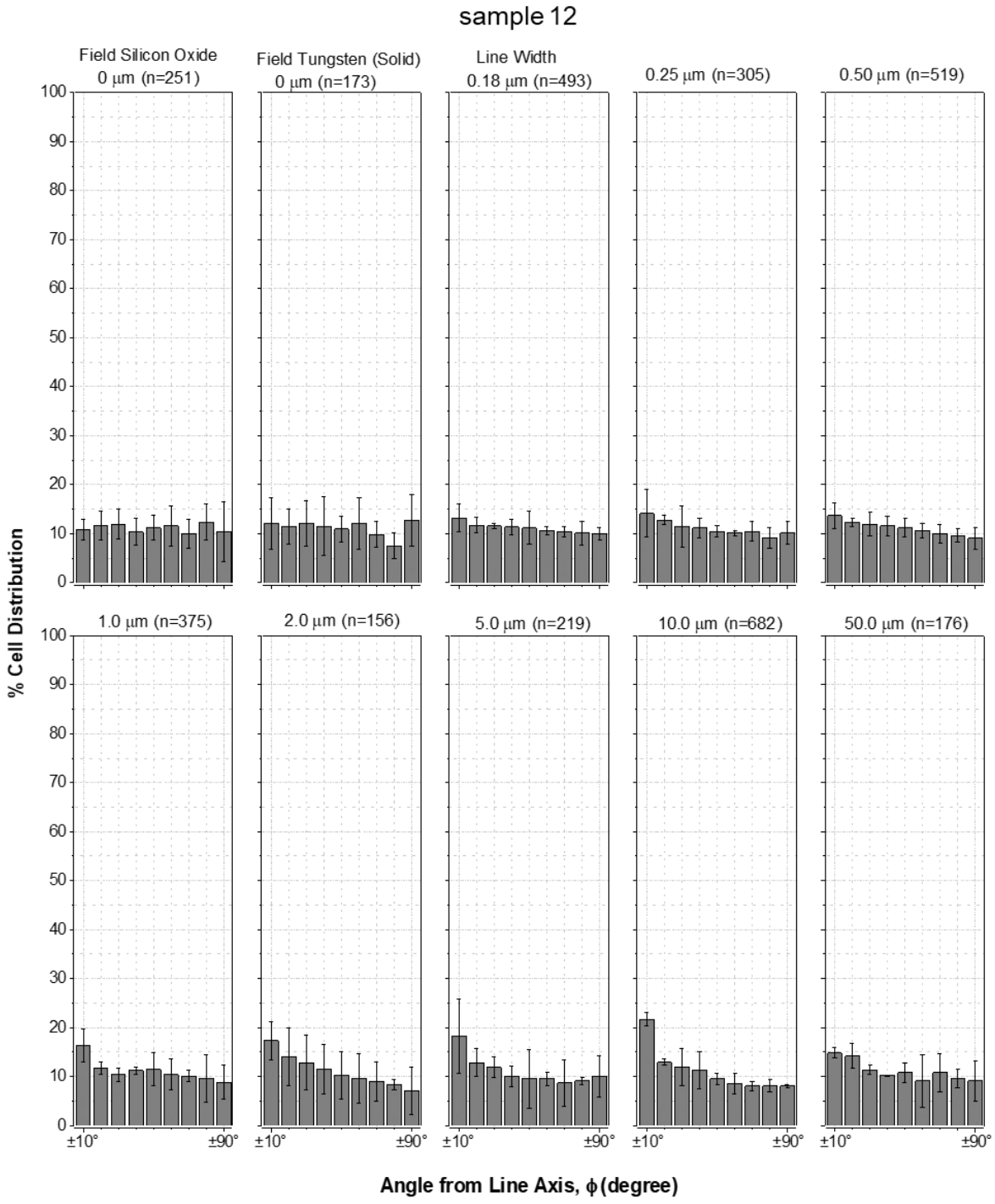

Figure 4-15 Alignment of Vero cells (incubated on pre-adsorbed vitronectin) as a function of metal lines width. From 0 μm (field oxide and field tungsten) to 50 μm. "n" is the number of cells inspected on each structure. Each bar represents the percentage of cells in a ±10° bin of deviations from the line axis. i.e., a cell with ϕ is -11° would be counted in the second bar from the right in each plot. Error bars correspond to one standard deviation from three different bins.

The summary of cell alignment data (ϕ in the range of $\pm 10°$) on 10x10 µm W and SiO_2 parallel lines comb structure are listed in Table 4-4. The 10x10 µm W/SiO_2 parallel lines comb structure was proven to be the pattern with the most potential to induce the highest preferential cell-substrate alignment.

Table 4-4 Summary of cell alignment distribution data incubated in different culture media on 10x10µm comb structures with an area of ~2.7 mm^2: number of measured cells, cell density, % population of cells and standard deviation (SD) with angle (ϕ) at ± 10° and ± 20° of the metal line axes. Initial cell concentration 5×10^4 cells/mL. SD represents one standard deviation from three independent groups of samples.

Sample Number	Matching Figure	Pre-adsorbed Protein	Pre-adsorbed Protein Concentration	Total Cell Count	Density (cell/mm^2) 10x10µm grid	% Cell Distribution	
						±10°	±20°
1	4-3	OptiPRO™	N/A	3,100	172	38.1±1.1	57.0±2.7
8	4-11	Pre-adsorbed Fibronectin	10 µg/mL	3,746	282	41.4±1.5	53.5±0.4
9	4-12	Pre-adsorbed Collagen	10 µg/mL	2,266	99	27.0±3.2	39.3±1.2
10	4-13	Pre-adsorbed FBS, rinsed with D-PBS prior to cell seeding	10 % FBS (v/v)	4,855	540	33.0±2.2	49.6±0.5
11	4-14	Pre-adsorbed FBS	10 % FBS (v/v)	5,495	249	41.4±8.3	54.8±5.7
12	4-15	Pre-adsorbed Vitronectin	10 µg/mL	3,536	379	21.7±1.4	34.6±0.7

All proteins were diluted in D-PBS solution prior to the pre-adsorption process

The summary of the comparison between the adhesion and alignment behaviors of Vero cells Table 4-3, Section 4.2.3.1, and Table 4-4, Section 4.2.3.1 is listed in Table 4-5.

Table 4-5 Summary of comparison data from the two protein-dependent alignment experiments including; the total number of measured cells, % population of cells and standard deviation (SD), the percentage of change for cell alignment (at ± 10°), and corresponding figure numbers. Initial cell concentration 5×10^4 cells/mL. Data obtained from comb structures with W/SiO_2 parallel lines of 10x10 µm

Sample Number	Matching Figures	Experiment	Culture Medium Component	Substrate Pre-treatment	Time		Total Cell Count	% Cell distribution ϕ in range ±10°	Alignment % of Change	% Cell distribution ϕ in range ±20°
					Protein Pre-adsorption	Cell Incubation				
1	4-3	OptiPRO™	OptiPRO™ Serum-Free	N/A	N/A	48 hrs.	3,100	38.1±1.1	-	57.0±2.7
2	4-4	Human Serum Albumin (HAS)	OptiPRO™ with HAS 10 µg/mL as a supplement	N/A	N/A	48 hrs.	2,409	95.3±0.7	-	97.0±0.7
3	4-5	Bovine Serum Albumin (BSA)	OptiPRO™ with BSA 10 µg/Ml as a supplement	N/A	N/A	48 hrs.	3,726	96.0±1.0	-	97.9±1.4
7	4-9	OptiPRO™ + Fibronectin	OptiPRO™ with 10 µg/ml FN as a supplemented	N/A	N/A	48 hrs.	4,402	45.7±4.0	~ 9.4% ↓	61.3±1.0
8	4-11	Pre-adsorbed Fibronectin	OptiPRO™ Serum-Free	10 µg/mL FN	24 hrs.	48 hrs.	3,746	41.4±1.5		53.5±0.4
6	4-8	OptiPRO™ + Collagen	OptiPRO™ with 10 µg/mL Coll-IV as a supplemented	N/A	N/A	48 hrs.	4,977	29.9±1.7	~ 9.7% ↓	44.2±1.6
9	4-12	Pre-adsorbed Collagen	OptiPRO™ Serum-Free	10 µg/mL Col-IV	24 hrs.	48 hrs.	2,266	27.0±3.2		39.3±1.2
5	4-7	OptiPRO™ + Vitronectin	OptiPRO™ with 10 µg/mL VN as a supplemented	N/A	N/A	48 hrs.	3,850	24.9±3.3	~ 12.9% ↓	36.1±3.4
12	4-15	Pre-adsorbed Vitronectin	OptiPRO™ Serum-Free	10 µg/mL VN	24 hrs.	48 hrs.	3,536	21.7±1.4		34.6±0.7
4	4-6	OptiPRO™ + 10 % FBS	OptiPRO™ with 10 % FBS as a supplemented	N/A	N/A	48 hrs.	5,446	61.6±2.7	-	72.6±1.4
10	4-13	Pre-adsorbed 10 % FBS. Substrate rinsed with D-PBS prior to cell deposition	OptiPRO™ Serum-Free	10% (v/v) FBS	24 hrs.	48 hrs.	4,855	33.0±2.2	~ 46.4% ↓	49.6±0.5
11	4-14	Pre-adsorbed 10 % FBS	OptiPRO™ Serum-Free	10% (v/v) FBS	24 hrs.	48 hrs.	5,495	41.4±8.3	~ 32.8% ↓	54.8±5.7

OptiPRO™ serum-free culture medium data is used as a control sample for comparison. All proteins were diluted in D-PBS solution prior to the pre-adsorption process.

Table 4-5 indicates that FBS in both sets of experiments continues to support the highest cell adhesion and growth. This is similar to findings reported by Felgueiras et al. (2015), Kyriakides (2015), Parhi, et al., (2010), Krishnan et al. (2006) and Hayman et al. (1985). However, when pre-adsorbed FBS was rinsed with D-PBS prior to seeding the cells, the substrate supported less cell adhesion and alignment (~46.4 %). Substrates with pre-adsorbed single protein or serum supported lower alignment and growth rates of cells. For single proteins, the decrease in the alignment rates varied between ~9.4 % for FN pre-adsorbed substrate, ~9.7 % for VN, and ~12.9 % for collagen pre-adsorbed substrate, which indicates performances that are independent of whether the protein used as a supplement or pre-adsorbed on the substrate. Similarly, substrates pre-coated with PBS showed a decrease in alignment and growth rates.

This is further illustrated in Figure 4-16 in which the percentage of cell nuclei aligned within ±10°, and ±20° of the tungsten lines y-axes were graphed as a function of (a) the culture medium used, or (b) the type pre-adsorbed protein. The alignment behaviors of adherent Vero cells on the 2D W/SiO_2 micron and sub-micron scale patterned substrate incubated in OptiPRO^{TM}, the serum-free medium supplemented by one of the serum single-species proteins or 10 % FBS based on data from Table 4-5, are further demonstrated in Figure 4-16(a), in which demonstrate the alignment of cells within ±10° (blue squares) and ±20° (gray circles) of the tungsten parallel lines y-axes. OptiPRO^{TM} was used as a control sample for comparison. Figure 4-16(b) exemplifies the alignment of cells within ±10° (blue squares) and ±20° (gray squares) from the tungsten parallel lines y-axes as a function of the pre-adsorbed protein on comb structures with line widths of 10 μm.

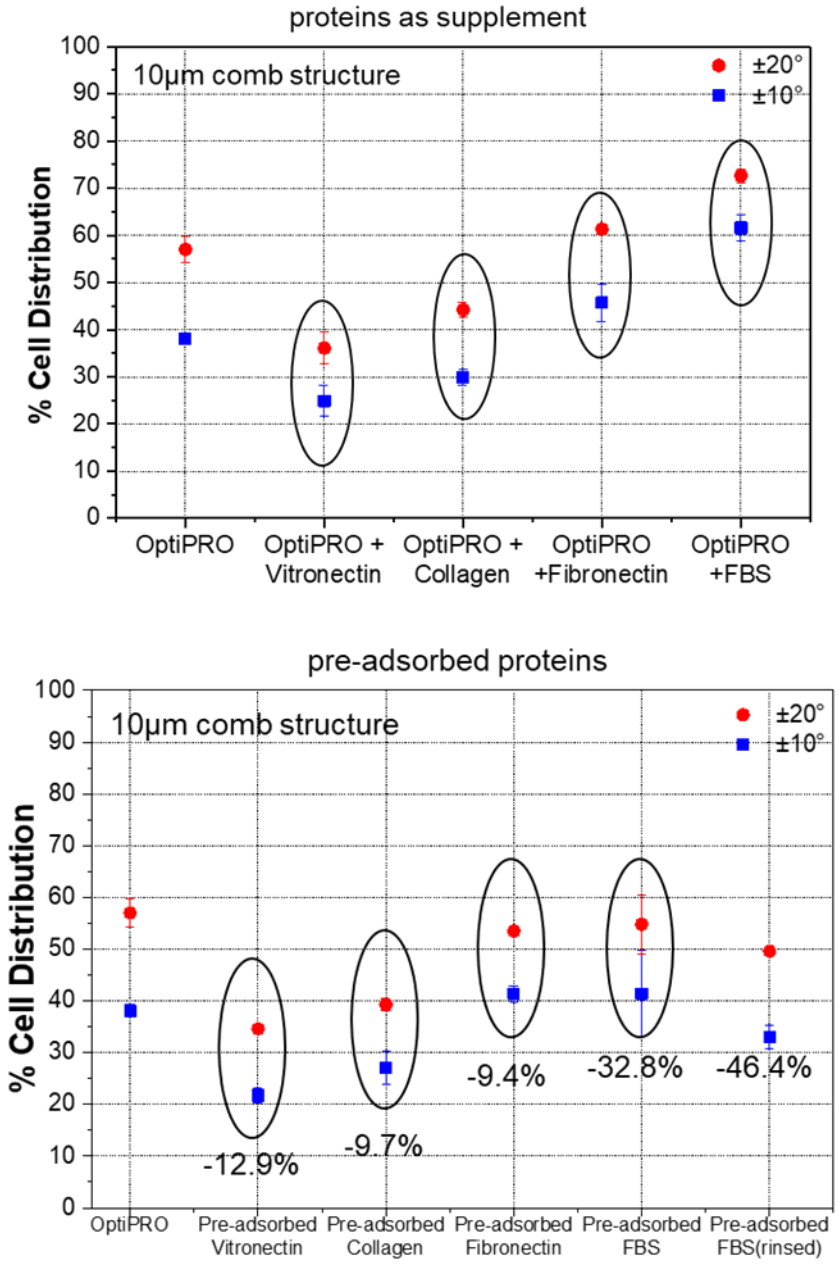

Figure 4-16 Percentage of cell alignment distribution in the range of ±10° (blue squares) and ±20° (gray circles) as a function of (a) single species proteins (FN, VN, Col) or FBS added as a supplement to OptiPRO™, the serum-free medium. (b) Pre-adsorbed single species proteins (FN, VN, Col) or FBS on the 2D substrates for 24 hours prior to seeding the cells. Individual proteins (supplement and pre-adsorbed) were added at a concentration of 10 µg/mL, while 10 % FBS was added on a volume basis. Error bars correspond to one standard deviation from three different groups.

4.3 Summary

In this chapter, the alignment and adhesion behaviors of Vero cells on the 2D W/SiO_2 engineered substrates were characterized and assessed. Herein, two sets of experiments were conducted; (1) single ECM proteins, and FBS were used as a supplement for OptiPro^{TM} a serum-free medium, and (2) single ECM proteins and FBS were pre-adsorbed on the substrates prior to seeding the cells. Thus, the characterization of cellular alignment and growth behaviors performed taking into consideration the cell-substrate interactions as a function of the cell-protein related mechanism, which in spite of the significant advancement in understanding the influence of proteins on the cellular behaviors, the disagreement among researchers is widely accepted when trying to the explain these mechanisms and commonly observed behaviors such as protein structural rearrangements, or aggregation (Rabe et al., 2011). However, and regardless of the precise mechanism, our results show that serum albumin (supplement for serum-free media), as verified in Section 4.2.3.1, and fibronectin and FBS (pre-adsorbed on the 2D micron and sub-micron scale patterned substrates) as validated in Section 4.2.3.2, played an important role in the alignment behavior of assessed Vero cells. Furthermore, it is worth indicating that sometimes formulating a relevant and applicable hypothesis to interpret the experimental data successfully is hindered by an insufficient level of understanding. In such cases, a data-driven approach can be developed, at which, the initial step is to start accumulating experimental data (produced and from future work) that may enhance our knowledge (Derda et al., 2010; Kell and Oliver, 2003).

Chapter 5

Manipulating Cell Behavior using a Novel 3D Tantalum and Silicon Oxide Patterned Substrate

This chapter is based on the following publication:

Moussa, H.I.; Logan, M.; Chan, W.; Wong, K.; Rao, Z.; Aucoin, M.G.; Tsui, T.Y., Materials 11, 2018, 1306.

This chapter will demonstrate the ability of an original three-dimensional tantalum/silicon oxide micron and sub-micron scale substrate to induce a preferential change in the cellular behavior of mammalian cells in response to the topographical features of the 3D micron and sub-micron scale patterned substrate understudy. The substrate consists of comb structures with silicon lines and tantalum trenches of equal width. In Chapter 3, we successfully tested the ability of the newly developed two-dimensional tungsten and silicon oxide micron and sub-micron scale patterned substrate to guide a cell-preferential adhesion, and alignment. This was done by attracting adherent Vero cells to targeted locations. These specific tungsten locations are inlaid parallel tungsten lines embedded in silicon oxide continuous phase that have no topographical features, and they were proven to have remarkably smooth, flat, continuous, and defect-free surfaces. This happened due to the selective adhesion of cells onto tungsten rather than silicon oxide, in the absence of any external mechanical stimuli. However, *in vivo*, cells are subjected to interactions with three-dimensional micron and sub-micron environments of ECM. This shows the importance of developing three-dimensional engineered substrates that may have the *in vitro* ability to mimic the effect of extracellular matrix in stimulating preferential cell behaviors. These behaviors were found to be different when tested on 3D systems rather than 2Ds (Hakkinen et al., 2011; Ochsner et al., 2007; Cukierman, Pankov, and Yamada, 2002).

Thus, this chapter demonstrates the ability of an original three-dimensional tantalum and silicon oxide micron and sub-micron scale patterned substrate to induce a preferential change in that cellular behavior of mammalian cells in response to the topographical features of the patterned substrate under study. The substrate consists of comb structures with equal-width silicon lines and tantalum trenches.

5.1 Background

The impacts of topography (Ning et al., 2016; Hakkinen et al., 2011; Choi et al., 2009; Loesberg et al., 2007), aspect ratio, shape (Kolind et al., 2010; Lord et al., 2010; Ochsner et al., 2007), and distribution of

microstructures (Nakamoto et al., 2014; Martinez et al., 2009) on the adhesion and change in morphology of cells are the subject of many scholarly works. However, all previously-mentioned literature used monolithic materials where the entire structures consisted of a single material, except for a few (Radtke et al., 2017; Poudel et al., 2013; Arnold et al., 2009). Many studies discussed the ability of cells to align themselves along the defined substrate surface morphologies (Sharma et al., 2016; Lu and Leng, 2008; Stevenson and Donald, 2009; Lu and Leng, 2003; Curtis and Wilkinson, 1997). This is known as the contact guidance phenomenon (Zhou, Yuan, Huang, and Chen, 2009; Teixeira et al., 2003; Brunette and Chehroudi, 1999; Meyle, Gültig, and Nisch, 1995; Wood, 1988). Many studies have also been concerned with the effects of depth and width of grooves on cell orientation (Stevenson and Donald, 2009; Lu and Leng, 2008; Loesberg, 2005; Lenhert, Meier, Meyer, Chi, and Wiesmann, 2005), but no consensus have been reached on the minimal depth and width needed for inducing cell orientation. These behaviors are cell type-related. Cells are also able to orient themselves on surfaces presenting nano-grooves (Lenhert et al., 2005).

Radtke et al. (2017), and Baranes, Shevach, Shefi, and Dvir (2016) developed innovative silver and gold biomaterials that can induce higher elongation behavior if cells. While micropatterning of proteins' topographical features (Sharma et al., 2016; Poudel et al., 2013; García-Parra et al., 2012; Pelaez-Vargas, et al., 2012; Versaevel, Grevesse, and Gabriel, 2012) or functionalized nanoparticles (Arnold et al., 2009; Cooke et al., 2008; Coussen, Choquet, Sheetz, and Erickson, 2002) provides the potential to manipulate the behavior of cells, only two-dimensional topographical features can be fabricated using these technologies, which restrict its applications. Hakkinen et al. (2011) underlined the effect of adsorbed proteins and structural dimensionality (3D and 2D) of the surface on the cell-substrate adhesion and ability of the cell to migrate and spread (area occupied per cell). This is similar to findings by Ochsner et. al. (2007); thus, comparing the change in cellular behaviors of cells on 2D and 3D structural topographies is problematic (Choi et al., 2015; Yang et al., 2009; Choi, et al., 2009; Kim , et al., 2006; Levenberg et al., 2003; Cukierman, Pankov, and Yamada, 2002).

The characterization of the ability of cells to adhere to a substrate reflects their behavior, and a multifaceted process that is regulated by protein-protein, protein-surface, protein-water, and water-surface interactions and cell signaling pathways. To be more specific, interactions that cause the formation of focal adhesion points are most important for their potential role in sensing the structural environment of the surrounding 3D topographies, cytoskeletal organization spreading, migration, and proliferation (Ferrari et al., 2010; Ryoo et al., 2010; Yim et al., 2010; Partridge and Marcantonio, 2006; Beningo, Dembo, Kaverina, Small, and Wang, 2001). Chapter 3 addressed the adhesion and the change in

morphology of mammalian cells on 2D W/SiO_2 patterned substrate. Their findings indicate that such changes are possible without the need for topographical features. Results demonstrate that the tendency of cells to change their morphology is induced by the need to maximize their contact area parallel to the y-axes of tungsten lines.

This chapter is intended to investigate and characterize the interactions between Vero cells and 3D micron and sub-micron patterned topographies entailing tantalum and silicon oxide parallel line/trench features ranging from ~210 nm to 100 μm. According to the initial hypothesis, cells may exhibit a preferential cellular behavior while interacting with the substrate 3D topographical tantalum features. This expected behavior is associated with preferred adhesion to tantalum as a result of its bioactive properties as a metal (Dolatshahi-Pirouz et al., 2010; Balla, Bodhak, Bose, and Bandyopadhyay, 2010) rather than silicon oxide. This predicted preferential adhesion is based on the work presented in Chapter 3 but on 2D W/SiO_2 substrates. However, in comparison to 2D substrates, it is hypothesized that the 3D topographical features will induce a higher cell elongation.

Additionally, the new substrates will provide the opportunity to observe the formation of focal adhesions and the cells' pseudopodia in action. That was unfeasible to do on the 2D surfaces characterized in Chapter 3. This chapter characterizes the alignment behaviors of cells relative to the y-axes of the tantalum trenches. Three attachment behaviors were identified based on the widths and spacing of lines and trenches, respectively. A mathematical model was used to understand the change in cellular morphologies as a function of the surface topographies. This chapter provides a unique opportunity to observe and understand the limitations of cellular pseudopodia projections.

5.2 Materials and Methods

5.2.1 Fabrication of the Tantalum/Silicon Oxide 3D Patterned Substrate

The 3D Ta/SiO_2 patterned substrates were fabricated and provided by Versum Materials, LLC (Tempe, AZ). The supplied substrates were fabricated using an advanced industrial-scale integrated circuit fabrication technique that comprises of Cu and Ta CMP and damascene integration on 200 mm silicon substrates (Doering and Nishi, 2007; Chen, 2007; Li Y., 2007), as illustrated in Figure 5-1. In brief, lithography and dry-etching methods were used to create the patterns of the parallel-line comb structure in the silicon oxide layer, which appears in blue (Doering and Nishi, 2007; Chen, 2007; Zantye, Kumar, and Sikder, 2004). This step was followed by depositing a thin seed layer of tantalum and copper in the patterned structures. CMP process was used to eliminate the unwanted copper and tantalum layers, and planarization was continued until the silicon oxide lines were uncovered as revealed in Figure 1(c) (Zhao

and Lu, 2013; Zhengfeng, Ling, Huan, and Luan, 2001; Steigerwald, Murarka, Gutmann, and Duquette, 1995; Stavreva , Zeidler, Plötner, and Drescher, 1995). Furthermore, in order to be able to use the substrates in direct contact with biological cells (Vincent, Duval , Hartemann, and Engels-Deutsch, 2017; Grass, Rensing, and Solioz, 2011), copper was chemically stripped and removed using ~42 % diluted nitric acid ACS Plus (Fisherbrand®, Fisher Scientific International Inc., Pittsburgh, PA) for ~45 minutes. Finally, stripped chips were rinsed with deionized water and anhydrous ethanol. The finished substrate consisted of a parallel-line comb structure with trench sidewalls and bottom surfaces coated with a thin layer of tantalum, while the top surfaces of the lines contained exposed silicon oxide (Figure 5-1).

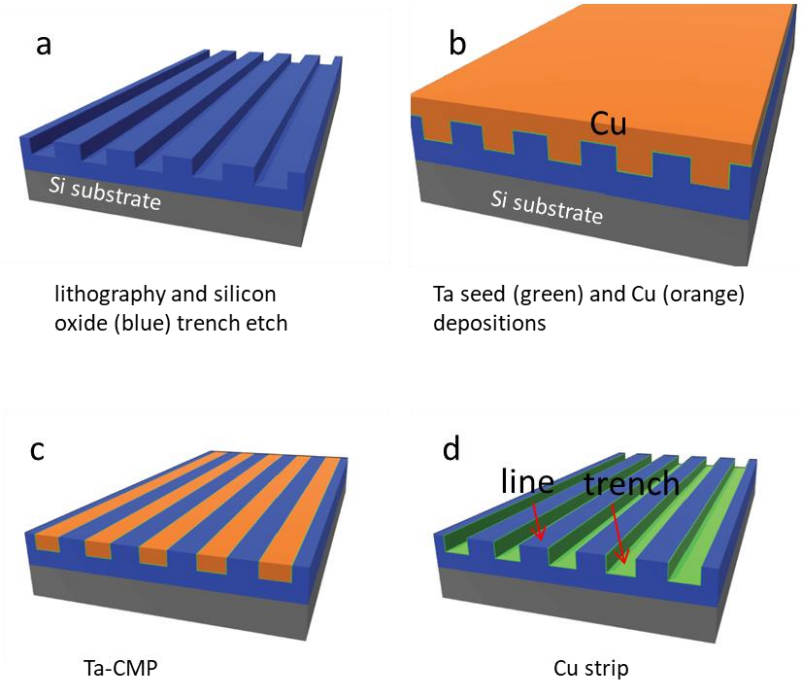

Figure 5-1 Simplified representation of the silicon oxide and tantalum (Ta) polished specimens. Parallel line/trench patterns were fabricated using Barrier-CMP process by lithographically creating inlaid trenches within the silicon oxide thin film (blue), followed by dry etching as in a. This step was followed by (b) the deposition of Ta (barrier layer) and copper film the patterned structures. (c) Chemical mechanical polishing was used to remove the excess copper and barrier subsequently. (d) Copper was stripped using nitric acid (Moussa et al., 2018a).

5.2.2 Cell Deposition, Fixation, Dehydration and Staining Protocols

Based on the same protocols described in Section 3.2.3.1, Vero cells were incubated on the 3D Ta/SiO2 substrate mentioned above. The American Type Culture Collection (ATCC, Manassas, Virginia) was the source for the Vero cells used in this experiment. Cells in a culture medium containing DMEM/F12 (1:1) media (Corning, New York, NY) were supplemented with 4 mM L-glutamine (Sigma-Aldrich, St. Louis,

MO) and essential amino acids. Furthermore, 10 % (v/v) FBS (Gibco™, Thermo Fisher Scientific, Waltham, MA, USA) was added to the culture medium; cells were seeded on the 3D substrates and incubated for 24 hours in 5 % CO_2 atmosphere at 37 °C. The substrates were decontaminated with 70 % ethanol for half a minute and then washed with D-PBS a saline solution prior to cells' deposition. The initial concentration of seeded cells is ~0.5×10^5 cells/mL. After 24 hours, the excess medium was removed, and the substrates were washed with D-PBS. For samples which are intended to be characterized using the fluorescence confocal microscope, adherent cells were fixed, permeabilized, and stained according to the method described in Moussa et al. (2018a). Fluorescence confocal microscopy was carried out at the University of Guelph using a Leica TCS SP5 confocal fluorescence microscope (Leica, Wetzlar, Germany). The cells were inspected with wavelengths in the ranges of 436–482 nm (for DAPI) and 650–700 nm (for CytoPainter F-actin) (Chapter 3, Section 3.2.3.1).

Substrates intended for characterization using scattering electron microscope were only fixed and dehydrated as discussed in Section 3.2.3. A Zeiss 1550 field-emission scanning electron microscope (Carl Zeiss AG, Oberkochen, Germany) was used with EHT of 7kV.

5.3 Results and Discussion

This section is intended to investigate whether the barrier-CMP substrates can be used to manipulate the orientation and alignment of Vero cells, as a result for the preferential adhesion of cells and the interaction with materials (Ta vs. SiO_2) and topography (lines vs. ditches). The experiments and results are vital for the viability of this research. The characterization of Vero cells alignment and change in morphology behaviors was done using the method described in Section 3.2.4.

Briefly, the changes in the morphology of the adherent cells were characterized using two different methods. (1) Nuclear orientation denoted by the angle ϕ, which is measured between the nucleus long axis and the tantalum ditches parallel lines y-axes (as demonstrated in Figure 3-6); (2) Nuclear elongation (deformation) ratio was measured and calculated as the ratio between a nucleus long and short axial length (L/S). As previously indicated in Chapter 3, ϕ and L/S were measured manually via Image Processing and Analysis in Java (ImageJ) software using lines of best fit, based on a visual estimate of the nucleus boundary.

5.3.1 Characterization of the Barrier-CMP Substrates

The fabricated specimens were inspected using SEM (make and model as listed in Chapter 3) of 70° tilted substrates. Typical SEM micrographs were generated for multiple comb structures with different parallel

silicon oxide lines (dark gray) and trenches covered with thin film tantalum (light gray) widths as illustrated in Figure 5-2. The trenches were measured to be ~500 nm deep. It is important to note that tantalum covered the sidewalls and bottoms of the trenches. Copper was fully stripped and the trenches are clean; smooth, and defect-free; and the trenches' sidewalls and bottom substrates were nearly perpendicular to each other. The root-mean-square (RMS) roughness of SiO_2 lines and Ta trenches were measured using AFM to be ~0.01-0.4 nm and ~0.5-1.0 nm, respectively.

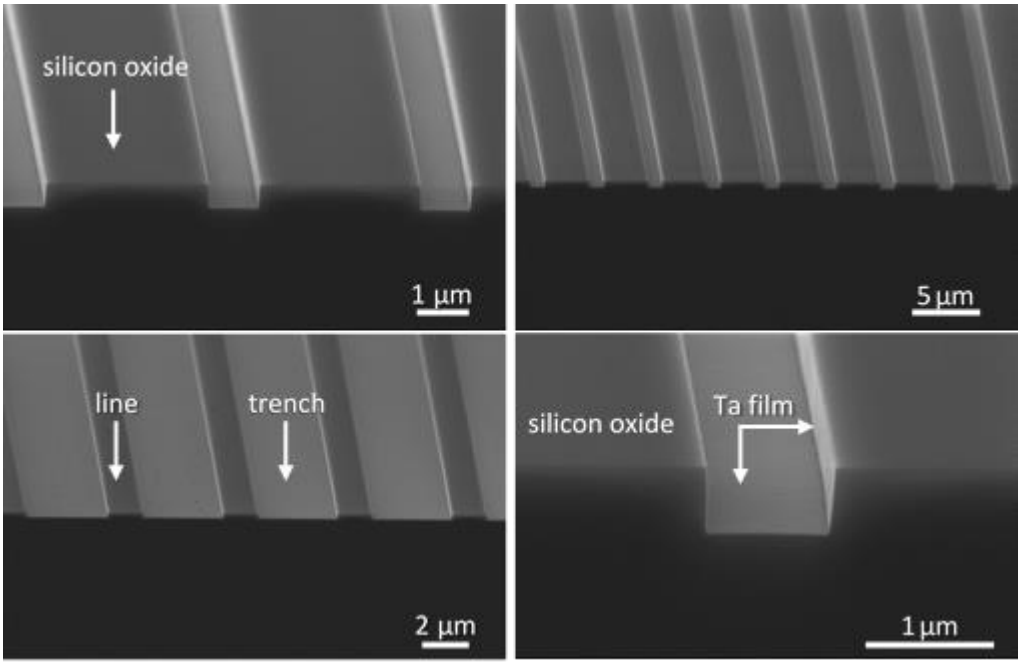

Figure 5-2 70° tilted SEM micrographs of barrier-CMP specimens after copper stripping with multiple lines and trench widths.

In total, ten different areas were inspected, divided one tantalum blanket film and nine comb structures with tantalum trench widths of 0.21, 0.26, 0.5, 1, 2, 5, 10, 50, and 100 µm. It is worth noting that, except for the 0.21 and 0.26 µm trench structures, all comb structures had widths of 0.15 and 0.24 µm for lines and trenches, respectively.

5.3.2 Pattern-Dependent Cell Alignment

The alignment behaviors of Vero cells as a function of trench widths were quantitatively assessed using typical micrographs generated using fluorescence confocal of adherent cells on isolated trenches, and comb structures with variable trench widths of 0.21, 0.26, 1, 10, and 50 µm are demonstrated in Figure 5-3. The white dashed lines (Figure 5-3 a, c, e, g, and i) demonstrate the trench boundary lines.

The nuclei were stained with blue DAPI, while the F-actin microfilaments appear in red due to staining with CytoPainter F-Actin. Fluorescence confocal images show that cells on isolated trenches were elongated and aligned in parallel to trench y-axes, while cells on blanket silicon oxide, pointed at with white arrows, were randomly oriented, had irregular shapes, and spread more. Similarly to the behavior of cells on isolated trenches, cells on dense comb structures (Figure 5-3 b, d, f, h, and j) tended to align their nuclei in the direction of the trench y-axes. Cells adherent on the 10 and 50 μm-wide comb structures seemed to restrict their physical location on the trench sidewalls and the bottom surfaces as they are covered with tantalum, but not on silicon oxide lines. Similarly to the random behavior of cells on silicon oxide blankets, cells adherent to tantalum blanket exhibited no preferred orientation or alignment. Figure 5-4 compares the alignment and spreading behaviors of Vero cells on tantalum and oxide blankets. Scanning Electron Microscope was also used to examine the alignment and spreading behaviors of the adherent cells on SiO_2/Ta comb structures, as exemplified in Figure 5-5. As expected, cells on trenchers wider than 10 μm tended to fully conceal themselves within the Ta-coated trenches, as inspected previously in Figure 5-3.

To quantitatively prove the observations from Figure 5-3, Figure 5-4, and Figure 5-5, the nuclei angular positions ϕ of the adherent cells (after 24 hours of incubation) were measured as a function of tantalum trenches width. The percentage of cells distribution in a ±10° interval from the y-axes of the trenches were produced and graphed as documented in Figure 5-6. The number of adherent cells inspected on the different substrates is referred to as "n". Results confirm the observations and demonstrate that cells were randomly aligned and irregularly spread in no preferential direction on the blanket tantalum. On the contrary, cells on comb structures tended to align in the direction of the trenches y-axes significantly. The positive correlation between the width of a trench and the alignment of cells reached a peak value at 10 μm wide Ta trenches, at which ~91 % of cells aligned within ±10° from the trench y-axes.

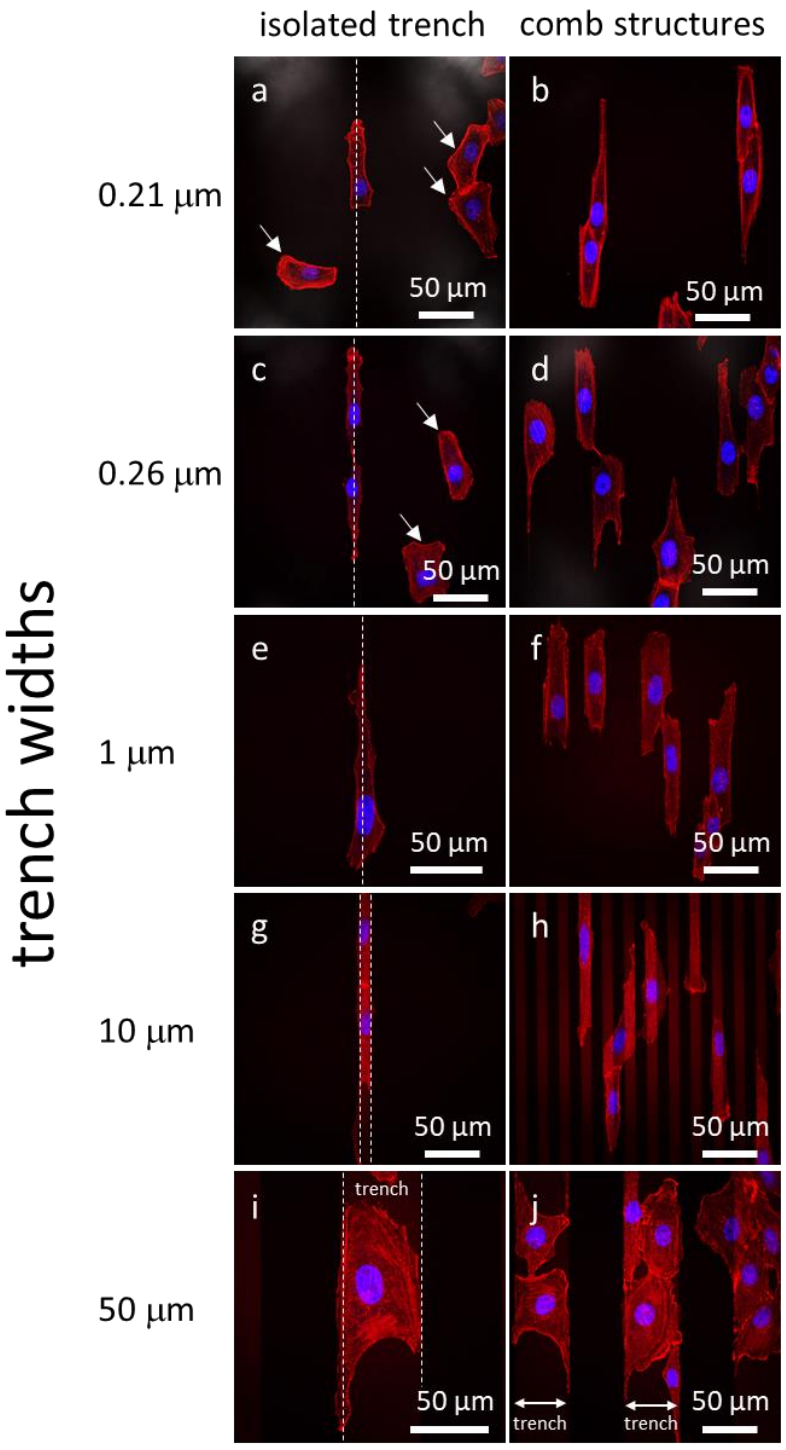

Figure 5-3 Images of Vero cells adherent on isolated trenches (a, c, e, g, i) and comb structures (b, d, f, h, j) with variable trench widths using fluorescence confocal microscope. Dashed white lines on a, c, e, g, and i, indicate boundaries of the isolated trenches. The nuclei are blue stained, and F-actin microfilaments are stained red. Incubation time is 24 hours (Moussa et al., 2018a).

It was proven that cells lose their preferential alignment to become disoriented and misaligned when Ta trenches become 50 and 100 μm wide. Data on nuclear elongation (deformation) of each adherent cell was calculated as a ratio (L/S) of the measured long (L) and short (S) axes of the nucleus. In a similar trend to cell alignment, cells on 10 μm wide trenches showed the highest elongation with L/S ratio of 2.98±0.82 in comparison to much smaller elongation for cells adherent to blanket Ta and 100 μm wide trenches with L/S of 1.64±0.44 and 1.49±0.32, respectively.

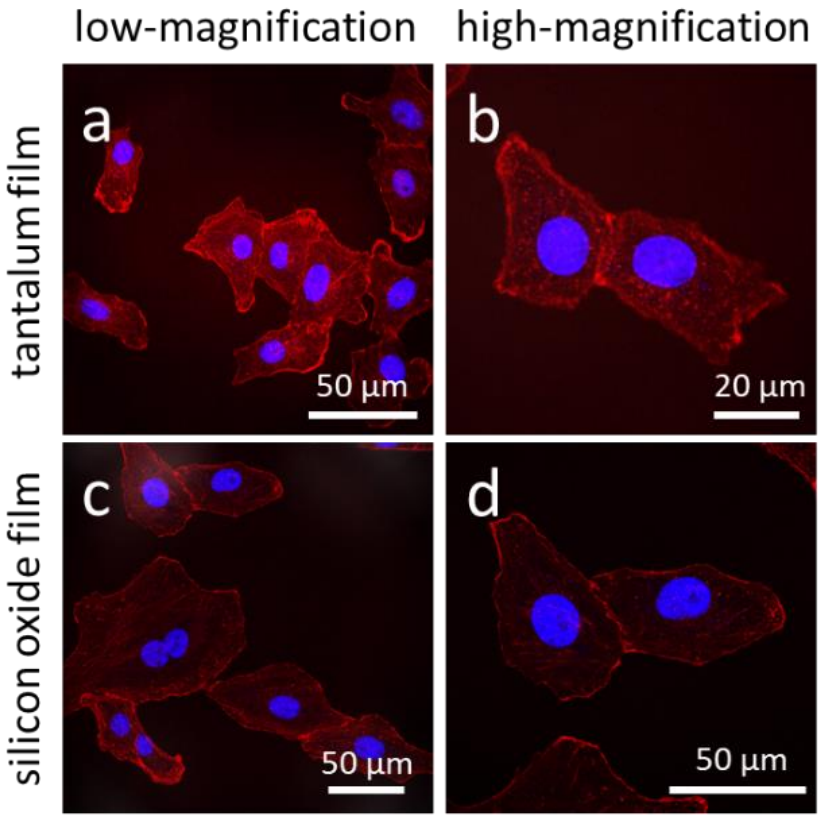

Figure 5-4 High and low magnification images of cells adherent to tantalum blanket (a, b) and to silicon oxide film (c, d) using fluorescence confocal microscope. The nuclei are stained in blue, and F-actin microfilaments are in red. Incubation time is 24 hours (Moussa et al., 2018a).

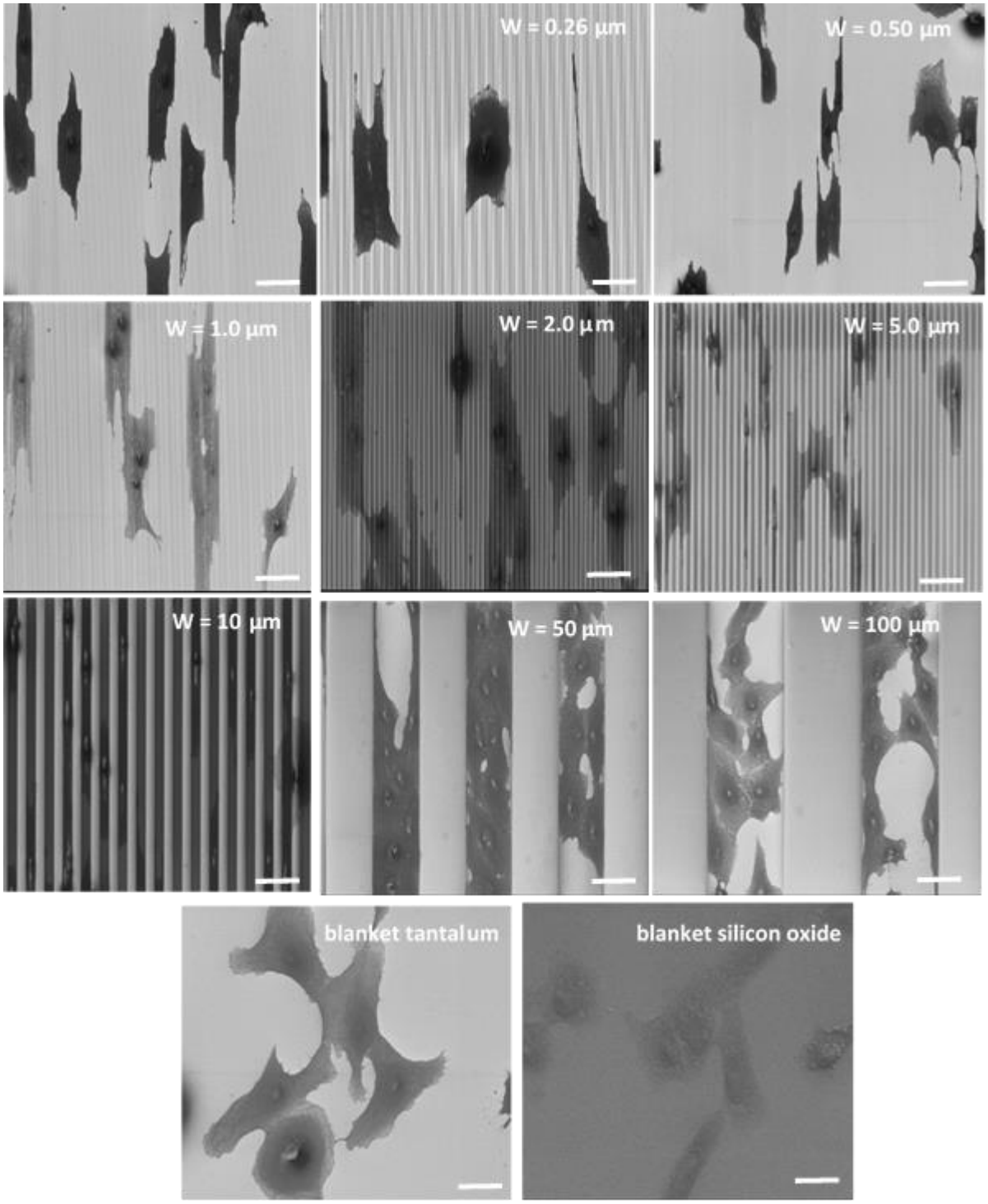

Figure 5-5 Typical SEM micrographs of adherent Vero cells on comb structures with different widths of the Ta trenches. The y-axes of the trenches are in the direction of the y-axes. Blanket tantalum and silicon oxide films with cells adherent on them are also included. Incubation time is 24 hours. Scale bar corresponds to 50 µm.

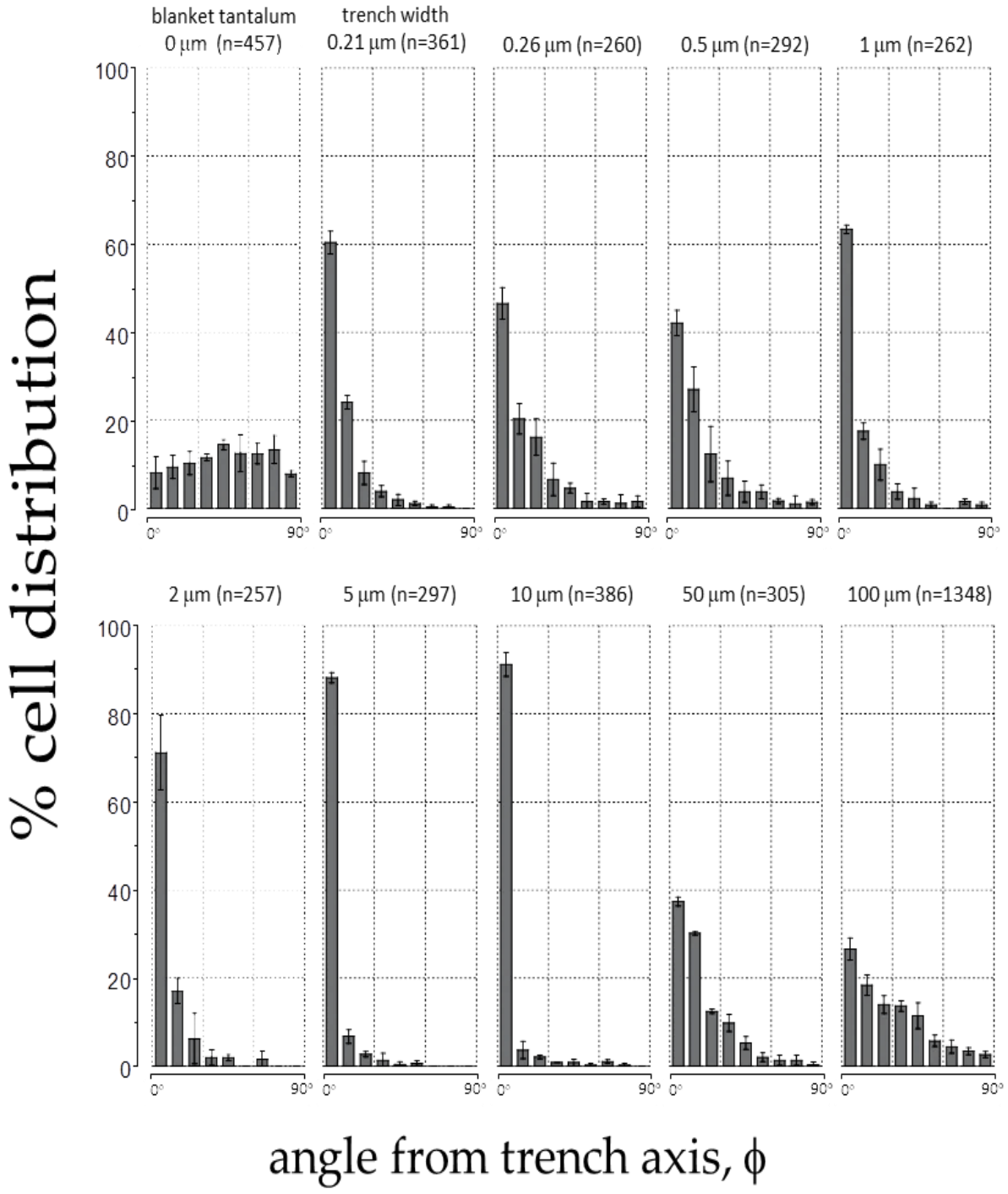

Figure 5-6 the alignment of adherent cells distribution characterized by the nuclei angular position ϕ as a function of the widths of the tantalum grooves. Blanket tantalum has 0 μm wide trenches. The number (n) of adherent cells assessed in each area is included in graphs. Each bin represents the percentage of the cell population in ±10° interval deviated from the trench y-axis. Standard deviation corresponds to values from three distinct groups (Moussa et al., 2018a).

The synopsis of all quantitative data from the pattern-dependent alignment (Section 5.3.2) is presented in Table 5-1

Table 5-1 Summary of experimental data includes dimensions and area of evaluated structures (Moussa et al., 2018a).

Widths (μm)		Inspected Comb Structure Area (mm^2)	Number of Cells on each comb structure (n)	Elongation ($\frac{L}{S}$ ± SD)	Percentage of Cells Alignment Angle ϕ within ± 10° from Trenches y-axes
Line	Trench				
0.15	0.21	1.8	361	2.09 ± 0.53	60.4 ± 2.6
0.24	0.26	1.8	260	1.92 ± 0.55	46.5 ± 3.6
0.50	0.50	1.8	292	1.86 ± 0.52	42.1 ± 2.9
1.0	1.0	1.8	262	2.38 ± 0.72	63.4 ± 0.9
2.0	2.0	1.8	257	2.67 ± 0.98	71.2 ± 8.5
5.0	5.0	1.8	297	2.45 ± 0.67	88.2 ± 1.2
10	10	1.8	386	2.98 ± 0.82	91.2 ± 2.7
50	50	1.8	305	1.94 ± 0.79	37.4 ± 1.0
100	100	6.6	1,348	1.49 ± 0.32	26.6 ± 2.5
Blanket Tantalum		1.8	457	1.64 ± 0.44	8.1 ± 3.6

Note: Value n is the total number of assessed cells, percentage of adherent cells aligned within ±10° of the lines y-axis, and L/S ratio between the long and short nuclei axes. Data correspond to one standard deviation

As summarized in Table 5-1, the results of this experiment can be hypnotized by a higher selective adhesion between cells and tantalum in comparison to silicon oxide lines. The surface energy of tantalum was experimentally found to be in the range of 2.902 -3.150 J/m^2 (Kiejna, 2005; Vitos, Ruban, Skriver, and Kollar, 1998; Skriver and Rosengaard, 1992). This value is much higher than the surface energy of virgin (0.0272 J/m^2), and chemical-mechanical polished silicon oxide (0.0296 J/m2) as reported by Thomas et al. (1996). This possible mechanism is similar to what has been discussed and demonstrated in Chapter 3. We tested the hypothesis of the selective adhesion of Vero cells to Ta compared to SiO_2. As developed and tested in Chapter 3, the mathematical model was used to calculate the Ta coverage area (sidewall coverage included) of an adherent cell, as a function of trench width. In the model, no preference was given to the bottom or sidewalls of the tantalum trenches. As shown in Figure 5-7(a) the changes in the morphology of cells on isolated trenches (elongated morphology), tantalum blanket and silicon oxide film (random morphology) were modeled to estimate the cell surface contact on tantalum. The different geometries of cells were overlaid on simulated tantalum and silicon oxide comb structures with multiple lines and trench widths, as in Figure 5-7(b). The cell area (with one of the three morphologies), which is in contact with tantalum, was plotted as a function of the Ta trench widths as

demonstrated in Figure 5-7(c). Simulated data show that, at the beginning, the coverage area decreased with width until it reached a minimum value, followed by an increase at a certain trench width until the cell was entirely on one Ta trench. This indicates that at trenches with smaller widths, the sidewalls did not contribute to the cell-Ta interaction. However, with the increase in trench width, the contribution of the sidewalls to the cell-Ta contact area increased. In Chapter 3, the suggestion was made that cells undergo morphological changes (elongation and alignment) to maximize their contact area with metal lines, and the cell-metal interaction was higher for elongated cells than randomly oriented ones. Thus, the coverage differences between elongated and each randomly oriented cell are graphed in Figure 5-7(d). It was observed that there are no coverage changes between 1 and 3 μm wide trenches.

Nevertheless, we noticed an increase in the coverage difference for trenches 3 to ~60 μm wide (Figure 5-7(d)). A peak coverage difference value was reached on trenches ~20 μm wide. This indicates a trend in the tendency of cells to elongate and increase their contact with Ta. Beyond 60 μm wide trenches, cells would no longer need to elongate since they would be in full contact with Ta.

Both the experimental and modeled data from Figure 5-6 and Figure 5-7 demonstrate the propensity of cells to maximize their contact area with Ta; however, the change in the morphology of cells on blanket tantalum or silicon oxide was more random than changes observed on comb structures with less than 3 μm wide. Even though the model was capable of predicting the behavior of cells, the 3D nature of the substrate added level of complexity that is not considered in this model.

5.3.3 Surface Topographies-Dependent Attachment Behaviors

Results from Figure 5-6 and Table 5-1 demonstrate the existence of three distinctive regimes in regards to the alignment and elongation of cells. These three regimes are the direct effect of comb structures' geometries on the cellular behavior of adherent Vero cells. This distinctive behavior was further investigated by characterizing the alignment and elongation behaviors of adherent cells as a function of the Ta trench widths. Results are plotted and presented in Figure 5-8.

Based on results from Section 5.3.2 and to help to understand the effect of comb structure geometries on the cellular change in morphology, the percentage of cells aligned within ±10° from the trenches y-axes and the nuclear elongation (L/S) was graphed as a function of trench widths (Figure 5-8). The cellular behavior was found to fall in three main categories, or regions arose from the trenches widths: (i) smaller than 1 μm; (ii) between 1–10 μm; and (iii) larger than 50 μm. Figure 5-8(a) reveals that cells in regions i and iii show a similar alignment trends in which cells express a rapid decrease in the percentage of aligned cells (within ±10°) parallel to trench y-axes as the width of the trenches increases between 0.21

and 0.5 μm, and from 50 to 100 μm. However, the portion of aligned cells in the region iii drops considerably in comparison to the region i toward a more random distribution as seen on blanket tantalum surface.

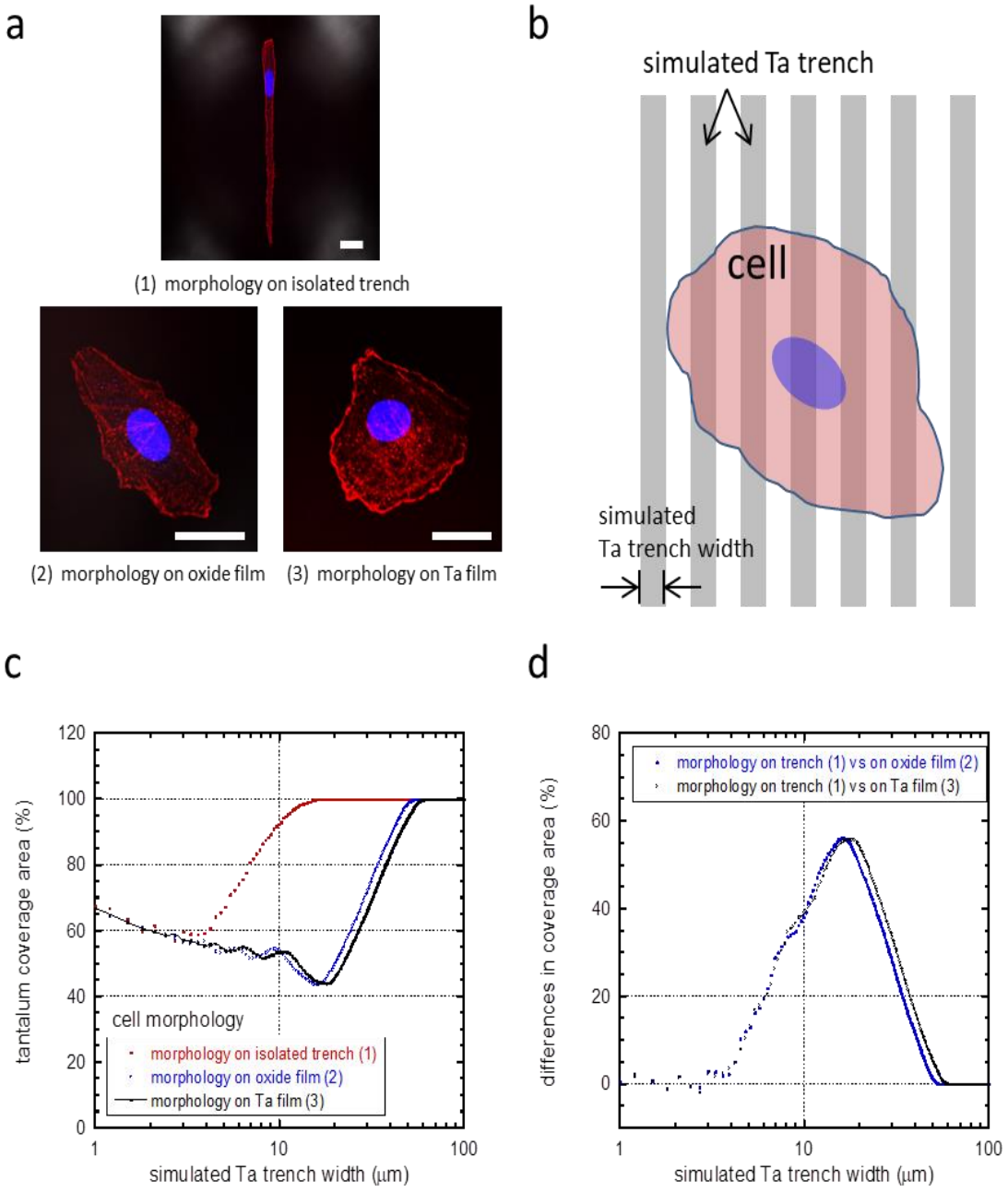

Figure 5-7 (a) The three morphologies used in the model (1) isolated trenches, (2) SiO_2 films, and (3) Ta films. Scale bar is 25 μm. (b) A simplified model for the cell on simulated comb structures. (c) Ta coverage area calculated from the model for cells with three different morphologies. (d) The difference in Ta coverage area between elongated morphology cell (1) and random-shaped cell morphology on blanket oxide (2) in blue, and tantalum films (3), in black (Moussa et al., 2018a).

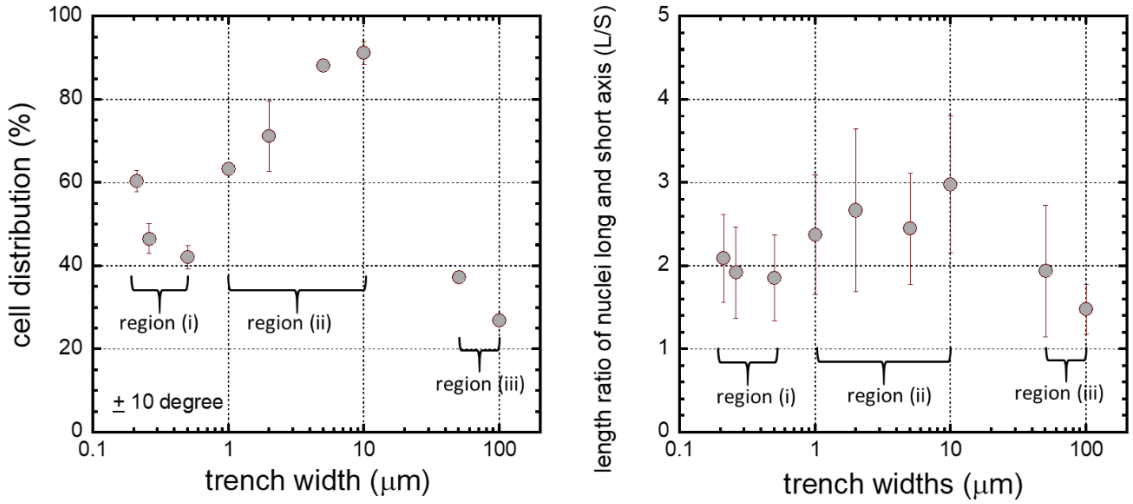

Figure 5-8 (a) Rate of cell (nucleus) alignment parallel within ±10° of the trenches y-axes as a function of different trench widths. (b) The change in the nucleus shape (L/S) as a function of trench widths. Three different regions were observed and identified: (i) 0.21–0.5 μm, (ii) 1–10 μm, and (iii) 50–100 μm, showing a strong correlation between alignment rates and L/S ratios on one side, and the width of trenches on the other side (Moussa et al., 2018a).

On the contrary, cells in the region ii showed different behavior in which the percentage of preferentially aligned cells increased as the trenches became wider (from 1 to 10 μm).

The change in the shape of the nucleus (L/S) was also measured. Results indicate that the effect of trench widths on the cellular elongation were identical to the alignment behaviors. Thus, similar regions were observed and defined, as illustrated in Figure 5-8 (b).

To further examine the three regions identified in Figure 5-8, we created high resolution 70° tilted SEM images. The intention was to characterize these regions by observing the cell-substrate interactions from the perspective of the cellular pseudopodia. These temporary cytoplasmic long projections were induced by cellular membrane microfilaments (Bogitsh, Carter, and Oeltm, 2013; Bornschlögl et al., 2013; Albuschies and Vogel, 2013). The top three images in Figure 5-9(a) show the ability of cellular pseudopods (marked with arrows) to cross the trenches like a suspension bridge without the need to establish any form of contact with the bottom. Surprisingly, the crossover of pseudopodia happened not at the top between the trenches but at an anchorage point often located at a depth of more than ~100 nm from the trench tops. These projections were observed to stay within the trench boarders, adherent to the sidewalls, rather than continuing to the top of the trenches. Such behaviors were identified within region i for 0.21 and 0.26 μm wide trenches.

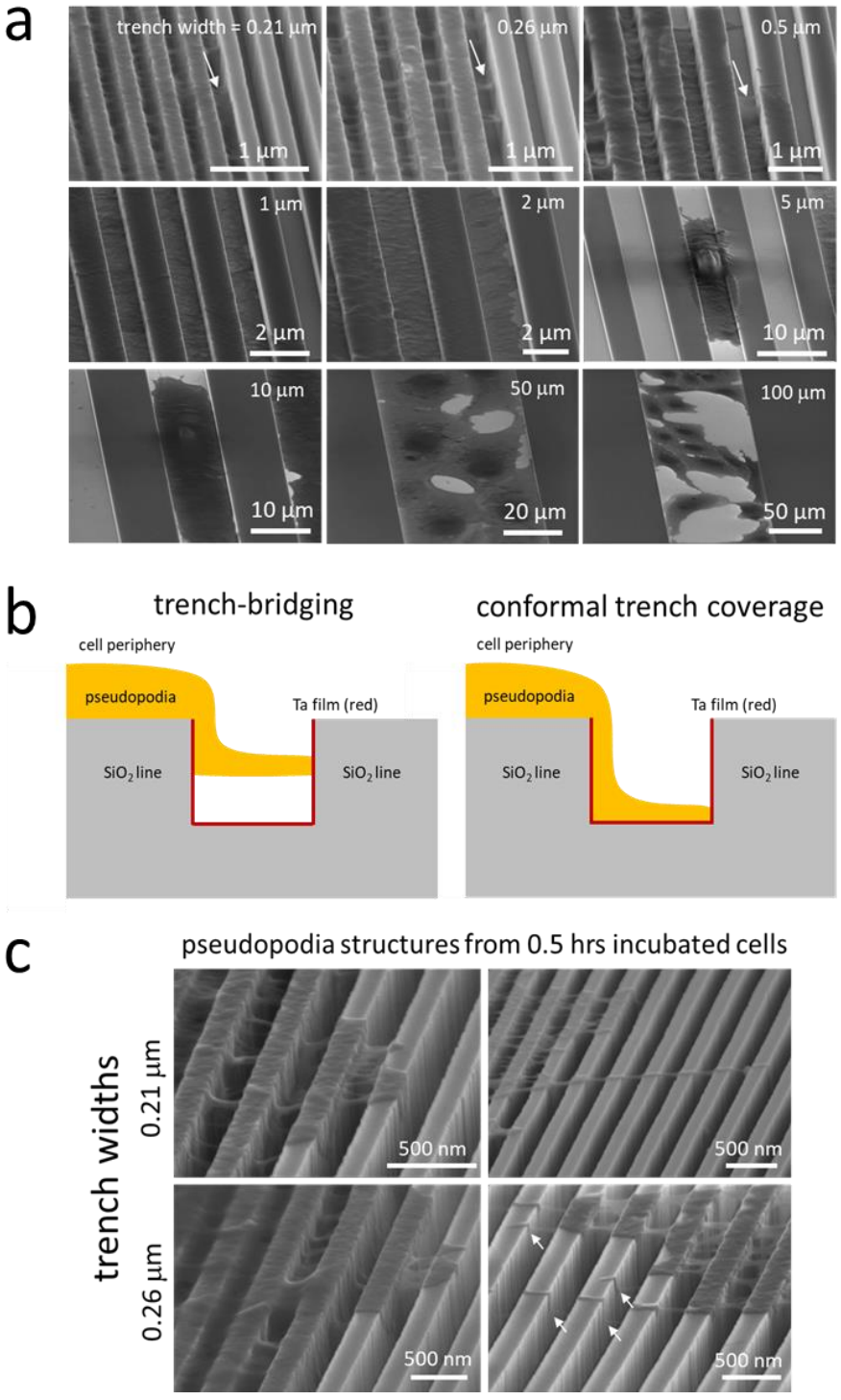

Figure 5-9 (a) High magnification 70° tilted SEM images of cell-substrate adhesion behaviors. White arrows are examples of pseudopodia bridging behaviors. The arrows in white point to pseudopodia projections bridging across the trenches (b) Simplified illustrations of the two spreading behaviors of pseudopodia as a function of trench width. (c) 70° tilted SEM images of cells incubated for 0.5 hours on comb structures with 0.21 and 0.26 µm wide trenches (Moussa et al., 2018a).

For 0.5 μm wide trenches, only very few of these projections were observed. These pseudopodia showed a dominant tendency to adhere to and cover the bottom surface of the trench.

To further explain these trench-bridging behaviors, Figure 5-9(b) shows simplified representations of these behaviors. The trench-bridging behaviors were observed to start briefly after cells were seeded on the substrate. Images in Figure 5-9 (c) represent 70° tilted high-magnification SEM images of cells after 0.5 hours of incubation on comb structures with 0.21 and 0.26 μm wide trenches. The micrographs confirm similar bridging behaviors of cellular pseudopodia for cells incubated for 24 hours, as verified in Figure 5-9 (a). These micrographs show that some of the anchorage points were stationed deep inside the trenches on the sidewalls. Images from Figure 5-9 reveal a sort of "physical limitation" in the capability of cells to regress within the trench, despite the ability of pseudopodia to enter the trenches. Appendix D, Figure S15 to Figure S17 provide supplementary images representing the formation of pseudopodia and bridging behaviors for cells adherent on 0.21 and 0.26 μm wide comb structures.

The cell-substrate interaction behaviors in region ii were unlike the cellular behaviors observed in region i. Region ii, includes comb structures with 1 to 10 μm wide trenches. The pseudopodium projections become dominant by surface coverage instead, as verified in Figure 5-9 (a), the 2nd raw of images (1, 2, and 5 μm wide trenches). Such morphological changes were also observed on the 10 μm wide comb structures during the early phases (0.5 and 2 hours) of the cell-substrate interactions (Figure 5-10). Figure 5-10(a)-(b) demonstrates that adherent cells spread on both silicon oxide lines and tantalum trenches, but preferentially align along the tantalum trenches, instead of silicon oxide lines. Figure 5-10(c) shows cytoplasmic projections with nano-scale diameters spreading perpendicular to the trench sidewalls as if they are sensing the surrounding environment and demonstrating the ability of cells to overcome such a barrier.

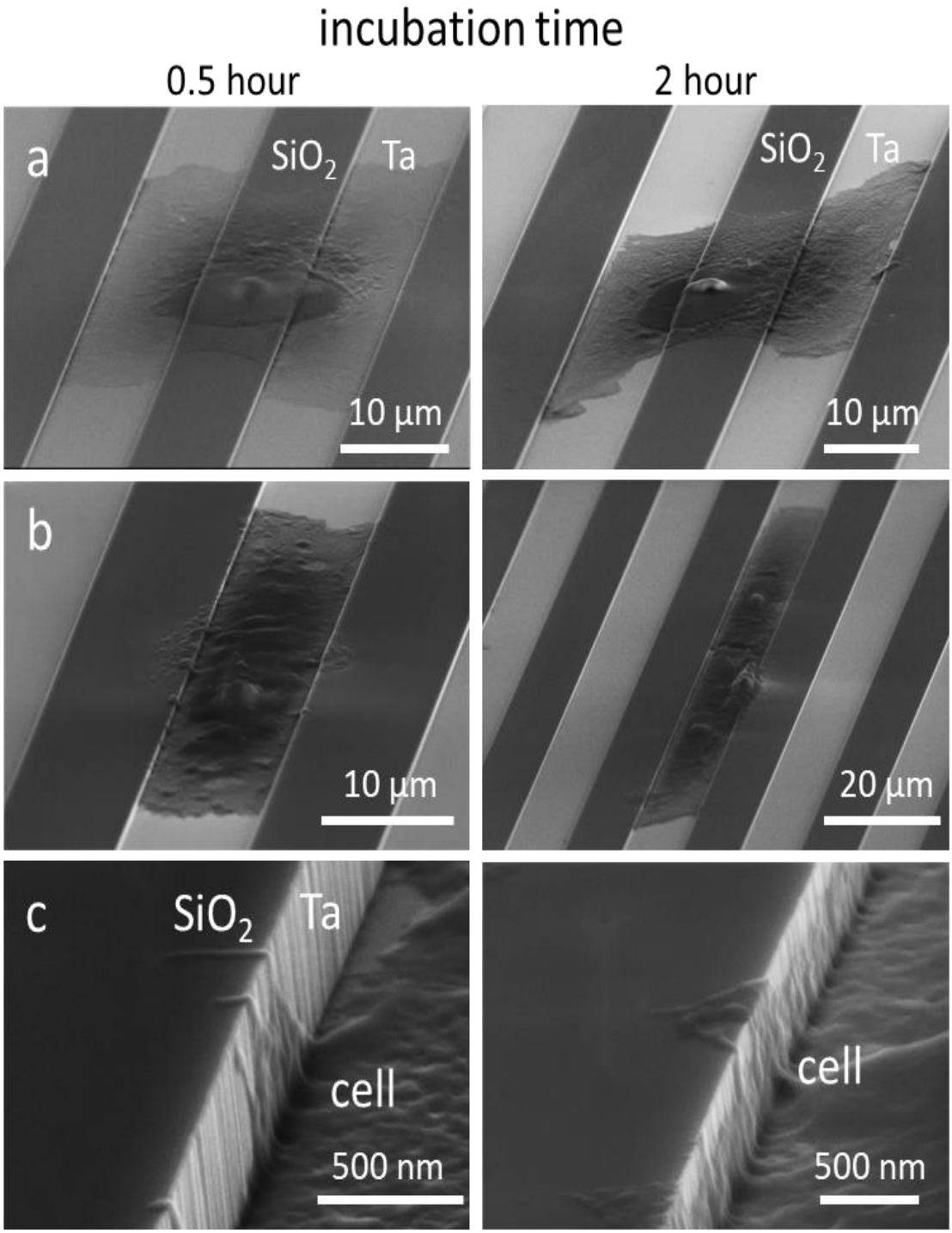

Figure 5-10 Representative 70° tilted low magnification SEM images after 0.5- and 2-hours of incubation time for cells on 10 µm wide trench comb structures with cell nuclei positioned on (a) silicon oxide lines and (b) tantalum layered trenches. (c) High-magnification images of pseudopodia on the sidewalls of 10 µm wide trenches (Moussa et al., 2018a).

In region iii, the trenches are 50 and 100 μm wide, which means they are wide enough to house multiple cells as previously demonstrated in Figure 5-3 to Figure 5-5. The majority of the adherent cells tend to show a random orientation similar to the behavior of adherent cells on blanket tantalum and silicon oxide film. This indicates that when the trenches are wide enough to accommodate the complete cell, cells will show a preferential adhesion on the Ta trenches, rather than the silicon oxide lines. However, a small percentage of cells localized themselves distinctively, favoring the 90° corner between the vertical and horizontal trench walls (Figure 5-11).

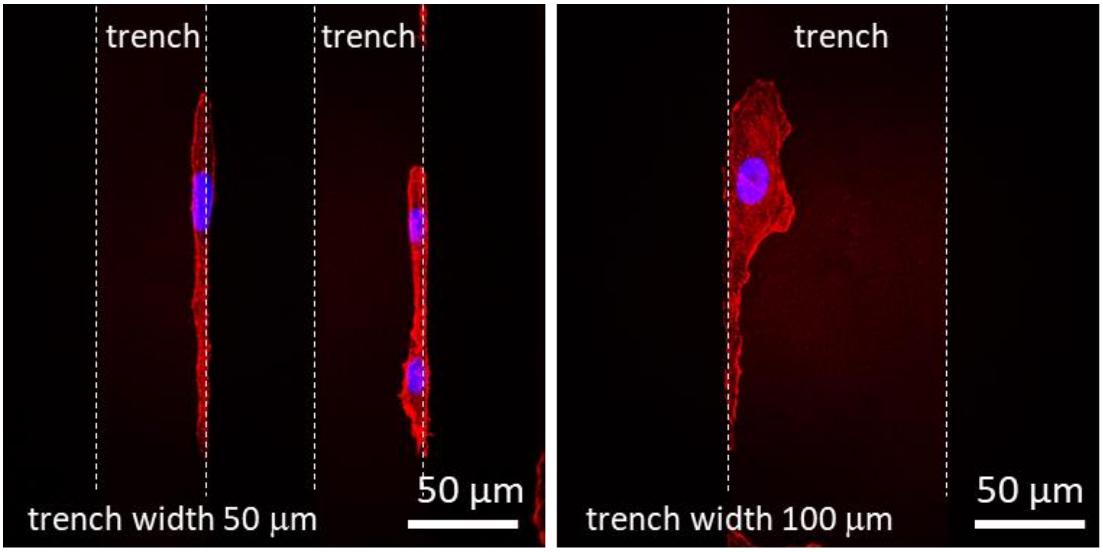

Figure 5-11 Fluorescent confocal images of cells on 50 and 100 μm wide trenches demonstrate the tendency of cells to locate themselves at the connection between the trench sidewall and flat bottom. The trench boundaries are highlighted by dashed lines (Moussa et al., 2018a).

The findings from Chapter 5 came broadly in agreement with findings by Sun, Xie, Chen, and Lam (2017); Sharma et al. (2016); Stevenson and Donald (2009); Yang et al. (2009); Martínez (2009); Lu and Leng (2008); Loesberg et al. (2007); Charest, Garcia, and King (2007); and Lenhert et al. (2005) in stating that cells require a cut-off trench width to induce a preferential alignment behavior in the direction of trench y-axes. This consensus was reached regardless of the type of cells assessed, biomaterials used, size/spacing of grooves and other experimental conditions.

5.3.4 Summary

This chapter investigated the adhesion behaviors and change in morphologies of adherent Vero cells incubated on a 3D Ta/SiO_2 micron and sub-micron scale patterned substrate. The substrate consists of silicon oxide lines and trenches layered with Ta. Two methods were used to characterize the cellular

behaviors on the substrate understudy: (1) high- and low-magnification 70° tilted SEM micrographs and (2) fluorescence confocal micrographs. The SEM images showed cytoplasmic projections at nanometer-scale crossing the trenches in a suspension bridge like extensions by using the trench sidewalls as a starting point. This was observed for trenches smaller than 0.5 μm wide. On broader trenches, adherent cells formed a layer of cytoplasmic projections to cover the trench, but no bridge-like formations were observed. We identified three different cellular trench widths-dependent regimes (behaviors). In region i with 0.21 to 0.5 μm wide trenches, the alignment of cells decreased with the increase of trench width. This can be explained by the absence of a physical barrier that may prevent cells from spreading perpendicularly to the trench y-axes. Region ii revealed an increase of the preferential alignment performance of cells on comb structures with trenches in range of 1 and 10 μm wide. This was driven by a highly selective cell-trenches tantalum layered adhesion. Region iii demonstrated a decrease in the preferential alignment behaviors in the direction of randomly oriented cells.

However, the findings of this chapter were not successful in isolating and describing the role of 3D topographical features from that of the materials' composition of the micron and sub-micron scale patterned substrate. Herein remains an essential question as to whether the topographical features are inducing the preferential alignment behaviors of adherent Vero cells or the composition of the micron and sub-micron scale patterned substrate.

Chapter 6
Manipulating Cell Behaviour Using 3D Tantalum Patterned Substrate

This chapter is based on the following publications:

Moussa, H.I.; Logan, M.; Wong, K.; Rao, Z.; Aucoin, M.G.; Tsui, T.Y., Micromechanics 9, 2018, 464

Tsui, T.Y.; Logan, M.; Moussa, H.; Aucoin, M.G., Materials 12, 2019, 114

A novel three-dimensional tantalum monolithic substrate consists of comb structures with equal width tantalum lines and trenches were developed to isolate the effect of material composition from the topographic effect of the novel 3D tantalum and silicon oxide (Ta/SiO_2) substrate developed in Chapter 5 to investigate the impact of micron and sub-micron scale 3D topographical features on manipulating the morphology and alignment behaviors of adherent mammalian Vero cells. This is important since tantalum is widely used in orthopedics, reconstructive surgeries, and surgical implant devices. The newly developed 3D tantalum substrates are topographically similar to the Ta/SiO_2 micron and sub-micron scale patterned substrates used in Chapter 5, Section 5.2.1. The difference is that herein manipulating the behavior of adherent cells will be a function of the surface topographical feature, rather than the composition of materials and topographical features as discussed in Chapter 5.

6.1 Background

Tantalum is widely used due to its biocompatibility (Wauthle et al., 2015) for medical applications, such as implants in hip and knee reconstructive surgeries (Patil, Lee, and Goodman, 2009), orthopedics (Paganias, Tsakotos, Koutsostathis, and Macheras, 2012), prostheses, and implants (Balla, Bose, Davies, and Bandyopadhyay, 2010). These implants are used in two forms: dense (Ren et al., 2015; Varitimidis, Dimitroulias, Karachalios, Dailiana, and Malizoscorrespo, 2009) or porous (Paganias et al., 2012, Balla et al., 2010). The elastic modulus and hardness of a tantalum thin film (100 nm) are measured to be 176.1 ± 3.6 GPa (Guisbiers, Herth, Buchaillot, and Pard, 2010), and 12.11 ± 0.46 GPa (Guisbiers et al., 2010), respectively. The surface energy of tantalum (~2.42 J/m^2) is higher than titanium (~2.0 J/m^2) and lower than tungsten (~3.3 J/m^2) (Tran et al., 2016). In comparison to titanium, porous tantalum was found to improve the adhesion, growth, and differentiation of osteoblast cells by 73 % and density of cells by six-fold when both metals are used under the same culture conditions (Balla et al., 2010). Thus, coating porous titanium (Wang et al., 2016) and carbon scaffolds (Wei et al., 2016) with a thin layer of tantalum

will help increase the Osseo-integration and ingrowth characteristics of the implant. Although tantalum is also proven effective (*in vivo* and *in vitro*) in improving the responses of cells, little knowledge is available on the effect of tantalum surfaces with nano-scale topographical features on the adhesion and change in morphology of cells. Such knowledge is vital to acquire since the tantalum implants may contain similar topographies that are formed during the fabrication as a result of mechanical polishing and handling.

The complexity of the in-vitro cell-substrate interactions and the different factors that may influence these interactions are well studied and documented in literature (Huang et al., 2016; Lv et al., 2015; Khalili and Ahmad, 2015; Martino et al., 2012; Rabe et al., 2011; Anselme et al., 2000; Sagvolden, et al., 1999). In particular, the effect of parallel lines surface topographies on the adhesion and change in morphology of cells (Joo et al., 2015; English et al., 2015; Nakamoto et al., 2014; Béduer et al., 2012; Fujita et al., 2009; Teixeira et al., 2006; Khan et al., 2005; Fan et al., 2000). Reviewing these papers and others was helpful in identifying some of the gaps that this chapter tries to address. To name a few: (1) The substrates were fabricated only using a handful of materials such as polymers, Si, and SiO_2. (2) The dimensions of the lines and grooves (ditches) were often limited to a small number and orders of magnitude, and this situation may restrict the ability to understand the effects of surface topographies on the behaviors of cells. (3) The cell-substrate interactions were assessed on topographical features on micron scale, and not on sub-micron features. However, it is clear that the cell-substrate interactions such as alignment and change in morphology vary considerably among the cell type and substrate materials. Currently, this is the first time in literature that a study discusses the change in the behavior of mammalian cells on tantalum surfaces with nano-scale features of lines and ditches (grooves). This is mainly due to complications associated with the fabrication of such metal substrates. Taking into consideration the promising biological features and performance of Ta, there is a need to further understand the effect of nano-textured tantalum substrate on the morphology of cell in addition to the fact that controlling the alignment behaviors of cells on a substrate will decrease the failure rate of implants (Barr, Hill, and Bayat, 2009; Zhao , Tsuru , Hayakawa, and Osaka, 2008).

This chapter will assess the impact of a tantalum-based substrate on the alignment and spreading behaviors of mammalian (Vero) cells. Nine comb structures were studied; each consisted of a wide range of parallel and equally wide Ta lines and ditches between 0.18 and 100 μm. The mechanism, by which Vero cells interact with the surrounding environment will be assessed by looking at the role of pseudopodia in cellular adhesion, and mobility. Such behaviors are influenced by complex protein interactions and pathways (Nobes and Hall, 1995; Ridley and Hall, 1992). Pseudopodia are usually

classified by their morphologies, to filopodia, reticulopodia, and axopodia (Albuschies and Vogel, 2013; Bornschlögl et al., 2013; Actor, 2012). The focus will be on pseudopodia with diameters smaller than 100 nm. Another critical aspect this chapter will examine is the response of adherent cells on multiple Ta comb structures with different geometries. The change in the morphology of adherent cells will be characterized using high-resolution images generated using SEM and fluorescence confocal microscopy. We chose tantalum because of its unique properties and applications, such as biocompatibility, and bioactivity (Bencharit et al., 2014), mechanical strength (Wauthle et al., 2015), corrosive resistance (Wang et al., 2012), and applications (Levine, Sporer, Poggie, Della Valle, and Jacobsa, 2006).

6.2 Materials and Methods

6.2.1 Fabrication of Tantalum 3D Monolithic Comb Structures

The new tantalum 3D structures used in this chapter were supplied by Versum Materials, LLC (Tempe, AZ), and similarly to all specimens used in this work, they were fabricated using a pioneer large-scale technique that is mainly used in the semiconductors industry (Doi, Marinescu, and Kurokawa, 2012; Fury, 2009; Seo and Lee, 2007; Seo and Lee, 2005; Larios, 2004; van Kranenburg et al., 1997). The fabrication steps were briefly discussed and demonstrated in Figure 6-1. A layer of silicon oxide was deposited on a silicon wafer with 20 mm of diameter using plasma-enhanced chemical vapor deposition (PE-CVD), on which the parallel lines and ditches comb structures were transferred using photolithography and dry etching (Cogez et al., 2011; Chen, 2007; Zantye et al., 2004). These comb structures are rectangular-shaped with areas equal to or larger than 1.8 mm^2 and consisted parallel lines (L) and trenches (T) of equal width. Tantalum thin layer and copper were then deposited on top of these structures using physical vapor deposition (PVD). The unwanted copper was removed using a combination of chemical and mechanical polishing techniques (Krishnan, Nalaskowski, and Cook, 2010; Chen, 2007; Baravelli, 2005). The final surfaces were flat, smooth, and defect free, and consisted of parallel lines of Ta and SiO_2. The residual copper in the trenches was removed by dipping the specimens in ~9.4 M, ACS Plus nitric acid (Fisherbrand®, Fisher Scientific International Inc., Pittsburgh, PA) for ~45 minutes. The copper-stripped specimens were rinsed by deionized water and ethanol. It is important to note that the depth (D) of the stripped trenches was the same at ~700 nm, all over the specimen.

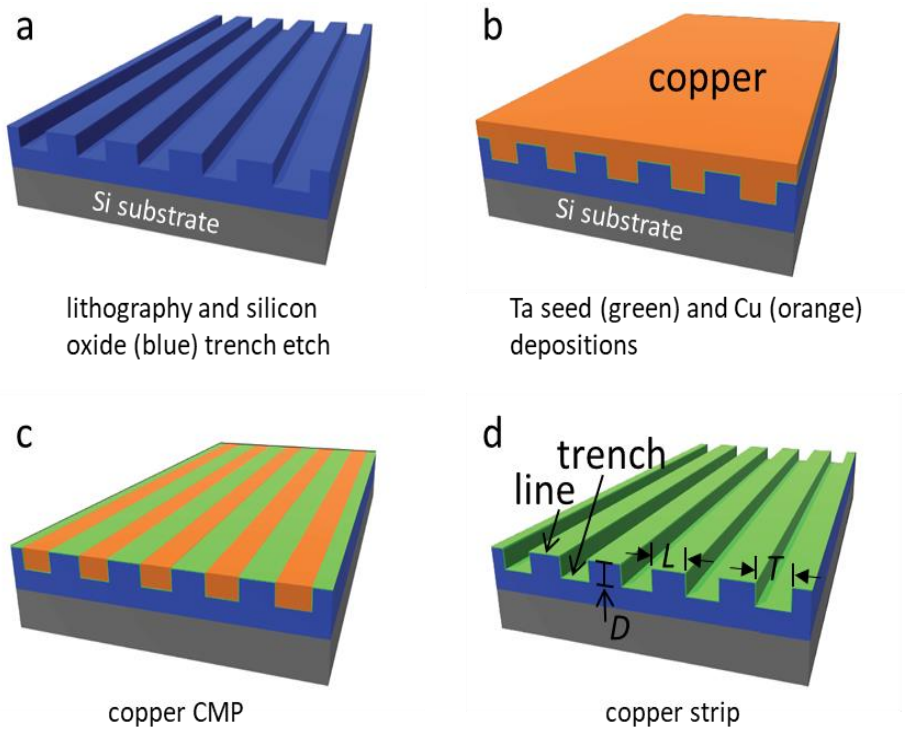

Figure 6-1 Simplified illustration of the fabrication process of tantalum-based comb structures (in green). (a) Desired topographical features are printed to the SiO_2 layer via photolithography and plasma etching. (b) Physical vapor deposition is used to deposit the Ta thin layer and copper film on the silicon substrate. (c) CMP process is used to remove the excess copper. (d) Stripping of copper by nitric acid to is used expose the 3D topographical features of symmetric Ta lines(L) and trenches (T), with the same depth (D) (Moussa et al., 2018b).

6.2.2 Cell Deposition, Fixation, Dehydration and staining Protocols

The detailed cell deposition procedures were similar to protocols discussed in Section 03.2.3.1. Vero cells (CCL-81) were sourced from the American Type Culture Collection (ATCC, Manassas, VA), and seeded in 1:1 volume of F12 (Corning, NY) media and Corning® Cellgro™ Dulbecco's Modified Eagle Media (DMEM). The media was supplemented with 4-mM L-glutamine (Sigma-Aldrich, St. Louis, MO) and Gibco™ 10 % (*v*/*v*) fetal bovine serum (FBS) by Thermo Fisher Scientific (Waltham, MA). Cells were incubated in tissue-culture-treated 175 cm^2 flasks (Corning Falcon, Corning, New York) at 37 °C in the presence of 5 % CO_2. Vero cells were seeded at a confluence of ~0.5×10^5 cells/mL at 37 °C for 0.5 to 24 hours on decontaminated copper-stripped tantalum substrates using 6-well tissue culture plates (Nunc, Thermo Scientific, Hvidovre, Denmark). Sterilization of the specimens was done by submerging them for 30 seconds in a 70 % ethanol solution and then washing them using Dulbecco's phosphate-buffered saline (D-PBS).

At the end of the incubation period, specimens with adherent cells were washed with a D-PBS solution and then fixed with a solution of 4 % methanol-free formaldehyde (Sigma-Aldrich, Oakville, ON) for one hour at room temperature. The fixed cells were permeabilized in a 0.1 % Triton-X 100 (Sigma-Aldrich) solution for 5 minutes. Specimens were rinsed with PBS and blocked with 2 mL of 1 % (*w/w*) bovine serum albumin (BSA) (Sigma-Aldrich). F-actin microfilament staining was conducted by soaking specimens for one hour in the deep red CytoPainter F-Actin stain (ab112127 Abcam, Cambridge, MA, USA) solution, which was diluted by a factor of 1000 in 1 % BSA. A solution of 0.4 μg/mL of the 4′,6-diamidino-2-phenylindole (DAPI) (Life Technologies, Waltham, MA) was used to stain the DNA (5 min). The staining procedures were done in the dark, and the specimens were rinsed twice with 2 mL D-PBS after each stain application. The final solution contained four drops of Prolong Gold anti-fade reagent (Life Technologies, Burlington, ON). Specimens were kept refrigerated at 4 °C. A Leica TCS SP5 confocal fluorescence microscope (Wetzlar, Germany) at the University of Guelph, Ontario was used to inspect stained samples with wavelengths in the range of 436 to 482 nm (for DAPI) and 650 to 700 nm (for CytoPainter F-Actin).

6.3 Results and Discussion

This section is intended to assess the interaction behavior of the adherent Vero cells on the 3D Ta substrates. We investigated the impact of Ta line widths on the preferential alignment of cells, and the nuclear deformation in the form of elongation by looking at the L/S ratio of the long and short nuclei axes. The experiments and results are vital for the viability of this research. The characterization of Vero cells alignment and change in morphology behaviors was done using the method described in Section 3.2.4.

Briefly, the morphological changes of each adherent cell were characterized using (1) Nuclear orientation denoted by the angle ϕ, which was measured between the nucleus long axis and the tantalum trench parallel lines y-axes (as demonstrated in Figure 3-6). (2) Nuclear elongation (deformation) ratio was measured and calculated as the ratio between a nucleus long and short axis length (L/S). As previously indicated in Chapter 3, ϕ and L/S were measured manually via Image Processing and Analysis in Java (ImageJ) software using lines of best fit, based on a visual estimate of the nucleus boundary.

6.3.1 Characterization of the Tantalum 3D Monolithic Substrates

The scanning electron microscope was used to generate representative micrographs of the copper-stripped Ta comb structures, as in Figure 6-2. These structures consist of parallel lines and trenches with equal

widths. Trenches are ~700 nm deep. The thickness of the tantalum layer is ~20 nm. The SEM micrographs reveal that the comb structures are copper-free and smooth. Most importantly, the trenches sidewalls are vertically aligned with the substrate surfaces. Supplementary images are available in Appendix E, Figure S19.

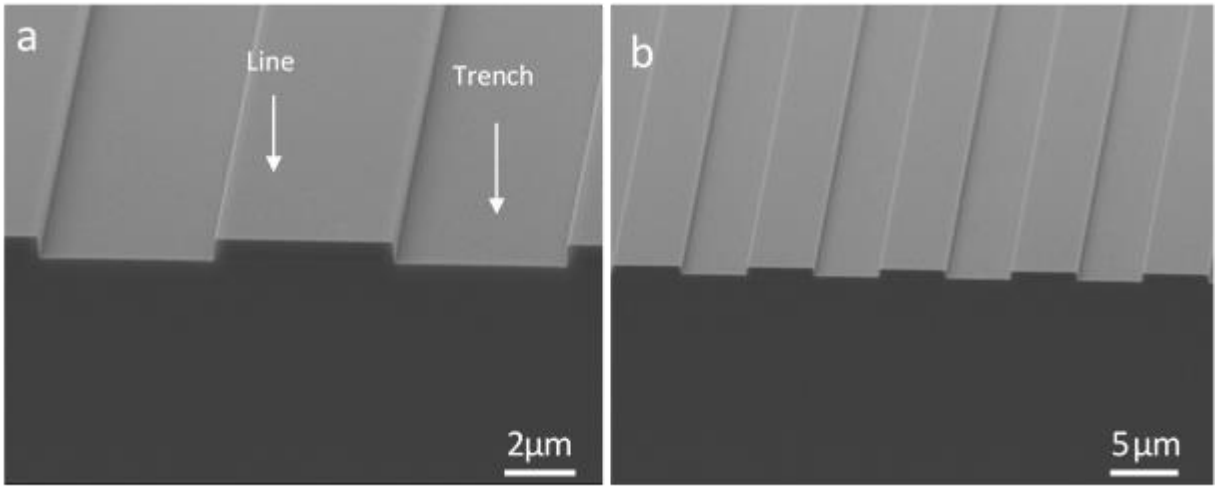

Figure 6-2 (a)-(b) High and low magnification 70° tilted SEM images for the equally wide tantalum lines and trenches 5 µm wide.

6.3.2 Patterns-Dependent Cell Alignment

This section uses a similar characterization method to those used in Chapter 3 and Chapter 5. Figure 6-3 includes typical top-down SEM images of adherent cells on the parallel lines comb structures, and the tantalum thin film blanket. Supplementary images similar to Figure 6-3 are available in Appendix E, Figure S20. As previously indicated, cells were incubated for 24 hours. Due to magnification, lines smaller than 1 µm wide cannot be seen on the comb structures; however, as illustrated in Figure 6-2, lines are vertically aligned. Adherent cells on comb structures with equally wide lines (L) and trenches (T) of 0.18, 0.25, 0.5, 1.0, 2.0, 5.0, and 10 µm are elongated in the direction of the lines y-axes. On the contrary, cells on 50 and 100 µm wide lines and trenches tend to maintain irregular shapes, with no preferential alignment behavior. This is similar to the behavior of cells on the tantalum thin film blanket.

To further affirm the observations from SEM images, representative micrographs obtained using confocal fluorescence microscopy were used to confirm the cell adhesion and alignment behaviors on 0.18, 10, and 50 µm wide parallel lines comb structures and tantalum blanket. The confocal fluorescence images are displayed in Figure 6-4. In these micrographs, cell nuclei are stained in blue, and F-actin microfilaments are in red. Figure 6-4 confirms our initial observations using SEM, indicating that cells on

0.18 and 10 µm comb structures show a tendency to elongate and align themselves in the direction of the lines y-axes.

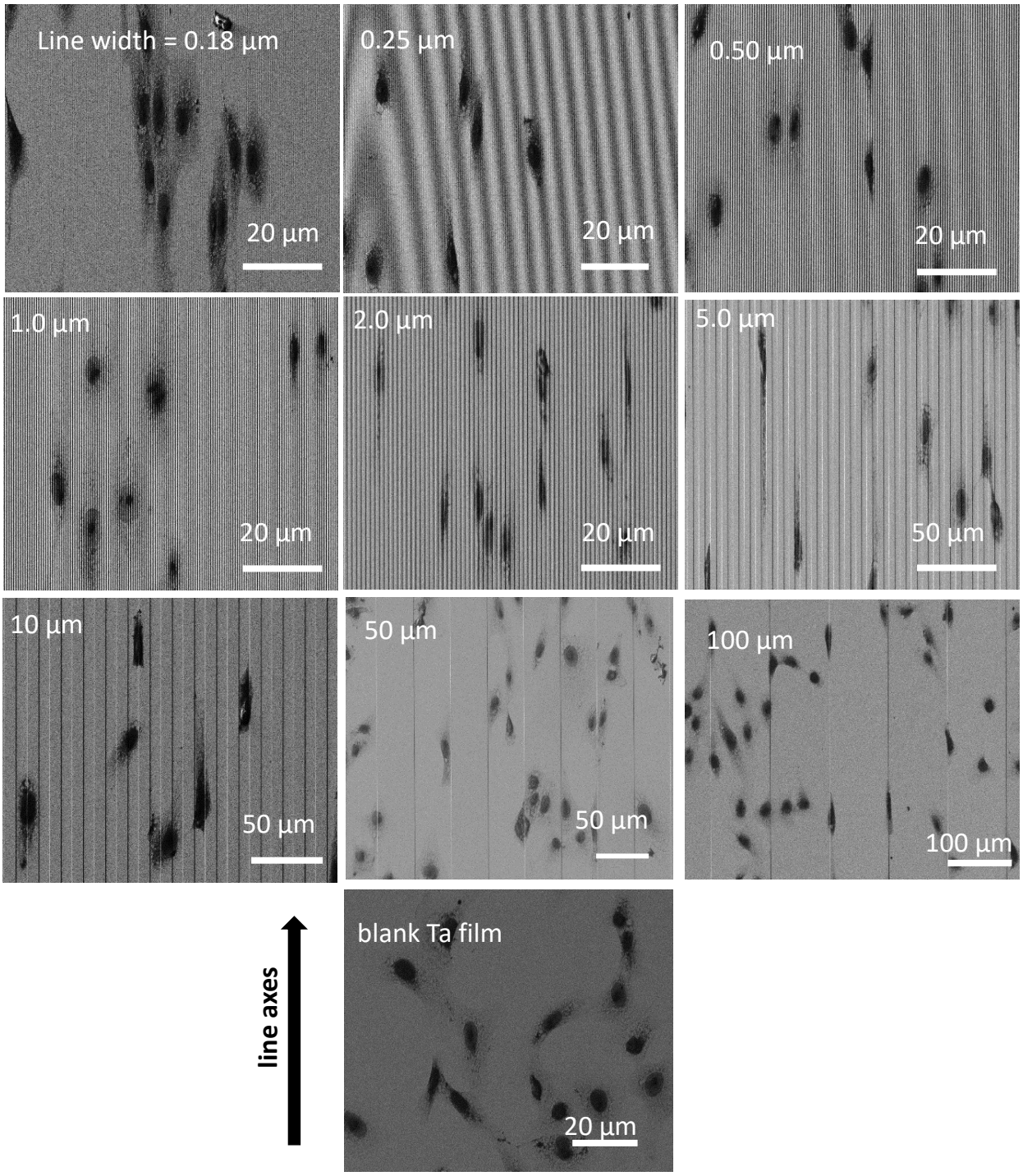

Figure 6-3 Typical top-down scanning electron microscopy (SEM) images of Vero cells adherent on multiple Ta film blanket and symmetric parallel lines comb structures. The line' width varies between 0.18 to 100 µm.

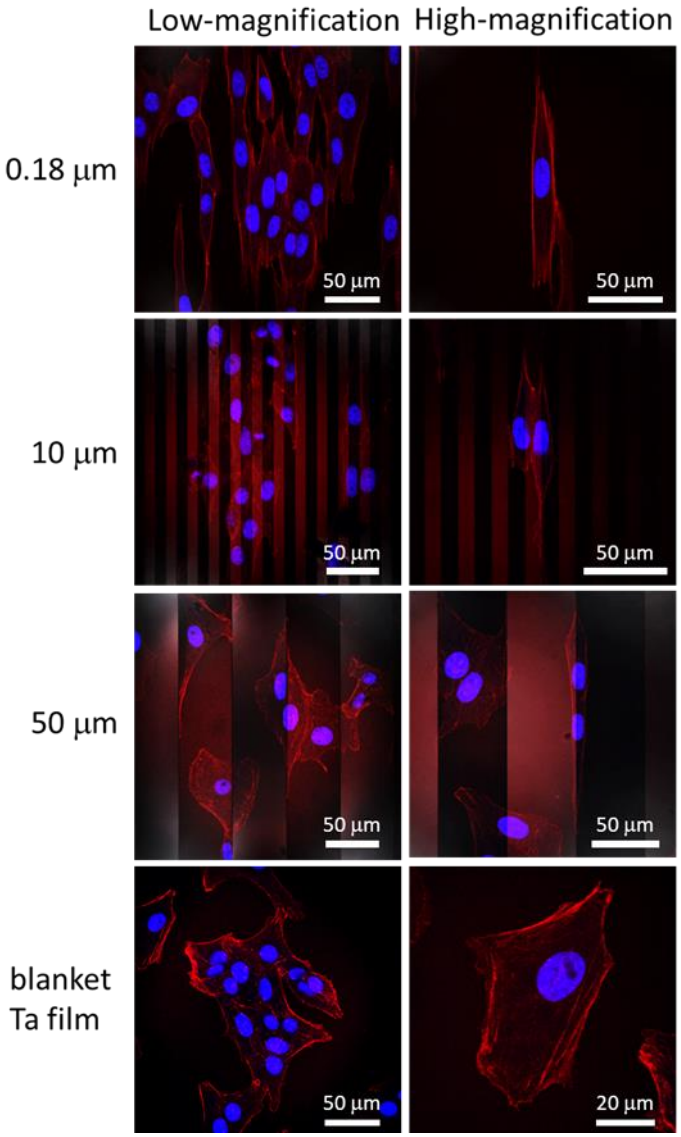

Figure 6-4 Typical images of adherent Vero cells on blanket Ta and comb structures with line widths of 0.18, 10, and 50 μm obtained using fluorescence confocal microscope. Cell nuclei are stained in blue, and F-actin microfilaments are in red (Moussa et al., 2018b).

On the other hand, cells adherent to 50 μm and Ta blanket look randomly oriented and misaligned. This indicates that cellular alignment and orientation behaviors are related and line-width dependent. To quantitatively confirm the observed cell alignment and elongation behaviors, we measured the angle ϕ positioned between the parallel lines y-axes and the nuclei long axes, and the dimensions (L and S) of the nuclei long and short axes. Figure 6-5 (a) shows the percentage of cell distribution as a function of the angle ϕ on different comb structures and blanket Ta. Error bars correspond to one standard deviation. Supplementary micrographs, similar to Figure 6-4 are available in Appendix E, Figure S21.

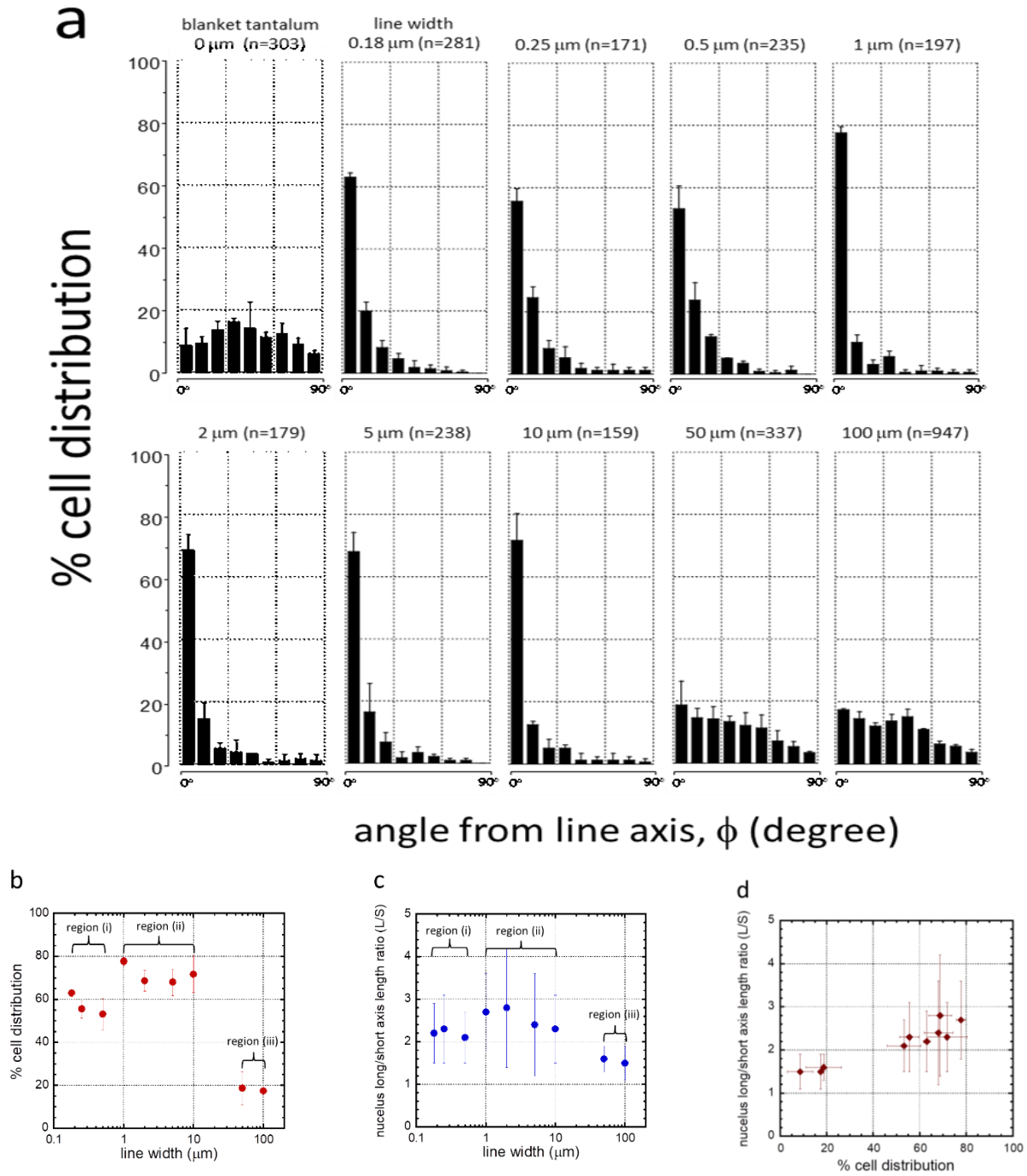

Figure 6-5 (a) Percentage of cell distribution aligned to the lines y-axes ϕ as a function of the comb structures line width and blanket tantalum films. The number of cells assessed (n) on each pattern. Data compiled in bars representing a ±10° bin of deviations from the line y-axis. (b) The population of cells aligned within ±10° of the comb structure line axes. (c) Nuclei L/S ratios as a function of comb structure line widths. (d) Nuclei L/S ratios as a function of cell population aligned within ± 10° of the trenches' y-axes (Moussa et al., 2018b).

The number of cells (n) assessed on each comb structure and blanket Ta are included in Figure 6-5(a). Adherent cells on Ta blanket and 50 and 100 μm wide lines are randomly oriented, with no preferential alignment behavior. However, cells on comb structures with 0.18 to 10 μm wide ta lines, show a much higher level of alignment and elongation parallel to the line y-axes. To further enhance the understanding of these cellular behaviors, Figure 6-5(b) plots the fraction of cells aligned within ±10° of the Ta lines y-axes as a function of the width of the parallel lines. Results highlight three main alignment behaviors (regions) based on the Ta line widths. (i) between 0.18 and 0.5 μm, (ii) 1-10 μm, and (iii) 50 and 100 μm.

In region I we observed a decrease in the percentage of cells aligned within ±10° of lines y-axes from 63.0 $\pm$1.4 % to 53.2$\pm$7.4 % followed by a decrease in the alignment of cells from 77.7$\pm$2.0 %, and 68.0$\pm$6.2 % between 1 and 10 μm wide parallel lines comb structures (region ii). The alignment of cells in region ii is higher than in region i. However, within region iii, the percentage of aligned cells (within ±10° of y-axes) shows a steep decrease in the alignment behavior of cells on comb structures with 50 and 100 μm wide parallel lines. Results indicate that less than 19 % of adherent cells will preferentially align themselves parallel to Ta line y-axes. Table 6-1 summarizes the quantitative data on the adhesion, alignment, and elongation behaviors of cells adherent on the assessed comb structures and tantalum thin film blanket. The table also includes the cell density on each of the assessed structures (comb and blanket).

Table 6-1 Data summary obtained from experimental data that includes: number of cells inspected (n), percent population of cells with $10° > \phi > -10°$ of the line axis, and axis length ratio (L/S) (Moussa et al., 2018b). The culture media initial cell concentration used was ~0.5×10^5 cells/mL. Data correspond to one standard deviation

Structure	Line/Trench Width (μm)	Area Comb Structure (mm^2)	Number of Cells (n)	Coverage ($cell/mm^2$)	$\frac{L}{S} \pm SD$	% of Population Aligned ±10° from Lines y-axes
1	0.18	1.8	281	156	2.2 $\pm$ 0.7	63.0 $\pm$ 1.4
2	0.25	1.8	171	95	2.3 $\pm$ 0.8	55.6 $\pm$ 4.1
3	0.5	1.8	235	131	2.1 $\pm$ 0.6	53.2 $\pm$ 7.4
4	1	1.8	197	109	2.7 $\pm$ 0.9	77.7 $\pm$ 2.0
5	2	1.8	179	99	2.8 $\pm$ 1.4	68.7 $\pm$ 4.9
6	5	1.8	238	132	2.4 $\pm$ 1.2	68.0 $\pm$ 6.2
7	10	1.8	159	88	2.3 $\pm$ 0.8	71.7 $\pm$ 8.6
8	50	1.8	337	187	1.6 $\pm$ 0.3	18.7 $\pm$ 7.7
9	100	6.6	947	143	1.5 $\pm$ 0.4	17.4 $\pm$ 0.3
10	blanket Ta	1.8	303	168	1.5 $\pm$ 0.4	8.6 $\pm$ 5.5

Additionally, the nuclear elongation (L/S) ratio as a function of the comb structures parallel lines width was also characterized as plotted in Figure 6-5(c). This is important to understand whether the alignment ϕ and elongation (L/S) behaviors are connected and interrelated as we observed, or not. Results demonstrate a close correlation between alignment rates and elongation of cells nuclei. Similar to Figure 6-5(b), three regions were also observed in Figure 6-5(c). On comb structures with line width in the range between 0.18 to 10 μm, cells showed significant elongation ratios. The highest elongation measured was for cells on 2 μm comb structure, with the L/S value of ~2.8 ± 1.4. However, cells adherent on blanket Ta and 50 and 100 μm comb structures, showed smaller L/S ratios between 1.5 ± 0.4 and 1.6 ± 0.3. The correlation between the L/S ratio and the cells alignment rates within ±10° of the line axes is shown in Figure 6-5. Results demonstrate a direct correlation between cell alignment and cell elongation.

Comparing the alignment results of Vero cells adherent onto 10x10 μm parallel lines comb structures on the 3D Ta/SiO_2 substrate, and on the 3D Ta monolithic substrate denote 17.4 % decrease in the alignment rate from 91.2±2.7 % (Figure 5-8, and Table 5-1) to 71.7±8.6 % (Figure 6-5, Table 6-1). Results indicate that the decrease in the alignment rates of Vero cells, as discussed above is the direct result of isolating the effect of the materials' composition of the 3D Ta/SiO_2 substrates.

6.3.3 Nanometer-Scale Morphology Analysis

6.3.3.1 Cell Behavior on Single Comb Structure

The cell-substrate nanometer-scale interactions were characterized using SEM by looking at the three alignment regions, as discussed in Section 6.3.2. High- and low-resolution 70° tilted SEM images were obtained for cells adherent on comb structures with 0.18, 0.25, 0.5, 1.0, 2.0, 5.0, 10, and 50 μm wide parallel lines as shown in Figure 6-6. Figure 6-6(a)-(b) shows 3D morphology of nanoscale pseudopodia for cells on 0.18 and 0.25 μm comb structures spreading parallel and perpendicular to the Ta line y-axes. One can observe short bridge-like projections (~50 nm diameter) perpendicular to the line y-axes, marked with red arrows. To further confirm these observations, adherent cells on 0.18 and 0.25 μm comb structures were inspected using 70° tilted SEM micrographs, as presented in Figure 6-7(a)-(b), respectively. Pseudopodia are marked with red arrows, extended across the trench to adhere to the sidewalls at locations ~80 nm lower than the trench top. It was observed that none of these made contact with the bottom of the trench. Such morphological change (referred to by Type 1) was also observed on 0.5 μm wide lines as in Figure 6-7(c). However, it was observed that these projections (on the 0.5 μm wide lines) would adhere to trench bottom too, as evident in Figure 6-6(c). Such behavior, is referred to as

Type 2. On comb structures with lines larger than 1 μm, Type 2 is the only morphology that was observed as in Figure 6-6(d-h).

The two distinctive morphological behaviors (Type I and Type 2) observed in Figure 6-7 were line width-dependent. However, we do not know whether these behaviors appear after 24 hours of incubation (Figure 6-6), or it occurs during the initial course of cell spreading. Thus, an experiment was conducted for Vero cells incubated on Ta substrates for 0.5 and 2 hours.

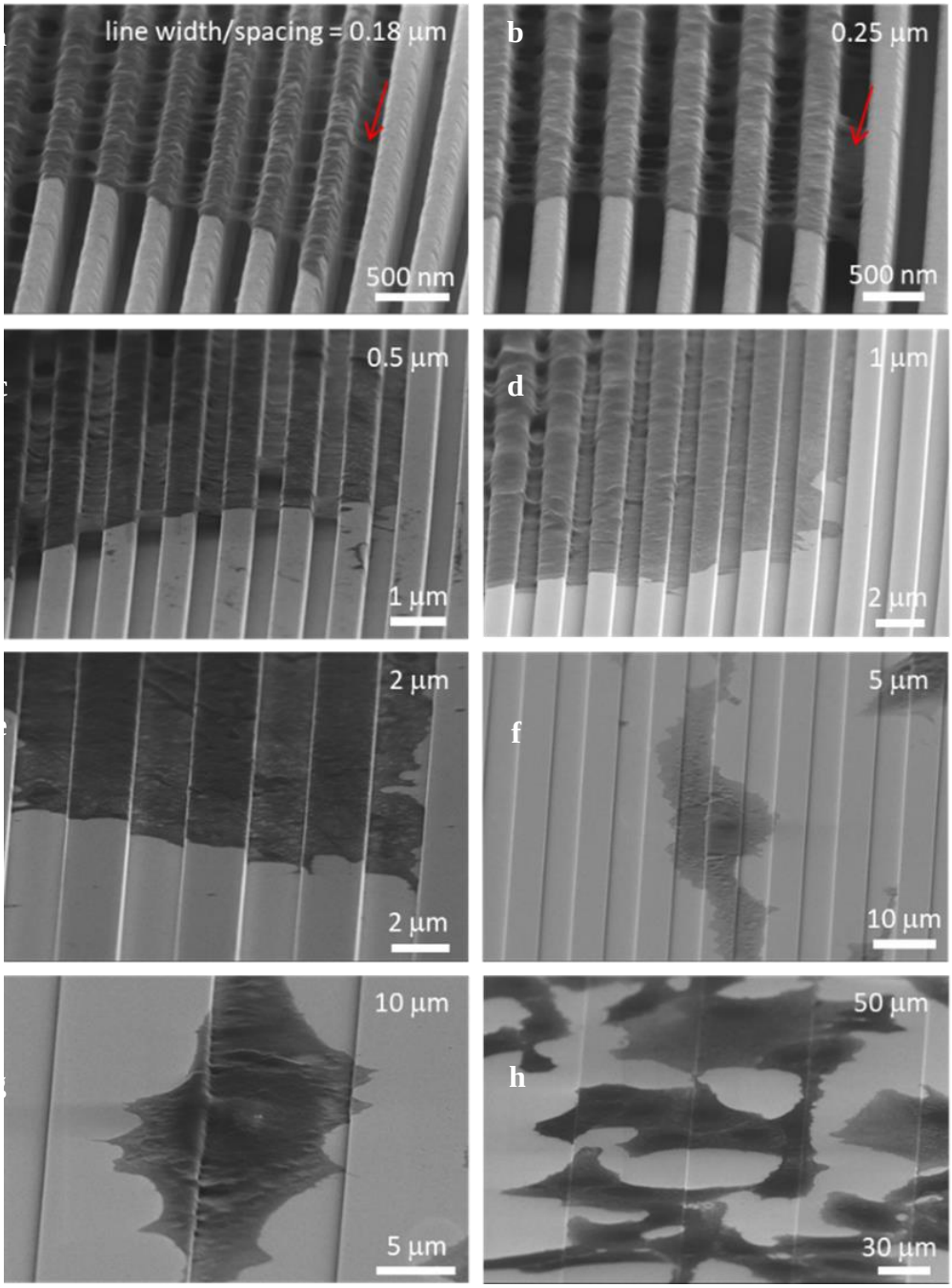

Figure 6-6 70° tilted SEM images of cells on comb structures with line widths of 0.18–50 µm. (a)-(b) Morphology Type 1: cells on 0.18 and 0.25 µm wide lines. Projections in contact with the top part and inside trench but not in contact with trench bottom. (e-h) Morphology Type 2: cells on lines larger than 1 µm show full surface coverage. (c) Morphologies Type 1 and Type 2 were observed for cells on 0.5 µm wide line comb structures. All cells were incubated on the structures for 24 hours (Moussa et al., 2018b).

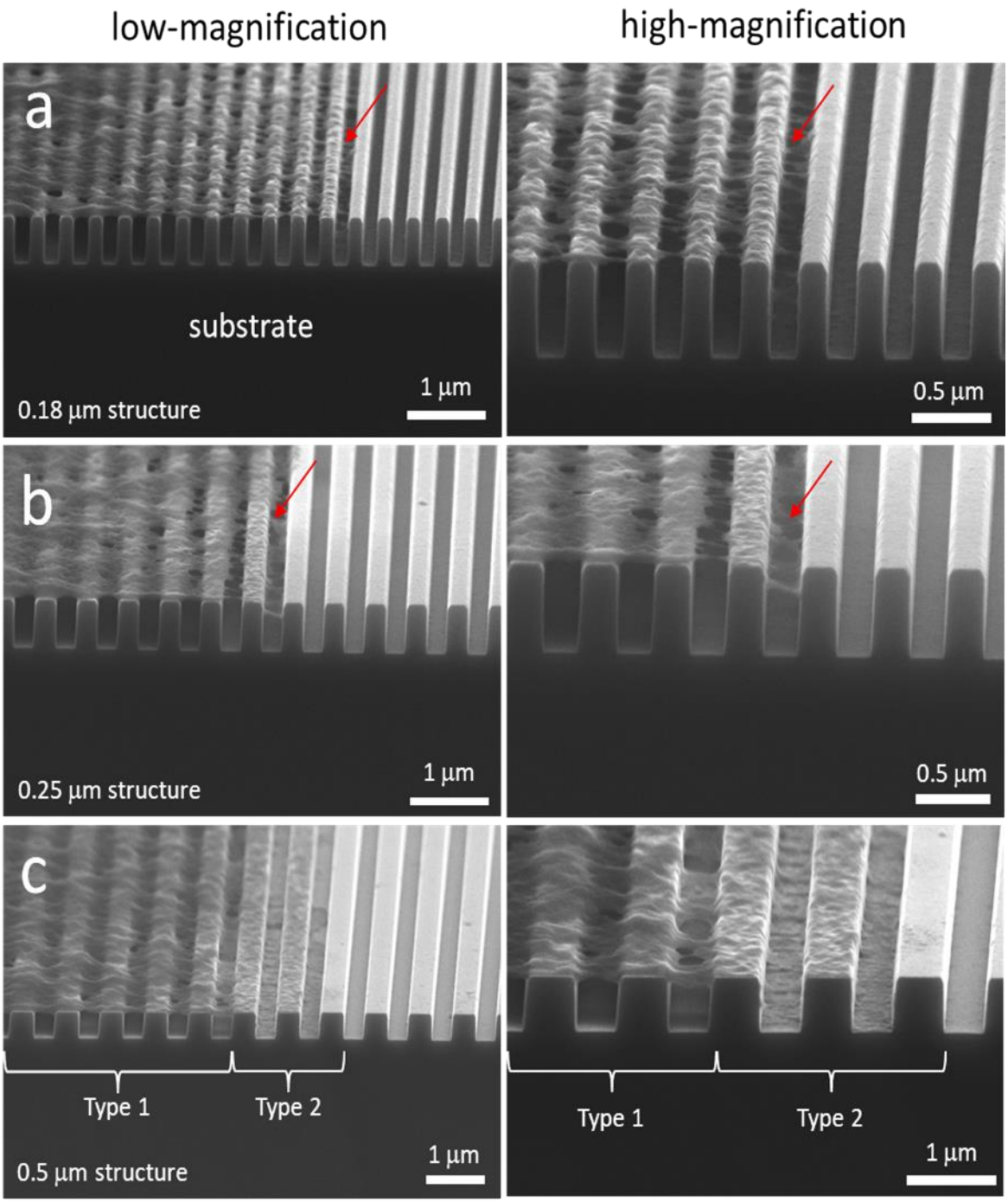

Figure 6-7 70° tilted SEM images of adherent cells on Ta and SiO_2 comb structures of (a) 0.18 µm, (b) 0.25 µm, and (c) 0.5 µm line widths. Two unique morphological behaviors. Type 1 cells on 0.18 µm and 0.25 µm wide lines structures were in contact with the top part of the trench but did not touch the flat bottom. Type 2 cells in full contact with the surface. Both morphologies were observed for cells on 0.5 µm wide lines comb structures. Cells incubation time is 24 hours. Cell confluence was ~5×10^5 cells/mL (Moussa et al., 2018b).

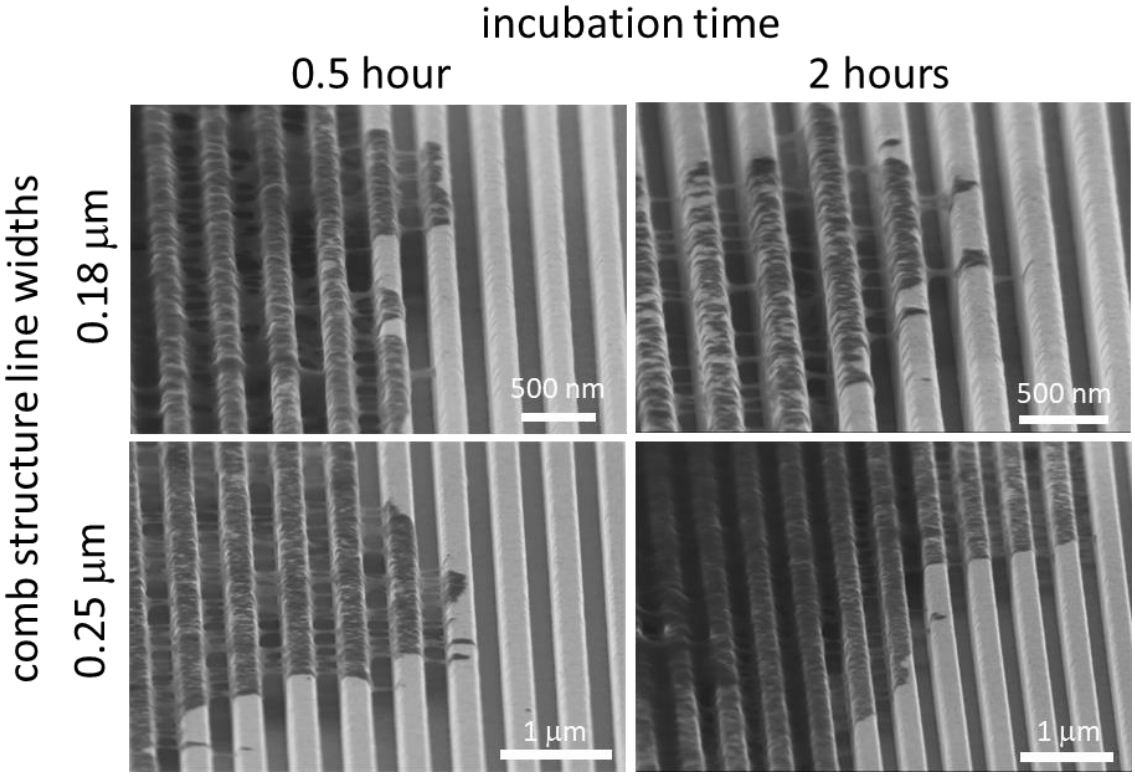

Figure 6-8 70° tilted SEM images of Type 1 cell morphology seen on comb structures with lines' width of 0.18 and 0.25 µm after 0.5 and 2 hours of incubation time (Moussa et al., 2018b).

The characterization of morphological behaviors (Type 1 and Type 2) of the adherent cells on comb structures with 0.18 and 0.25 µm wide lines was done using high-resolution SEM images, as demonstrated in Figure 6-8. Images prove that Type 1 pseudopodia happened as early as 0.5 hours after initial cell deposition. Most of the projections were observed to cross the trenches to adhere to the opposite sidewall, and some crossed directly between the lines' top surfaces. However, no projections were found to contact the flat bottom of the trench. Additional supportive images similar to the ones provided in Figure 6-8 are available in Appendix E, Figure S22, and Figure S23.

The effect of topographical features and their dimensions (e.g., depth, width, and spacing) on the change in the behavior and morphology of cells was well investigated in literature (Nakamoto et al., 2014; Ventre, Natale, Rianna, and Netti, 2014; Ventre, Causa, and Netti, 2012; Lamers et al., 2010; Loesberg et al., 2007; Teixeria et al., 2003). According to Ventre et al. (2012), Lamers et al. (2010), and Loesberg et al. (2007), the alignment of fibroblast and osteoblast cell on line structures is generally triggered by grooves at least 35 nm deep. This was hypothesized by the assumption that grooves with a smaller depth would be filled by proteins from the culture medium (Lamers et al., 2010; Toworfe et al., 2004).

Furthermore, Loesberg et al. (2007) and Lamers et al. (2010) reported a minimum width of 80–100 nm for lines and trenches to effectively induce cellular alignment. This is similar to the findings of this chapter, which indicate a minimum width of 180 nm and a depth of ~700 nm is required to stimulate the cell alignment. The spacing between lines was also reported by Ventre et al. (2012) to influence the spreading behaviors of cells, as reported in this chapter for Type 1 and Type 2. Ventre et al. (2012) observed that cells demonstrated the ability to glide on substrates with dense patterned structures (40 nm ≤ depth ≤ 100 nm) without the need to contact the trenches' flat bottoms. This is consistent with the findings of this chapter based on Figure 5-6, which indicate that cells can crossover trenches and lines 250 nm wide without the need to contact the bottom of the trench. However, a different spreading behavior was observed when the spacing between lines increased. In that case, cells tended to incline into the trench causing a full contact between the cell and bottom of the trench (Ventre et al., 2012; Zahor, Radko, Vago, Vago, and Gheber, 2007; Teixeria et al., 2003). Ventre et al. (2012) proposed that in order for cells to descend into the trench, the trench width must be at least 1 μm and the line width should be wider than 0.1 μm. Findings by Zahor et al. (2007) demonstrated that elongated cells tend to decline into a 5 μm wide trench rather than cross over the trench. Our findings from Figure 6-6 and Figure 6-7 came in consensus with findings by Zahor et al. (2007), in which we demonstrated that 68.0±6.2 % of cells on 5 μm line width and 71.7±8.6 % of cells on 10 μm line width were aligned and elongated in full contact with the bottom of the trench.

6.3.3.2 Single Cell Adhesion on Multiple Structures

The effect of surface topographies on the morphologies of the adherent cells is undisputable (Sung, Yang, Yeh, and Cheng, 2016; Qi et al., 2013; Yim et al., 2010; Anselme et al., 2010; Yang et al., 2009). These observations were based on the behavior of cells on homogeneous surfaces (with or without topographical features). However, it is still ambiguous how cells will behave if adherent (at the same time) on one substrate with two different topographical features. This section investigated such behavior simultaneously by looking at a cell adherent on blanket tantalum and 0.18 μm comb structure. Illustrative low magnification 70° tilted SEM images were used to demonstrate the location of the cell under study as in Figure 6-9(a)-(b). The images show that approximately ~50 % of the cell and its nucleus are located on the smooth tantalum blanket and ~50 % on the comb structure. The micrographs show two distinctive behaviors. On smooth blanket tantalum, the cell was spread without any favorable orientation, and it was noted that some of the actin cytoskeletons in proximity to the comb structures gave the impression that has stretched along the line axes suggesting that mechanical strains were conveyed across the cell;

however, the elongation of the cell may have been held up by the portion of the cell that was anchored on the flat surface. On the contrary, the part of the cell on the comb structure was elongated and aligned parallel to the line y-axes.

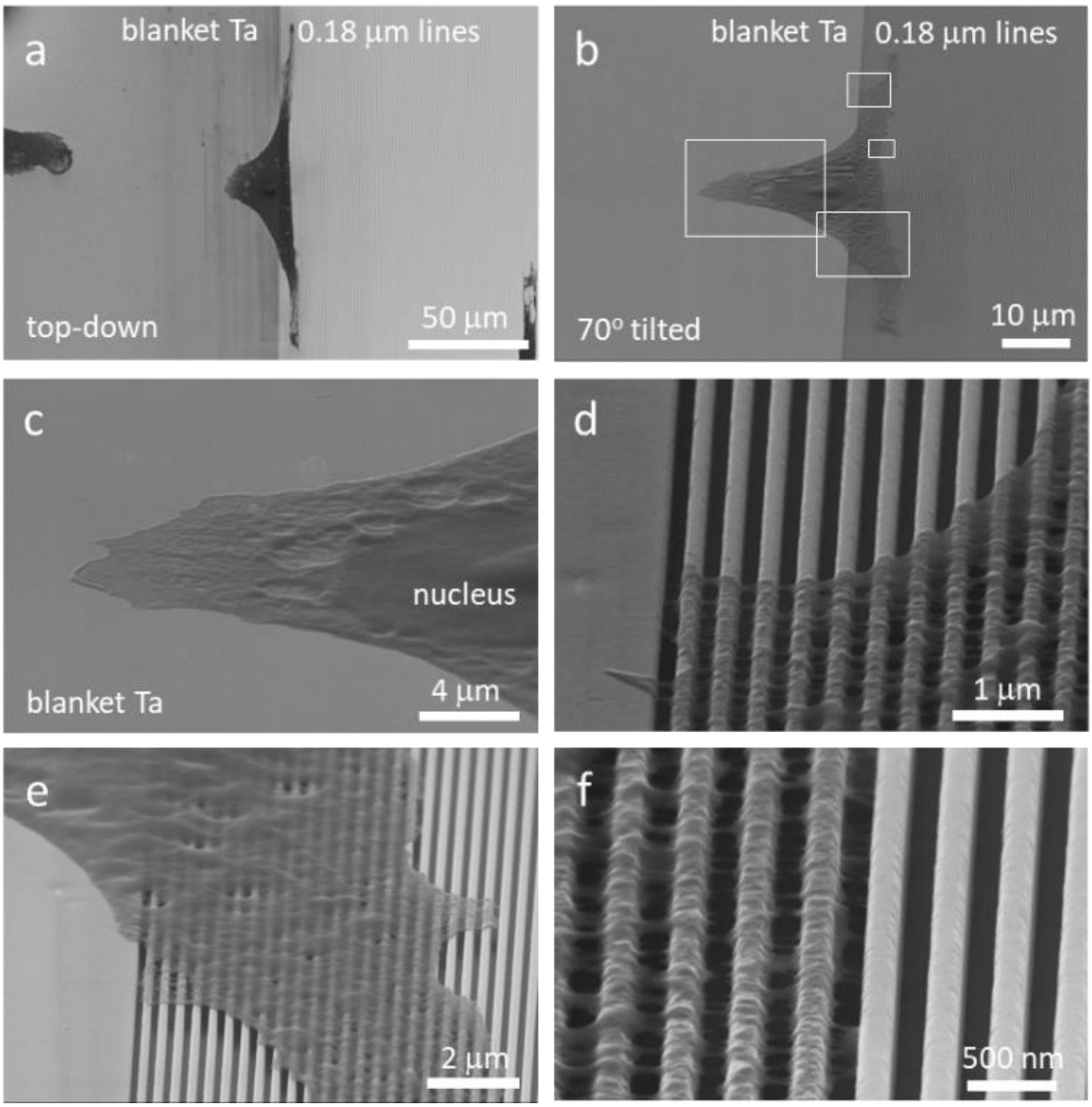

Figure 6-9 (a) Typical and (b) 70° tilted SEM images of a Vero cell adherent at the same time on a flat Ta area, and 0.18 µm wide parallel lines. (c)-(e) The cell is partially adherent on two topographically distinctive areas, a Ta blanket (flat), and a comb structure (patterned). (d)-(**f**) High magnification 70° tilted images of the adherent cell cytoplasmic projections on a comb structure (Moussa et al., 2018b).

Figure 6-9(d),(f) shows high-magnification SEM images focused on the part of the cell on the comb structure that unveiled Type 1 morphological behavior with the majority of the cellular materials either floating on the top surfaces of the Ta lines or being stretched across the trench in a bridge-like extensions in a similar behavior like observed in Figure 6-7. These observations could be regarded as the ability of cells to control their morphologies at a localized level. Figure S23 presents additional SEM images of an adherent cell on the 0.25 μm comb structures after 0.5 hours of incubation.

The observed cellular morphological changes (e.g., elongation and alignment) as presented in Figure 6-4 to Figure 6-7 can be explained by the outsized mechanical constraints (spacing and depth of trenches) that prevent the cells from spreading horizontally in the direction of the line x-axes. In order for the cell to spread horizontally, cellular components need to overtake the physical obstacles by floating over or plunging down and up the trench sidewalls. In contrast, the ability of cells to spread and elongate parallel to the line y-axes were not hindered by constraints caused by the topographical features of the surface. It was observed that the ability of cells to move and spread horizontally is affected by the topographical features of the surface. Thus it is pattern-dependent (Luzhansky et al., 2018; Wu, Giri, Sunb, and Wirtz, 2014; Cavalcanti-Adam et al., 2007). The number of sidewalls per unit length in the horizontal direction parallel to the lines x-axes is negatively correlated with the width of parallel lines in the comb structure line widths. Therefore, it is safe to assume that cells will travel a long distance on a dense comb structure than on a lower density comb structure or a flat surface with no sidewalls. Therefore, this hypothesis supports the experimental data, which shows a higher cellular alignment and elongation on dense line patterns than on flat surfaces. This may not explain the minor decrease in the alignment rate of cells with the increase in the widths of the parallel lines from 0.18 to 0.5 μm; furthermore, it may look like contradictory to the above-mentioned hypothesis. However, this inconsistency between the hypothesis and experimental data could be explained by the different cell-spreading mechanisms (Type 1 vs. Type 2). Figure 6-7 and Figure 6-8 proved that during the Type 1 spreading process, pseudopodia tend to form contact points with the sidewalls at a depth of ~80 nm from the top of the lines and then, a bridge across the trench toward the opposite sidewall. This happened without covering the entire sidewalls or establishing contacts with trench's bottom surface.

With a simple calculation, we could estimate the distance travelled by the pseudopodia on the 0.18 μm comb structures was ~18 % smaller than the traveled distance on 1 μm comb structure, but ~44 % higher than flat surfaces. This was accompanied by a higher alignment rate on 0.18 μm than on blanket ta. The cell alignment dynamics suggested in this section was consistent with findings by Zhou, Shi, Hu, and

Chenac (2013), which reported an increase in the alignment of cells with the increase in the depth of the groove.

6.4 Summary

We investigated the change in the behavior of adherent mammalian Vero cells on the newly developed 3D monolithic tantalum-coated substrate. These Ta-coated comb structures consist of parallel lines and ditches with equal widths ranging between 0.18 to 100 μm. Cells aligned the most on 1 μm wide lines at ~78 % parallel to the lines y-axes. The adherent cells exhibited two distinctive line- and trench widths-dependent cellular pseudopodium morphologies. Type 1, was found on comb structures with line widths smaller than 0.5 μm on which the nanometer-scale cellular projections bridged across the trenches without the need to establish contacts with the bottom surfaces. These projections can be seen formed after 0.5 hours of incubation time. Type 2 cells fully adapted and spread with the surface topographies on the comb structures with line widths larger than 1 μm. Results also denoted that individual cells can exhibit multiple morphological behaviors when they come in contact with two different surface topographies at the same time.

However, the most important outcome of Chapter 6 is to understand the isolated effect of the material composition on the alignment behavior of adherent cells.

Chapter 7
Conclusion and Future Work

The original objectives of this study, as stated in Chapter 1, Section 1.3, are revisited in this chapter to demonstrate the fulfillment of these objectives. Additionally, Chapter 7 provides recommendations for future research opportunities.

7.1 Conclusion

In vivo, biological systems are captivating, resilient, complicated, and hard to imitate. Understanding how these systems function is essential to replicate them *in vitro*. Thus, it is vital to attain tools with specific abilities to mimic the chemical and physical functions of these *in vivo* environments. Extracellular matrix-inspired engineered substrates embrace the promise to induce targeted cell-substrate interactions to control the behavior of biological cells. Such biologically-mimicked biomaterials may hold a potential solution for a complex problem.

This thesis presented viable alternatives for the engineered substrates that are currently in use. Some of the physical and mechanical features make the substrates presented in this work desirable as biologically active mimics. The newly developed substrates were used as structural support for the assessed cells, and they also provided contact guidance for their biological functions, such as adhesion, and alignment. This was done by using custom-designed 2D, and 3D engineered patterned surfaces with different materials. Contact guidance is defined as the ability of the topographical features of a substrate to induce changes in the biological functions of cells (Flemming, Murphy, Abrams, Goodman, and Nealey, 1999).

It is essential to emphasize that the comparison between the effect of the 2D and the 3D substrates on the alignment behavior of cells is hindered by the following:

I. the difference in the effect of surface topography (2D vs. 3D)
II. the difference in the effect of substrate materials (tungsten vs. tantalum)
III. the difference in the effect of surface properties of W in comparison to Ta (e.g., roughness, surface energy, contact angle)

Chapter 3 presented a novel two-dimensional silicon oxide-based micron and sub-micron scale patterned substrate. The substrates were fabricated by means of a highly advanced process used in the semiconductor industry. The substrates consisted of micron- and sub-micron scale tungsten metal line structures inlaid in thin-film silicon oxide. The combination of scalable fabrication process of CMP and

the properties of the surface (flatness, smoothness, and the defect-free), with a very low surface roughness of ~0.26 – 0.44 nm, in addition to the potential to create unlimited numbers of designs with high precision, demonstrated the potential of these substrates as biological mimics. Surface characterization was done using scattering electron microscopy and atomic force microscopy. Four types of cells were tested on these substrates, seeded, and allowed to grow. The alignment behaviors of cells on both the symmetrical and asymmetrical parallel line comb structures were assessed and characterized as a function of (1) parallel lines width, W/SiO_2 line widths, (2) incubation time (0.5-72 hours), (3) serum content in the culture medium, and (4) the presence of a bacterial toxin (Antimycin A). Experimental results indicated that all the assessed cells were preferentially attracted to tungsten rather than silicon oxide parallel lines and surfaces, but with different magnitude. For example, ~1 % of Vero cells were found adherent to silicon oxide. The preferential adhesion of cells onto tungsten lines happened in the absence of external mechanical stimuli.

Furthermore, results showed selectivity to the tungsten line geometric parameters, such as line width and spacing. The maximum alignment rate was achieved on 10 μm lines width comb structures. These phenomena were explained using two mathematical models designed to predict the pattern-dependent cell dynamics on the symmetric and asymmetric comb structures. The models were designed to describe the cellular geometries as a function of pattern width and spacing, which showed that cells would rearrange their morphologies to maximize their contact with the inlaid tungsten lines. Additionally, the reusability of these engineered substrates was tested, by removing adherent (fixed and dehydrated) cells from an already used substrate, using simple mechanical scrubbing. The scrubbed substrate was used to seed new cells on, and results proved that the re-worked substrates maintained their alignment functions.

Chapter 4 tested and compared the alignment behaviors of adherent Vero cells on two-dimensional tungsten and silicon oxide micron and sub-micron scale patterned substrates as a function of single-species serum proteins or FBS as (i) supplement to the serum-free medium and (ii) pre-adsorbed on the substrate before seeding the cells. Results indicate that as a supplement, albumins had the highest impact on the alignment of cells, but the lowest effect on the cell adhesion. Vitronectin had the lowest impact on the alignment behavior of cells when added as a supplement to OptiPRO, the SFM. As expected, OptiPRO supplemented with 10 % FBS supported the maximum cell growth. However, when single species serum proteins (FN, VN, and Col) or FBS were pre-adsorbed on the substrate prior to seeding the cells, individual proteins, specifically FN, VN, and Col-IV induced comparable alignment behaviors to those observed when they used as a supplement for OptiPRO (SFM). Pre-adsorbed FBS supported the highest growth performance; however, the alignment behavior, and growth rate of cells were negatively

affected by rinsing the pre-adsorbed FBS with D-PBS before seeding the cells. Nevertheless, pre-adsorbed fibronectin and FBS induced the highest alignment rates amongst all single proteins and FBS (rinsed).

Chapter 5 presented a novel 3D Ta/SiO_2 micron and sub-micron scale patterned substrate. The 3D substrates used in this section consist of dense comb structures with parallel lines of equal widths and trenches. The goal was to examine the morphological changes of mammalian (Vero) cells deposited on these substrates as a function of the widths of silicon oxide lines and tantalum trenches. High-resolution images were generated using scattering electron microscopy and fluorescence microscopy to characterize the alignment and elongation behaviors of adherent cells. Results proved that the alignment behavior of the adherent cells was dependent on Ta trench width. Three adhesion dynamics were observed corresponding to the different spreading mechanism. Region i includes cells adherent on Ta trenches 0.21 to 0.5 μm wide (thin trenches). The adherent cells had a tendency to cross over the trench openings. Region ii consists of cells adherent on trenches with higher widths than those in Region i. The widths of these trenches varied between 1 and 10 μm. Cells were observed to fully adhere (conform) to the topographical features of the trench. The trenches from region iii in this group were wider than 10 μm, and the majority of the adherent cells in that region were randomly spread, with no preferential alignment similar to cells on blanket tantalum; however, a substantial percentage of cells adhered to the junctions in the corner between the sidewalls and the bottom. Results indicate that cells align the most in trenches 10 μm wide. Pseudopods projections (with an effective diameter of ~50 nm) were observed extending to help to stabilize the adhesion of cells onto the tantalum surface.

Chapter 6 presented a new developed three-dimensional silicon oxide-based substrates tantalum coated comb structures with parallel equal widths lines and trenches 0.18 to 100 μm wide. Tantalum is widely used in surgical implants. However, the interaction between the substrate and the cells at a nano level is still untested. Scanning electron microscopy and fluorescence confocal microscopy were used to characterize the interaction between Vero cells and the 3D tantalum substrates, and the change in the morphology of the adherent cells. Results demonstrate that ~53–77 % of cells adherent on lines are smaller than 10 μm wide and are aligned within ±10° of the lines y-axes.

On the contrary, not more than 19 % of cells on 50 and 100 μm line widths exhibited a preferential alignment behavior. Two types of cell morphologies were observed, both proved to be line-width-dependent. The pseudopod projections of cells on lines 0.5 μm wide and smaller tend to cross the ditch between two lines without the need to contact the flat bottom of the trench. On the other hand, the

pseudopod extensions from cells adherent to lines wider than 0.5 μm, tend to cover the entire trench sidewalls and the bottom surfaces of comb structures. Additionally, a cell simultaneously adherent on multiple surfaces with different topographical features (e.g., comb structures and blanket Ta) will exhibit two distinctive morphological behaviors; each behavior will be similar to the type of morphology observed for cells individually contacting these surfaces.

7.2 Recommended Future Work

7.2.1 Continue Working on the Time-Dependent Alignment Study

Chapter 3, Section 3.3.1.3 presents the preliminary results for the time-dependent Vero cells alignment behavior on comb structures with line width of 10 μm. Further examination to assess the alignment behaviors of cells on the rest of the comb structures for different incubation times is required. This would help to complete the full picture of cell alignment behavior as a function of time on symmetric comb structures.

Additionally, it is recommended to assess the alignment behavior of cells as a function of time on asymmetric comb structures. In this study, as presented in Chapter 3, Section 3.3.1.6, we have only assessed the alignment behavior of cells on a small sample of asymmetric comb structures. However, the 2D W/SiO_2 substrate consists of more asymmetric comb structures such as 1.5x0.5 μm, 0.5x1.5 μm, 3x7 μm, 7x3 μm, 10x90 μm, and 90x10 μm.

7.2.2 Complete the Bacterial Toxin (antimycin A) Study

Section 3.3.3, demonstrated the negative impact of antimycin A, when added to the culture medium, on the alignment behavior of dermal fibroblast (GM5565) cells and their densities, as a function of time on comb structures with 10 μm symmetric comb structures. Thus, completing the full picture by assessing the behavior of cells in the presence of antimycin A as a function of time on symmetrical and asymmetric comb structures would be essential for understanding the behavior of cells in the presence of antimycin A.

7.2.3 Effect of Albumin on the Behavior of Cells on Ta/SiO_2 3D Substrate

Results from Section 5.3.2, indicated that ~91 % of Vero cells adherent on the Ta/SiO_2 3D micron and sub-micron scale patterned substrate aligned within ±10° parallel to the Ta trench y-axes. Cells were incubated in a baseline medium containing 10% FBS. This is the maximum alignment rate observed on any tested substrates. On the other hand, results from Chapter 4, Section 4.2.3.1, proved that using 10 μg/mL of bovine serum albumin (BSA) as a supplement for serum-free culture media instead of 10 %

FBS induced an increase in the alignment rate of Vero cells incubated on the 2D W/SiO_2 substrate by ~30 %. Thus, it would be reasonable to assess the alignment behavior of Vero cells on the 3D Ta/SiO_2 micron, and sub-micron scale patterned substrate using SFM supplemented with 10 μg/mL of BSA.

References

Abe, T., Steigmeier, E., Hagleitner, W., and Pidduck, A. (1992). Microroughness Measurements on Polished Silicon Wafers. *Japanese Journal of Applied Physics, 31*(3R), 712-728.

Abe, T., Steigmeier, E., Hagleitner, W., and Pidduck, A. (Japanese Journal of Applied Physics). Microroughness Measurements on Polished Silicon Wafers. *1992, 31*(3R), 712-728.

Acikgoz, C., Hempeniusa, M. A., Huskens, J., and Vancso, G. J. (2011). Polymers in Conventional and Alternative Lithography for the Fabrication of Nanostructures. *European Polymer Journal, 47*(11), 2033-2052. doi:10.1016/j.eurpolymj.2011.07.025

Adams, T., Anwar, R., Mfarej, M., Rundatz, T., Coyle, M., and McLaughlin, J. (2015). Nutritional Stress of Cultured Vero Cells Causes Altered Growth and Morphology as Seen in Neoplastic Transformation. *American Journal of Undergraduate Research, 12*(3), 63-75.

Albanese, A., and Chan, W. (2011). Effect of Gold Nanoparticle Aggregation on Cell Uptake and Toxicity. *ACS Nano, 5*(7), 5478-5489. doi:10.1021/nn2007496

Albuschies , J., and Vogel, V. (2013). The Role of Filopodia in the Recognition of Nanotopographies. *Scientific Reports, 3*, Article number: 1658. doi:10.1038/srep01658

Alkilany, A., and Murphy, C. (2010). Toxicity and cellular uptake of gold nanoparticles: what we have learned so far? *Journal of Nanoparticle Research, 12*(7), 2313-2333. doi:10.1007/s11051-010-9911-8

Altankov, G., Richau, K., and Groth, T. (2003). The role of surface zeta potential and substratum chemistry for regulation of dermal fibroblasts interaction. *Materials Science and Engineering Technology, 34*(12), 1120-1128. doi:10.1002/mawe.200300699

Ammerman, N., Beier-Sexton, M., and Azad, A. (2008). Growth and Maintenance of Vero Cell Lines. *Current Protocols in Microbiology, APPENDIX, Appendix–4E.* doi:10.1002/9780471729259.mca04es11

Anker, J., Hall, W., Lyandres, O., Shah , N., Zhao, J., and Van Duyne, R. (2008). Biosensing with plasmonic nanosensors. *Nature Materials, 7*, 442-453. doi:10.1038/nmat2162

Anselme , K., Ploux , L., and Ponche, A. (2010). Cell/Material Interfaces: Influence of Surface Chemistry and Surface Topography on Cell Adhesion. *Journal of Adhesion Science and Technology, 24*(5), 831-852. doi:10.1163/016942409X12598231568186

Anselme, K., and Bigerelle, M. (2005). Topography effects of pure titanium substrates on human osteoblast long-term adhesion. *Acta Biomaterialia, 1*(2), 211-222. doi:10.1016/j.actbio.2004.11.009

Anselme, K., and Bigerelle, M. (2006). Modelling approach in cell/material interactions studies. *Biomaterials, 27*(8), 1187-1199. doi:j.biomaterials.2005.10.009

Anselme, K., Bigerelle, M., Noel, B., Dufresne, E., Judas, D., Iost, A., and Hardouin, P. (2000). Qualitative and quantitative study of human osteoblast adhesion on materials with various surface roughnesses. *Journal of Biomedical Materials Research, 49*(2), 155-166. doi:10.1002/(SICI)1097

Arima, Y., and Iwata, H. (2015). Preferential adsorption of cell adhesive proteins from complex media on self-assembled monolayers and its effect on subsequent cell adhesion. *Acta Biomaterialia, 26*, 72-81. doi:0.1016/j.actbio.2015.08.033

Armentano, I., Arciola, C., Fortunati, E., Ferrari, D., Mattioli, S., Amoroso, C., . . . Visai, L. (2014). The Interaction of Bacteria with Engineered Nanostructured Polymeric Materials: A Review. *The Scientific World Journal, 2014*, 410423 (18pp). doi:10.1155/2014/410423

Arnold, M., Schwieder, M., Blümmel, J., Cavalcanti-Adam, E., López-Garcia, M., Kessler, H., . . . Spatz, J. (2009). Cell interactions with hierarchically structured nano-patterned adhesive surfaces. *Soft Matter, 5*, 72-77. doi:10.1039/B815634D

Arora, M. (2013). Cell Culture Media: A Review. *Materials and Methods, 3*(175), 29. doi:10.13070/mm.en.3.175

Arora, P., Bhide, V., Chen , A., McCulloch, C., and Ko, K. (2001). Cell-cell adhesion in human fibroblasts requires calcium signaling. *Journal of Cell Science, 114*(6), 1155-1167.

Atiquzzaman, F. (2012). Chemical Mechanical Planarization of Electronic Materials (Master's Thesis). Tampa, FL: University of South Florida.

Aubin, H., Nichol, J., Hutson, C., Bae, H., Sieminski, A., Cropek, D., . . . Khademhosseini, A. (2010). Directed 3D cell alignment and elongation in microengineered hydrogels. *Biomaterials, 31*(27), 6941-6951. doi:10.1016/j.biomaterials.2010.05.056

Aumailley, M. (2013). The laminin family. *Cell Adhesion 7 Migration, 7*(1), 48-55. doi:10.4161/cam.22826

AZoM. (2001, Dec. 13). *Silica - Silicon Dioxide (SiO2).* Retrieved from AZO Materials: https://www.azom.com/article.aspx?ArticleID=1114#

Baac, H., Lee, J.-H., Seo, J.-M., Park, T., Chung, H., Lee, S.-D., and Kim, S. (2004). Submicron-scale topographical control of cell growth using holographic surface relief grating. *Materials Science and Engineering: C, 24*(1-2), 209-212. doi:10.1016/j.msec.2003.09.009

Bacakova, L., Filova, E., Parizek, M., Ruml, T., and Svorcik, V. (2011). Modulation of cell adhesion, proliferation and differentiation on materials designed for body implants. *Biotechnology Advances, 29*(6), 739-767. doi:10.1016/j.biotechadv.2011.06.004

Badami, D., Jahed, Z., Seo, B., Burek, M., and Tsui, T. (2015). Microstructural and Geometrical Effects on the Deformation Behavior of Sub-micron Scale Nanocrystalline Copper Pillars. *Metallurgical and Materials Transactions A, 47*(3), 1061-1071. doi:10.1007/s11661-015-3276-7

Baker, D., Harrison, N., Maltby, E., Smith, K., Moore, H., Shaw, P., . . . Andrews, P. (2007). Adaptation to culture of human embryonic stem cells and oncogenesis in vivo. *Nature Biotechnology, 25*(2), 207-215. doi:10.1038/nbt1285

Balcells , M., and Edelman, E. (2002). Effect of pre-adsorbed proteins on attachment, proliferation, and function of endothelial cells. *Journal of Cellular Physiology, 191*(2), 155-161. doi:10.1002/jcp.10087

Balcells , M., and Edelman, E. (2002). Effect of pre-adsorbed proteins on attachment, proliferation, and function of endothelial cells. *Journal of Cellular Physiology, 191*(2), 155–161. doi:10.1002/jcp.10087

Balla, V., Bodhak, S., Bose, S., and Bandyopadhyay, A. (2010). Porous tantalum structures for bone implants: Fabrication, mechanical and in vitro biological properties. *Acta Biomaterialia, 6*(8), 3349-3359. doi:10.1016/j.actbio.2010.01.046

Banerjee, G., and Rhoades, R. L. (2008). *Chemical Mechanical Planarization Historical Review and Future Direction* (Vol. 13). Gilbert, AZ, USA: ECS Transactions.

Banhegyi, G. (2015, Jan. 09). *What is the difference between top down and bottom up methods for creating nano-structures?* Retrieved from Research Gate: https://www.researchgate.net

Baranes, K., Shevach, M., Shefi, O., and Dvir, T. (2016). Gold Nanoparticle-Decorated Scaffolds Promote Neuronal Differentiation and Maturation. *Nano Letters, 16*(5), 2916-2920. doi:10.1021/acs.nanolett.5b04033

Baravelli, E. (2005, Sep. 27). *Introduction to VLSI Fabrication Technologies.* Retrieved from University of Bologna, Department of Electronics, Computer Science and Systems: http://www-micro.deis.unibo.it/

Barnthip, N., Noh, H., Leibner, E., and Vogler, E. (2008). Volumetric interpretation of protein adsorption: kinetic consequences of a slowly-concentrating interphase. *Biomaterials, 29*(21), 3062-3074. doi:10.1016/j.biomaterials.2008.03.043

Barnthip, N., Parhi, P., Golasb, A., and Vogler, E. (2009). Volumetric interpretation of protein adsorption: Kinetics of protein-adsorption competition from binary solution. *Biomaterials, 30*(33), 6495-6513. doi:10.1016/j.biomaterials.2009.08.016

Barrett, P., Berezuk, G., Fritsch, S., Aichinger, G., Hart, M., El-Amin, W., . . . Ehrlich, H. (2011). Efficacy, safety, and immunogenicity of a Vero-cell-culture-derived trivalent influenza vaccine: a multicentre, double-blind, randomised, placebo-controlled trial. *The Lancet, 377*(9767), 751-759. doi:10.1016/S0140-6736(10)62228-3

Baszkin, A., and Lyman , D. (2004). The interaction of plasma proteins with polymers. I. Relationship between polymer surface energy and protein adsorption/desorption . *Journal of Biomedical Materials Research, 14*(4), 393-403.

Bauer, T., McDermid , H., Budarf , M., Van Keuren , M., and Blomberg, B. (1993). Physical location of the human immunoglobulin lambda-like genes, 14.1, 16.1, and 16.2. *lmmunogene~cs, 38*, 387-399.

Baujard-Lamotte, L., Noinville, S., Goubard, F., Marque, P., and Pauthe, E. (2008). Kinetics of conformational changes of fibronectin adsorbed onto model surfaces. *Colloids and Surfaces B: Biointerfaces, 63*(1), 129-137. doi:10.1016/j.colsurfb.2007.11.015

Beaudoin, S., Boning, D., and Raghavan, S. (1999). Chemical Mechanical Polishing (CMP) Overview. Arizona, USA.

Beckman Institute . (2011, July 09). *Cells' Get Sticky with Calcium*. Retrieved from Theoretical and Computational Biophysics group: http://www.ks.uiuc.edu/Research/cadherin/

Belaadi, N., Aureille , J., and Guilluy, C. (2016). Under Pressure: Mechanical Stress Management in the Nucleus. *Cells, 5*(27), 1-11. doi:10.3390/cells5020027

Beningo, K., Dembo, M., Kaverina, I., Small, J., and Wang, Y.-l. (2001). Nascent Focal Adhesions Are Responsible for the Generation of Strong Propulsive Forces in Migrating Fibroblasts. *The Journal of Cell Biology, 153*(4), 881-888. doi:10.1083/jcb.153.4.881

Berens, M., Rief, M., Loo, M., and Giese, A. (1994). The role of extracellular matrix in human astrocytoma migration and proliferation studied in a microliter scale assay. *Clinical and Experimental Metastasis, 12*(6), 405-415.

Berne, C., Ducret, A., Hardy, G., and Brun, Y. (2015). Adhesins involved in attachment to abiotic surfaces by Gram-negative bacteria. *Microbiology Spectrum, 3*(4). doi:10.1128/microbiolspec.MB-0018-2015

Biazar, E., Heidari, M., Asefnezhad, A., and Montazeri, N. (2011). The relationship between cellular adhesion and surface roughness in polystyrene modified by microwave plasma radiation. *International Journal of Nanomedicine, 6*, 631-639. doi:10.2147/IJN.S17218

Biela, S., Su, Y., Spatz, J., and Kemkemer, R. (2009). Different Sensitivity of Human Endothelial Cells, Smooth Muscle Cells and Fibroblasts to Topography in the Nano-Micro Range. *Acta Biomaterialia, 5*(7), 2460–2466. doi:10.1016/j.actbio.2009.04.003

Biggs, M., Richards , R., Gadegaard, N., Wilkinson, C., and Dalby, M. (2007). The Effects of Nanoscale Pits on Primary Human Osteoblast Adhesion Formation and Cellular Spreading. *Journal of Materials Science: Materials in Medicine, 18*(2), 399-404.

Bizzarri, M., Monici, M., and van Loon, J. (2015). How Microgravity Affects the Biology of Living Systems. *BioMed Research International, 2015*(Article ID 863075), 1-4. doi:10.1155/2015/863075

Blau, A., Weinl, C., Mack, J., Kienle, S., Jung, G., and Ziegler, C. (2001). Promotion of neural cell adhesion by electrochemically generated and functionalized polymer films. *Journal of Neuroscience Methods, 112*(1), 65-73. doi:10.1016/S0165-0270(01)00458-7

Bogitsh, B., Carter, C., and Oeltm, T. (2013). Chapter 3 - General Characteristics of the Euprotista (Protozoa). In B. J. Bogitsh, C. E. Carter, and T. N. Oeltm, *Human Parasitology (Fourth Edition)* (pp. 37-51). Waltham, MA: Academic Press. doi:10.1016/B978-0-12-415915-0.00003-0

Boisseau, P., and Loubaton, B. (2011). Nanomedicine, nanotechnology in medicine. *Comptes Rendus Physique, 12*(7), 620-636. doi:10.1016/j.crhy.2011.06.001

Bornschlögl, T., Romero, S., Vestergaard, C., Joanny, J.-F., Van Nhieu, G., and Bassereau, P. (2013). Filopodial retraction force is generated by cortical actin dynamics and controlled by reversible tethering at the tip. *PNAS, 110*(47), 18928-18933. doi:10.1073/pnas.1316572110

Bourget, J.-M., Guillemette, M., Veres, T., Auger , F., and Germain, L. (2013). Alignment of Cells and Extracellular Matrix Within Tissue-Engineered Substitutes. In R. Pignatello (Ed.), *Advances in Biomaterials Science and Biomedical Applications* (pp. 365-390). Rijeka, Croatia: InTech. doi:10.5772/54142

Brash, J. (1988). Protein interactions with solid surfaces following contact with plasma and blood. *Macromolecular Symposia, 17*(1), 441-452. doi:10.1002/masy.19880170133

Brunette, D., and Chehroudi, B. (1999). The Effects of the Surface Topography of Micromachined Titanium Substrata on Cell Behavior in Vitro and in Vivo. *Journal of Biomechanical Engineering , 121*(1), 49-57.

Brunner, D., Frank, J., Appl, H., Schöffl, H., Pfaller, W., and Gstraunthaler, G. (2010). Serum-free Cell Culture: The Serum-free Media Interactive Online Database. *ALTEX, 27*(1), 53-62. doi:10.14573/altex.2010.1.53

Brusic, V., Edelstein, D., Feeney, P., Guthrie, W., Jaso, M., Kaufman, F., . . . Thompson , D. (2003). *United States of America Patent No. US 6632377 B1.*

Burridge, K., and Wennerberg, K. (2004). Rho and Rac Take Center Stage. *Cell, 116*(2), 167-179. doi:10.1016/S0092-8674(04)00003-0

Burzo, M., Komarov, P., and Raad, P. (2003). Thermal transport properties of gold-covered thin-film silicon dioxide. *IEEE Transactions on Components and Packaging Technologies, 26*(1), 80-88. doi:10.1109/TCAPT.2003.811467

Byron, A., Humphries , J., and Humphries, M. (2013). Defining the extracellular matrix using proteomics. *International Journal of Experimental Pathology, 94*(2), 75-92. doi:10.1111/iep.12011

Cai, K., Dong, H., Chen, C., Yang, L., Jandt, K. D., and Deng, L. (2009). Inkjet printing of laminin gradient to investigate endothelial cellular alignment. *Colloids and Surfaces B: Biointerfaces, 72*(2), 230-235. doi:10.1016/j.colsurfb.2009.04.008

Cao, N., Chen, X., and Schreyer, D. (2012). Influence of Calcium Ions on Cell Survival and Proliferation in the Context of an Alginate Hydrogel. *ISRN Chemical Engineering, 2012, Article ID 516461,* 9 pages. doi:10.5402/2012/516461

Carré , A., and Lacarrière, V. (2010). How Substrate Properties Control Cell Adhesion. A Physical-Chemical Approach. In A. Carré, and K. Mittal (Eds.), *Surface and Interfacial Aspects of Cell Adhesion* (pp. 3-18). Leiden, The Netherlands: Koninklijke Brill NV.

Casaroli Marano, R., and Vilaro, S. (1994). The Role of Fibronectin, Laminin, Vitronectin and Their Receptors on Cellular Adhesion in Proliferative Vitreoretinopathy. *Investigative Ophthalmology and Visual Science , 35*(6), 2791-2803.

Cavalcanti-Adam, E., Volberg, T., Micoulet, A., Kessler, H., Geiger, B., and Spatz, J. (2007). Cell Spreading and Focal Adhesion Dynamics Are Regulated by Spacing of Integrin Ligands. *Biophysical Journal, 92*(8), 2964-2974. doi:10.1529/biophysj.106.089730

Cha, P., Krishnan, A., Fiore, V., and Vogler, E. (2008). Interfacial Energetics of Protein Adsorption from Aqueous Buffer to Surfaces with Varying Hydrophilicity. *Langmuir, 24*(6), 2553–2563. doi:10.1021/la703310k

Chan, C.-Y., and Tambyah, P. (2012). Preflucel®: a Vero-cell culture-derived trivalent influenza vaccine. *11*(7), 759-773. doi:10.1586/erv.12.55

Chang, H.-Y., Huang, C.-C., Lin, K.-Y., Kao, W.-L., Liao, H.-Y., You, Y.-W., . . . Shyue, J.-J. (2014). Effect of Surface Potential on NIH3T3 Cell Adhesion and Proliferation. *Journal of Physical Chemistry, 118*, 14464−14470. doi:10.1021/jp504662c

Chang, H.-Y., Kao, W.-L., You, Y.-W., Chu, Y.-H., Chu, K.-J., Chen, P.-J., . . . Shyue, J.-J. (2016). Effect of surface potential on epithelial cell adhesion, proliferation and morphology. *Colloids and Surfaces B: Biointerfaces, 141*, 179-186. doi:10.1016/j.colsurfb.2016.01.049

Charest, J., Garcia, A., and King, W. (2007). Myoblast alignment and differentiation on cell culture substrates with microscale topography and model chemistries. *Biomaterials, 28*(13), 2202–2210. doi:10.1016/j.biomaterials.2007.01.020

Chelli, B., Barbalinardo, M., Valle, F., Greco, P., Bystrenova, E., Bianchi, M., and Biscarini, F. (2014). Neural cell alignment by patterning gradients of the extracellular matrix protein laminin. *Interface Focus, 4*(1), 20130041. doi:10.1098/rsfs.2013.0041

Chen, C., Tan, J., and Tien, J. (2004). Mechanotransduction at Cell-Matrix and Cell-Cell Contacts. *Annual Review of Biomedical Engineering, 6*, 275-302. doi:10.1146/annurev.bioeng.6.040803.140040

Chen, L., Ma, K., Han, J., Chen, Q., and Zhu, Y. (2017). Chapter Eleven - Monitoring Mitophagy in Mammalian Cells. *Methods in Enzymology, 588*, 187-208.

Chen, W.-K. (Ed.). (2007). *The VLSI Handbook. 2nd ed.* New York: CRC Press, Taylor and Francis Group.

Cheng , C.-M., LeDuc , P., and Lin, Y.-W. (2011). Localized bimodal response of neurite extensions and structural proteins in dorsal-root ganglion neurons with controlled polydimethylsiloxane substrate stiffness. *Journal of Biomechanics, 44*(5), 856-862. doi:10.1016/j.jbiomech.2010.12.006

Cheung, K. C., and Renaud, P. (2006). BioMEMS for medicine: On-chip cell characterization and implantable microelectrodes. *Solid-State Electronics, 50*(4), 551-557. doi:10.1016/j.sse.2006.03.023

Chieh, H.-F., Sun, Y., Liao, J.-D., Su, F.-C., Zhao, C., Amadio, P., and An, K.-N. (2014). Effects of cell concentration and collagen concentration on contraction kinetics and mechanical properties in a bone marrow stromal cell-collagen construct. *Journal of Biomedical Materials Research Part A, 93*(3), 1132–1139. doi:10.1002/jbm.a.32606

Chierico, L., Joseph, A., Lewis, A., and Battaglia, G. (2014). Live cell imaging of membrane / cytoskeleton interactions and membrane topology. *Scientific Reports, 4*(Article number: 6056). doi:10.1038/srep06056

Chithrani , B., Ghazani, A., and Chan, W. (2006). Determining the Size and Shape Dependence of Gold Nanoparticle Uptake into Mammalian Cells. *Nano Letters, 6*(4), 662-668. doi:10.1021/nl052396o

Cho , S., and Chae, J. (2009). A New Protein Sensor Platform Based on Competitive Protein Adsorption for Thyroglobulin Detection. *AMSE. Journal of Medical Devices, 3*(2), 027539-027539-1. doi:10.1115/1.3147513

Choi, C.-H., Heydarkhan-Hagvall, S., Wu, B., Dunn, J., Beygui, R., and Kim, C.-J. (2009). Cell Growth as a Sheet on Three-Dimensional Sharp-Tip Nanostructures. *Journal of Biomedical Materials Research Part A, 89*(3), 804-817. doi:10.1002/jbm.a.32101

Choi, J.-Y., Alford, T., and Honsberg, C. (2015). Fabrication of Periodic Silicon Nanopillars in a Two-Dimensional Hexagonal Array with Enhanced Control on Structural Dimension and Period. *Langmuir, 31*(13), 4018–4023. doi:10.1021/acs.langmuir.5b00128

Chung, I.-C., Li, C.-W., and Wang, G.-J. (2013). The Influence of Different Nanostructured Scaffolds on Fibroblast Growth. *Science and Technology of Advanced Materials, 14*(4), 044401 (10pp). doi:10.1088/1468-6996/14/4/044401

Chuvilin, A. (2015, Jan. 09). *What is the difference between top down and bottom up methods for creating nano-structures?* Retrieved from Research Gate: https://www.researchgate.net

Coelho, N., Gonza´lez-Garcı´a, C., Salmeron-Sanchez, M., and Altankov, G. (2011). Arrangement of Type IV Collagen and Laminin on Substrates with Controlled Density of –OH Groups. *Tissue Engineering: Part A, 17*(17-18), 2245-2257. doi:10.1089/ten.tea.2010.0713

Cogez, P., Graef, M., Huizing, B., Mahnkopf, R., Ishiuchi, H., Shindo, J., . . . Steff, I. (2011). *International Technology Roadmap for Semiconductors 2011 Edition - Executive Summary.* Washington D.C., USA: Semiconductor Industry Association.

Cooke , M., Phillips , S., Shah, D., Athey, D., Lakey, J., and Przyborski, S. (2008). Enhanced cell attachment using a novel cell culture surface presenting functional domains from extracellular matrix proteins. *Download PDF, 56*(2), 71–79. doi:10.1007/s10616-007-9119-7

Costa, K., Hucker, W., and Yin, F.-P. (2002). Buckling of actin stress fibers: A new wrinkle in the cytoskeletal tapestry. *Cell Motility and the Cytoskeleton, 52*(4), 266-274. doi:10.1002/cm.10056

Coursey, J., Schwab, D., Tsai, J., and Dragoset, R. (2015, Sept. 30). *Atomic Weights and Isotopic Compositions (Version 4.1).* Retrieved from The National Institute of Standards and Technology (NIST) : http://physics.nist.gov

Cousins, B., Doherty, P., Williams, R., Fink, J., and Garvey, M. (2004). The Effect of Silica Nanoparticulate Coatings on Cellular Response. *Journal of Materials Science: Materials in Medicine, 15*(4), 355-359.

Coussen, F., Choquet, D., Sheetz, M., and Erickson, H. (2002). Trimers of the fibronectin cell adhesion domain localize to actin filament bundles and undergo rearward translocation. *Journal of Cell Science, 115* (12), 2581-2590.

Coutinho , C., and Gupta, V. (2011). Chapter 30: Chemical Mechanical Polishing: Role of Polymeric Additives and Composite Particles in Slurries. In M. Kutz (Ed.), *Applied Plastics Engineering Handbook - Processing and Materials* (pp. 519-532). Oxford, UK: Elsevier Inc. Retrieved from http://app.knovel.com

Coutinho, C. A., Mudhivarthi, S., Kumar, A., and Gupta, V. (2008). Novel ceria–polymer microcomposites for chemical mechanical polishing. *Applied Surface Science, 255*(5, Part 2), 3090–3096. doi:10.1016/j.apsusc.2008.08.093

Cukierman, E., Pankov, R., and Yamada, K. (2002). Cell interactions with three-dimensional matrices. *Current Opinion in Cell Biology, 14*(5), 633-640. doi:10.1016/S0955-0674(02)00364-2

Cunningham, D., and You, Z. (2015). In vitro and in vivo model systems used in prostate cancer research. *Journal of Biological Methods, 2*(1), e17. doi:10.14440/jbm.2015.63

Curtis, A., and Wilkinson, C. (1997). Topographical control of cells. *Biomaterials, 18*(24), 1573-1583. doi:10.1016/S0142-9612(97)00144-0

Dalby, M. J., Gadegaard, N., Riehle, M. O., Wilkinson, C. D., and Curtis, A. (2004b). Investigating filopodia sensing using arrays of defined nano-pits down to 35 nm diameter in size. *The International Journal of Biochemistry and Cell Biology, 36*(10), 2005-2015. doi:10.1016/j.biocel.2004.03.001

Dalby, M. J., Riehle, M. O., Sutherland, D. S., Agheli, H., and Curtis, A. S. (2004a). Use of Nanotopography to Study Mechanotransduction in Fibroblasts – Methods and Perspectives. *European Journal of Cell Biology, 83*(4), 159-169. doi:10.1078/0171-9335-00369

Dalby, M. J., Riehle, M., Johnstone, H., Affrossman, S., and Curtis, A. (2002). In Vitro Reaction of Endothelial Cells to Polymer Demixed Nanotopography. *Biomaterials, 23*(14), 2945-2954. doi:10.1016/S0142-9612(01)00424-0

Dalby, M., Andar, A., Nag, A., Affrossman, S., Tare, R., McFarlane, S., and Oreffo, R. (2008). Genomic Expression of Mesenchymal Stem Cells to Altered Nanoscale Topographies. *5*(26), 1055-1065. doi:10.1098/rsif.2008.0016

Dalby, M., Riehle, M., Yarwood, S., Wilkinson, C., and Curtis, A. (2003). Nucleus Alignment and Cell Signaling in Fibroblasts: Response to a Micro-grooved Topography. *Experimental Cell Research, 284*(2), 272-280. doi:10.1016/S0014-4827(02)00053-8

Darling, E., Zauscher, S., Block, J., and Guilak, F. (2007). A Thin-Layer Model for Viscoelastic, Stress-Relaxation Testing of Cells Using Atomic Force Microscopy: Do Cell Properties Reflect Metastatic Potential? *Biophysical Journal, 92*(5), 1784-1791. doi:10.1529/biophysj.106.083097

de Oliveira Souza, M. C., da Silva Freire, M., and Castilho, L. d. (2005). Influence of culture conditions on Vero cell propagation on non-porous microcarriers. *Brazilian Archives of Biology and Technology, 48(spe)*, 71-77. doi:10.1590/S1516-89132005000400009

Dee , K., Puleo , D., and Bizio, R. (2002). Chapter 3: Protein-Surface Interactions. In K. C. Dee, D. A. Puleo, and R. Bizio, *An Introduction To Tissue-Biomaterial Interactions: Tissue-Biomaterial* (pp. 37-52). Hoboken, NJ: John Wiley and Sons, Inc. doi:10.1002/0471270598.ch3

Delivopoulos , E., Ouberai, M., Coffey, P., Swannd, M., Shakesheff , K., and Wellanda, M. (2015). Serum protein layers on parylene-C and silicon oxide: Effect on cell adhesion. *Colloids and Surfaces B: Biointerfaces, 126*, 169-177. doi:10.1016/j.colsurfb.2014.12.020

Derda, R., Musah, S., Orner, B., Klim, J., Li, L., and Kiesslin, L. (2010). High-Throughput Discovery of Synthetic Surfaces That Support Proliferation of Pluripotent Cells. *Journal of the American Chemical Society , 132*(4), 1289-1295. doi:10.1021/ja906089g

Doering, R., and Nishi, Y. (2007). *Handbook of Semiconductor Manufacturing Technology. Second Edition.* New York, NY: CRC Press, Talyor and Francis Group.

Doi, T., Marinescu, I. D., and Kurokawa, S. (2012). Chapter 2: Details of the Fabrication Process for Devices with a Silicon Crystal Substrate. In T. Doi, I. D. Marinescu, and S. Kurokawa, *Advances in CMP/Polishing Technologies for the Manufacturing of Electonic Devices* (pp. 3-13). Waltham, MA, USA: Elsevier Inc.

Dolatshahi-Pirouz, A., Jensen, T., Kraft, D. C., Foss, M., Kingshott, P., Hansen, J. L., . . . Besenbacher, F. (2010). Fibronectin Adsorption, Cell Adhesion, and Proliferation on Nanostructured Tantalum Surfaces. *ACS Nano, 4*(5), 2874–2882. doi:10.1021/nn9017872

Dong, Z., Kennedy, S., and Wu, Y. (2011). Electrospinning Materials for Energy-related Applications and Devices. *Journal of Power Sources, 196*(11), 4886-4904. doi:10.1016/j.jpowsour.2011.01.090

Du, J., Zhang, L., Yang, Y., Li, W., Chen, L., Ge, Y., . . . Gu, L. (2010). ATP depletion-induced actin rearrangement reduces cell adhesion via p38 MAPK-HSP27 signaling in renal proximal tubule cells. *Cellular Physiology and Biochemistry, 25*(4-5), 501-510. doi:10.1159/000303055

Edwards , J., Robson, R., and Campbell , G. (1987). A major difference between serum and fibronectin in the divalent cation requirement for adhesion and spreading of BHK21 cells. *Journal of Cell Science, 87*, 657-665.

Ehrlich, H., Berezukb, G., Fritsch, S., Aichingerc, G., Singer, J., Portsmouth, D., . . . Barrett, P. (2012). Clinical Development of a Vero Cell Culture-derived Seasonal Influenza Vaccine. *Vaccine, 30*(29), 4377-4386. doi:10.1016/j.vaccine.2011.11.114

Elhofy, A. (2014). *Serum and its applicability and use in cell culture.* Retrieved from Essential Pharmaceuticals: https://www.essentialpharma.com/

El-Kareh, B. (1995). *Fundamentals of Semiconductor Processing Technologies.* Dordrecht, The Netherlands: Kluwer Academic Publishers. doi:10.1007/978-1-4615-2209-6

Ellmerer, M., Schaupp, L., Brunner, G., Sendlhofer , G., Wutte, A., Wach, P., and Pieber, T. (2000). Measurement of interstitial albumin in human skeletal muscle and adipose tissue by open-flow microperfusion. *American Journal of Physiology-Endocrinology and Metabolism , 278*, E352-E356. doi:10.1152/ajpendo.2000.278.2.E352

Emsley, J. (2011). *Nature's Building Blocks: An A-Z Guide to the Elements, 2nd Edition.* New York: Oxford University Press.

Esch, T., Lemmon , V., and Banker, G. (1999). Local Presentation of Substrate Molecules Directs Axon Specification by Cultured Hippocampal Neurons. *Journal of Neuroscience, 19*(15), 6417-6426. doi:10.1523/JNEUROSCI.19-15-06417.1999

Eskin, S., Horbett, T., McIntire, L., Mitchell, R., Ratner, B., Schoen, F., and Yee, A. (2004). Chapter 3: Some Background Concepts. In B. D. Ratner, A. S. Hoffman, F. J. Schoen, and J. E. Lemons (Eds.), *Biomaterials Science. An Introduction to Materials in Medicine. 2nd Edition* (pp. 237-245). San Diego: Academic Press.

Extrand, C. (2016). Uncertainty in contact angle measurements from. *Journal of Adhesion Science and Technology, 30*(15), 1597-1601. doi:10.1080/01694243.2016.1142799

Fabrizius-Homan, D., and Cooper, S. (1991). Competitive adsorption of vitronectin with albumin, fibrinogen, and fibronectin on polymeric biomaterials. *Journal of Biomedical Materials Research, 25*, 953-971. doi:10.1002/jbm.820250804

Fabrizius-Homan, D., Cooper, S., and Mosher, D. (1992). The ex vivo effect of preadsorbed vitronectin on platelet activation. *Thrombosis and Haemostasis, 68*(2), 194-202. doi:10.1055/s-0038-1656348

Fan, Y., Cui, F., Chen, L., Zhai, Y., and Xu, Q. (2000). Improvement of neural cell adherence to silicon surface by hydroxyl ion implantation. *Surface and Coatings Technology, 131*(1-3), 355-359. doi:10.1016/S0257-8972(00)00812-4

Fang, C.-Y., Wu, C.-C., Fang, C.-L., Chen, W.-Y., and Chen, C.-L. (2017). Long-term growth comparison studies of FBS and FBS alternatives in six head and neck cell lines. *PLoS ONE, 12*(6), e0178960. doi:10.1371/journal.pone.0178960

Feeney, P. (2010). CMP for Metal-gate Integration in Advanced CMOS Transistors. *Solid State Technology*, Cover Article.

Felgueiras , H., Evans , M., and Migonney, V. (2015). Contribution of fibronectin and vitronectin to the adhesion and morphology of MC3T3-E1 osteoblastic cells to poly (NaSS) grafted Ti6Al4V. *Acta Biomaterialia, 25*, 225-233. doi:10.1016/j.actbio.2015.09.030

Ferrari, A., Cecchini , M., Serresi, M., Faraci, P., Pisignano, D., and Beltram, F. (2010). Neuronal polarity selection by topography-induced focal adhesion control. *Biomaterials, 31*(17), 4682-4694. doi:10.1016/j.biomaterials.2010.02.032

Filipponi , L., and Sutherland, D. (2013). *Nanotechnologies: Principles, Application, Implications and Hands-on Activities.* Luxembourg: European Commission: Directorate-General for Research and Innovation Industrial technologies (NMP). doi:10.2777/76945

Finlayson, B., Schnick, R. A., Cailteux, R. L., DeMong , L., Horton , W., and McClay , W. (2011). Assessment of Antimycin a Use in Fisheries and its Potential for Reregistration. *Fisheries, 27*(6), 10-18. doi:10.1577/1548-8446(2002)027<0010:AOAAUI>2.0.CO;2

Flemming, R., Murphy, C., Abrams, G., Goodman, S., and Nealey, P. (1999). Effects of synthetic micro- and nano-structured surfaces on cell behavior. *Biomaterials, 20*(6), 573-588. doi:10.1016/S0142-9612(98)00209-9

Francis, G. (2010). Albumin and mammalian cell culture: implications for biotechnology applications. *Cytotechnology, 62*, 1-16. doi:10.1007/s10616-010-9263-3

Fu, J., Wang, Y.-K., Yang, M. T., Desai, R. A., Yu, X., Liu, Z., and Chen, C. S. (2010). Mechanical Regulation of Cell Function with Geometrically Modulated Elastomeric Substrates. *Nature Methods, 7*(9), 733–736. doi:10.1038/nmeth.1487

Fujita, S., Ohshima, M., and Iwata, H. (2009). Time-lapse observation of cell alignment on nanogrooved patterns. *Journal of the Royal Society Interface, 6*(3), S269-S277. doi:10.1098/rsif.2008.0428.focus

Fukumoto, H., Hishimac, T., Hasegawa, H., Saeki, H., Kuroda , M., and Katanoa, H. (2016). Evaluation of Vero-cell-derived simian endogenous retrovirus infection in humans by detection of viral genome in clinicopathological samples and commercialized vaccines and by serology of Japanese general population. *Vaccine, 34*(24), 2700-2706. doi:10.1016/j.vaccine.2016.04.031

Fury, M. (2009). Milestones in a Quarter Century of CMP – Plenary. In G. Banerjee, Y. Obeng, V. Desai, and K. Sundaram (Ed.), *215th ECS Meeting. 19 (7),* pp. 3-11. San Francisco, CA: The Electrochemical Society. doi:10.1149/1.3123769

Gao , L., and McCarthy, T. (2009). Wetting 101°. *Langmuir, 25*(24), 14105–14115. doi:10.1021/la902206c

García-Parra, P., Cavaliere, F., Maroto, M., Bilbao, L., Obieta, I., de Munain, A., . . . Izeta, A. (2012). Modeling neural differentiation on micropatterned substrates coated with neural matrix components. *Frontiers in Cellular Neuroscience, 6*(10), Article 10, 1-12. doi:10.3389/fncel.2012.00010

Geiger, B., Bershadsky, A., Pankov, R., and Yamada, K. (2001). Transmembrane crosstalk between the extracellular matrix-cytoskeleton crosstalk. *Molecular Cell Biology, 2*(11), 793-805. doi:10.1038/35099066

Giese, A., Rief, M. D., Loo, M. A., and Berens, M. E. (1994). Determinants of Human Astrocytoma Migration. *cancer Research, 54*(14), 3897-3904.

Gigout, A., Jolicoeur, M., and Buschmann, M. (2005). Low calcium levels in serum-free media maintain chondrocyte phenotype in monolayer culture and reduce chondrocyte aggregation in suspension culture. *Osteoarthritis and Cartilage, 13,* 1012-1024. doi:10.1016/j.joca.2005.06.003

Gleiter, H. (1995). Nanostructured materials: state of the art and perspectives. *Nanostructured Materials, 6*(1-4), 3-14. doi:10.1016/0965-9773(95)00025-9

Godfrey, M. (2009). Chapter 22 - Extracellular Matrix. In P. Barnes, J. Drazen, S. Rennard, and N. Thomson (Eds.), *Asthma and COPD. Basic Mechanisms and Clinical Management. 2nd Edition* (pp. 265-274). Cambridge: Academic Press. doi:10.1016/B978-0-12-374001-4.00022-5

Gong, N., Chen, S., Jin, S., Zhang, J., Wang, P., and Liang, X.-J. (2015). Effects of the physicochemical properties of gold nanostructures on cellular internalization. *Regenerative Biomaterials,* 273-280. doi:10.1093/rb/rbv024

Gonzalez-Perez, F., Udina, E., and Navarro, X. (2013). Extracellular Matrix Components in Peripheral Nerve Regeneration. *International Review of Neurobiology, 108,* 257-275. doi:10.1016/B978-0-12-410499-0.00010-1

Grass, G., Rensing, C., and Solioz, M. (2011). Metallic Copper as an Antimicrobial Surface. *Applied and Environmental Microbiology, 77*(5), 1541–1547. doi:10.1128/AEM.02766-10

Greene, S., and Pohanish, R. (Eds.). (2005). *Sittig's Handbook of Pesticides and Agricultural Chemicals.* Norwich, NY: William Andrew Publishing.

Groth, T., and Altankov, G. (1996). Fibroblast spreading and proliferation on hydrophilic and hydrophobic surfaces is related to tyrosine phosphorylation in focal contacts. *Journal of Biomaterials Science, Polymer Edition, 7*(3), 297-305. doi:10.1163/156856295X00337

Grzesik, W. (1997). Integrins and bone--cell adhesion and beyond. *Archivum Immunologiae et Therapiae Experimentalis, 45*(4), 271–275.

Grzesik, W., and Robey, p. (1994). Bone matrix RGD glycoproteins: immunolocalization and interaction with human primary osteoblastic bone cells in vitro. *Journal of Bone and Mineral Research, 9*(4), 487-496. doi:10.1002/jbmr.5650090408

Guclu , C., Tamma, V., Wickramasinghe, H., and Capolino, F. (2015). Photoinduced magnetic force between nanostructures. *Physical Review B, 92*(23), 235111 (8pp). doi:10.1103/PhysRevB.92.235111

Guida , L., Oliva , A., Assunta Basile, M., Giordano, M., Nastri , L., and Annunziata, M. (2013). Human Gingival Fibroblast Functions are Stimulated by Oxidized Nano-structured Titanium Surfaces. *Journal of Dentistry , 41*(10), 900-907. doi:10.1016/j.jdent.2013.07.009

Guo , T., Ringel , J., Lim , C., Bracaglia , L., Noshin , M., Baker , H., . . . Fisher, J. (2018). Three-dimensional extrusion printing induces polymer molecule alignment and cell organization within engineered cartilage. *Journal of Biomedical Materials Research Part A, 106*(8), 2190-2199. doi:10.1002/jbm.a.36426

Gupta, T. (1979). Aluminum alloy as an interconnecting material in the fabrication of integrated circuits. *Microelectronics Reliability, 19*(4), 337-343. doi:10.1016/0026-2714(79)90150-1

Haase, K., Macadangdang, J., Edrington, C., Cuerrier, C., Hadjiantoniou, S., Harden, J., . . . Pelling, A. (2016). Extracellular Forces Cause the Nucleus to Deform in a Highly Controlled Anisotropic Manner. *Scientific Reports, 6:21300*, 1-11. doi:10.1038/srep21300

Hajj, G., Lopes, M., Mercadante, A., Veiga, S., da Silveira, R., Santos, T., . . . Martins, V. (2007). Cellular prion protein interaction with vitronectin supports axonal growth and is compensated by integrins. *Journal of Cell Science, 120*, 1915-1926. doi:10.1242/jcs.03459

Hakkinen, K., Harunaga, J., Doyle, A., and Yamada, K. (2011). Direct Comparisons of the Morphology, Migration, Cell Adhesions, and Actin Cytoskeleton of Fibroblasts in Four Different Three-

Dimensional Extracellular Matrices. *Tissue Engineering. Part A, 17*(5-6), 713-724. doi:10.1089/ten.tea.2010.0273

Hallab, N., Bundy, K., O'Connor, K., and Jacobs, J. (2001). Evaluation of Metallic and Polymeric Biomaterial Surface Energy and Surface Roughness Characteristics for Directed Cell Adhesion. *Tissue Engineering, 7*(1), 55-71. doi:10.1089/107632700300003297

Hartrianti, P., Ling, L., Mei-Ming, L., Ow, K., Samsonraj, R., Sow, W., . . . Ng, K. (2015). Modulating Mesenchymal Stem Cell Behavior Using Human Hair Keratin-Coated Surfaces. *Stem Cells International, 2015*(Article ID 752424), 9 pages. doi:10.1155/2015/752424

Hashimoto , M., and Imazato, S. (2015). Cytotoxic and genotoxic characterization of aluminum and silicon oxide nanoparticles in macrophages. *Dental Materials , 31*(5), 556-564. doi:10.1016/j.dental.2015.02.009

Hasirci, V., and Kenar, H. (2006). Novel Surface Patterning Approaches for Tissue Engineering and their Effect on Cell Behavior. *Nanomedicine, 1*(1), 73-90. doi:10.2217/17435889.1.1.73

Haugsten, E., Wiedlocha, A., Olsnes, S., and Wesche, J. (2010). Roles of Fibroblast Growth Factor Receptors in Carcinogenesis. *Molecular Cancer Research, 8*(11), 1439-1452. doi:10.1158/1541-7786.MCR-10-0168

Hayman , E., Pierschbacher , M., Suzuki, S., and Ruoslahti, E. (1985). Vitronectin--a major cell attachment-promoting protein in fetal bovine serum. *160*(2), 245-258.

Haynes, W., Lide, D., and Bruno, T. (Eds.). (2015). *CRC Handbook of Chemistry and Physics, 96th Edition.* Boca Raton, FL: CRC Press and Taylor and Francis Group .

Hlady, V., Buijs, J., and Jennisse, H. P. (1999). Methods for Studying Protein Adsorption. *Methods Enzymol, 309*, 402-429. doi:10.1016/S0076-6879(99)09028-X

Hobertt, T. (2004). The role of adsorbed protein in tissue response to biomaterials. In F. Schoen , and J. Lemons (Eds.), *Biomaterials Science: An Introduction to Materials in Medicine* (pp. 237-246). San Diego: Elsevier Academic Press.

Hong, S., Ergezen, E., Lec, R., and Barbee, K. (2006). Real-time analysis of cell-surface adhesive interactions using thickness shear mode resonator. *Biomaterials, 27*(34), 5813-5820.

Hook, A. (2014). Chapter 4: Polymer Microarrays for High Throughput Biomaterials Discovery . In E. Palmer, *Cell-Based Microarrays* (pp. 53-74). New York: Springer.

Horbett, T. A. (2004). The role of adsorbed protein in tissue response to biomaterials. In F. Schoen , and J. Lemons (Eds.), *Biomaterials Science: An Introduction to Materials in Medicine* (pp. 237-246). San Diego: Elsevier Academic Press.

Horbett, T., and Schway , M. (1988). Correlations between mouse 3T3 cell spreading and serum fibronectin adsorption on glass and hydroxyethylmethacrylate-ethylmethacrylate copolymers. *Journal of Biomedical Materials Research, 22*(9), 763-793.

Hu, J., Hardy, C., Chen, C.-M., Yang, S., Voloshin, A., and Liu, Y. (2014). Enhanced Cell Adhesion and Alignment on Micro-Wavy Patterned Surfaces. *PLOS ONE, 9*(8), e104502. doi:10.1371/journal.pone.0104502

Hu, W., Crouch, A. S., Miller, D., Aryal, M., and Luebke, K. J. (2010). Inhibited Cell Spreading on Polystyrene Nanopillars Fabricated by Nanoimprinting and in Situ Elongation. *Nanotechnology, 21*(38), 385301 (6pp). doi:10.1088/0957-4484/21/38/385301

Huang, H.-H., Ho, C.-T., Lee, T.-H., Lee, T.-L., Liao, K.-K., and Chen, F.-L. (2004). Effect of surface roughness of ground titanium on initial cell adhesion. *Biomolecular Engineering, 21*(3-5), 93-97. doi:10.1016/j.bioeng.2004.05.001

Huang, Q., Antensteiner, M., Liu, X. Y., Lind, C., and Vogler, E. A. (2016). Graphical analysis of mammalian cell adhesion in vitro. *Vogler, 148*, 211-219. doi:10.1016/j.colsurfb.2016.07.022

Huang, Q., Lin, L., Yang, Y., Hu, R., Vogler, E. A., and Lin, C. (2012). Role of trapped air in the formation of cell-and-protein micropatterns on superhydrophobic/superhydrophilic microtemplated surfaces. *Biomaterials, 33*(33), 8213-8820. doi:10.1016/j.biomaterials.2012.08.017

Hudalla, G., and Murphy, W. (2011). Chemically well-defined self-assembled monolayers for cell culture: toward mimicking the natural ECM. *Soft Matter, 7*(20), 9661-9571. doi:10.1039/C1SM05596H

Huggins, D., Marsh, M., and Payne, M. (2011). Thermodynamic Properties of Water Molecules at a Protein–Protein Interaction Surface. *Journal of Chemical Theory and Computation , 7*(11), 3514–3522. doi:10.1021/ct200465z

Hughes , R., Pena , S., Clark , J., and Dourmashkin , R. (1979). Molecular requirements for adhesion and spreading of hamster fibroblasts. *Experimental Cell Research, 121*(2), 307-314.

Hussainova , I. (2010). MTX9100 Nanomaterials. Lecture 5: Fundamentals of Nanomaterials [PowerPoint Slides]. Tallinn, Estonia. Retrieved from https://www.ttu.ee

Inbe, T. (2004). *US Patent No. US6705922 B1: Method and apparatus for polishing a semiconductor substrate wafer*.

Iorio, V., Troughton, L., and Hamill, K. (2015). Laminins: Roles and Utility in Wound Repair. *Advances in Wound Care, 4*(4), 250-263. doi:10.1089/wound.2014.0533

ITIA. (2011). *Tungsten Properties*. Retrieved from International Tungsten Industry Association : http://www.itia.info/tu

Jager, M., Zilkens, C., Zanger, K., and Krauspe, R. (2007). Significance of Nano- andMicrotopography for Cell-Surface Interactions in Orthopaedic Implants. *Journal of Biomedicine and Biotechnology, 2007*, Article ID 69036, 19 pages. doi:10.1155/2007/69036

Jahed, Z., Molladavoodi, S., Seo, B., Gorbet, M., Tsui, T., and Mofrad, M. (2014). Cell Responses to Metallic Nanostructure Arrays with Complex Geometries. *Biomaterials, 35*(34), 9363-9371. doi:10.1016/j.biomaterials.2014.07.022

Jefferson, J., and Shankland, S. (2008). Chapter 21 - Molecular Mechanisms of Proteinuria. In D. Mount , and M. Pollak (Eds.), *Molecular and Genetic Basis of Renal Disease* (pp. 373-389). Philadelphia: Saunders Elsevier. doi:10.1016/B978-1-4160-0252-9.50025-2

Jin, Y.-H., Lee, S.-H., Shim, H.-W., Ko, K., and Kim, D.-W. (2010). Tailoring High-surface-area Nanocrystalline TiO2 Polymorphs for High-power Li-Ion Battery Electrodes. *Electrochimica Acta, 55*(24), 7315-7321. doi:10.1016/j.electacta.2010.07.027

Jing, L., YuHong, L., YuanJing, D., DaChuan, Y., XinChun, L., and JianBin, L. (2013). Achievement of a near-perfect smooth silicon surface. *Science China Technological Sciences, 56*(1), 2847-2853. doi:10.1007/s11431-013-5364-5

Johnson, D., Ang, C., Bednar, A., and Inouye, L. (2010). Tungsten effects on phosphate-dependent biochemical pathways are species and liver cell line dependent. *Toxicological Sciences, 116*(2), 523-532. doi:10.1093/toxsci/kfq124

Joo, S., Kim, J., Lee, E., Hong, N., Sun, W., and Nam, Y. (2015). Effects of ECM protein micropatterns on the migration and differentiation of adult neural stem cells. *Scientific Reports, 5*(13043), 12 pages. doi:10.1038/srep13043

Kalghatgi, S., Spina, C., Costello, J., Liesa, M., Morones-Ramirez, J., Slomovic, S., . . . Collins, J. (2013). Bactericidal Antibiotics Induce Mitochondrial Dysfunction and Oxidative Damage in Mammalian Cells. *Science Translational Medicine, 5*(192), 192ra85. doi:10.1126/scitranslmed.3006055

Kao, P., Parhi, P., Krishnan, A., Noh, H., Haider, W., Tadigadapa, S., . . . Vogler, E. (2010). Volumetric interpretation of protein adsorption: Interfacial packing of protein adsorbed to hydrophobic surfaces from surface-saturating solution concentrations. *Biomaterials, 32*(4), 969-978. doi:10.1016/j.biomaterials.2010.09.075.

Karlsson, L. (2009). *Differentiation of Human Dermal Fibroblasts: A New Tool in Vascular Tissue Engineering. Ph.D. Thesis.* Linköping, Sweden: Linköping University.

Kasemo, B. (2002). Biological Surface Science. *Current Opinion in Solid State and Materials Science, 3*(5), 451-459. doi:10.1016/S1359-0286(98)80006-5

Kell , D., and Oliver, S. (2003). Here is the evidence, now what is the hypothesis? The complementary roles of inductive and hypothesis-driven science in the post-genomic era. *BioEssays, 26*(1), 99-105. doi:10.1002/bies.10385

Kern, T., Yang, Y., Glover, R., and Ong, J. L. (2005). Effect of Heat-Treated Titanium Surfaces on Protein Adsorption and Osteoblast Precursor Cell Initial Attachment. *Implant Dentistry, 14*(1), 70-76. doi:10.1097/01.id.0000154795.93155.ee

Keswani, M., and Han, Z. (2015). Chapter 4 - Post-CMP Cleaning. In D. i. Methods, R. Kohli, and K. Mittal (Eds.). Oxford: Elsevier. doi:10.1016/B978-0-323-29961-9.00004-1

Khain, E., Katakowski, M., Hopkins, S., Szalad, A., Zheng, X., Jiang, F., and Chopp, M. (2011). Collective behavior of brain tumor cells: The role of hypoxia. *Physical Review E, 83*(3), 031920 (6). doi:10.1103/PhysRevE.83.031920

Khalili , A., and Ahmad, M. (2015). A Review of Cell Adhesion Studies for Biomedical and Biological Applications. *International Journal of Molecular Sciences, 16*(8), 18149–18184. doi:10.3390/ijms160818149

Khan, S., Auner, G., and Newaz, G. (2005). Influence of nanoscale surface roughness on neural cell attachment on silicon. *Nanomedicine: Nanotechnology, Biology, and Medicine, 1*(2), 125-129. doi:10.1016/j.nano.2005.03.007

Khanna, V. K. (2016). Chapter 24: Bottom-up Nanofabrication. In V. K. Khanna, *Nanoelectronics, Integrated* (pp. 397-417). New Delhi: Springer. doi:10.1007/978-81-322-3625-2_24

Kiejna, A. (2005). Surface atomic structure and energetics of tantalum. *Surface Science, 598*(1-3), 276-284. doi:10.1016/j.susc.2005.09.029

Kim , J.-Y., Jang, D., and Greer, J. (2010). Tensile and compressive behavior of tungsten, molybdenum, tantalum and niobium at the nanoscale. *Acta Materialia, 58*(7), 2355-2363. doi:10.1016/j.actamat.2009.12.022

Kim , Y.-L., Im , Y.-J., Lee, Y.-K., Ha , N.-C., Bae, Y.-S., Lim , S.-M., . . . Im, D.-S. (2006). Albumin functions as an inhibitor of T cell adhesion in vitro. *Biochemical and Biophysical Research Communications, 351*(4), 953-957. doi:10.1016/j.bbrc.2006.10.143

Kim, H. (2013). Fabrication of Three-Dimensional Nanostructures for Thermal Study. Master's Thesis. Urbana, Illinois, USA: University of Illinois.

King , M., and Radicchi-Mastroianni, M. (2002). Antimycin A-induced apoptosis of HL-60 cells. *Cytometry, 49*(3), 106-112. doi:10.1002/cyto.10156

Ko, K., Arora, P., Bhide, V., Chen, A., and McCulloch, C. (2001). Cell-cell adhesion in human fibroblasts requires calcium signaling. *Journal of Cell Science, 114*(6), 1155-1167. Retrieved from http://jcs.biologists.org/content/joces/114/6/1155.full.pdf

Koch , T., Münster, S., Bonakdar, N., Butler, J., and Fabry, B. (2012). 3D Traction Forces in Cancer Cell Invasion. *PLoS ONE, 7*(3), e33476. doi:10.1371/journal.pone.0033476

Koch, C. C. (2009). Nanostructured Materials: An Overview. In M. Zehetbauer, and Y. Zhu (Eds.), *Bulk Nanostructured Materials* (pp. 3-20). Weinheim, Germany: WILEY-VCH Verlag GmbH and Co. KGaA.

Kolind, K., Dolatshahi-Pirouz, A., Lovmand, J., Pedersen, F., Foss, M., and Besenbacher, F. (2010). A Combinatorial Screening of Human Fibroblast Responses on Micro-structured. *Biomaterials, 31*(35), 9182-9191. doi:10.1016/j.biomaterials.2010.08.048

Koubassova, N., and Tsaturyan, A. (2011). Molecular mechanism of actin-myosin motor in muscle. *Biochemistry Moscow, 76*(13), 1484–1506. doi:10.1134/S0006297911130086

Krishnan, A., Cha, P., Liu, Y.-H., Allara, D., and Vogler, E. (2006). Interfacial energetics of blood plasma and serum adsorption to a hydrophobic self-assembled monolayer surface. *Biomaterials, 27*(17), 3187-3194. doi:10.1016/j.biomaterials.2005.12.032

Krishnan, A., Sturgeon, J., Siedleck, C., and Vogler, E. (2004). Scaled interfacial activity of proteins at the liquid-vapor interface. *Journal of Biomedical Materials Research Part A, 68*(3), 544-557. doi:10.1002/jbm.a.20104

Krishnan, M., Nalaskowski, J., and Cook, L. (2010). Chemical Mechanical Planarization: Slurry Chemistry, Materials, and Mechanisms. *Chemical Reviews, 110*(1), 178–204. doi:10.1021/cr900170z

Kroshian, V., Sheridan, A., and Lieberthal, W. (1994). Functional and cytoskeletal changes induced by sublethal injury in proximal tubular epithelial cells. *American Physiological Society, 266*(1), F21-F30. doi:10.1152/ajprenal.1994.266.1.F21

Krotz, D. (2014, March 04). *Scientists show which surfaces attract clingy Staph bacteria*. Retrieved from Lawrence Berkeley National Laboratory: http://vcresearch.berkeley.edu/

Kuo, W., Chueh, D.-Y., and Chen, P. (2014). Investigation of size-dependent cell adhesion on nanostructured interfaces. *Journal of Nanobiotechnology, 12*(54), 10. doi:10.1186/s12951-014-0054-4

Kwon, K., Choi, S., Lee, S., Kim, B., Lee, S., Park, M., . . . Suh, K. (2007). Label-free, microfluidic separation and enrichment of human breast cancer cells by adhesion difference. *Lab on a Chip, 7*(11), 1461-1468. doi:10.1039/b710054j

Kyriakides, T. (2015). Chapter 5 – Molecular Events at Tissue–Biomaterial Interface. In S. Badylak (Ed.), *Host Response to Biomaterials* (pp. 81-116). Tokyo: Academic Press. doi:10.1016/B978-0-12-800196-7.00005-0

Lacouture , M., Schaffer , J., and Klickstein, L. (2009). A Comparison of Type I Collagen, Fibronectin, and Vitronectin in Supporting Adhesion of Mechanically Strained Osteoblasts. *Journal of Bone and Mineral Research, 17*(3), 481-492. doi:10.1359/jbmr.2002.17.3.481

Lai, J.-Y. (2001). Mechanics, Mechanisms and Modeling of the Chemical Mechanical Polishing Process (Ph.D. Thesis). Cambridge, MA: Massachusetts Institute of Technology (MIT).

Lamers, E., van Horssen, R., Riet, J., van Delf, F., Luttge, R., Walboomers, X., and Jansen, J. (2010). The influence of nanoscale topographical cues on initial osteoblast morphology and migration. *e-Cells and Materials Journal , 20*, 329-343.

Lammerding, J. (2011). Mechanics of the Nucleus. *Comprehensive Physiology, 1*(2), 783-807. doi:10.1002/cphy.c100038

Larios, J. (2004). CMP Cleaning. In M. Oliver (Ed.), *Chemical-Mechanical Planarization of Semiconductor Materials* (pp. 251-281). Berlin: Springer . doi:10.1007/978-3-662-06234-0_8

Lassner, E., and Schubert, W.-D. (1999). *Tungsten: Properties, Chemistry, Technology of the Element, Alloys, and Chemical Compounds.* New York: Kluwer Academic / Plenum.

LeBaron, R., and Athanasiou, K. (2000). Ex vivo synthesis of articular cartilage. *Biomaterials, 21*(24), 2575-2587. doi:10.1016/S0142-9612(00)00125-3

Lee, D., Lee, H., and Jeong, H. (2016). Slurry Components in Metal Chemical Mechanical Planarization (CMP) Process: A Review. *International Journal of Precision Engineering and Manufacturing, 17*(12), 1751-1762. doi:10.1007/s12541-016-0201-y

Lee, T., Lee, I., Choi, B., and Park, Y. (2009). *USA Patent No. US 20090001340 A1*.

Lenhert, S., Meier, M.-B., Meyer, U., Chi, L., and Wiesmann, H. (2005). Osteoblast alignment, elongation and migration on grooved polystyrene surfaces patterned by Langmuir–Blodgett lithography. *Biomaterials, 26*(5), 563-570. doi:10.1016/j.biomaterials.2004.02.068

Letourneau, P. (2008). Axonal Pathfinding: Extracellular Matrix Role. In L. Squire (Ed.), *Encyclopedia of Neuroscience* (pp. 1139-1145). Oxford: Academic Press. doi:10.1016/B978-0-12-809324-5.02630-4

Levenberg, S., Huang, N., Lavik, E., Rogers, A., Itskovitz-Eldor, J., and Langer, R. (2003). Differentiation of Human Embryonic Stem Cells on Three-dimensional Polymer Scaffolds. *PROC National Academy of Science of the United States of America, 100*(22), 12741–12746. doi:10.1073/pnas.1735463100

Li, P., Wang, D., Li, H., Yu, Z., Chen, X., and Fang, J. (2014). Identification of nucleolus-localized PTEN and its function in regulating ribosome biogenesis. *Molecular biology Reports, 41*(10), 6383–6390. doi:10.1007/s11033-014-3518-6

Li, Y. (2007). *Microelectronic Applications of Chemical Mechanical Planarization.* Hoboken, New Jersey, USA: John Wiley and Sons, Inc.

Li, Y., Qian, F., Xiang, J., and Liebe, C. (2006). Nanowire electronic and optoelectronic devices. *Materials Today, 9*(10).

Lim, J. L. (2004). Systematic variation in osteoblast adhesion and phenotype with substratum surface characteristics. *Journal of Biomedical Materials Research Part A, 68A*(3), 504–512. doi:10.1002/jbm.a.20087

Lim, J.-H., Park , J.-H., and Park, J.-G. (2013). Effect of iron(III) nitrate concentration on tungsten chemical-mechanical-planarization performance. *Applied Surface Science, 282*(1), 512-517. doi:10.1016/j.apsusc.2013.06.003

Lim, G., Lee, J.-H., Son, J.-W., Lee, H.-W., and Kim, J. (2006). Oxidation Behavior of Tungsten in H2O2- and Fe(NO3)3-Base Aqueous Slurries. *Journal of The Electrochemical Society, 135*(5), B169-B172.

Lin, C.-Y., Li, L.-T., and Su, W.-T. (2014). Three-dimensional chitosan scaffolds influence the extracellular matrix expression in Schwann cells. *Materials Science and Engineering: C, 42*, 474-478. doi:10.1016/j.msec.2014.05.063

Lin, J.-H., Chang, H.-Y., Kao, W.-L., Lin, K.-Y., Liao, H.-Y., You, Y.-W., . . . Shyue, J.-J. (2014a). Effect of Surface Potential on Extracellular Matrix Protein Adsorption. *Longmuir, 30*(34), 10328-10335. doi:10.1021/la5020362

Lin, L., Wang, H., Ni, M., Rui, Y., Cheng, T.-Y., Cheng, C.-K., . . . Lin, C. (2014). Enhanced osteointegration of medical titanium implant with surface modifications in micro/nanoscale structures. *Journal of Orthopaedic Translation, 2*(1), 35-42. doi:10.1016/j.jot.2013.08.001

Lisdero, C., Carreras, M., Meulemans, A., Melani, M., Aubier, M., Boczkowski, J., and Poderoso, J. (2004). The mitochondrial interplay of ubiquinol and nitric oxide in endotoxemia. *Methods in Enzymology, 382*, 67-81. doi:10.1016/S0076-6879(04)82004-4

Liu, X., Lim, J., Donahue, H., Dhurjati, R., Mastro, A., and Vogler, E. (2007). Influence of substratum surface chemistry/energy and topography on the human fetal osteoblastic cell line hFOB 1.19: Phenotypic and genotypic responses observed in vitro. *Biomaterials, 28*(31), 4535-4550. doi:j.biomaterials.2007.06.016

Liu, Y., Lin, I.-K., and Zhang, X. (2008). Mechanical properties of sputtered silicon oxynitride films by nanoindentation. *Materials Science and Engineering: A, 489*(1-2), 294-301. doi:10.1016/j.msea.2008.01.063

Llobet, L., Montoya, J., López-Gallardo, E., and Ruiz-Pesini, E. (2015). Side Effects of Culture Media Antibiotics on Cell Differentiation. *Tissue Engineering Part C: Methods, 21*(11), 1143-1147. doi:10.1089/ten.tec.2015.0062

Loesberg, W., Riet, J., van Delft, F., Schön, P., Figdor, C., Speller, S., . . . Jans, J. (2007). The threshold at which substrate nanogroove dimensions may influence fibroblast alignment and adhesion. *Biomaterials, 28*(27), 3944-3951. doi:10.1016/j.biomaterials.2007.05.030

Loesberg, W., Walboomers, X., van Loon, J., and Jansen, J. (2005). The effect of combined cyclic mechanical stretching and microgrooved surface topography on the behavior of fibroblasts. *Journal of Biomedical Materials Research Part A, 75A*(3), 723-732. doi:10.1002/jbm.a.30480

Lord, M., Foss, M., and Besenbacher, F. (2010). Influence of Nanoscale Surface Topography on Protein Adsorption and Cellular Response. *NanoToday, 5*(1), 66-78. doi:10.1016/j.nantod.2010.01.001

Lu, J., Su, T., and Penfold, J. (1999). Adsorption of Serum Albumins at the Air/Water Interface. *Langmuir, 15*(20), 6975–6983. doi:10.1021/la990131h

Lu, X., and Leng, Y. (2003). Quantitative analysis of osteoblast behavior on microgrooved hydroxyapatite and titanium substrata. *Journal of Biomedical Materials Research Part A, 66A*(3), 677-687. doi:10.1002/jbm.a.10022

Lu, X., and Leng, Y. (2008). Comparison of the Osteoblast and Myoblast Behavior on Hydroxyapatite Microgrooves. *Journal of Biomedical Materials Research Part B: Applied Biomaterials, 90B*(1), 438-445. doi:10.1002/jbm.b.31304

Ludwig, F., Pacetti, S., Hossainy, S., and Davalian, D. (2011). *United States Patent No. US 8,048,448 B2* .

Lutanie, E., Voegel, J., Schaaf, P., Freund, M., Cazenave, J., and Schmitt, A. (1992). Competitive adsorption of human immunoglobulin G and albumin: Consequences for structure and reactivity of the adsorbed layer. *Proceedings of the National Academy of Sciences of the United States of America, 89*(20), 9890-9894.

Luzhansky, I., Schwartz, A., Cohen, J., MacMunn, J., Barney, L., Jansen, L., and Peyton, S. (2018). Anomalously diffusing and persistently migrating cells in 2D and 3D culture environments. *APL Bioengineering, 2*, 026112. doi:10.1063/1.5019196

Lv, H., Huang , S., Mercadé-Prieto, R., Wu, X., and Chen, X. (2015). *Colloids and Surfaces B: Biointerfaces, 129*(47), 154–160. doi:10.1016/j.colsurfb.2015.03.042

Lv, L., Liu, Y., Zhang, P., Zhang, X., Liu, J., Chen, T., . . . Zhou, Y. (2015). The nanoscale geometry of TiO2 nanotubes influences the osteogenic differentiation of human adipose-derived stem cells by modulating H3K4 trimethylation. *Biomaterials, 39*, 193-205. doi:10.1016/j.biomaterials.2014.11.002

Lv, L., Liu, Y., Zhang, P., Zhang, X., Liu, J., Chen, T., . . . Zhou, Y. (2015b). The nanoscale geometry of TiO2 nanotubes influences the osteogenic differentiation of human adipose-derived stem cells by modulating H3K4 trimethylation. *Biomaterials, 39*, 193-205. doi:10.1016/j.biomaterials.2014.11.002

Lymberis, A. (2010). Micro-nano-biosystems: An overview of European research. *Minimally Invasive Therapy and Allied Technologies, 19*(3), 136-143. doi:10.3109/13645706.2010.481392

Ma, Y., Iyer, R., de Castro Brás, L., Toba, H., Yabluchanskiy, A., Deleon-Pennell, K., . . . Lindsey, M. (2015). Chapter 4 - Cross Talk Between Inflammation and Extracellular Matrix Following Myocardial Infarction. In *Inflammation in Heart Failure* (pp. 67-79). Cambridge: Academic Press. doi:10.1016/B978-0-12-800039-7.00004-9

Mahesparan, R., Tysnes, B. B., Edvardsen, K., Haugeland, H. K., Garcia Cabrera, I., Lund-Johans, M., . . . Bjerkvig, R. (1997). Role of high molecular weight extracellular matrix proteins in glioma cell migration. *Neuropathology and Applied Neurobiology, 23*(2), 102-112. doi:j.1365-2990.1997.tb01192.x

Mann, J., Lam, R., Weng, S., Sun, Y., and Fu, J. (2012). A Silicone-Based Stretchable Micropost Array Membrane for Monitoring Live-Cell Subcellular Cytoskeletal Response. *Lab on a Chip, 12*(4), 731-740. doi:10.1039/c2lc20896b

Marks, P., Hendey, B., and Maxfield, F. (1991). Attachment to Fibronectin or Vitronectin Makes Human Neutrophil Migration Sensitive to Alterations in Cytosolic Free Calcium Concentration. *The Journal of Cell Biology, 112*(1), 149-158.

Martin, J., Schwartz, Z., Hummert, T., Schraub, D., Simpson, J., Lankford Jr., J., . . . Boyan, B. (1995). Effect of titanium surface roughness on proliferation, differentiation, and protein synthesis of

human osteoblast-like cells (MG63). *Journal of Biomedical Materials Research, 29*(3), 389-401. doi:10.1002/jbm.820290314

Martínez, E., Engel, E., Planell, J., and Samitier, J. (2009). Effects of Artificial Micro- and Nano-structured Surfaces on Cell Behaviour. *Annals of Anatomy, 191*(1), 126-135. doi:10.1016/j.aanat.2008.05.006

Martini, S., Bonechi, C., Foletti, A., and Rossi, C. (2013). Water-Protein Interactions: The Secret of Protein Dynamics. *The Scientific World Journal, 2013*(Article ID 138916), 6. doi:10.1155/2013/138916

Martino , S., D'Angelo , F., Armentano , I., Kenny , J., and Orlacchio, A. (2012). Stem cell-biomaterial interactions for regenerative medicine. *Biotechnology Advances, 30*(1), 338-351. doi:j.biotechadv.2011.06.015

Matsushita, T., Kawakubo, Y., Sawano, M., and Funatsu, K. (2000). Vitronectin enhances adhesion force and tPA production of weakly adherent 293 cells exposed to a shear stress. *Cytotechnology, 32*(3), 181-190. doi:10.1023/A:1008140632747

Matsuzaka, N., Nakayama, M., Takahashi, H., Yamato, M., Kikuchi, A., and Okano, T. (2013). terminal-Functionality Effect of Poly(N-Isopropylacrylamide) Brush Surfaces on Temperature-Controlled Cell Adhesion/Detachment. *Biomacromolecules, 14*(9), 3164-3171. doi:10.1021/bm400788p

McConnell, D. R., and Hurst, A. M. (2014a). *United States Patent No. 8,858,819.*

McConnell, D. R., and Hurst, A. M. (2014b). *United States Patent No. 8,790,521 B2.*

McNamara, L. E., McMurray, R. J., Biggs, M. J., Kantawong, F., Oreffo, R. O., and Dalby, M. J. (2010). Nanotopographical Control of Stem Cell Differentiation. *Journal of Tissue Engineering, 1*(1), 120623 (13pp). doi:10.4061/2010/120623

Mejillano, M., Kojima, S.-i., Applewhite, D., Gertler, F., Svitkina, T., and Borisy, G. (2004). Lamellipodial Versus Filopodial Mode of the Actin Nanomachinery: Pivotal Role of the Filament Barbed End. *Cell, 118*(3), 363-373. doi:10.1016/j.cell.2004.07.019

Merten, O.-W. (2015). Advances in cell culture: anchorage dependence. *Philosophical Transactions of the Royal Society B Biological Sciences*, 1661:20140040. doi:10.1098/rstb.2014.0040

Meyle , J., Gültig , K., and Nisch , W. (1995). Variation in contact guidance by human cells on a microstructured surface. *Journal of Biomedical Materials Research, 29*(1), 81-88. doi:10.1002/jbm.820290112

Michaelis, S., Robelek , R., and Weg, J. (2011). Studying Cell–Surface Interactions In Vitro: A Survey of Experimental Approaches and Techniques. In C. Kasper, F. Witte , and R. Pörtner (Eds.),

Advances in Biochemical Engineering/Biotechnology. Tissue Engineering III: Cell - Surface Interactions for Tissue Culture (Vol. 126, pp. 33-66). Berlin Heidelberg: Springer-Verlag. doi:10.1007/10_2011_112

Miyamoto, Y., Izumi, M., Ishizaka, S., and Hayashi, M. (1989). Adsorption of Vitronectin in Human Serum onto Plastics is Augmented by Sodium Dodecyl Sulfate. *Cell Structure and Function, 14*(2), 151-162. doi:https://doi.org/10.1247/csf.14.151

Morrow, K., and Sha, M. (2013). *Vero Cell-based Vaccine Production: Rabies and Influenza Cell lines, Media and Bioreactor Options.* Hamburg, Germany: Eppendorf, Inc. Retrieved from http://www.eppendorf.com

Mortimer, C., Burke , L., and Wright, C. (2016). Microbial Interactions with Nanostructures and their Importance for the Development of Electrospun Nanofibrous Materials used in Regenerative Medicine and Filtration. *Journal of Microbial and Biochemical Technology, 8*(3), 195-201. doi:10.4172/1948-5948.1000285

Moussa, H. I., Logan, M., Chang, W. Y., Wong, K., Rao, Z., Aucoin, M. G., and Tsui, T. Y. (2018a). Pattern-Dependent Mammalian Cell (Vero) Morphology on Tantalum/Silicon Oxide 3D Nanocomposites. *Materials, 11*(8), 1306. doi:10.3390/ma11081306

Moussa, H. I., Logan, M., Wong, K., Rao, Z., Aucoin, M. G., and Tsui, T. Y. (2018b). Nanoscale-Textured Tantalum Surfaces for Mammalian Cell Alignment. *Micromachines, 9*(9), 464. doi:10.3390/mi9090464

Moussa, H., Logan, M., Siow, G., Phann, D., Rao, Z., Aucoin , M., and Tsui , T. (2017). Manipulating mammalian cell morphologies using chemical-mechanical polished integrated circuit chips. *Science and Technology of Advanced Materials, 8*(1), 839-856. doi:10.1080/14686996.2017.1388135

Muñoz-Noval , A., Sánchez-Vaquero, V., Punzón-Quijorna , E., Torres-Costa , V., Gallach-Pérez , D., González-Méndez , L., . . . Manso-Silván, M. (2012). Aging of porous silicon in physiological conditions: Cell adhesion modes on scaled 1D micropatterns. *Journal of Biomedical Materials Research Part A, 100A*(6), 1615-1622. doi:10.1002/jbm.a.34108

Murarka, S., Verner, I., and Gutmann, R. (2000). *Copper - Fundamental Mechanism for Microelectronic Applications.* Hoboken, New Jersey: John Wiley and Sons, Inc.

Murayama, A., Sugiyama, N., Wakita, T., and Kato, T. (2016). Completion of the Entire Hepatitis C Virus Life Cycle in Vero Cells Derived from Monkey Kidney. *mBio, 7*(3). doi:10.1128/mBio.00273-16

Murphy-Ullrich, J. (2001). The de-adhesive activity of matricellular proteins: is intermediate cell adhesion an adaptive state? *The Journal of Clinical Investigation, 107*(7), 785-790. doi:10.1172/JCI12609

Nahapetian, A., Thomas, J., and Thilly, W. (1986). Optimization of environment for high-density Vero cell culture: effect of dissolved oxygen and nutrient supply on cell growth and changes in metabolites. *Journal of Cell Science, 81*, 65–103.

Nakamoto, T., Wang, X., Kawazoe, N., and Chen, G. (2014). Influence of micropattern width on differentiation of human mesenchymal stem cells to vascular smooth muscle cells. *Colloids and Surfaces B: Biointerfaces, 122*, 316-323. doi:10.1016/j.colsurfb.2014.06.013

NCBI. (1987). *Medical Subject Headings (MeSH): Vero Cells*. Retrieved July 05, Assessed 2016, from National Center for Biotechnology Information (NCBI): http://www.ncbi.nlm.nih.gov/

Nelea , V., and Kaartinen, M. (2010). Periodic beaded-filament assembly of fibronectin on negatively charged surface. *Journal of Structural Biology, 170*(1), 50-59. doi:10.1016/j.jsb.2010.01.009

Nikalje, A. P. (2015). Nanotechnology and its Applications in Medicine. *Medicinal chemistry, 5*(2), 081-089. doi:10.4172/2161-0444.1000247

Ning, D., Duong, B., Thomas, G., Qiao, Y., Ma, L., Wen, Q., and Su, M. (2016). Mechanical and Morphological Analysis of Cancer Cells on Nanostructured Substrates. *Langmuir, 32*(11), 2718-2723. doi:10.1021/acs.langmuir.5b04469

Nir, S., and Nieva, J. (2003). Uptake of Liposomes by Cells: Experimental Procedures and Modeling. *Liposomes, Part B, 372*, 235-248. doi:10.1016/S0076-6879(03)72013-8

Noh, H., and Vogler, E. (2006). Volumetric interpretation of protein adsorption: Partition coefficients, interphase volumes, and free energies of adsorption to hydrophobic surfaces. *Biomaterials, 27*(34), 5780-5793. doi:10.1016/j.biomaterials.2006.07.038

Noh, H., and Vogler, E. (2007). Volumetric interpretation of protein adsorption: Competition from mixtures and the Vroman effect. *Biomaterials, 28*(3), 405-422. doi:10.1016/j.biomaterials.2006.09.006

Noh, H., Yohe, S., and Vogler, E. (2008). Volumetric interpretation of protein adsorption: Ion-exchange adsorbent capacity, protein pI, and interaction energetics. *Biomaterials, 29*(13), 2033-2048. doi:10.1016/j.biomaterials.2008.01.017

Norde , W., and Haynes, C. (1995). Chapter 2: Reversibility and the Mechanism of Protein Adsorption. In T. Horbett, and J. Brash (Eds.), *Proteins at Interfaces II: Fundamentals and Applications* (pp. 26-40). Washington, DC: American Chemical Society. doi:10.1021/bk-1995-0602.ch002

Norde, W., and Lyklea, J. (1990). Why proteins prefer interfaces. *Journal of Biomaterial Science, 2*(3), 183-202.

Nune, K., and Misra, R. (2014). Pre-adsorption of protein on electrochemically grooved nanostructured stainless steel implant and relationship to cellular activity. *J Biomed Nanotechnology, 10*(7), 1320-1335. doi:10.1166/jbn.2014.1811

Nur-E-Kamal, A., Ahmed, I., Kamal, J., Schindler, M., and Meiners, S. (2006). Three-Dimensional Nanofibrillar Surfaces Promote Self-Renewal in Mouse Embryonic Stem Cells. *Stem Cells, 24*(2), 426-433. doi:10.1634/stemcells.2005-0170

Ochsner, M., Dusseiller, M., Grandin, H., Luna-Morris, S., Textor, M., Vogel, V., and Smith, M. (2007). Micro-well arrays for 3D shape control and high-resolution analysis of single cells. *Lab on a Chip, 7*(8), 1074-1077. doi:10.1039/b704449f

Ochsner, M., Dusseiller, M., Grandin, H., Luna-Morris, S., Textor, M., Vogelb , V., and Smith, M. (2007). Micro-well arrays for 3D shape control and high-resolution analysis of single cells. *Lab on a Chip, 7*, 1074–1077. doi:10.1039/b704449f

Oliver, W., and Pharr, G. (1992). An improved technique for determining hardness and elastic modulus using load and displacement sensing indentation experiments. *Journal of Materials Research*, 1564-1583. doi:10.1557/JMR.1992.1564

Orgovan, N., Peter, B., Bősze, S., Ramsden, J., Szabó , B., and Horvath, R. (2014). Dependence of cancer cell adhesion kinetics on integrin ligand surface density measured by a high-throughput label-free resonant waveguide grating biosensor. *Scientific Reports, 4*(Article number 4034), 1-8. doi:doi:10.1038/srep04034

Orner, B., Derda, R., Lewi, R., Thomson, J., and Kiessling, L. (2004). Arrays for the Combinatorial Exploration of Cell Adhesion. *Journal of the American Chemical Society, 126*(35), 10808-10809. doi:10.1021/ja0474291

Oshida, Y., and Lim, Y. (2001). Initial contact angle measurements on variously treated dental/medical titanium materials. *Bio-medical materials and engineering, 11*(4), 325-341.

Pakiela, Z., Lewandowska, M., and Kurzydlowski, K. (2011). The Effect of Microstructural Features on the Mechanical Properties of Nanocrystalline Metals. In J. Li (Ed.), *Mechanical Properties of Nanocrystalline Materials* (pp. 133-162). Singapore: Pan Stanford Publishing Pte. Ltd.

Palmer, C., Mycielska, M., Burcu, H., Osman, K., Collins, T., Beckerman, R., . . . Djamgo, M. (2008). Single cell adhesion measuring apparatus (SCAMA): application to cancer cell lines of different

metastatic potential and voltage-gated Na+ channel expression. *European Biophysics Journal, 37*(4), 359–368. doi:10.1007/s00249-007-0219-2

Pan, Z., Yan, C., Peng, R., Zhao, Y., He, Y., and Ding, J. (2012). Control of cell nucleus shapes via micropillar patterns. *Biomaterials, 33*(6), 1730-1735. doi:j.biomaterials.2011.11.023

Parhi, P., Golas, A., and Vogler, E. (2010). Role of Proteins and Water in the Initial Attachment of Mammalian Cells to Biomedical Surfaces: A Review. *Journal of Adhesion Science and Technology, 24*(5), 853-888. doi:10.1163/016942409X12598231567907

Parhi, P., Golas, A., Barnthip, N., Noh, H., and Vogler, E. (2009). Volumetric interpretation of protein adsorption: Capacity scaling with adsorbate molecular weight and adsorbent surface energy. *Biomaterials, 30*(36), 6814-6824. doi:10.1016/j.biomaterials.2009.09.005

Park , J., Bauer , S., von der Mark, K., and Schmuki, P. (2007). Nanosize and Vitality: TiO2 Nanotube Diameter Directs Cell Fate. *Nano Letters, 7*(6), 1686-1691. doi:10.1021/nl070678d

Partridge, M., and Marcantonio, E. (2006). Initiation of Attachment and Generation of Mature Focal Adhesions by Integrin-containing Filopodia in Cell Spreading. *Molecular Biology of the Cell, 17*(10), 4237-4248. doi:10.1091/mbc.E06-06-0496

Patrauchan, M., Sarkisova, S., and Sauer, K. (2005). Calcium influences cellular and extracellular product formation during biofilm-associated growth of a marine Pseudoalteromonas sp. *Microbiology, 151*, 2885-2897. doi:10.1099/mic.0.28041-0

Pelaez-Vargas, A., Gallego-Perez, D., Higuita-Castro, N., Carvalho, A., Grenho, L., Arismendi, J., . . . Monteiro , F. (2012). Chapter 11: Micropatterned Coatings for Guided Tissue Regeneration in Dental Implantology. In S. Gowder (Ed.), *Cell Interaction* (pp. 273-302). Rijeka, Croatia: InTech. doi:10.5772/50838

Pennisi, C., Sevcencu, C., Dolatshahi-Pirouz, A., Foss, M., Lundsgaard Hansen, J., Nylandsted Larsen, A., . . . Yoshida, K. (2009). Responses of Fibroblasts and Glial Cells to Nanostructured Platinum Surfaces. *Nanotechnology, 20*(38), 385103 (9pp). doi:10.1088/0957-4484/20/38/385103

Percell Biolytica. (n.d.). *Growth of Vero and GMK Cells. Application Note 115.* Retrieved 02 06, 2019, from Percell Biolytica: http://percell.se/115.pdf

Petiot, E., Guedon, E., Blanchard, F., Geny, C., Pinton, H., and Marc, A. (2010). Kinetic Characterization of Vero Cell Metabolism in a Serum-Free Batch Culture Process. *Biotechnology and Bioengineering, 107*(1), 143-153. doi:1002/bit.22783

Philp , D., Chen , S., Fitzgerald, W., Orenstein , J., Margolis, L., and Kleinman, H. (2005). Complex Extracellular Matrices Promote Tissue-Specific Stem Cell Differentiation. *Stem Cells, 23*(2), 288-296. doi:10.1634/stemcells.2002-0109

Pierres, A., Benoliel , A., and Bongrand, P. (2002). Cell fitting to adhesive surfaces: A prerequisite to firm attachment and subsequent events. *European Cells and Materials*, 31-45. doi:10.22203/eCM.v003a04

Pimpin , A., and Srituravanich, W. (2012). Review on Micro- and Nanolithography Techniques and Their Applications. *Engineering Journal, 16*(1), 37-56. doi:10.4186/ej.2012.16.1.37

Plank, M., and Simpson, M. (2012). Models of collective cell behaviour with crowding effects: comparing lattice-based and lattice-free approaches. *Journal of The Royal Society Interface, 9*, 2983–2996. doi:10.1098/rsif.2012.0319

Plansee. (Assessed 2016, July 04). *Tungsten.* Retrieved from Plansee High-Performance Materials: https://www.plansee.com

Plantman, S. (2013). Proregenerative Properties of ECM Molecules. *BioMed Research International, 2013 (Article ID 981695)*, 11. doi:10.1155/2013/981695

Pohl, K., Bartelt, M., Figuera, d., Bartlet, N., Hrbek, J., and Hwang, R. (1999). Identifying the forces responsible for self-organization of nanostructures at crystal surfaces. *Nature, 397*(6716), 238-241. doi:10.1038/16667

Pokropivny, V., and Skorokhod, V. (2007). Classification of Nanostructures by Dimensionality and Concept of Surface Forms Engineering in Nanomaterial Science. *Materials Science and Engineering, 27*(5-8), 990-993. doi:10.1016/j.msec.2006.09.023

Polyudova, T., Eroshenko, D., and Korobov, V. (2017). Plasma, serum, albumin, and divalent metal ions inhibit the adhesion and the biofilm formation of Cutibacterium (Propionibacterium) acnes. *AIMS Microbiology, 4*(1), 165–172. doi:10.3934/microbiol.2018.1.165

Ponche, A., Bigerelle, M., and Anselme, K. (2010). Relative influence of surface topography and surface chemistry on cell response to bone implant materials. Part 1: Physico-chemical effects. *Proceedings of the Institution of Mechanical Engineers, Part H: Journal of Engineering in Medicine , 224*(12), 1471-1486. doi:10.1243/09544119JEIM900

Ponsonnet, L., Reybier, K., Jaffrézic, N., Comte, V., Lagneau, C., Michèle, L., and Martelet, C. (2003). Relationship Between Surface Properties (Roughness, Wettability) of Titanium and Titanium Alloys and Cell Behaviour. *Materials Science and Engineering: C, 23*(4), 551-560. doi:10.1016/S0928-4931(03)00033-X

Poudel, I., Lee, J., Tan, L., and Lim, J. (2013). Micropatterning-retinoic acid co-control of neuronal cell morphology and neurite outgrowth. *Acta Biomaterialia, 9*(1), 4592-4598. doi:10.1016/j.actbio.2012.08.039

Prahalad, P., Calvo, I., Waechter, H., Matthews, J., Zuk, A., and Matli, K. (2004). Regulation of MDCK cell-substratum adhesion by RhoA and myosin light chain kinase after ATP depletion. *American Physiological Society, 286*(3), C693-C707. doi:10.1152/ajpcell.00124.2003

Prewitz, M., Seib, F., von Bonin, M., Friedrichs, J., Stißel, A., Niehage, C., . . . Werner, C. (2013). Tightly anchored tissue-mimetic matrices as instructive stem cell microenvironments. *nature Method, 10*(8), 788-794. doi:10.1038/nmeth.2523

Protein adsorption on titanium surfaces and their effect on osteoblast attachment. (2003). *Journal of Biomedical Materials Research Part A, 67A*(1), 344-349. doi:10.1002/jbm.a.10578

PubChem. (2019, Mar. 24). *Silica.* Retrieved from PubChem. U.S. National Library of Medicine: https://pubchem.ncbi.nlm.nih.gov/compound/Silica#section=Top

Puckett, S. D., Taylor, E., Raimondo, T., and Webster, T. J. (2010). The relationship between the nanostructure of titanium surfaces and bacterial attachment. *Biomaterials, 31*(4), 706-713. doi:10.1016/j.biomaterials.2009.09.081

Qi, L., Li, N., Huang, R., Song, Q., Wang, L., Zhang, Q., . . . Cheng, G. (2013). The Effects of Topographical Patterns and Sizes on Neural Stem Cell Behavior. *PLoS ONE, 3*, e59022. doi:10.1371/journal.pone.0059022

Qu, Z., Rausch-Fan, X., Wieland, M., Matejka, M., and Schedle, A. (2007). The initial attachment and subsequent behavior regulation of osteoblasts by dental implant surface modification. *Journal of Biomedical Materials Research, 82A*(3). doi:10.1002/jbm.a.31023

Quinlan, C., Gerencser, A., Treberg, J., and Brand, M. (2011). The mechanism of superoxide production by the antimycin-inhibited mitochondrial Q-cycle. *Journal of Biological Chemistry, 286*(36), 31361-31372. doi:10.1074/jbc.M111.267898

Rabe, M., Verdes, D., and Seeger, S. (2011). Understanding protein adsorption phenomena at solid surfaces. *Advances in Colloid and Interface Science, 162*(1-2), 87-106. doi:10.1016/j.cis.2010.12.007

Radtke, A., Jędrzejewski, T., Kozak, W., Sadowska, B., Więckowska-Szakiel, M., Talik, E., . . . Piszczek, P. (2017). Optimization of the Silver Nanoparticles PEALD Process on the Surface of 1-D Titania Coatings. *Nanomaterials, 7*(7), 193 (19 pages). doi:10.3390/nano7070193

Raman, N., and Atkinson, S. (1999). Rho controls actin cytoskeletal assembly in renal epithelial cells during ATP depletion and recovery. *American Physiological Society, 276*(6), C1312-C1324. doi:10.1152/ajpcell.1999.276.6.C1312

Rance, G., Marsh, D., Bourne, S., Reade , T., and Khlobystov, A. (2010). van der Waals Interactions between Nanotubes and Nanoparticles for Controlled Assembly of Composite Nanostructures. *ACS Nano, 4*(8), 4920-4928. doi:10.1021/nn101287u

Rapuano, B., and MacDonalda, D. (2011). Surface oxide net charge of a titanium alloy: Modulation of fibronectin-activated attachment and spreading of osteogenic cells. *Colloids and Surfaces B: Biointerfaces, 82*(1), 95-103. doi:10.1016/j.colsurfb.2010.08.023

Rasmussen, C., Reynolds, P., Petersen, D., Hansson , M., McMeeking , R., Dufva, M., and Gadegaard, N. (2016). Enhanced Differentiation of Human Embryonic Stem Cells Toward Definitive Endoderm on Ultrahigh Aspect Ratio Nanopillars. *Advanced Functional Materials, 26*(6), 815-823. doi:10.1002/adfm.201504204

Redey, S., Nardin, M., Bernache–Assolant, D., Rey, C., Delannoy, P., Sedel, L., and Marie, P. (2000). Behavior of human osteoblastic cells on stoichiometric hydroxyapatite and type A carbonate apatite: role of surface energy. *Journal of Biomedical Materials Research, 50*(3), 353-364. doi:10.1002/(SICI)1097-4636(20000605)50:3<353::AID-JBM9>3.0.CO;2-C

Reith, A., Bjerkvig, R., and Rucklidge, G. (1994). Laminin: a potential inhibitor of rat glioma cell invasion in vitro. *Anticancer Research, 14*(3A), 1071-1076.

Renner , L., and Weibel, D. (2011). Physicochemical regulation of biofilm formation. *MRS Bulletin, 36*(5), 347–355. doi:10.1557/mrs.2011.65

Rhoades, R. (2008). The Dark Art of CMP. *Future Fab International, 24*, 76-85. Retrieved from http://www.entrepix.com/

Rico, F., Chu, C., Abdulreda, M., Qin, Y., and Moy, V. (2010). Temperature Modulation of Integrin-Mediated Cell Adhesion. *Biophysical Journal, 99*(5), 1387-1396. doi:10.1016/j.bpj.2010.06.037

Roach, P., Farrar, D., and Perry, C. (2005). Interpretation of Protein Adsorption: Surface-Induced Conformational Changes. *Journal of American Chemical Society, 127*(22), 8168-8173. doi:10.1021/ja042898o

Robert , A., and Freitas Jr., J. (2005). "What is nanomedicine?," Nanomed. Nanotechnol. *Nanomedicine: Nanotechnology, Biology and Medicine, 1*(1), 2-9. doi:10.1016/j.nano.2004.11.003

Rosales-Leal, J., Rodríguez-Valverde, M., Mazzaglia, G., Ramón-Torregrosa, P., Díaz-Rodríguez, L., García-Martínez, O., . . . Cabrerizo-Vílchez, M. (2010). Effect of roughness, wettability and

morphology of engineered titanium surfaces on osteoblast-like cell adhesion. *Colloids and Surfaces A: Physicochemical and Engineering Aspects, 365*(1-3), 222-229. doi:10.1016/j.colsurfa.2009.12.017

Royal Society of Chemistry [RSC]. (retrieved 2019, March 09). *Periodic Table: Tungsten*. Retrieved from Royal Society of Chemistry: http://www.rsc.org/

Ruggeri, Z., and Jackson, S. (2013). Chapter 20 – Platelet Thrombus Formation in Flowing Blood. In A. Michelson (Ed.), *Platelets. third Edition* (pp. 399-423). Tokyo: Academic Press. doi:10.1016/B978-0-12-387837-3.00020-1

Rupp, F., Liang, L., Geis-Gerstorfer, J., Scheideler, L., and Hü, F. (2018). Surface characteristics of dental implants: A review. *Dental Materials, 34*(1), 40-57. doi:10.1016/j.dental.2017.09.007

Russell, P., and Kingsley, E. (2003). Human Prostate Cancer Cell Lines. In P. Russell, P. Jackson, and E. Kingsley (Eds.), *Prostate Cancer Methods and Protocols. Methods in Molecular Medicine*™ (Vol. 81, pp. 21-39). Totowa, NJ: Springer. doi:10.1385/1-59259-372-0:21

Rycenga, M., Cobley, C., Zeng, J., Li, W., Moran, C., Zhang, Q., . . . Xia, Y. (2011). Controlling the Synthesis and Assembly of Silver Nanostructures for Plasmonic Applications. *Chemical Reviews, 111*(6), 3669-3712. doi:10.1021/cr100275d

Ryoo, S.-R., Kim, Y.-K., Kim, M.-H., and Min, D.-H. (2010). Behaviors of NIH-3T3 Fibroblasts on Graphene/Carbon Nanotubes: Proliferation, Focal Adhesion, and Gene Transfection Studies. *ACS Nano, 4*(11), 6587-6598. doi:10.1021/nn1018279

Sabharwal , S., and Schumacker, P. (2014). Mitochondrial ROS in cancer: initiators, amplifiers or an Achilles' heel? *Nature Reviews Cancer volume, 14*, 709-721.

Sáenz-Morales, D., Escribese, M., Stamatakis, K., García-Martos, M., Alegre, L., Conde, E., . . . García-Bermejo, M. (2006). Requirements for proximal tubule epithelial cell detachment in response to ischemia: Role of oxidative stress. *Experimental Cell Research, 312*(19), 3711-3727. doi:10.1016/j.yexcr.2006.05.024

Sagvolden, G., Giaever, I., Pettersen, E., and Feder, J. (1999). Cell adhesion force microscopy. *Biophysics, 96*(2), 471–476. doi:10.1073/pnas.96.2.471

Saha, R., and Nix, W. (2002). Effects of the substrate on the determination of thin film mechanical properties by nanoindentation. *Acta Materialia, 50*(1), 23-38. doi:10.1016/S1359-6454(01)00328-7

Salatin, S., Dizaj, S., and Khosroushahi, A. (2015). Effect of the surface modification, size, and shape on cellular uptake of nanoparticles. *39*(8), 881-890. doi:10.1002/cbin.10459

Schmidt , D., Waldeck, H., and Kao, W. (2009). Protein Adsorption to Biomaterials. In D. Puleo, and R. Bizios (Eds.), *Biological Interactions on Materials Surfaces. Understanding and Controlling Protein, Cell, and Tissue Responses* (pp. 1-18). New York, NY: Springer. doi:10.1007/978-0-387-98161-1_1

Schwierz, F. (2010). Graphene transistors. *Nature Nanotechnology, 5*, 487-496. doi:10.1038/nnano.2010.89

Scotchford, C., Gilmore, C., Cooper, E., Leggett, G., and Downe, S. (2002). Protein adsorption and human osteoblast-like cell attachment and growth on alkylthiol on gold self-assembled monolayers. *Journal of Biomedical Materials Research Part A, 59*(1), 84-99. doi:10.1002/jbm.1220

Seiffert, D., and Smith, J. (1997). The Cell Adhesion Domain in Plasma Vitronectin Is Cryptic. *The Journal of Biological Chemistry, 272*(21), 13705–13710. doi:10.1074/jbc.272.21.13705

Sena, L., and Chandel, N. (2012). Physiological roles of mitochondrial reactive oxygen species. *Molecular Cell, 48*(2), 158-167. doi:10.1016/j.molcel.2012.09.025

Seo, B. B., Jahed, Z., Coggan, J. A., Chau , Y., Rogowski, J., Gu, F., . . . Tsui, T. (2017). Mechanical Contact Characteristics of PC3 Human Prostate Cancer Cells on Complex-Shaped Silicon Micropillars. *Materials, 10*(8), 892 (16 pages). doi:10.3390/ma10080892

Seo, Y.-J., and Lee, W.-S. (2005). Effects of different oxidizers on the W-CMP performance. *Materials Science and Engineering: B, 118*(1-3), 281-284. doi:10.1016/j.mseb.2004.12.064

Seo, Y.-J., and Lee, W.-S. (2007). Effects of oxidant additives for exact selectivity control of W- and Ti-CMP process. *Microelectronic Engineering, 77*(2), 132-138. doi:10.1016/j.mee.2004.10.003

Shadel, G., and Horvath, T. (2015). Mitochondrial ROS Signaling in Organismal Homeostasis. *Cell, 163*(3), P560-569. doi:10.1016/j.cell.2015.10.001

Sharma, A., Zbarska, S., Petersen, E., Marti, M., Mallapragada, S., and Sakaguchi, D. (2016). Oriented growth and transdifferentiation of mesenchymal stem cells Schwann cell fate on micropatterned substrates. *Journal of Bioscience and Bioengineering, 121*(3), 325-335. doi:10.1016/j.jbiosc.2015.07.006

Shen, J., Ly , K., and Hoang, Y. (2012). Chapter 5 - Cell Culture Medium. In J. Loring , and S. Peterson (Eds.), *Human Stem Cell Manual (Second Edition)* (pp. 53-69). London: Academic Press. doi:10.1016/B978-0-12-385473-5.00005-9

Shibata, Y., and Tanimoto, Y. (2015). A review of improved fixation methods for dental implants. Part I: Surface optimization for rapid osseointegration. *Journal of Prosthodontic Research, 59*(1), 20-33. doi:10.1016/j.jpor.2014.11.007

Shih, T., and Twu, J.-C. (2000). *US Patent No. US 6153526 A: Method to remove residue in wolfram CMP*.

Shinji, H., Yosizawa, Y., Tajima, A., Iwase, T., Sugimoto, S., Seki, K., and Mizunoe, Y. (2011). Role of Fibronectin-Binding Proteins A and B in In Vitro Cellular Infections and In Vivo Septic Infections by Staphylococcus aureus. *Infection and immunity, 79*(6), 2215-2223. doi:10.1128/IAI.00133-11

Shoulders, M., and Raines, R. (2009). Collagen Structure and Stability. *Annual Review of Biochemistry, 78*, 929-958. doi:10.1146/annurev.biochem.77.032207.120833

Siddiqui, J., and Frederick , T. (2005). *United States Patent No. 6,893,476 B2*.

Sigma Aldrich. (assessed 2016a, July 07). *VERO Cell Line*. Retrieved from Sigma Aldrich: http://www.sigmaaldrich.com/

Sigma-Aldrich. (2016b, Nov. 25). *QT 35*. Retrieved from Sigma-Aldrich: http://www.sigmaaldrich.com/

Sigma-Aldrich. (retrieved 2017, May 04). *Human Albumin*. Retrieved from Sigma-Aldrich: http://www.sigmaaldrich.com/life-science/metabolomics/enzyme-explorer/enzyme-reagents/human-albumin.html

Silva, G. (2006). Neuroscience nanotechnology: progress, opportunities and challenges. *Nature Reviews Neuroscience, 7*(1), 65-74. doi:10.1038/nrn1827

Silver, F., and Birk, D. (1984). Molecular structure of collagen in solution: comparison of types I, II, III and V. *International Journal of Biological Macromolecules, 6*(3), 125-132. doi:10.1016/0141-8130(84)90052-7

Silver, J., Lin , H.-B., and Cooper, S. (1993). Effect of protein adsorption on the sulphonated polyurethanes. *Biomaterials, 14*(11), 834-844. doi:10.1016/0142-9612(93)90005-M

Singer, P. (1998). Tantalum, copper and Damascene: The Future of Interconnects. *Semiconductor International, 21*(6), 90-98.

Singhana, B., Slattery, P., Chen, A., Wallace, M., and Melancon, M. (2014). Light-activatable gold nanoshells for drug delivery applications. *AAPS Pharm SciTech, 15*(3), 741-752. doi:10.1208/s12249-014-0097-8

Sitterley, G., Karmiol, S., Manaster, E., and Ryn, J. (2008). Attachment and Matrix Factors. *Sigma Life Science BioFiles, 3*(8). Retrieved from https://www.sigmaaldrich.com/content/dam/sigma-aldrich/flashapps/biofiles-movie/pdf/biofiles_issue3.8.pdf

Skriver, H. L., and Rosengaard, N. M. (1992). Surface energy and work function of elemental metals. *Physical Review B, 46*(11), 7157-7168. doi:10.1103/PhysRevB.46.7157

Smith, L., Liu, X., Hu, J., and Ma, P. (2009). The Influence of Three-dimensional Nanofibrous Scaffolds on the Osteogenic Differentiation of Embryonic Stem Cells. *Biomaterials, 30*(13), 2516-2522. doi:10.1016/j.biomaterials.2009.01.009

Sniadecki, N., Desai, R., Alom Ruiz, S., and Chen, C. (2006). Nanotechnology for Cell–Substrate Interactions. *Annals of Biomedical Engineering, 34*(1), 59-74. doi:10.1007/s10439-005-9006-3

South Bay Technology. (retrieved 2017). *Applications Laboratory Report 86. Evaluating Surface Roughness of Si Following Selected Lapping and Polishing Processes.* San Clemente, CA: South Bay Technology, INC.

Stavreva , Z., Zeidler, D., Plötner, M., and Drescher, K. (1995). Chemical Mechanical Polishing of Copper for Multilevel Metallization. *Proceedings of the First European Workshop on Materials for Advanced Metallization, 91*(1-4), 192-196. doi:10.1016/0169-4332(95)00118-2

Steele, J., Johnson, G., and Underwood, P. (1992). Role of serum vitronectin and fibronectin in adhesion of fibroblasts following seeding onto tissue culture polystyrene. *Journal of Biomedical Materials Research, 26*, 861-884.

Stefano, G., Samuel, J., and Kream, R. (2017). Antibiotics May Trigger Mitochondrial Dysfunction Inducing Psychiatric Disorders. *Medical Science Monitor, 23*, 101-106. doi:10.12659/MSM.899478

Steigerwald, J., Murarka, S., Gutmann, R., and Duquette, D. (1995). Chemical processes in the chemical mechanical polishing of copper. *Materials Chemistry and Physics*(41), 217-228. doi:10.1016/0254-0584(95)01516-7

Stevenson , P., and Donald, A. (2009). Identification of Three Regimes of Behavior for Cell Attachment on Topographically Patterned Substrates. *Langmuir, 25*(1), 367-376. doi:10.1021/la802859v

Su, Y.-C., and Riesbeck, K. (2018). Chapter 33 - Vitronectin. In S. Barnum, and T. Schein (Eds.), *The Complement FactsBook (Second Edition)* (pp. 351-360). Cambridge: Academic Press. doi:10.1016/B978-0-12-810420-0.00033-X

Sun, B., Xie, K., Chen, T.-H., and Lam, R. (2017). Preferred cell alignment along concave microgrooves. *RSC Advances, 7*(11), 6788–6794. doi:10.1039/c6ra26545f

Sung, C.-Y., Yang, C.-Y., Yeh, J., and Cheng, C.-M. (2016). Integrated Circuit-Based Biofabrication with Common Biomaterials for Probing Cellular Biomechanics. *Trends in Biotechnology, 34*(2), 171-186. doi:10.1016/j.tibtech.2015.11.005

Suryanarayana, C., and Koch, C. C. (2000). Nanocrystalline materials – Current research and future directions. *Hyperfine Interactions, 130*(1), 5-44.

Szunerits , S., Barras, A., Khanal, M., Pagneux, Q., and Boukherroub, R. (2015). Nanostructures for the Inhibition of Viral Infections. *Molecules, 20*(8), 14051-14081. doi:10.3390/molecules200814051

Tagaya, M., Ikoma, T., Hanagata, N., Yoshioka, T., and Tanaka, J. (2011). Competitive adsorption of fibronectin and albumin on hydroxyapatite nanocrystals. *Science and Technology of Advanced Materials, 12*(3), 034411 (7pp).

Takeichi, M., and Osada, T. (1972). Roles of Magnesium and Calcium ions in Cell-to-Substrate Adhesion. *Experimental Cell Research, 74*(1), 51-60. doi:10.1016/0014-4827(72)90480-6

Tamada, Y., and Ikada, Y. (1993). Effect of Preadsorbed Proteins on Cell Adhesion to Polymer Surfaces. *Journal of Colloid and Interface Science, 155*(2), 334-339. doi:10.1006/jcis.1993.1044

Tan, J., Tien, J., Pirone, D., Gary, D., Bhadriraju, K., and Chen, C. (2003). Cells Lying on a Bed of Microneedles: An Approach to Isolate Mechanical Force. *PNAS, 100*(4), 1484-1489. doi:10.1073/pnas.0235407100

Tanaka, K. (2013). Chapter 36 - Transfusion and Coagulation Therapy. In H. Hemmings, Jr., and T. Egan, *Pharmacology and Physiology for Anesthesia. Foundations and Clinical Application* (pp. 628-642). Philadelphia: Saunders Elsevier. doi:10.1016/B978-1-4377-1679-5.00036-3

Teixeira, A., Abrams, G., Bertics, P., Murphy, C., and Nealey, P. (2003). Epithelial Contact Guidance on Well-defined Micro- and Nanostructured Substrates. *Journal of Cell Science, 116 (Pt 10)*, 1881-1892. doi:10.1242/jcs.00383

Teixeira, A., McKie, G., Foley, J., Bertics, P., and Nealey, P. (2006). The Effect of Environmental Factors on the Response of Human Corneal Epithelial Cells to Nanoscale Substrate Topography. *Biomaterials, 27*(21), 3945-3954. doi:10.1016/j.biomaterials.2006.01.044

Thakar, R., Ho, F., Huang , N., Liepmann, D., and Li, S. (2003). Regulation of Vascular Smooth Muscle Cells by Micropatterning. *Biochemical and Biophysical Research Communications, 307*(4), 883–890. doi:10.1016/S0006-291X(03)01285-3

Tharmalingam, S., Daulat, A., Antflick, J., Ahmed, S., Nemeth, E., Angers , S., . . . R. Hampson, D. (2011). Calcium-sensing Receptor Modulates Cell Adhesion and Migration via Integrins. *The Journal of Biological Chemistry, 286*(47), 40922-40933. doi:10.1074/jbc.M111.265454

Thomas, R., Kaufman, F., Kirleis, J., and Beisky, R. (1996). Wettability of Polished Silicon Oxide Surfaces. *Journal of the Electrochemical Society, 143*(2), 643-648. doi:10.1149/1.1836494

Tighe, B., and Mann, A. (2011). Chapter 13 - Sulphonated biomaterials as glycosaminoglycan mimics in wound healing. In D. Farrar (Ed.), *Advanced Wound Repair Therapies* (pp. 321-257). Oxford: Woodhead Publishing Limited. doi:10.1533/9780857093301.2.321

Timoshevskii, V., Ke, Y., Guo, H., and Gall, D. (2008). The influence of surface roughness on electrical conductance of thin Cu films: An ab initio study. *Journal of Applied Physics, 103*, 113705:1-4. doi:doi.org/10.1063/1.2937188

Tiwari, J., Tiwari, R., and Kim, K. (2012). Zero-dimensional, One-dimensional, Two-dimensional and Three-dimensional Nanostructured Materials for Advanced Electrochemical Energy Devices. *Progress in Materials Science, 57*(4), 724-803. doi:10.1016/j.pmatsci.2011.08.003

Todd, D., Connor , T., Creelan, J., Borghmans, B., Calvert, V., and McNulty, M. (1998). Effect of multiple cell culture passages on the biological behaviour of chicken anaemia virus. *Avian Pathology, 27*(1), 74-79. doi:10.1080/03079459808419277

Tomellini, R., Faure, U., and Panzer, O. (2006). *Nanomedicine: Nanotechnology for Health - Strategic Research Agenda.* Luxembourg: European Commission.

Torres-Costa, V., Martínez-Muñoz, G., Sánchez-Vaquero, V., Muñoz-Noval, Á., Punzón-Quijorna, E., Gallach-Pérez, D., . . . García-Ruiz, J. (2012). Engineering of silicon surfaces at the micro- and nanoscales for cell adhesion and migration control. *International Journal of Nanomedicine, 7*, 623-630. doi:10.2147/IJN.S27745

Toworfe , G., Composto , R., Adams, C., Shapiro , I., and Ducheyne, P. (2004). Fibronectin adsorption on surface-activated poly(dimethylsiloxane) and its effect on cellular function. *71*(3), 449-461. doi:10.1002/jbm.a.30164

Tran, R., Xu, Z., Radhakrishnan, B., Winston, D., Sun, W., Persson , K., and Ping Ong, S. (2016). Surface energies of elemental crystals. *Scientific Data, 3:160080*, 1-13. doi:10.1038/sdata.2016.80

Tremel, A., Cai, A., Tirtaatmadja, N., Hughes, B., Stevens, G., Landman, K., and O'Connor, A. (2009). Cell migration and proliferation during monolayer formation and wound healing. *Chemical EngineeringScience, 64*(2), 247--253. doi:10.1016/j.ces.2008.10.008

Trono , J., Mizumo, K., Yusa, N., Matsukawa, T., Yokoyama, K., and Uesaka, M. (2011). Size, concentration and incubation time dependence of gold nanoparticle uptake into pancreas cancer cells and its future application to X-Ray Drug Delivery System. *Journal of Radiation Research, 52*(1), 103-109.

Tsui , T., Logan, M., Moussa, H., and Aucoin , M. (2019). What's Happening on the Other Side? Revealing Nano-Meter Scale Features of Mammalian Cells on Engineered Textured Tantalum Surfaces. *Materials, 12*(1), 114. doi:10.3390/ma12010114

Tsytsikova, L. (2009). *Global List of Organizations and Efforts Related to Nanotechnology, Nanoscience, Nanomaterials, and Food and Agriculture Products.* Washington, DC: North American Branch of The International Life Sciences Institute. Retrieved from http://www.ilsi.org/

Underwood, P. A., and Bennett, F. (1989). A comparison of the biological activities of the cell-adhesive proteins vitronectin and fibronectin. *Journal of Cell Science, 93*, 641-649.

Uppuluri, S., Kinzel, E., Li, Y., and Xu, X. (2010). Parallel optical nanolithography using nanoscale bowtie aperture array. *29*(18), 7369-7375. doi:10.1364/OE.18.007369

Vaidya, S. S., and Ofoli, R. Y. (2005). Adsorption and Interaction of Fibronectin and Human Serum Albumin at the Liquid-Liquid Interface. *Langmuir, 21*(13), 5852–5858. doi:10.1021/la046766k

Valamehr, B., Jonas, S., Polleux, J., Qiao, R., Guo, S., Gschweng, E., . . . Wu, H. (2008). Hydrophobic surfaces for enhanced differentiation of embryonic stem cell-derived embryoid bodies. *PNAS, 105*(38), 14459–14464.

Valster, A., Tran, N., Nakada, M., Berens, M., Chan, A., and Symons, M. (2005). Cell migration and invasion assays. *Methods, 37*(2), 208-215. doi:10.1016/j.ymeth.2005.08.001

van Kranenburg, H., van Corbach, H., Woerlee, P., and Lohmeier, M. (1997). W-CMP for sub-micron inverse metallization. *Microelectronic Engineering, 33*(1-4), 241-248. doi:10.1016/S0167-9317(96)00050-0

Ventre, M., Causa, F., and Netti, P. (2012). Determinants of cell-material crosstalk at the interface: towards engineering of cell instructive materials. *The Journal of the Royal Society Interface, 9*(74), 2017-2032. doi:10.1098/rsif.2012.0308

Ventre, M., Natale, C., Rianna, C., and Netti, P. (2014). Topographic cell instructive patterns to control cell adhesion, polarization and migration. *Journal of The Royal Society Interface, 11*(100). doi:10.1098/rsif.2014.0687

Verdu´, E., Labrador, R. O., Rodrıguez, F. J., Ceballos, D., Fores, J., and Navarro, X. (2002). Alignment of collagen and laminin-containing gels improve nerve regeneration within silicone tubes. *Restorative Neurology and Neuroscience, 20*(5), 169-79.

Versaevel, M., Grevesse , T., and Gabriel, S. (2012). Spatial coordination between cell and nuclear shape within micropatterned endothelial cells. *Nature Communication, 3*, Article number: 671. doi:10.1038/ncomms1668

Vincent , M., Duval , R., Hartemann , P., and Engels-Deutsch, M. (2017). Contact killing and antimicrobial properties of copper. *Journal of Applied Microbiology, 124*(5), 1032-1046. doi:10.1111/jam.13681

Vitos , L., Ruban , A., Skriver, H., and Kollar, J. (1998). The surface energy of metals. *Surface Science, 1-2*, 186-202. doi:10.1016/S0039-6028(98)00363-X

Vogler, E. (1998). Structure and reactivity of water at biomaterial surfaces. *Advances in Colloid and Interface Science, 74*(1-3), 69-117. doi:10.1016/S0001-8686(97)00040-7

Vogler, E. (2011). The Goldilocks Surface. *Biomaterials, 32*(28), 6670-6675. doi:10.1016/j.biomaterials.2011.05.066

Vogler, E. (2012). Protein adsorption in three dimensions. *Biomaterials, 33*(5), 1201-1237. doi:10.1016/j.biomaterials.2011.10.059

Vullers, R., van Schaijk, R., Doms, I., Van Hoof, C., and Mertens, R. (2009). Micropower energy harvesting. *Solid-State Electronics, 53*(7), 684-693. doi:10.1016/j.sse.2008.12.011

Wagner , W., Wein , F., Roderburg , C., Saffrich , R., A., D., Eckstein , V., and Ho, A. (2008). Adhesion of human hematopoietic progenitor cells to mesenchymal stromal cells involves CD44. *Cells Tissues Organs, 188*(1-2), 160-169. doi:10.1159/000112821

Walther , D. C., and Ahn, J. (2011). Advances and challenges in the development of power-generation systems at small scales. *Progress in Energy and Combustion Science, 37*(5), 583-610. doi:10.1016/j.pecs.2010.12.002

Wang, B., Weldon, A., Kumnorkaew, P., Xu, B., Gilchrist, J., and Cheng, X. (2011). Effect of Surface Nanotopography on Immunoaffinity Cell Capture in Microfluidic Devices. *Langmuir, 0*(0 (proofing)). doi:10.1021/la2015868@proofing

Wang, S., Wan, Y., and Liu, Y. (2014). Effects of Nanopillar Array Diameter and Spacing on Cancer Cell Capture and Cell Behaviors. *Nanoscale, 6*(21), 12482-12849. doi:10.1039/c4nr02854f

Wang, X., Liu, H., Zhu, M., Cao, C., Xu, Z., Tsatskis, Y., . . . Sun, Y. (2018). Mechanical stability of the cell nucleus – roles played by the cytoskeleton in nuclear deformation and strain recovery. *Journal of Cell Science*, 1-10. doi:10.1242/jcs.209627

Wang, Y., Black, K., Luehmann, H., Li, W., Zhang, Y., Cai, X., . . . Xia, Y. (2013). Comparison Study of Gold Nanohexapods, Nanorods, and Nanocages for Photothermal Cancer Treatment. *ACS Nano, 7*(3), 2068-2077. doi:10.1021/nn304332s

Webb, K., Hlady, V., and Tresco, P. (1998). Relative importance of surface wettability and charged functional groups on NIH 3T3 fibroblast attachment, spreading, and cytoskeletal organization. *Journal of Biomedical Materials Research, 41*(3), 422-430.

Wertz , C., and Santor, M. (2001). Effect of Surface Hydrophobicity on Adsorption and Relaxation Kinetics of Albumin and Fibrinogen: Single-Species and Competitive Behavior. *Langmuir, 17*(10), 3006-3016. doi:10.1021/la0017781

Willerth, S. (2017). *Chapter 5 - Natural biomaterials for engineering neural tissue from stem cells.* Cambridge: Academic Press. doi:10.1016/B978-0-12-811385-1.00005-4

Williams, D. (2008). On the mechanisms of biocompatibility. *Biomaterials, 29*(20), 2941-2953. doi:10.1016/j.biomaterials.2008.04.023

Wilson, C., Clegg, R., Leavesley, D., and Pearcy, M. (2005). Mediation of Biomaterial–Cell Interactions by Adsorbed Proteins: A Review. *Tissue Engineering, 11*(1-2), 1-18. doi:10.1089/ten.2005.11.1

Wimley, W. C., and Hristova, K. (2014). Interfacially active peptides and proteins. *Biochimica et Biophysica Acta (BBA) - Biomembranes, 1838*(9). doi:10.1016/j.bbamem.2014.06.001

Witten, M., Sheppard, P., and Witten, B. (2012). Tungsten Toxicity. *Chemico-Biological Interactions, 196*(3), 87-88. doi:10.1016/j.cbi.2011.12.002

Wójciak-Stothard, B., Curtis, A., Monaghan, W., Macdonald, K., and Wilkinson, C. (1996). Guidance and Activation of Murine Macrophages by Nanometric Scale Topography. *Experimental Cell Research, 223*(2), 426-435. doi:10.1006/excr.1996.0098

Wolfenson, H., Lavelin, I., and Geiger, B. (2013). Dynamic regulation of the structure and functions of integrin adhesions. *Developmental Cell, 24*(5), 447-458. doi:10.1016/j.devcel.2013.02.012

Wood, A. (1988). Contact guidance on microfabricated substrata: the response of teleost fin mesenchyme cells to repeating topographical patterns. *Journal of Cell Science, 90 (Pt 4)*, 667-681.

Wu, G., Wang, J., Chen, X., and Wang, Y. (3013). Impact of self-assembled monolayer films with specific chemical group. *Journal of Biomedical Materials research A, 120A*(10), 3439-3445. doi:10.1002/jbma.35007

Wu, P.-H., Giri, A., Sun, S. X., and Wirtz, D. (2014). Three-dimensional cell migration does not follow a random walk. *PNAS, 111*(11), 3949–3954. doi:10.1073/pnas.1318967111

Wu, S., Zuber, F., Brugger, J., Maniura-Weberc, K., and Ren, Q. (2016). Antibacterial Au Nanostructured Surfaces. *Nanoscale, 8*(5), 2620-2625. doi:10.1039/c5nr06157a

Xio, B., Rao, F., Guo, Z.-y., Sun, X., Wang, Y.-g., Liu, S.-y., . . . Lu, S.-b. (2016). Extracellular matrix from human umbilical cord-derived mesenchymal stem cells as a scaffold for peripheral nerve regeneration. *Neural Regeneration Research, 11*(7), 1172-1179. doi:10.4103/1673-5374.187061

Xu, J., and Mosher, D. (2011). Fibronectin and Other Adhesive Glycoproteins. In R. Mecham (Ed.), *The Extracellular Matrix: an Overview* (pp. 41-75). Berlin: Springer-Verlag GmbH.

Yamane, T., Nagai, N., Katayam, S.-i., and Todoki, M. (2002). Measurement of thermal conductivity of silicon dioxide thin films using a 3v method. *Journal of Applied Physics, 91*(12), 9772-9776. doi:10.1063/1.1481958

Yang, J.-Y., Ting, Y.-C., Lai, J.-Y., Liu, H.-L., Fang, H.-W., and Tsai, W.-B. (2009). Quantitative Analysis of Osteoblast-like Cells (MG63) Morphology on Nanogrooved Substrata with Various Groove and Ridge Dimensions. *Journal of Biomedical Materials Research, 90*(3), 629-640. doi:10.1002/jbm.a.32130

Yang, L., Jiang, Z., Zhou, L., Zhao, K., Maa, X., and Cheng, G. (2017). Hydrophilic cell-derived extracellular matrix as a niche to promote adhesion and differentiation of neural progenitor cells. *RSC Advances, 7*(72), 45587–45594. doi:10.1039/c7ra08273h

Yang, S., Ye, R., Han, B., Wei, C., and Yang, X. (2014). Ecotoxicological Effect of Nano-silicon Dioxide Particles on Daphnia Magna. *Integrated Ferroelectrics, 154*(1), 64-72. doi:10.1080/10584587.2014.904143

Yang, Y. C. (2003). Protein adsorption on titanium surfaces and their effect on osteoblast attachment. *Journal of Biomedical Materials Research Part A, 67A*(1), 344-349. doi:10.1002/jbm.a.10578

Yang, Y., Cavin, R., and Ong, J. (2003). Protein adsorption on titanium surfaces and their effect on osteoblast attachment. *Journal of Biomedical Materials Research Part A, 67A*(1), 344-349. doi:10.1002/jbm.a.10578

Yao, N. (Ed.). (2007). *Focused Ion Beam Systems: Basics and Applications.* Cambridge, UK: Cambridge University Press.

Yatohgo, T., Izumi, M., Kashiwagi, H., and Hayashi, M. (1988). Novel Purification of Vitronectin from Human Plasma by Heparin Affinity Chromatography. *Cell Structure and Function, 13*(4), 281-292. doi:10.1247/csf.13.281

Yim, E., Darling, E., Kulangara, K., Guilak, F., and Leong, K. (2010). Nanotopography-induced changes in focal adhesions, cytoskeletal organization, and mechanical properties of human mesenchymal stem cells. *Biomaterials, 31*(6), 1299-1306. doi:10.1016/j.biomaterials.2009.10.037

Ying, P., Jin, G., and Tao, Z. (2001). Effects of surface chemistry and protein competitive adsorption on cell adhesion. *23rd Annual EMBS International Conference* (pp. 2957-2960). Istanbul, Turkey : Institute of Electrical and Electronics Engineers (IEEE). doi:10.1109/IEMBS.2001.1017412

You, B., and Park, W. (2010). The effects of antimycin A on endothelial cells in cell death, reactive oxygen species and GSH levels. *Toxicology in Vitro, 24*(4), 1111-1118. doi:10.1016/j.tiv.2010.03.009

Yurchenco, P., and Cheng, Y.-S. (1993). Self-assembly and calcium-binding sites in laminin. A three-arm interaction model. *The Journal of Biological Chemistry, 268*(23), 17286-17299.

Zahor, D., Radko, A., Vago, R., Vago, R., and Gheber, L. (2007). Organization of mesenchymal stem cells is controlled by micropatterned silicon substrates. *Materials Science and Engineering C, 27*(1), 117-121. doi:10.1016/j.msec.2006.03.005

Zantye, P., Kumar, A., and Sikder, A. (2004). Chemical mechanical planarization for microelectronics applications. *Materials Science and Engineering: R: Reports, 45*(3-6), 89-220. doi:10.1016/j.mser.2004.06.002

Zhang , W., and Liu, Q. (2010). Chapter 2: Cell Culture on Chips. In P. Wang and Q. Liu (Eds.), *Cell-based Biosensors: Principles and Applications* (pp. 13-33). Boston, MA: Artich House.

Zhang, L., and Webster, T. (2013). Chapter 17 – Nanotopography of biomaterials for controlling cancer cell function. In K. Park (Ed.), *Biomaterials for Cancer Therapeutics* (pp. 461-487). Oxford: Woodhead Publishing Limited. doi:10.1533/9780857096760.4.461

Zhang, Y., Yang, M., Portney, N., Cui, D., Budak, G., Ozbay, E., . . . Ozkan, C. (2008). Zeta potential: a surface electrical characteristic to probe the interaction of nanoparticles with normal and cancer human breast epithelial cells. *Biomedical Microdevices, 10*(2), 321–328. doi:10.1007/s10544-007-9139-2

Zhao , D., and Lu, X. (2013). Chemical Mechanical Polishing: Theory and Experiment. *Friction, 1*(4), 306–326. doi:10.1007/s40544-013-0035-x

Zhao, D., and Lu, X. (2013). Chemical mechanical polishing: Theory and experiment. *Friction, 1*(4), 306–326. doi:10.1007/s40544-013-0035-x

Zhao, G., Schwartz, Z., Wieland, M., Rupp, F., Geis-Gerstorfer, J., Cochran, D., and Boyan, B. (2005). High surface energy enhances cell response to titanium substrate microstructure. *74*(1), 49-58. doi:10.1002/jbm.a.30320

Zhengfeng, W., Ling, Y., Huan, N., and Luan, T. (2001). *Chemical Mechanical Planarization. Technical Report (PT/01/1003/JT).* Singapore: Singapore Institute of Manufacturing Technology (SIMTech). Retrieved from SIMTech.a-star.edu.sg

Zhou, F., Yuan, L., Huang, H., and Chen, H. (2009). Phenomenon of "contact guidance" on the surface with nano-micro-groove-like pattern and cell physiological effects. *Chinese Science Bulletin, 54*(18), 3200-3205. doi:10.1007/s11434-009-0366-1

Zhou, X., Shi, J., Hu, J., and Chenac, Y. (2013). Cells cultured on microgrooves with or without surface coating: correlation between cell alignment, spreading and local membrane deformation. *Materials Science and Engineering: C, 33*(2), 855-863. doi:10.1016/j.msec.2012.11.011

Zhu, W., Gehron Robey, P., and Boskey, A. (2008). CHAPTER 9 - The Regulatory Role of Matrix Proteins in Mineralization of Bone. In R. Marcus, D. Feldman, D. Nelson, and C. Rosen (Eds.), *Osteoporosis (Third Edition). Volume I* (pp. 191-240). Cambridge: Academic Press. doi:10.1016/B978-012370544-0.50011-2

Zhu, Y., Chen, G., Chen, L., Zhang, W., Feng, D., Liu, L., and Chen, Q. (2014). Chapter Three - Monitoring Mitophagy in Mammalian Cells. *Methods in Enzymology, 547*, 39-55. doi:10.1016/B978-0-12-801415-8.00003-5

Zhuo, R., Siedlecki, C., and Vogler, E. (2006). Autoactivation of blood factor XII at hydrophilic and hydrophobic surfaces. *Biomaterials, 27*(24), 4325-4332. doi:10.1016/j.biomaterials.2006.04.001

Zinger, O., Anselme, K., Denzer, A., Habersetzer, P., Wieland, M., Jeanfils, J., . . . Landolt, D. (2004). Time-dependent morphology and adhesion of osteoblastic cells on titanium model surfaces featuring scale-resolved topography. *Biomaterials, 14*, 2695-2711. doi:10.1016/j.biomaterials.2003.09.111

Appendix A

Table S1 the physical, chemical and mechanical properties of tungsten

Property	SiO2	Literature
Physical State at 20 °C and Appearance	Colourless crystals, insoluble in water	(PubChem, 2019)
Hardness at 20 °C	4.5-9.5 GPa	(AZoM, 2001)
Modulus of Elasticity at 20 °C	66-69.3 GPa	(El-Kareh, 1995) (Oliver and Pharr, 1992)
Surface Energy	0.0296 J/m^2	(Thomas et al., 1996)
Density at 20 °C	2.18-2.27 g/cm^{-3}	(El-Kareh, 1995)
Thermal Conductivity at 20 °C	1.1-1.4 $Wm^{-1}K$	(Burzo et al., 2003) (Yamane et al., 2002) (El-Kareh, 1995)
Electrical Resistivity at 20 °C	$1x10^{23}$ μΩ.cm	(El-Kareh, 1995)
Electrical Conductivity		
Melting Point	~1700 °C	(El-Kareh, 1995)
Boiling Point	2230 °C	(PubChem, 2019)
Crystal structure	Amorphous	(El-Kareh, 1995)
Specific Heat Capacity at 20 °C	$1.0x10^3$ J/kg.K	
The coefficient of Linear Thermal Expansion at 20 °C	$5.6x10^{-7}$ K^{-1}	
Application	Electronic components	

Appendix B

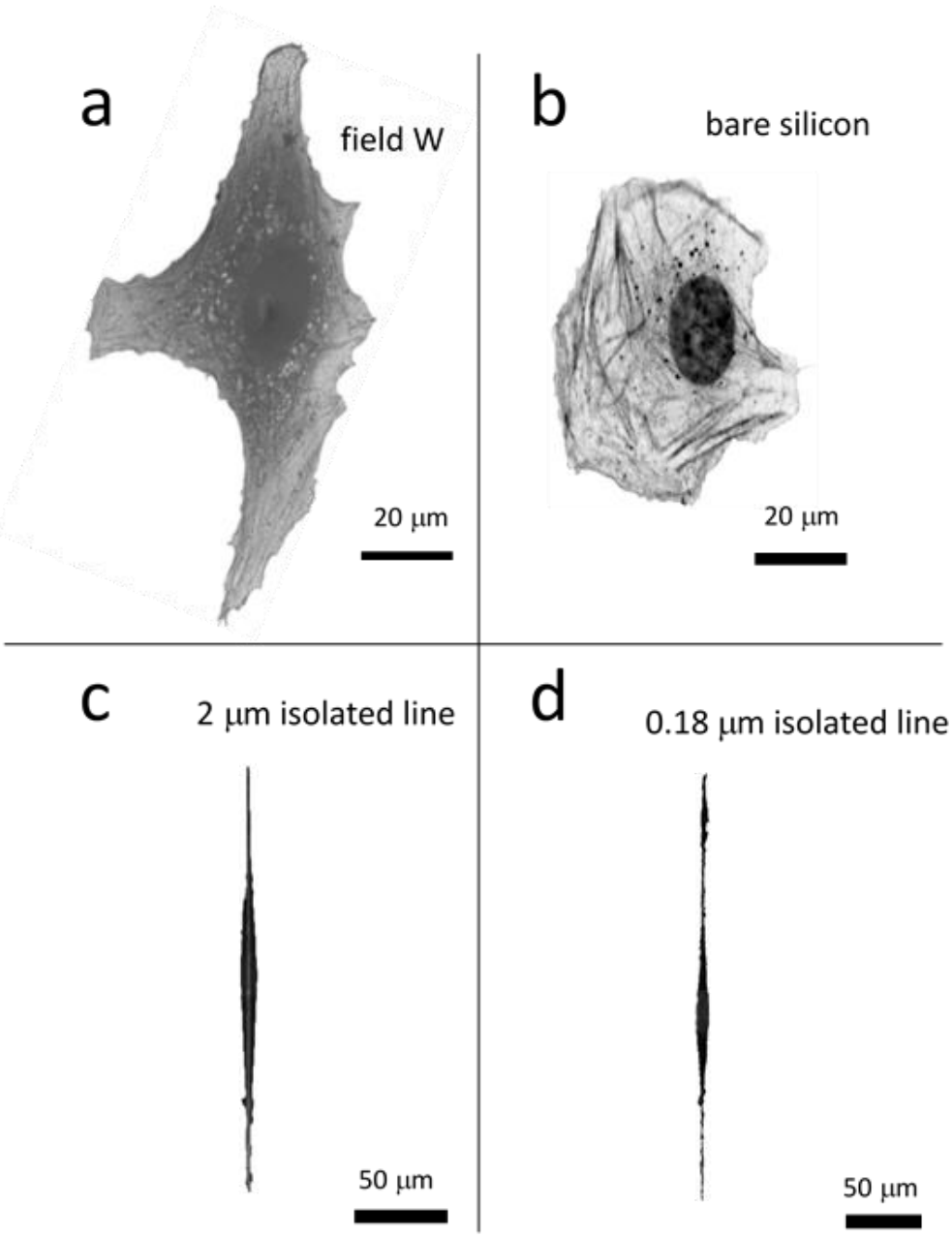

Figure S1 Geometries of different cells used in the mathematical model. Cells were chosen from actual cells adhered on (a) solid tungsten area, (b) bare silicon, (c) 2 μm, and (d) 0.18 μm wide isolated tungsten lines (Moussa et al., 2017)

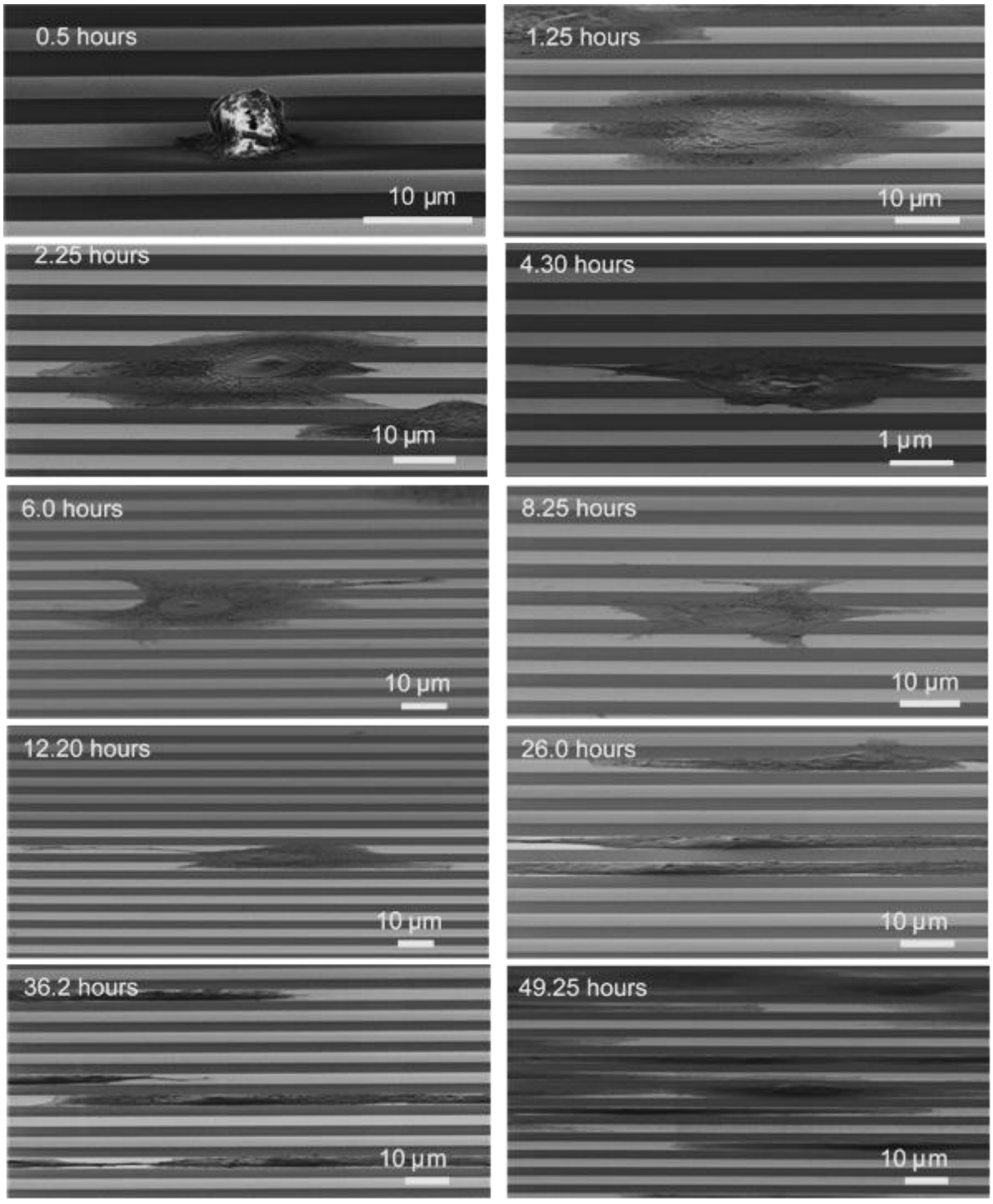

Figure S2 SEM micrographs (70^{o} tilted) of Vero cells on 10 µm comb structures with incubation time from 0.5 to 49.25 hours.

Appendix C

OptiPRO Reference Sample

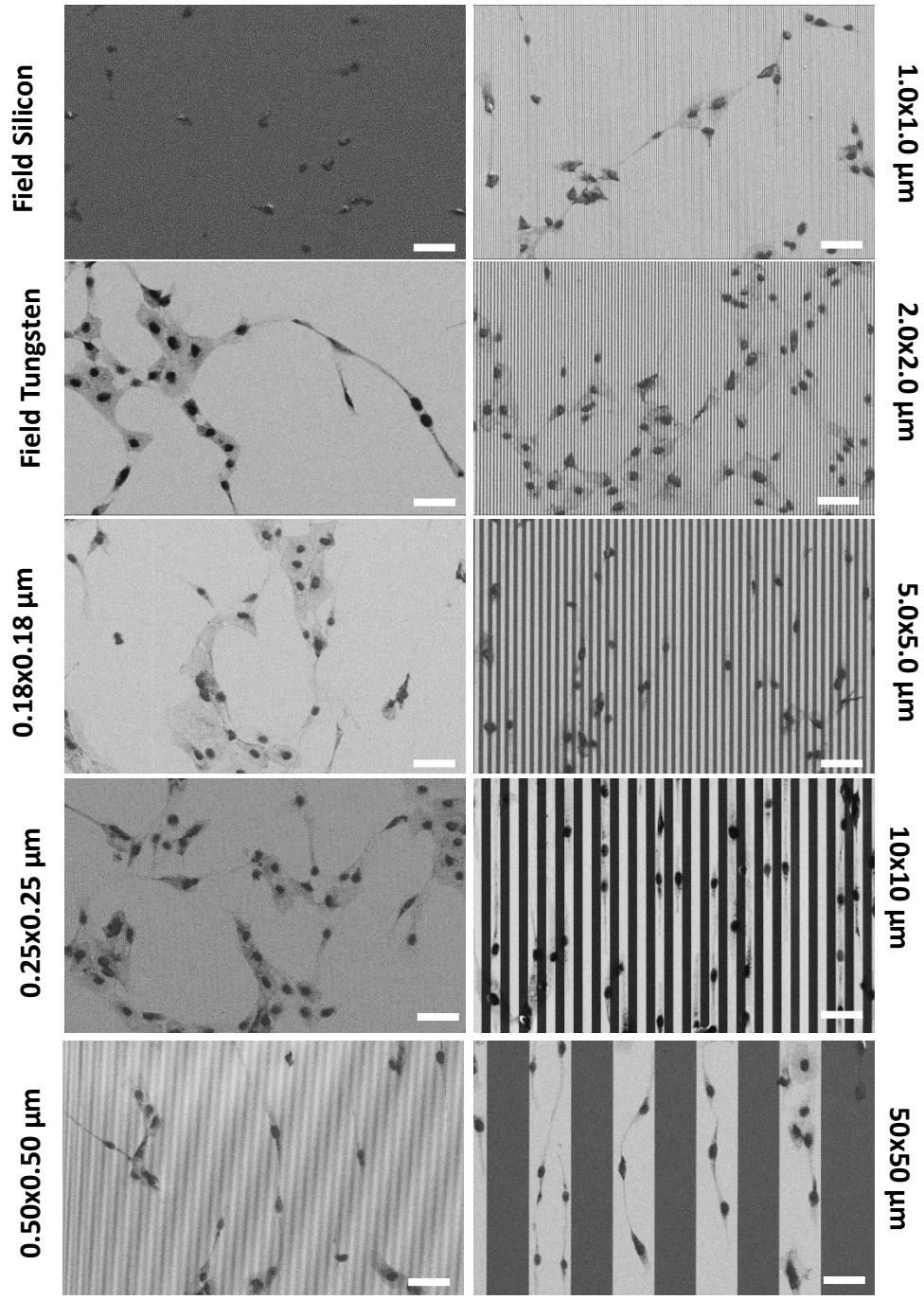

Figure S3 Typical top-down SEM images of Vero cells adherent on comb structures with different tungsten line widths incubated for 48 hours in OptiPRO™ culture medium. All scale bars are equal and represent 50 µm. OptiPRO™ is used as a reference for all protein-dependent experiments.

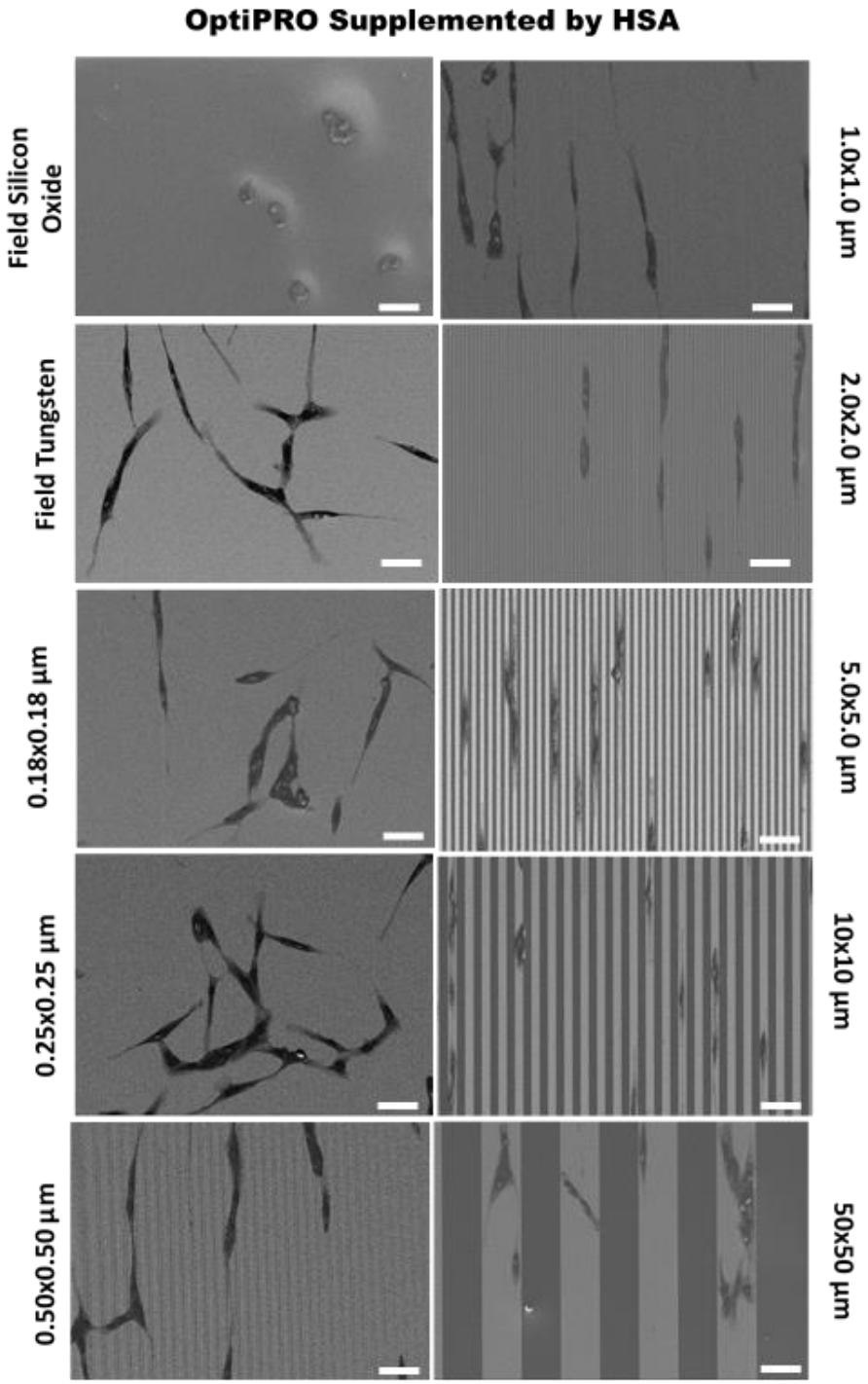

Figure S4 Typical top-down SEM images of Vero cells adherent on comb structures with different tungsten line widths incubated for 48 hours in OptiPROTM culture medium supplemented with 10 µg/mL HSA. All scale bars are equal and represent 50 µm.

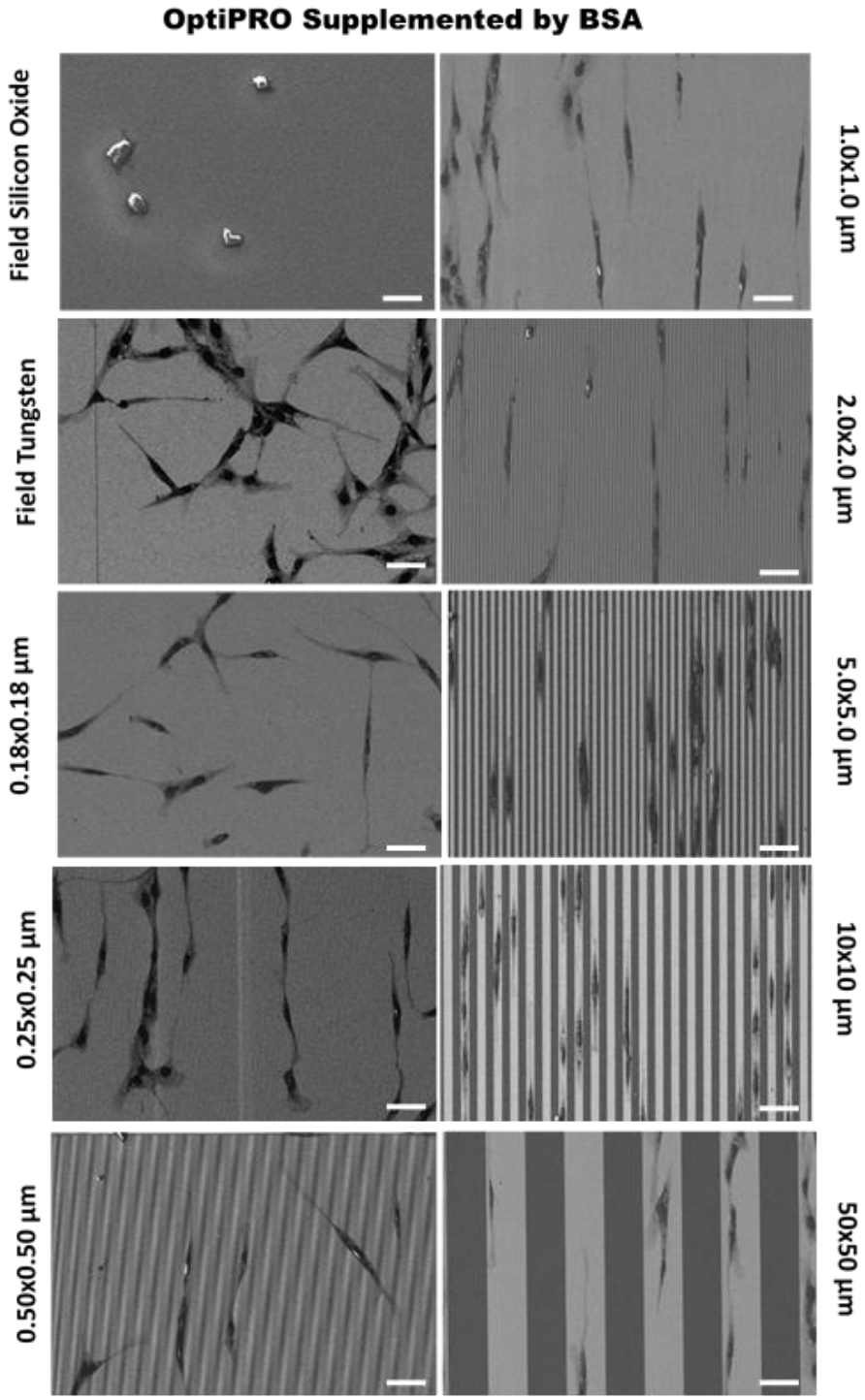

Figure S5 Typical top-down SEM images of Vero cells adherent on comb structures with different tungsten line widths incubated for 48 hours in OptiPRO™ culture medium supplemented with 10 µg/mL BSA. All scale bars are equal and represent 50 µm.

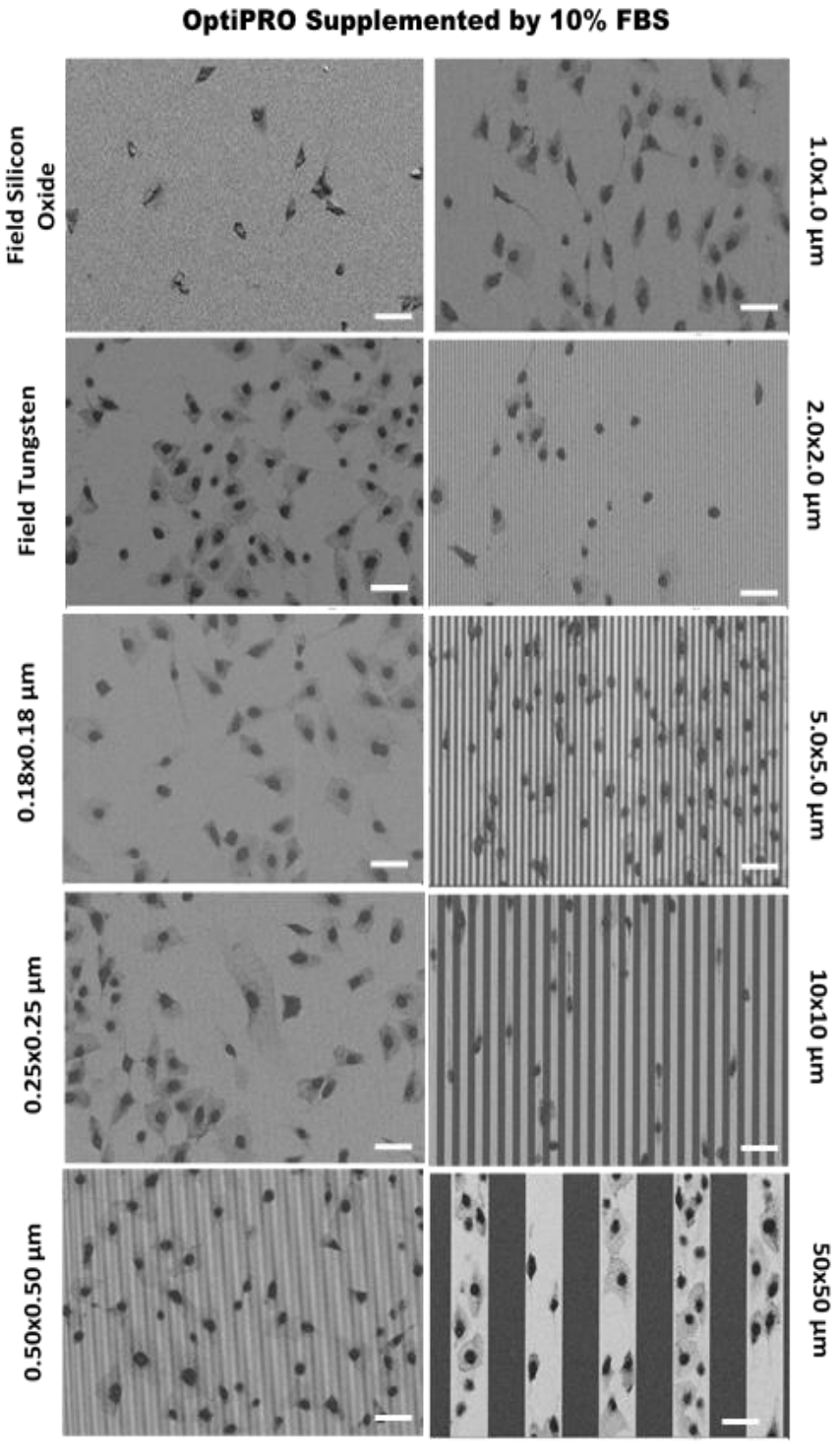

Figure S6 Typical top-down SEM images of Vero cells adherent on comb structures with different tungsten line widths incubated for 48 hours in OptiPRO™ culture medium supplemented with 10 % FBS. All scale bars are equal and represent 50 µm.

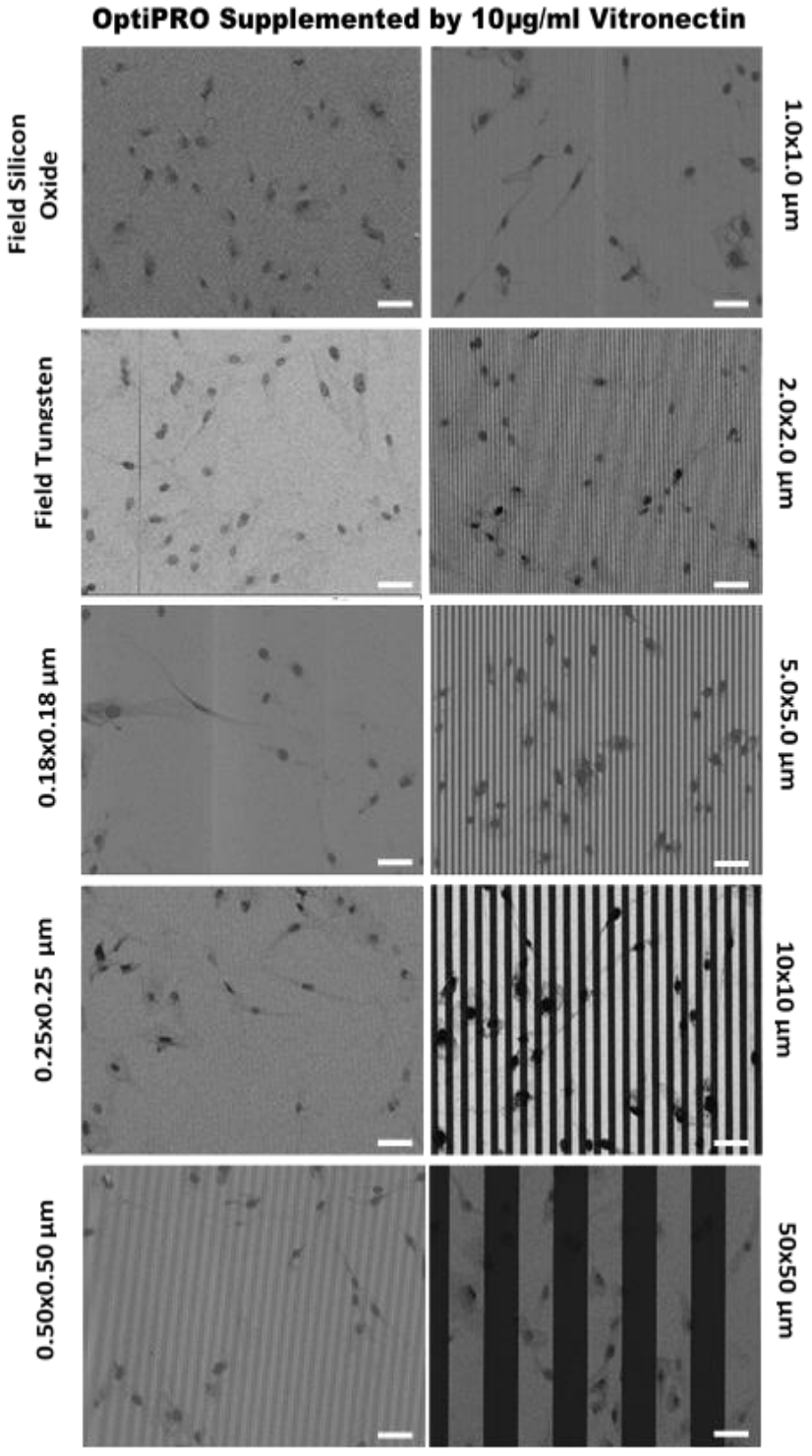

Figure S7 Typical top-down SEM images of Vero cells adherent on comb structures with different tungsten line widths incubated for 48 hours in OptiPRO™ culture medium supplemented with 10 µg/mL vitronectin. All scale bars are equal and represent 50 µm.

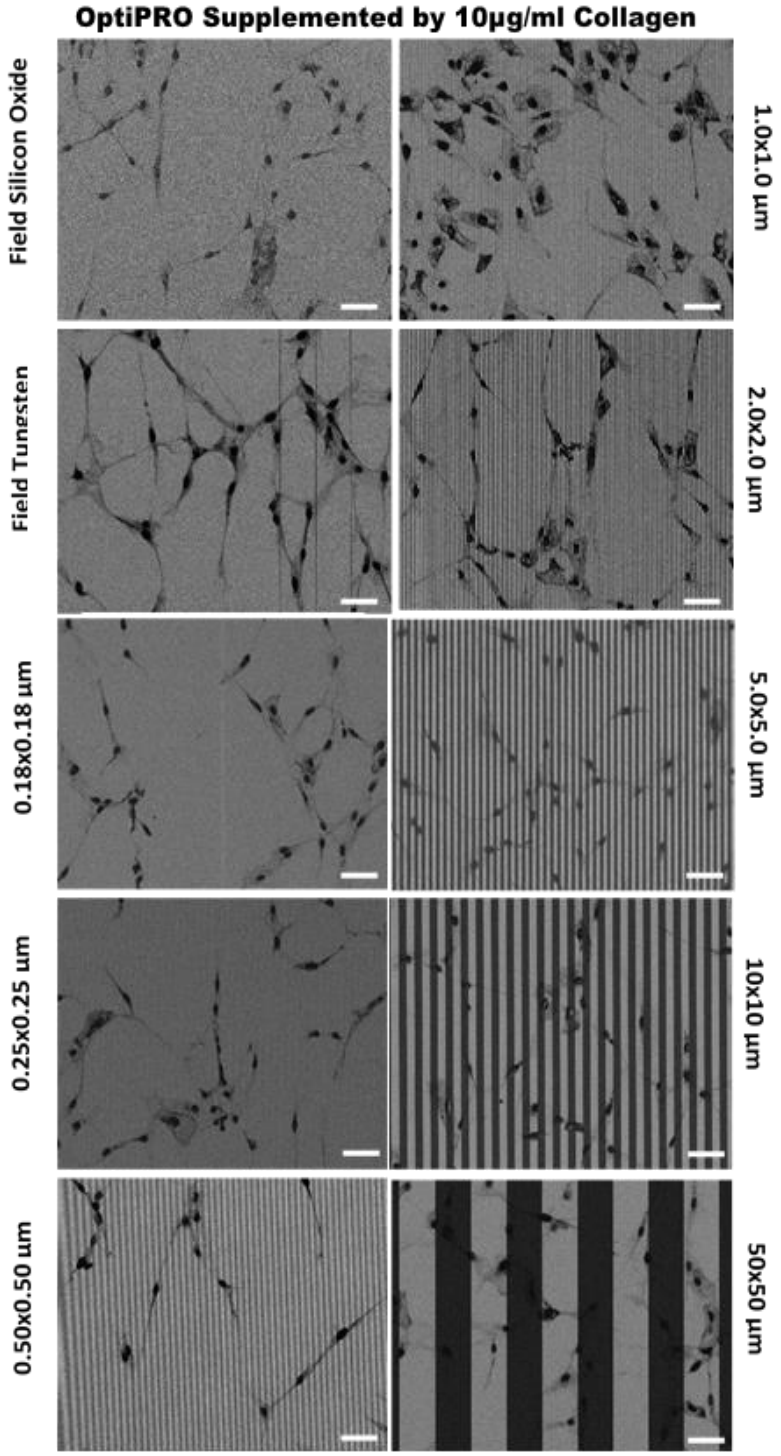

Figure S8 Typical top-down SEM images of Vero cells adherent on comb structures with different tungsten line widths incubated for 48 hours in OptiPRO™ culture medium supplemented with 10 µg/mL collagen. All scale bars are equal and represent 50 µm.

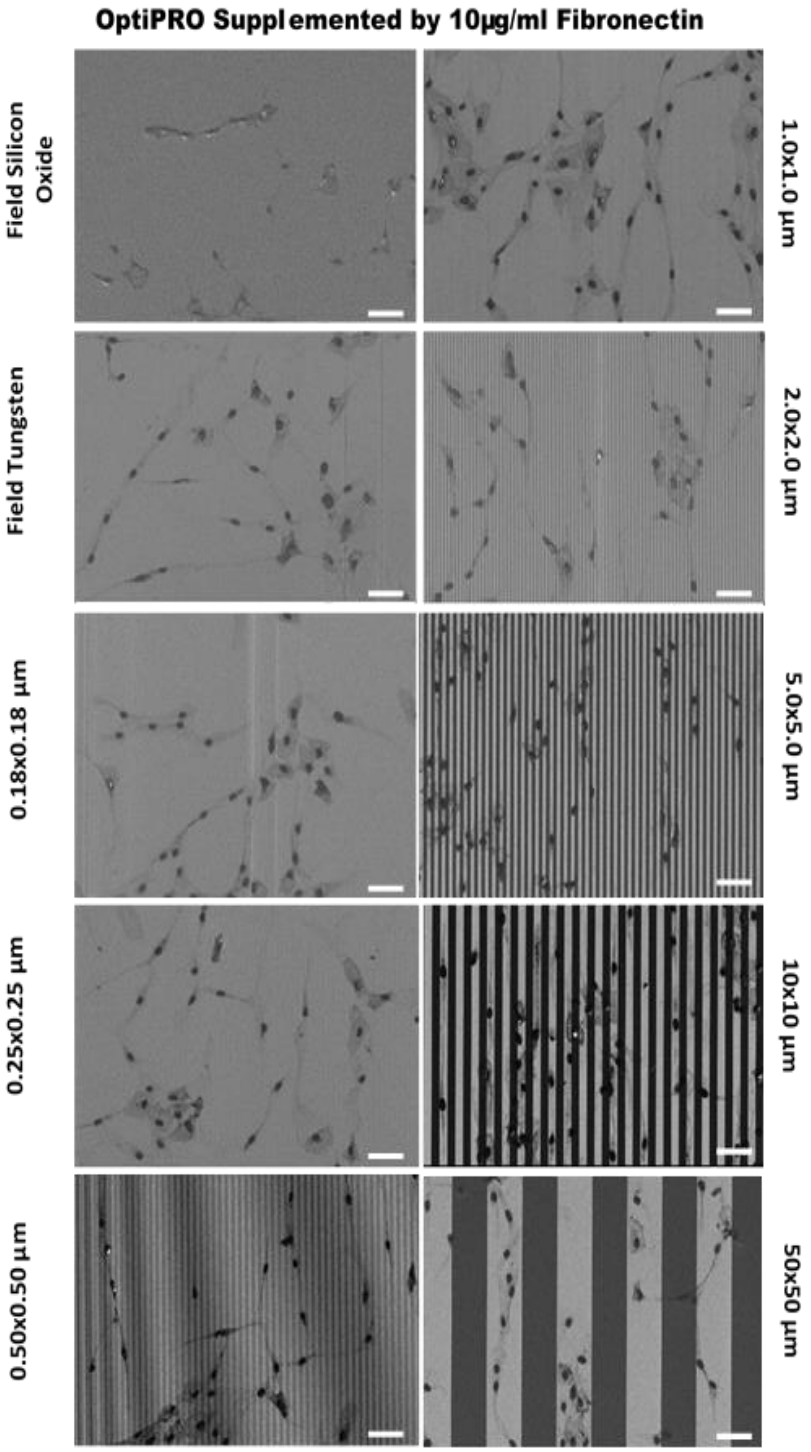

Figure S9 Typical top-down SEM images of Vero cells adherent on comb structures with different tungsten line widths incubated for 48 hours in OptiPRO™ culture medium supplemented with 10 µg/mL fibronectin. All scale bars are equal and represent 50 µm.

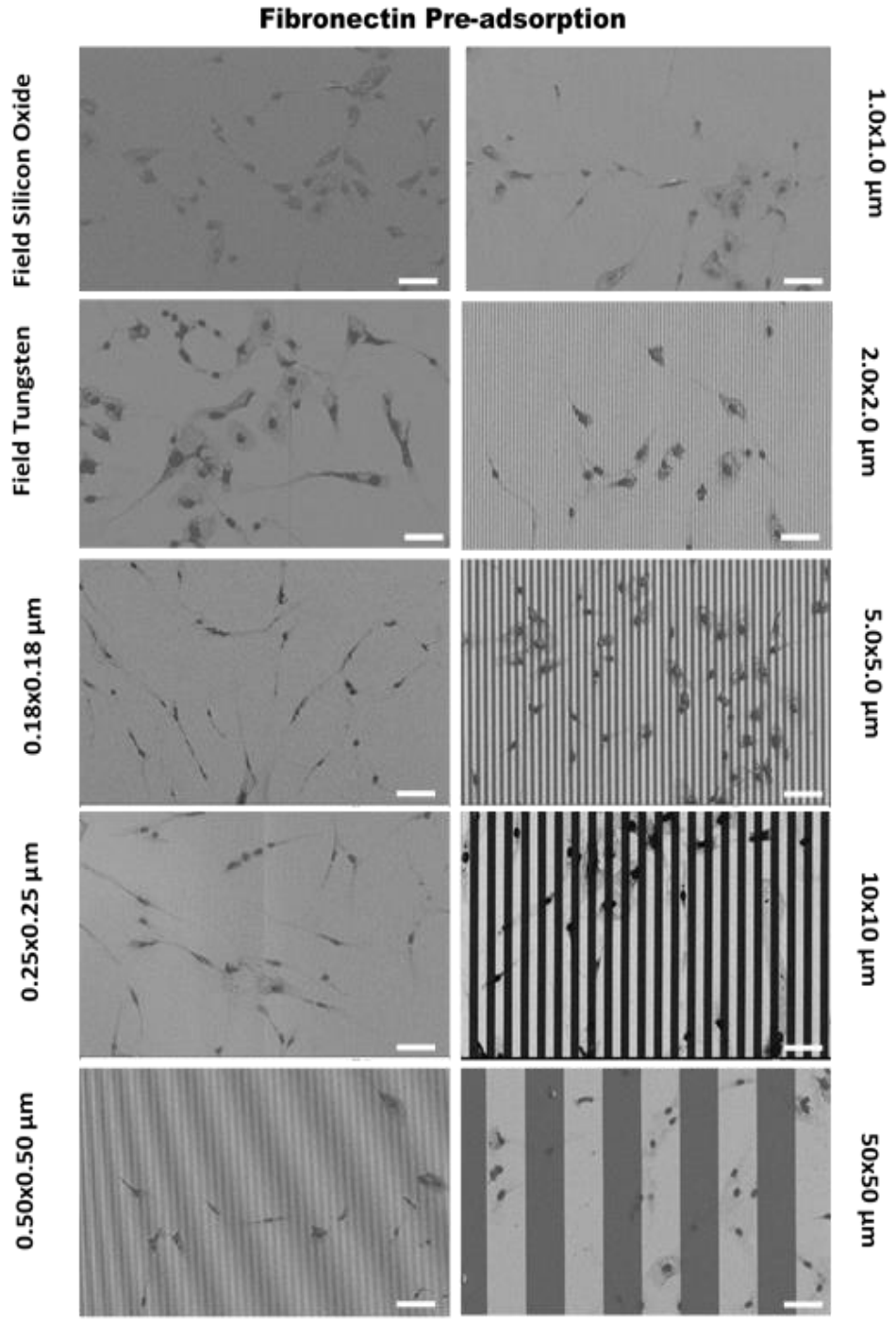

Figure S10 Representative top-down SEM images of Vero cells adherent on comb structures with different tungsten line widths incubated for 48 hours in OptiPRO™ culture medium. The substrate was submerged in a D-PBS solution containing 10 µg/mL fibronectin for 24 hours prior to seeding the cells. All scale bars are equal and represent 50 µm

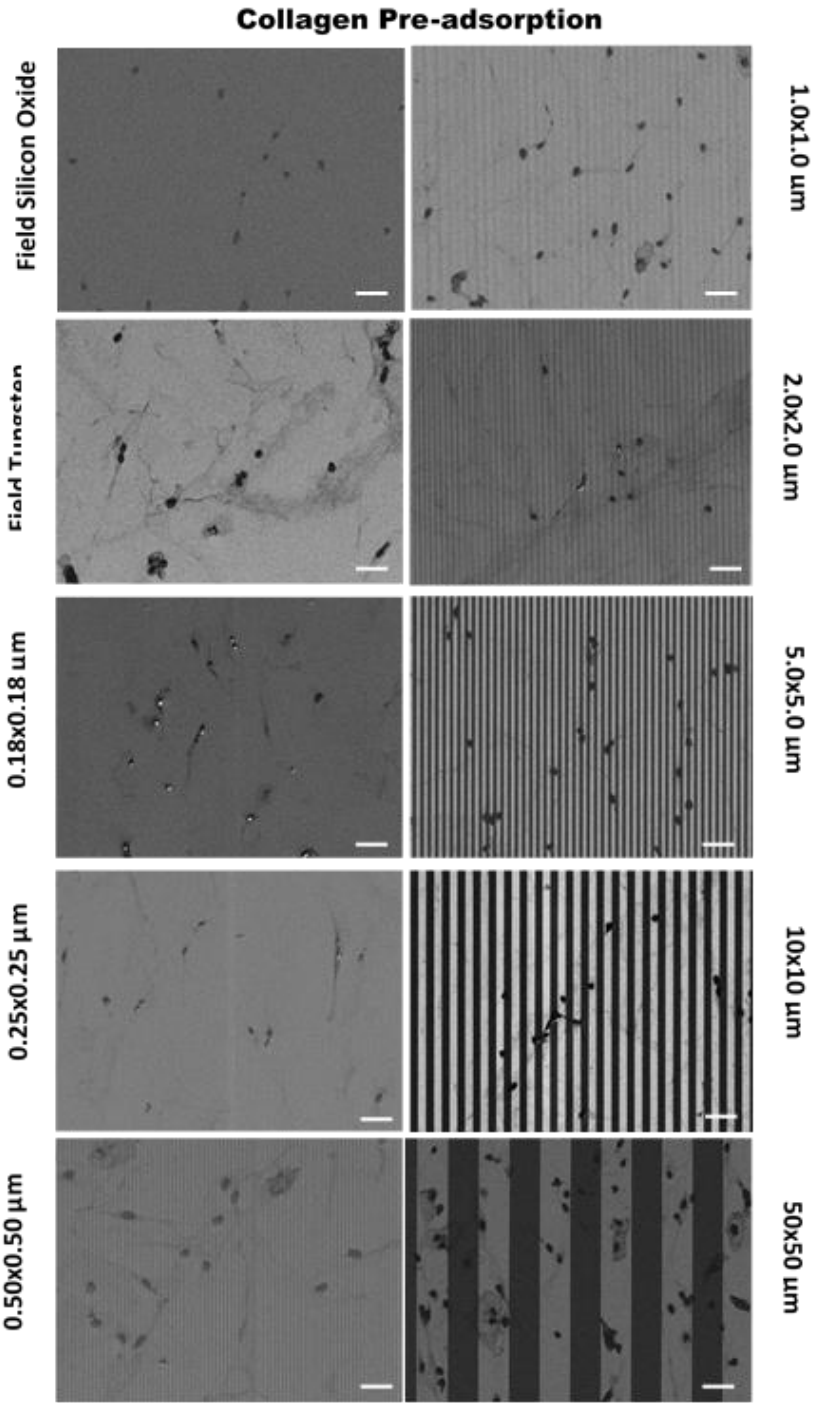

Figure S11 Representative top-down SEM images of Vero cells adherent on comb structures with different tungsten line widths incubated for 48 hours in OptiPRO^{TM} culture medium. The substrate was submerged in a D-PBS solution containing 10 µg/mL collagen for 24hours prior to seeding the cells. All scale bars are equal and represent 50 µm.

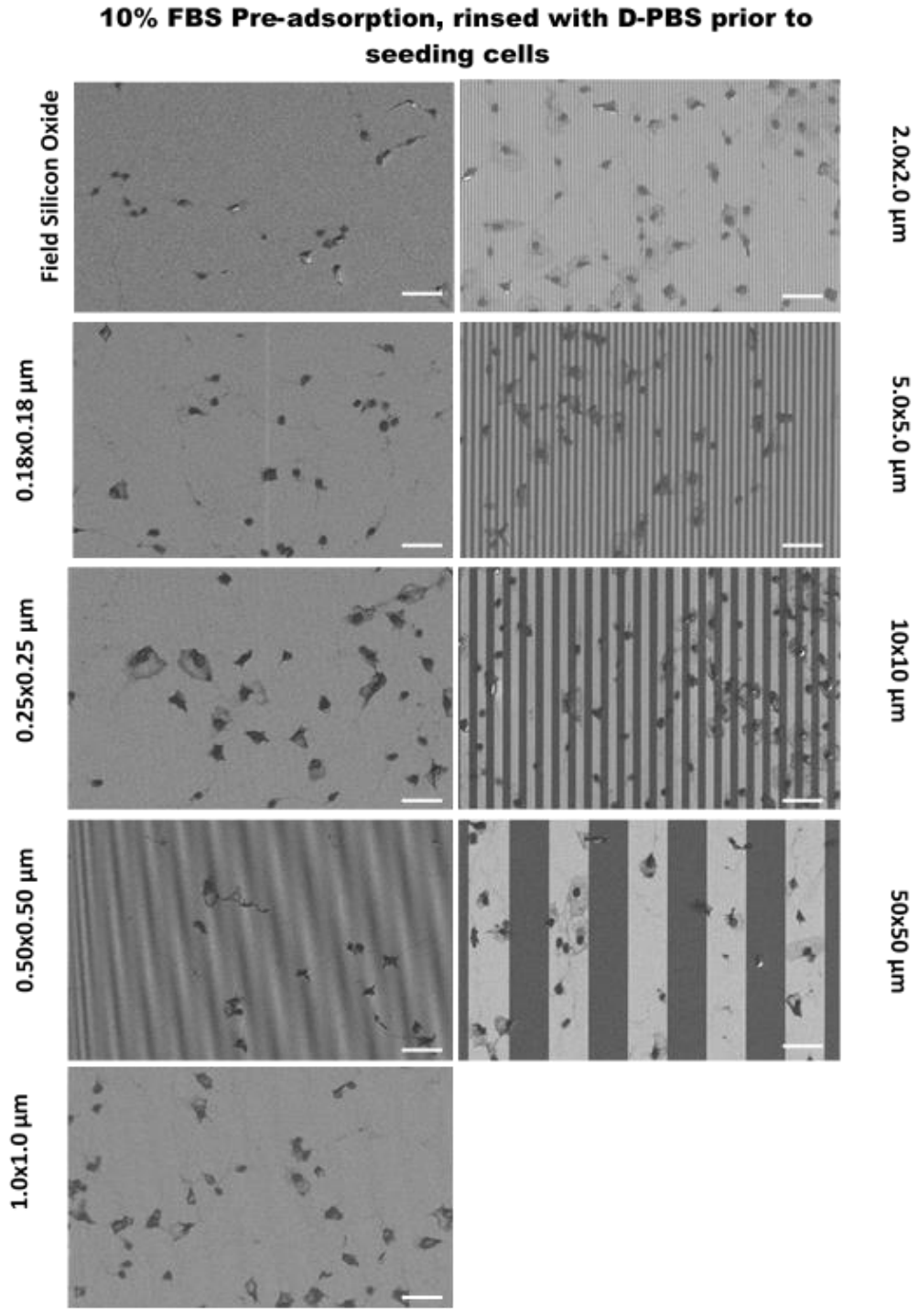

Figure S12 Representative top-down SEM images of Vero cells adherent on comb structures with different tungsten line widths incubated for 48 hours in OptiPRO™ culture medium. The substrate was submerged in a D-PBS solution containing 10 % FBS for 24hours, then rinsed with D-PBS prior to seeding the cells. All scale bars are equal and represent 50 µm.

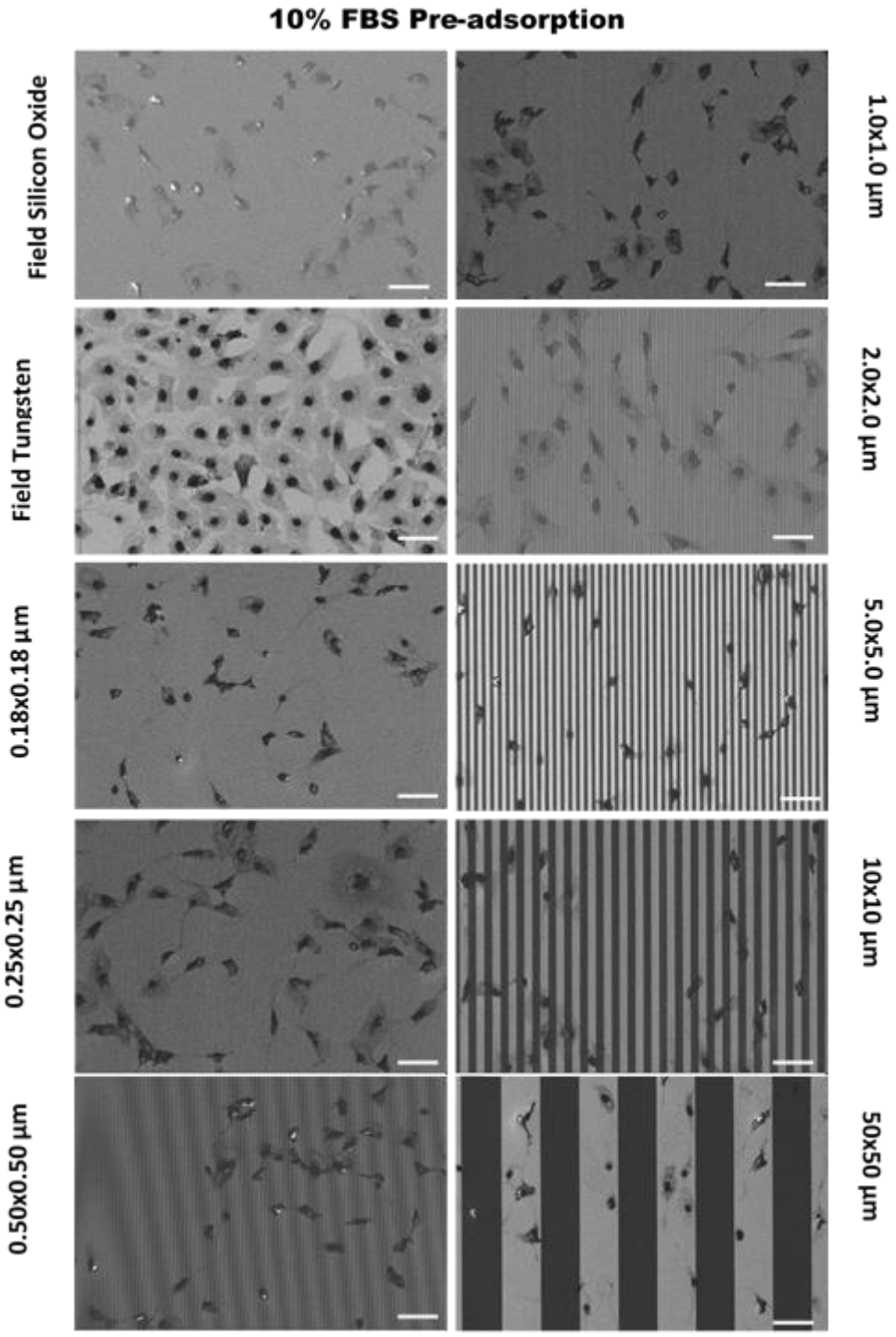

Figure S13 Representative top-down SEM images of Vero cells adherent on comb structures with different tungsten line widths incubated for 48 hours in OptiPRO™ culture medium. The substrate was submerged in a D-PBS solution containing 10 % FBS for 24hours prior to seeding the cells. All scale bars are equal and represent 50 µm.

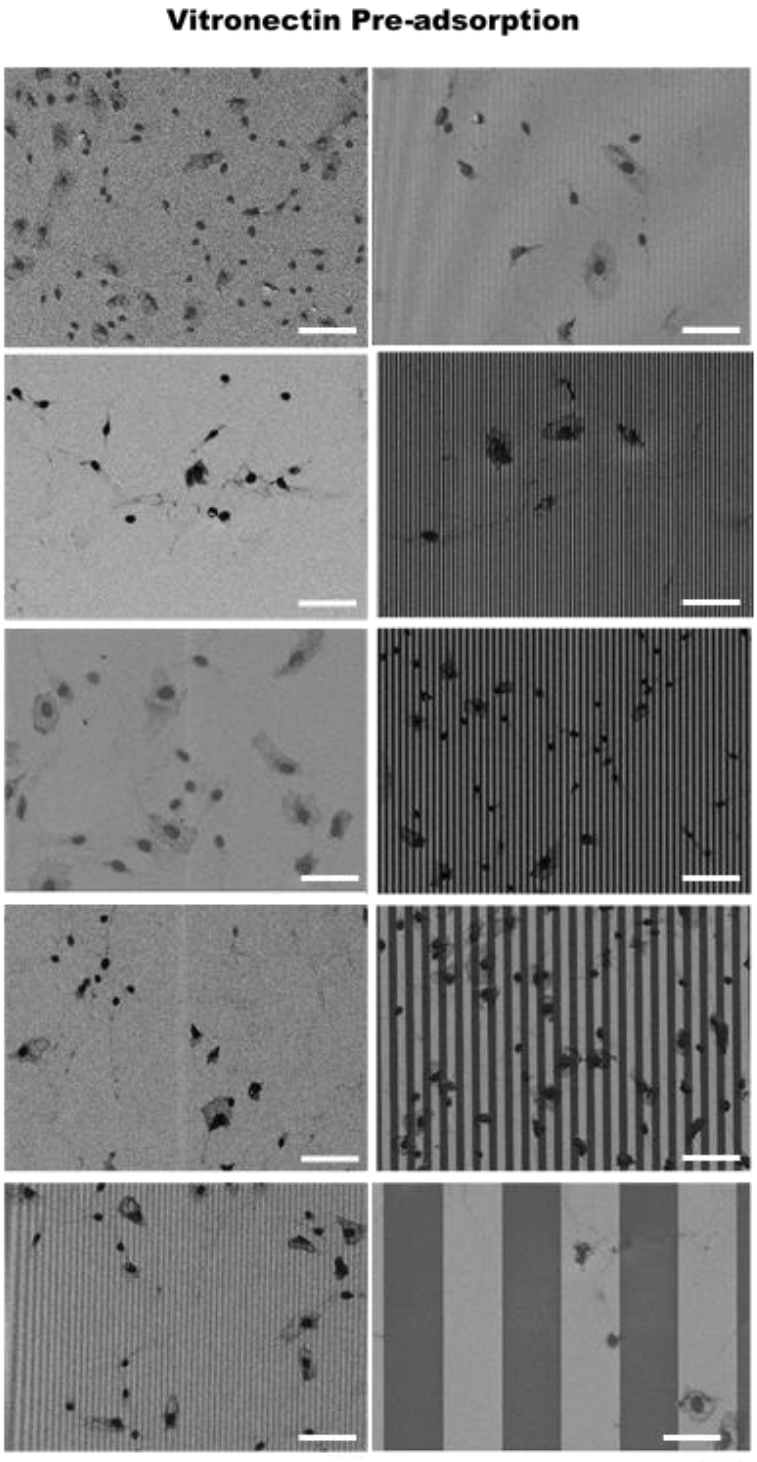

Figure S14 Representative top-down SEM images of Vero cells adherent on comb structures with different tungsten line widths incubated for 48 hours in OptiPRO™ culture medium. The substrate was submerged in a D-PBS solution containing 10 µg/mL vitronectin for 24hours prior to seeding the cells. All scale bars are equal and represent 50 µm.

Appendix D

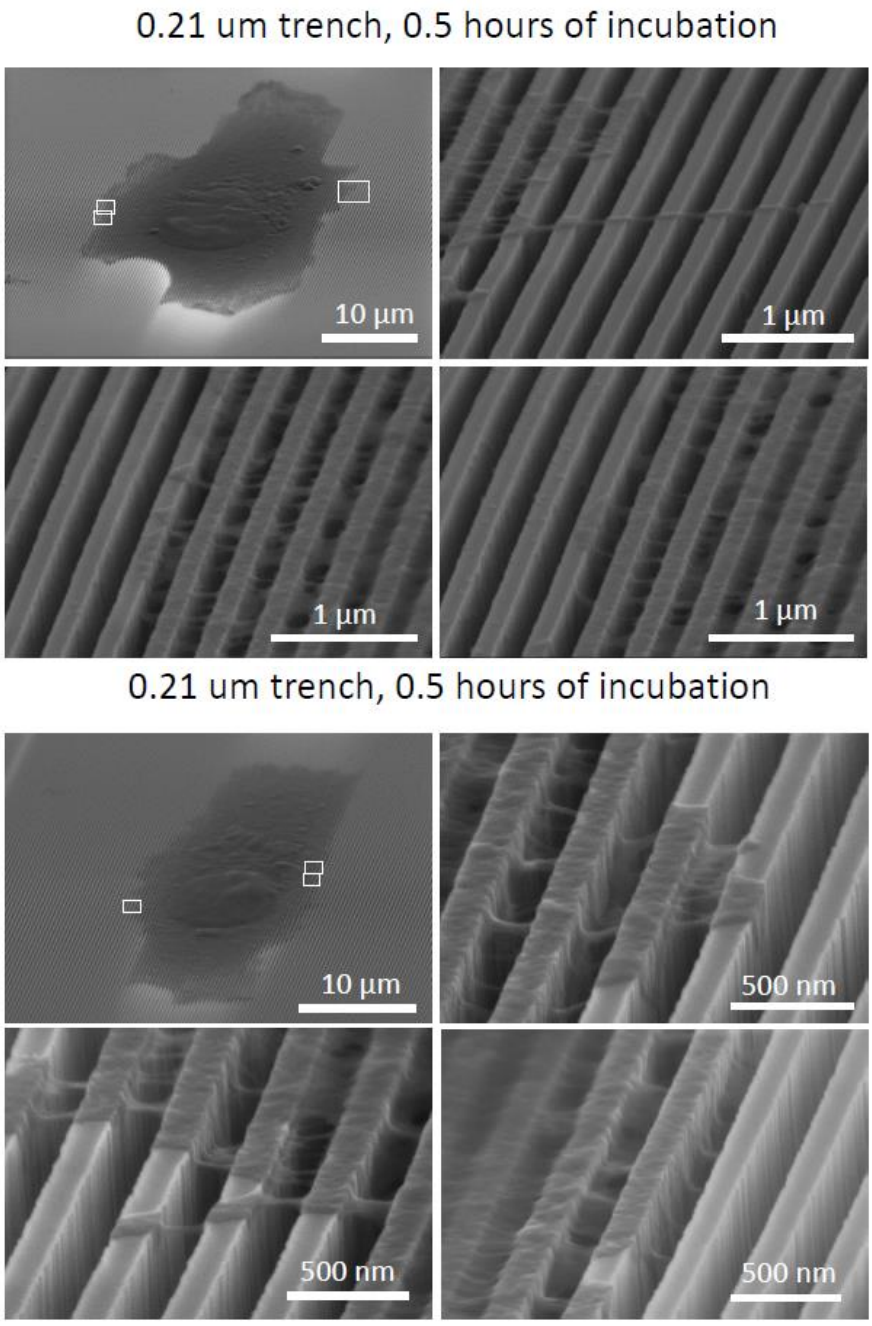

Figure S15 (a) and (b) 70° tilted SEM images of cells-substrate interactions on 0.21 µm wide trenches for cells incubated for 0.5 hours (Moussa et al., 2018a)

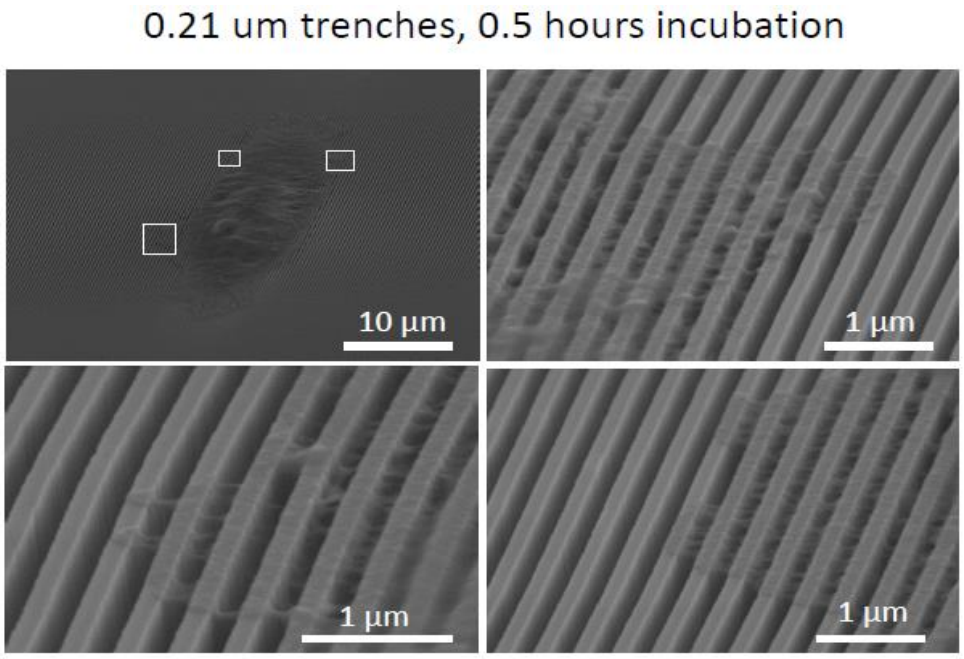

Figure S16 70° tilted SEM images of cells-substrate interactions on 0.21 µm wide trenches for cells incubated for 0.5 hours (Moussa et al., 2018a)

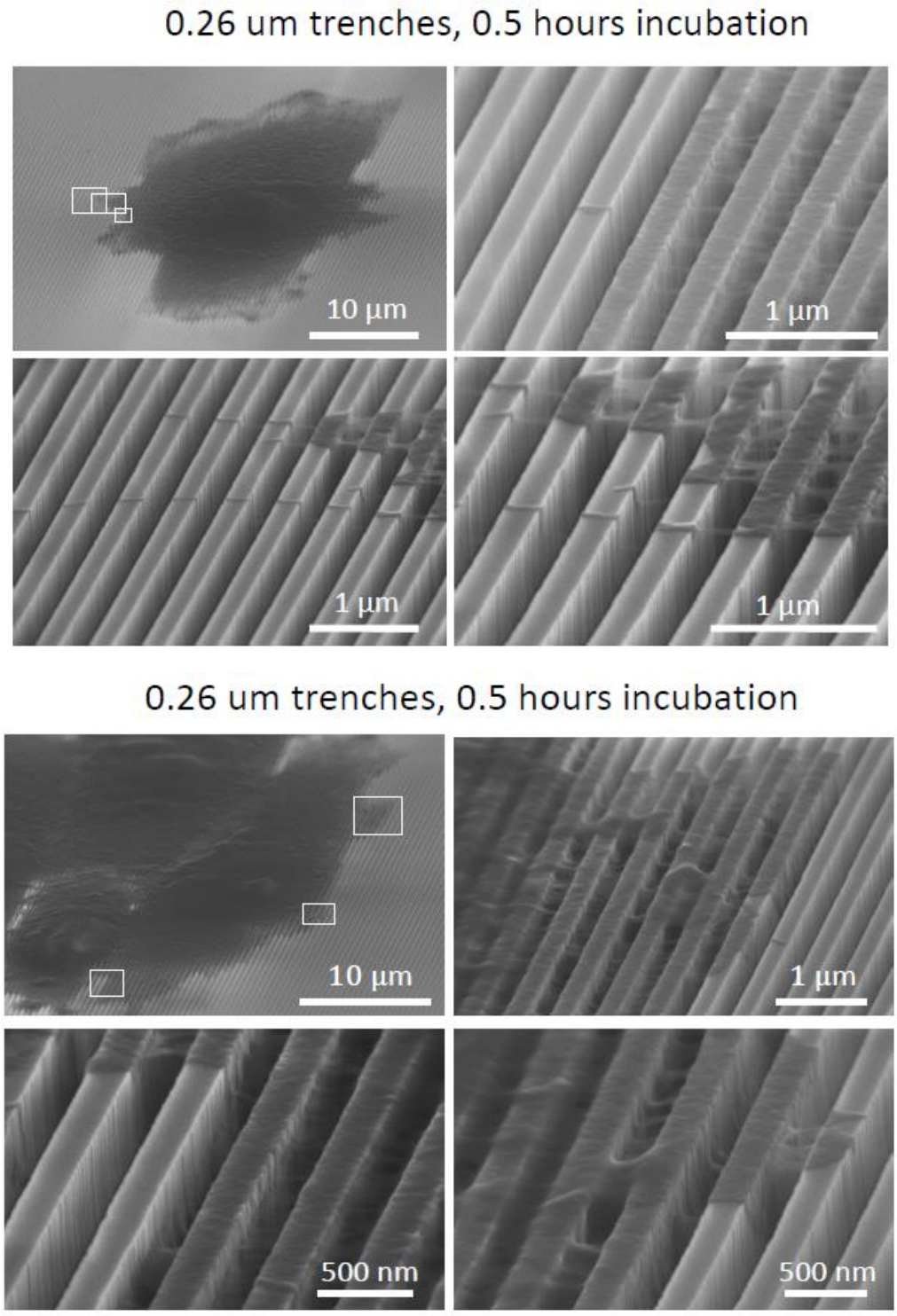

Figure S17 (a) and (b) 70° tilted SEM images of cell-substrate interactions on 0.26 µm wide trenches for cells incubated for 0.5 hours (Moussa et al., 2018a)

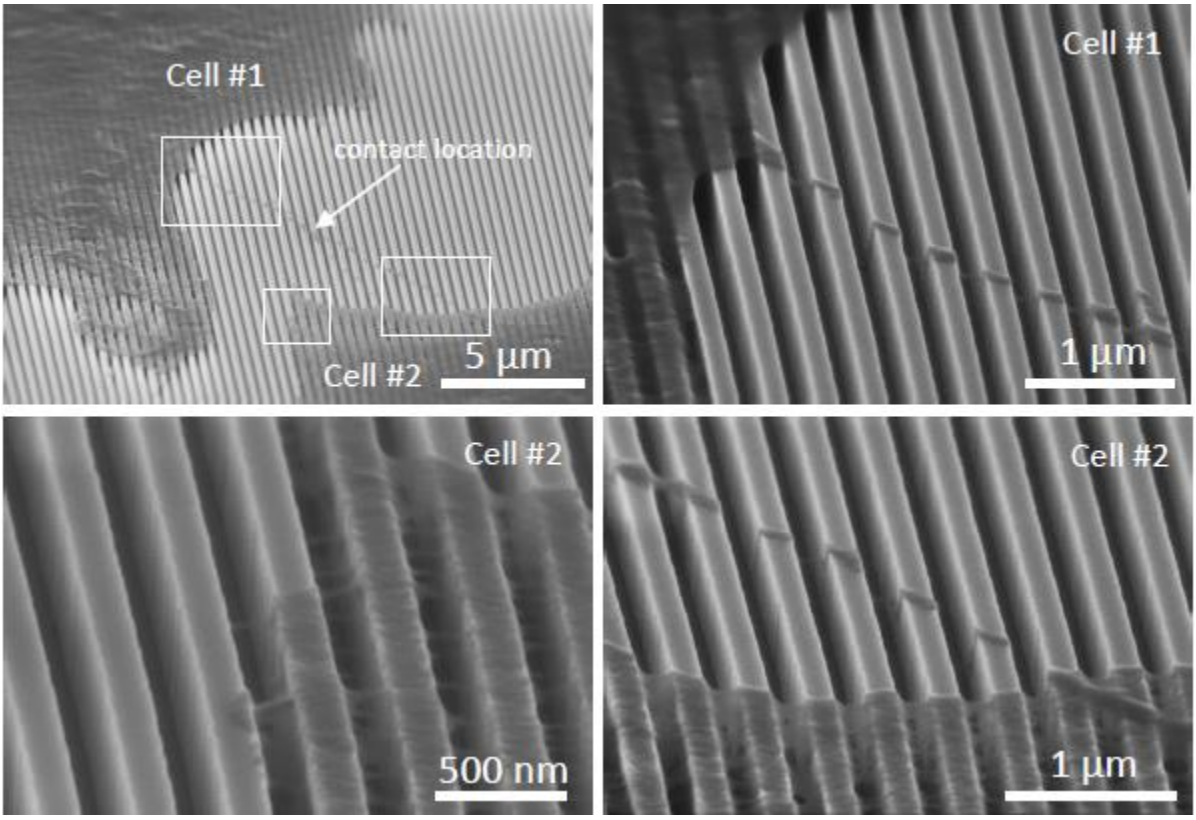

Figure S18 70° tilted SEM images of cell-substrate interactions on 0.21 µm wide trenches for cells incubated for 24 hours. Pseudopodia projections from two neighboring cells in contact on dense comb structures (Moussa et al., 2018a)

Appendix E

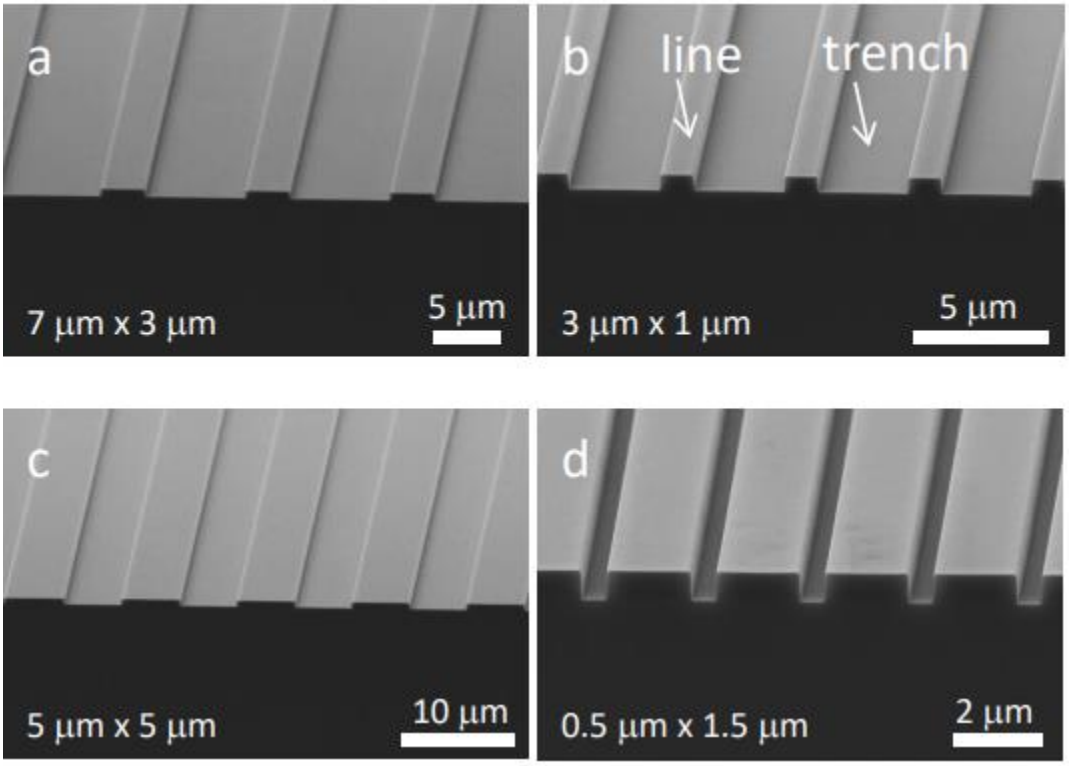

Figure S19 70° tilted SEM micrographs of copper stripped comb structures. Both the lines and trenches are coated with a thin film of Ta. Trenches are 700 nm deep (Moussa et al., 2018b)

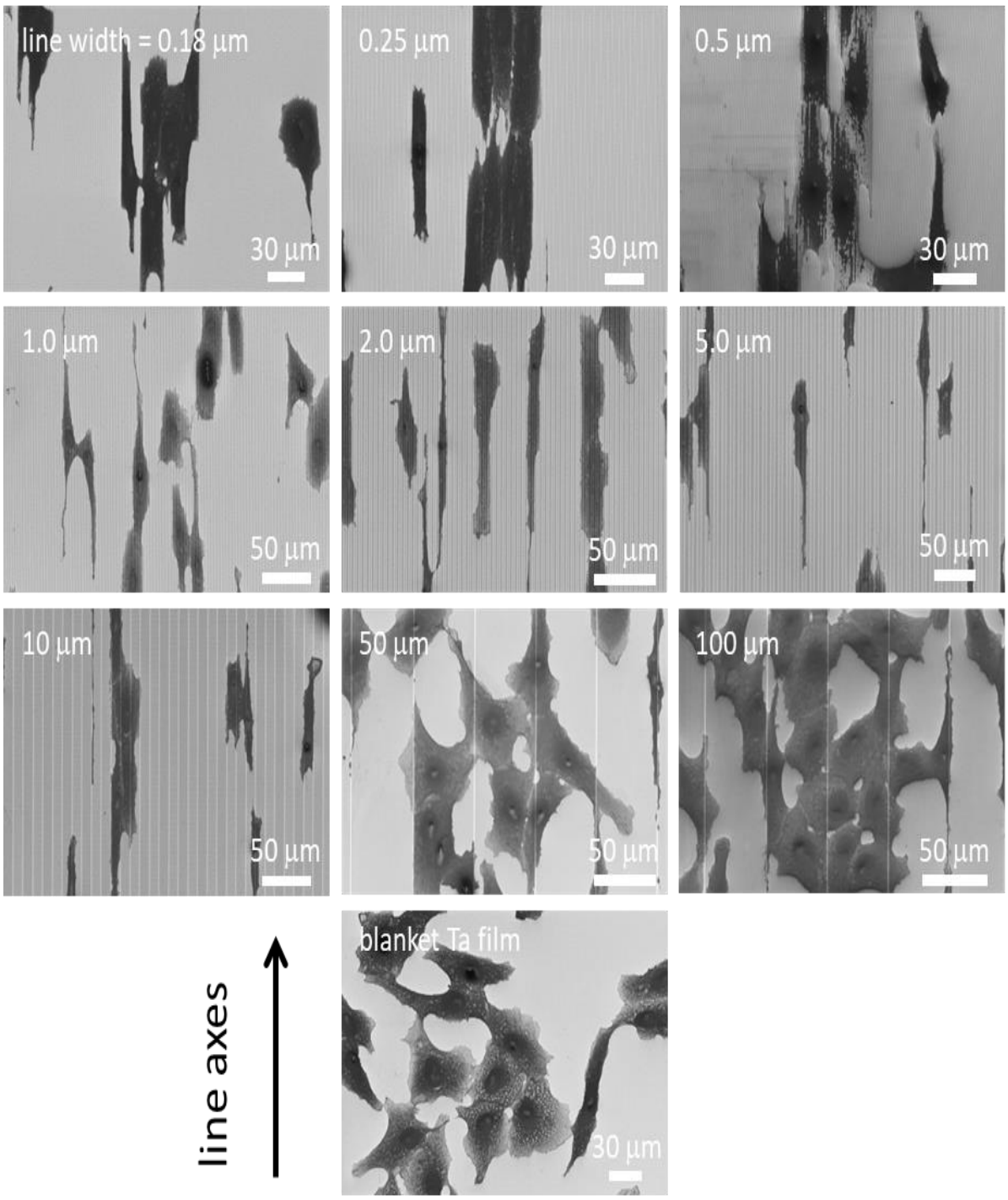

Figure S20 Representative top-down scanning electron microscopy (SEM) micrographs of adherent cells on different comb structures and blanket tantalum (Ta) film. Results show that adherent cells are aligned to the line axes on structures with line widths in the range of 0.18 to 10 µm. In contrast, cells on the 50 µm and 100 µm structures do not align well with the line axes—they are similar to cells (Moussa et al., 2018b)

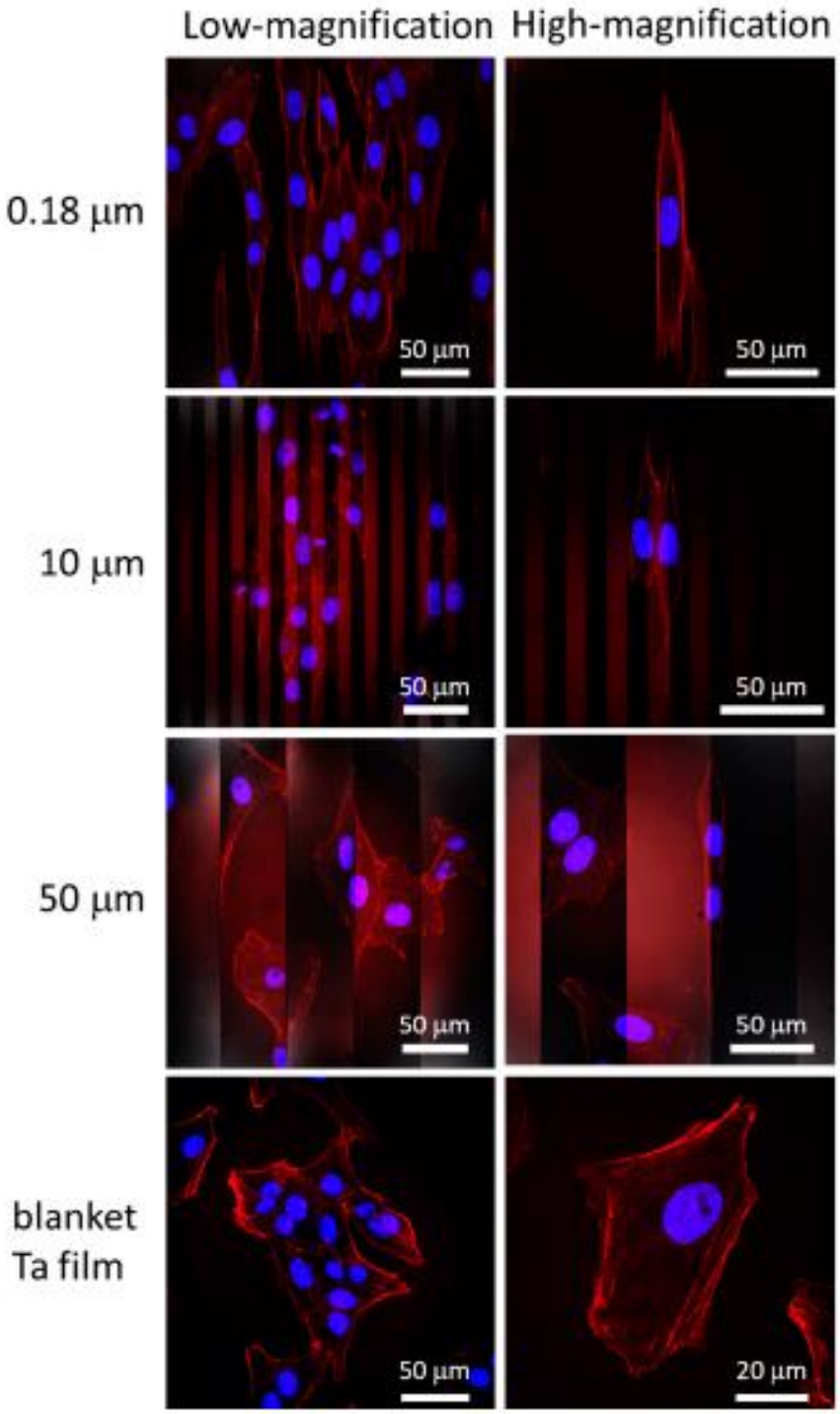

Figure S21 Typical high and low magnification fluorescence confocal images for adherent cells on comb structures with line widths of 0.25, 0.5, 1.0, and 10 µm. Cells incubated for 24 hours (Moussa et al., 2018b)

0.5 hour incubation on 0.18 μm comb structure

(a)

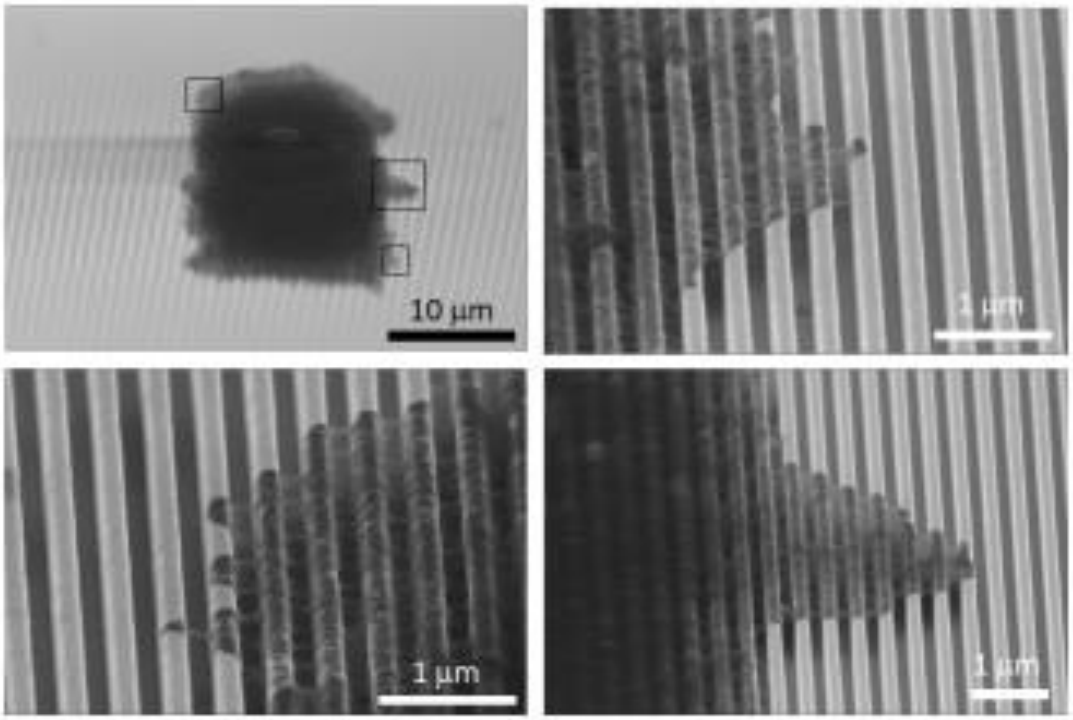

0.5 hour incubation on 0.25 μm comb structures

(b)

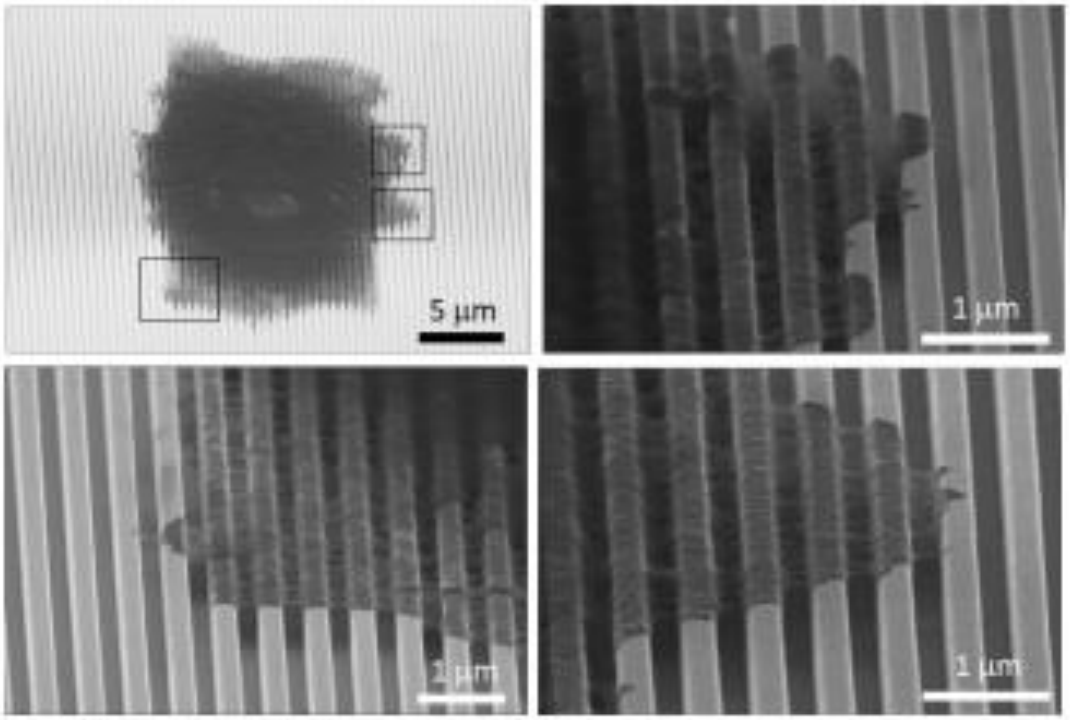

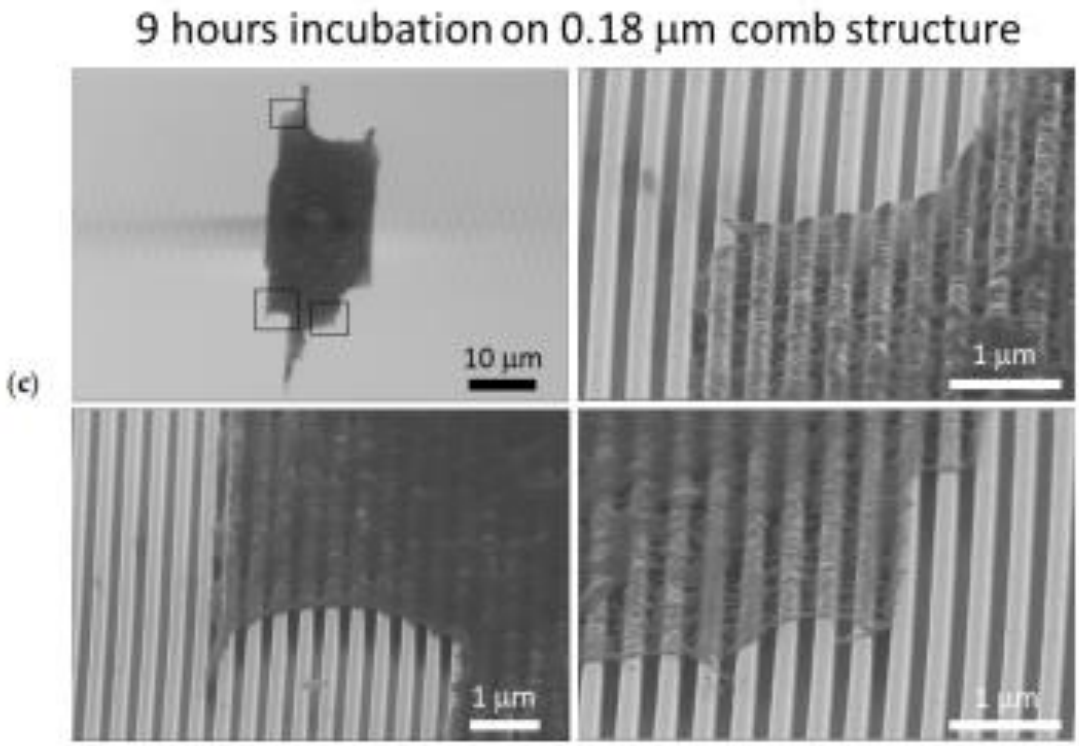

Figure S22 70° tilted SEM images of a single cell after incubated for 0.5-hour not fully spread on (a) 0.18 µm and (b) 0.25 µm wide lines comb structure. Morphologies of the pseudopod's extensions resemble the ones from cells incubated for 24 hours. (c) 70° tilted SEM images of a fully spread cell adherent after 9 hours of incubation on 0.18 µm comb structure (Moussa et al., 2018b).

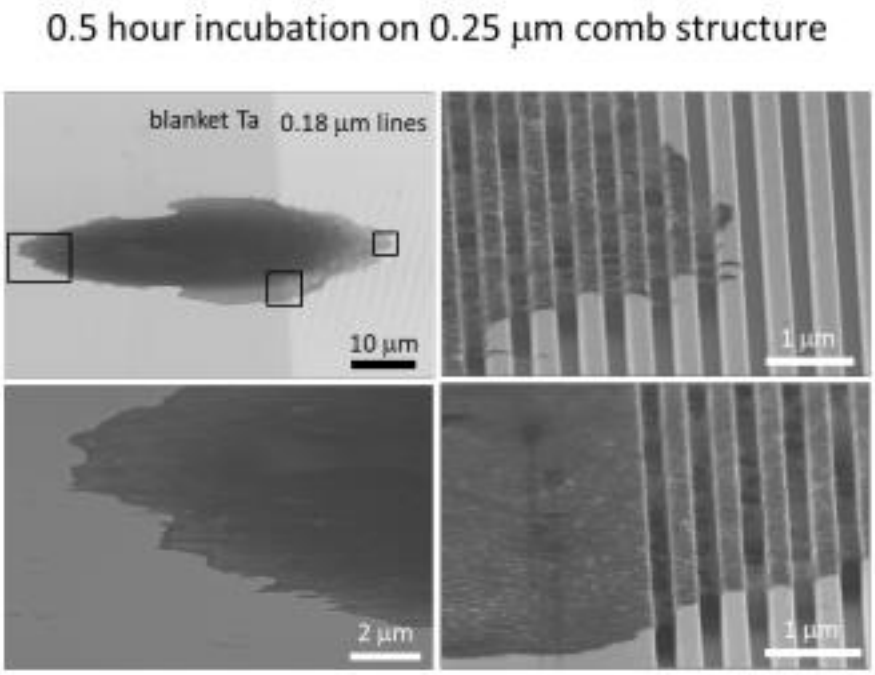

Figure S23 70° tilted SEM images for a not fully spread cell incubated for 0.5 hours and adherent on Ta blanket and 0.25 µm wide lines comb structure at the same time (Moussa et al., 2018b).